The Distribution of Trace Metals and their Relationship to Net Community Production during Two Marine Heatwave Events in the Subarctic Northeast Pacific Ocean

by

Robyn Corinne Taves
B.Sc., Vancouver Island University, 2017

A Thesis Submitted in Partial Fulfillment
of the Requirements for the Degree of

MASTER OF SCIENCE

in the School of Earth and Ocean Sciences

University of Victoria

We acknowledge and respect the lək̓ʷəŋən peoples on whose traditional territory the university stands and the Songhees, Esquimalt and W̱SÁNEĆ peoples whose historical relationships with the land continue to this day.

Supervisory Committee

The Distribution of Trace Metals and their Relationship to Net Community Production during Two Marine Heatwave Events in the Subarctic Northeast Pacific Ocean

by

Robyn Corinne Taves
B.Sc., Vancouver Island University, 2017

Supervisory Committee

Dr. Jay T. Cullen, School of Earth and Ocean Sciences
Supervisor

Dr. Diana E. Varela, School of Earth and Ocean Sciences
Departmental Member

Dr. Roberta C. Hamme, School of Earth and Ocean Sciences
Departmental Member

Abstract

The marine biological carbon pump (BCP) leads to the transfer of carbon from the atmosphere to the ocean interior through the growth of photosynthetic plankton in the euphotic zone and subsequent sinking of particulate matter to depth. In the subarctic northeast Pacific Ocean, the BCP is limited by the availability of the micro-nutrient iron (Fe) in the offshore, high nutrient, low chlorophyll (HNLC) region and by the macronutrient nitrate in the coastal region. In the last decade, two atmospheric events led to anomalously high sea surface temperatures, or marine heatwaves, in 2014-2015 and 2019 that were related to changes in the phytoplankton community composition and the BCP. Given that the bioavailability of trace metals can control microbial community composition, and important rate processes related to the BCP, we studied the spatial and temporal variation in the distribution of dissolved trace metals manganese, iron, cobalt, nickel, copper, and cadmium and macronutrients nitrate, phosphate, and silicic acid from 5 stations along the Line P Time Series transect in the subarctic northeast Pacific Ocean from winter (February) and summer (August) 2012-2019. In 2014 the mixed layer shallowed by diminished winter storm mixing, resulted in lower trace metal and macronutrient concentrations, but sustained dissolved iron and net community production (NCP) in the offshore, while the coastal region biogeochemistry remained similar to previous years (2012-2013). In 2015, further mixed layer shallowing allowed for similarly diminished trace metal (most notably iron), macronutrient concentrations, and NCP in the offshore and coastal regions. The phytoplankton community in the offshore shifted towards a higher relative abundance of pico-nano size species in both 2014 and 2015, with biomass sustained in 2014 and reduced in 2015. During the second marine heatwave event in 2019, the offshore was subject to similar winter mixed layer shallowing, warming, and reduced macronutrient concentrations. In the summer, surface trace metal and macronutrient concentrations were greatly diminished, resulting in nitrate limitation in the offshore. As the oceans continue to warm in response to anthropogenic CO_2, a likely consequence may be more frequent, and severe, marine heatwaves that can have internal and external effects on micro-macronutrient distributions, phytoplankton production, and the efficiency of the biological carbon pump.

Table of Contents

Table of Contents

Table of Contents

List of Tables

List of Figures

Acknowledgements

Firstly, I would like to thank Jay Cullen. Thank you for being you. You have been an amazing mentor and educator to me throughout the years. If I had a question or lacked understanding, you were there to provide the answer with as much detail as possible. I want to thank you for being an ally to women in science, not only because you educate many of us, but because you understand that it can be more difficult for us in this field, and you continue to have an open mind. You have shown me the support that is required for women to feel heard, respected, and safe in science. What I really want to thank you for is your empathy and understanding that life is not perfect. You have been supportive from the beginning with my familial circumstances and have allowed me to take the time I needed to support them, as well as myself. I am eternally grateful for this.

As much of my time was spent in the lab, I would like to thank Jody Spence. Thank you for all of your hard hours of prepping and running the ICP. Beyond the instrument time, you have been a mentor during my time at UVic. Thank you for helping me strengthen my analytical skills and teaching me the ins and outs of the ICP. Thank you for always being there when I had questions – you were always happy to help in any way possible. I appreciate everything you have done for me and I will miss our ICP prep chats about science and life.

Thank you to my committee members Roberta Hamme and Diana Varela. Unfortunately, we did not get to see much of either due to the pandemic. However, I appreciate the support that I knew was there the entire time. Special thanks to Roberta for listening and caring for her fellow women in science.

I would like to thank all of the members of the Cullen Lab group. Melissa and Meghan, although covid-19 put a physical wedge between us, I want to thank you for being amazing women and I can't wait to build our friendships. Tia, without a doubt you were the best lab mate in the history of lab mates. Thanks for being yourself, supporting me during tough times, and being my friend. Annaliese, thank you for teaching me the ins and outs of the lab and the seaFAST. Most importantly, thank you for making me feel welcome and for being my friend.

Big thank you to Marie Robert and all of the crew and scientists of the CCGS John P. Tully. Marie, thank you for always being flexible with our trace metal needs and for welcoming me onto the cruises. To the Boson Johnny and all of the crew, thank you so much. I couldn't have conducted sampling without you. You were all so helpful, patient, and kind throughout the trace metal process – which is not easy.

Lastly, I would like to thank my friends and family, starting with my friends. Thank you to all of my close friends whom I consider family for listening and supporting me during the highs and lows of grad school. Special thanks to Ahron and Sile. Thanks to Ahron for answering all of my simple matlab questions, without you I wouldn't have nice figures. Thanks to Sile for always being there, 24/7 whenever I needed a friend. Thank you both for all of our fun times of having dinner and watching scary movies. To my family, this wouldn't be possible without you. Thank you to my parents for supporting me throughout my entire life and my academic career. Thank you to my sister for having a similar sense of humour and laughing at my memes. Thank you to my partner Tim for taking care of me in all ways, but especially for taking us out to dinner when we were too exhausted to make it. Thank you to our family cat Buoy, she has been the best emotional support kitty who provides entertainment and softness for all. Finally, thank you to my niece Sophia for grounding me, making me laugh, and loving me unconditionally.

Dedication

This thesis is dedicated to my entire family. To my parents, for putting in the hard work and dedication it takes to raise their children and grandchild. To my sister, who is teaching the future generation with empathy and respect. To my partner Tim, who has been by my side and made every day a little easier. Finally to my niece Sophia, you will be able to accomplish any goals you have, and your family will love and support you to make sure you meet your own definition of success.

Chapter 1: Introduction

1.1 Trace Metal Biogeochemistry

Trace metals are metallic elements that are found in the environment at very low concentrations. In seawater, trace metals occur at concentrations within the range of 10^{-15} (fmol/L) to 10^{-6} (µmol/L) (Bruland and Lohan 2003). Types of trace metals include some transition metals that are essential for biochemical functions, but can behave as toxins at higher concentrations. In marine phytoplankton, trace metals are used in a variety of biological processes including, but not limited to, photosynthesis, respiration, carbon acquisition, and nitrogen assimilation (Morel *et al.* 2003). They act as metal centers in metalloenzymes as well as electron donors and acceptors in the cell (Robbins *et al.* 2020).

In seawater, trace metals are typically grouped into four distinct types, or combinations of these, based on their vertical depth profiles: I) conservative-type distribution, II) nutrient-type distribution, III) scavenged-type distribution, and IV) hybrid-type distribution (Bruland and Lohan 2014). Conservative-type distributions remain relatively constant from surface to depth. Species that display conservative-type distributions are typically oxyanions or mono-covalent cations, and have uniform concentrations across ocean basins (Bruland and Lohan 2014). Nutrient-type distributions have low concentrations at the surface due to assimilation by marine microbes and subsequent export to depth, with organic-matter. Dissolved concentrations increase with increasing depth, as organic matter is oxidized and metals are released in the deep ocean (Bruland and Lohan 2014). The trace elements zinc (Zn) and cadmium (Cd) are the most noteworthy of nutrient-type, as their acute surface depletions and dramatic concentration profiles are exemplarily of the distribution. Scavenged-type distributions have the highest concentrations proximate to trace metal sources (eg. Atmospheric deposition), and decrease with distance and/or depth in the water column. Examples of species with this distribution include manganese (Mn), aluminum (Al), and lead (Pb). They typically have short residence times in the ocean and have a high affinity for particles (Bruland and Lohan 2014). Hybrid-type distribution trace metals are influenced by both scavenging and recycling. Some metals, such as iron (Fe), can either be assimilated at the surface by marine microbes (nutrient-type) or have a surface maxima due to external inputs (scavenged-type) (Bruland and Lohan 2014).

Sources of trace metals include both internal and external inputs in oceanic environments. External inputs predominantly include riverine, atmospheric, benthic, and hydrothermal sources (Bruland and Lohan 2014). Internal sources include processes that recycle trace metals scavenged to particles and the release of some species in the suboxic waters of oxygen minimum zones (OMZ) (Landing and Bruland 1980; Klinkhammer and Bender 1980; Bruland and Lohan 2014). In coastal regions, the predominant source of trace metals comes from riverine input, as well as atmospheric, benthic, and internal recycling. Further from the coast and ocean margins, the upper layer of offshore environments can be heavily influenced by atmospheric and internal recycling inputs, while the deep ocean is influenced by benthic and hydrothermal sources.

To better interpret the distributions of trace metals in coastal and offshore environments, it is important to have a rudimentary understanding of the physical, chemical, and biological requirements

of individual metal species. In addition, it is imperative to understand the potential internal and external sources of trace species and how they might affect spatial and temporal distributions. The aim of this thesis is to observe the spatial and temporal distributions of manganese (Mn), iron (Fe), cobalt (Co), cadmium (Cd), nickel (Ni), and copper (Cu) to better understand the biogeochemical effects of recently documented marine heatwaves in the subarctic northeast Pacific Ocean.

Table 1. Physical and Chemical Properties of Manganese, Iron, Cobalt, Cadmium, Nickel, and Copper

Property	**Manganese**	**Iron**	**Cobalt**	**Nickel**	**Copper**	**Cadmium**
Atomic Number	25	26	27	28	29	48
Atomic Weight	54.938	55.845	58.933	58.693	63.546	112.41
Atomic Radius (Angstroms)	1.40[a]	1.40[a]	1.35[a]	1.35[a]	1.35[a]	1.55[a]
Electron Configuration	[Ar] $3d^5$ $4s^2$	[Ar] $3d^6$ $4s^2$	[Ar] $3d^7$ $4s^2$	[Ar] $3d^8$ $4s^2$	[Ar] $3d^9$ $4s^2$	[Kr] $4d^{10}$ $5s^2$
Melting Point (°C)	1246	1538	1495	1455	1084.62	321.07
Boiling Point (°C)	2061	2861	2900	2913	2562	766.9
Density (g cm^{-3})	7.470	7.874	8.9000	8.908	8.960	8.650
Common Oxidation States	+2, +3, +4, +6, +7	+2, +3	+2, +3	+2	+1, +2	+2
Ionic Radius Mn^{2+} (pm)	70	70	70	70	73	95
Reduction Potential (E°)	-1.185[b]	-0.447[b]	-0.28[b]	-0.257[b]	+0.34[b]	-0.4030[b]
First Ionization Energy (kJ mol^-)	717.3	762.5	760.4	737.1	745.5	867.8
Second Ionization Energy (kJ mol^-)	1509.0	1561.9	1648	1753.0	1957.9	1631.4

[a] Slater, 1964

[b] Neth *et al.* 2016

1.2 Manganese in the Ocean

Manganese (Mn) is a first row transition metal with an atomic number and weight of 25 and 54.938 g/mol, respectively. It is highly redox sensitive element with 5 common oxidation states. The physical and chemical properties of Mn are shown in Table 1. In the subarctic northeast Pacific, the depth profile is a modified nutrient-type profile with three maxima located at the surface, the oxygen minimum zone (OMZ), and near hydrothermal vent sites in the deep ocean (Landing and Bruland 1980). Typically, Mn concentrations are elevated at the surface by external sources such as riverine, continental shelf sediment, and aeolian dust inputs (Landing and Bruland 1980; Bishop and Fleisher 1987; Lam *et al.* 2006). During the spring/summer growing seasons, Mn is scavenged by phytoplankton in the mixed layer, diminishing surface dissolved (passing through a 0.2 µm pore size filter) Mn (dMn). At mid depths near the OMZ (500-1200m), where dO_2 concentrations are low but non-zero, the second maxima of Mn corresponds to the reduction of solid Mn species, the breakdown of organic matter, or anoxic sediment transport from the slope (Landing and Bruland 1980; Klinkhammer and Bender 1980). In the deep ocean (>2000m), the third Mn maxima originates from either Mn rich hydrothermal fluid

input or resuspension of sediments, with the latter likely a less efficient source (Landing and Bruland 1980; Von Damm 1980; Klinkhammer and Bender 1980).

1.2.1 Manganese Phytoplankton Assimilation

During oxygenic photosynthesis, Mn is an essential component of the oxygen evolving complex (OEC) in photosystem II (Vinyard *et al.* 2013). The OEC utilizes the high redox potential of Mn species to oxidize water to oxygen (O_2) (Vinyard *et al.* 2013). Therefore, Mn is imperative for the function and growth of marine prokaryotic and eukaryotic photosynthetic organisms. In addition, during the process of converting water to O_2, highly reactive oxygen species, including superoxide (O_2^-), can form as a result. In order to protect the cell from damage, a family of Mn-containing enzymes known as superoxide dismutases (SODs) catalyze the dismutation of O_2^- to O_2 (Morel *et al.* 2003). The Mn-containing SODs become most important during times of Fe limitation when oxidative stress increases. Diatoms that are Fe stressed require higher Mn quotas compared to those that are replete in Fe, where the Mn-containing SOD's make up for a large portion of the intracellular Mn quotas (Peers and Price 2004).

1.3 Iron in the Ocean

Iron (Fe) is a first row transition metal with an atomic number of 26 and mass of 55.845 g/mol, as shown in Table 1. Fe is commonly found in the +2 and +3 oxidation states, and is easily oxidized from soluble Fe^{2+} to insoluble Fe^{3+} in oxygenated waters. As Fe^{3+} is thermodynamically favourable in seawater and insoluble, surface concentrations are depleted in open ocean environments that extend far from continental inputs (Rue and Bruland 1995). The depth profile of dissolved Fe is a hybrid-type profile (nutrient and scavenged-type). Surface Fe is scavenged by active uptake by phytoplankton and adsorption to reactive particle surfaces, resulting in concentrations less than 0.5 nM dissolved Fe (Landing and Bruland 1987; Bruland *et al.* 2014). Below the euphotic zone concentrations begin to increase as particles and organic aggregates breakdown and release Fe into the water column. Near the OMZ there is evidence of soluble Fe release in suboxic waters likely originating from lateral transport (Landing and Bruland 1987; Bruland *et al.* 2014). Deep water Fe concentrations can be some of the lowest in the vertical profile, with at times having a maxima due to resuspension of sediments and hydrothermal fluid (Landing and Bruland 1987; Bruland *et al.* 2014)

Iron enrichment experiments have shown that in the open ocean, high nitrate low chlorophyll (HNLC) regions, addition of Fe stimulates rates of productivity and allows for drawdown of macronutrients (Martin *et al.* 1989; Martin 1990; Martin *et al.* 1994). These early experiments suggest that inputs of Fe from the atmosphere or continental margin are essential for ocean productivity in the HNLC, and limit the growth of phytoplankton in the region. In regions with minimal input from externally sourced Fe, the residence time of surface dissolved Fe is on the order of 1.3 years (Moore *et al.* 2004). The dissolved Fe is predominantly complexed with organic ligands which are bioavailable to some marine phytoplankton, facilitating uptake and assimilation (Rue and Bruland 1995).

1.3.1 Iron Phytoplankton Assimilation

For photosynthetic organisms, Fe is the most prevalent transition metal used during the light reactions of photosynthesis. Raven (1990) observed 3 Fe atoms in PSII, 12 in photosystem I (PSI), and 8 within the electron transport chain. Due to the high requirement of Fe, it is no surprise that the function and growth of marine phytoplankton and heterotrophic bacteria depends on the presence of adequate, bioavailable Fe in the environment (Granger and Price 1999; Morel *et al.* 2003). When Fe is replete in the ocean, similar to Mn, Fe can also be used as a metal center in SOD (Raven 2019).

Another important role of Fe for phytoplankton is in the production and acquisition of biologically available nitrogen. Nitrate reductase (NR) is an enzyme used to reduce NO_3^- to NO_2^-, and is an Fe containing cytochrome that requires 2 Fe atoms for proper function (Morel *et al.* 2003). During times of Fe limitation, larger diatoms become stressed and are unable to assimilate NO_3 and utilize other forms of nitrogen, similar to that smaller phytoplankton are able to acquire nitrogen through different pathways that require less Fe (Price *et al.* 1994; Morel *et al.* 2003).

As Fe in the surface ocean is present predominantly in the scarce oxidized form of Fe^{3+}, phytoplankton have adapted to access inorganic Fe^{3+} by assimilating Fe^{3+} organic ligand complexes, which tend to be thermodynamically stable. Fe-binding, marine siderophores are produced by cyanobacteria and heterotrophic bacteria (Barbeau *et al.* 2003). Siderophores are able to bind to Fe^{3+}, and can either be photo-reduced to Fe^{2+} or assimilated by phytoplankton and later reduced (Maldonado and Price 1999). In HNLC regions, concentrations of dissolved Fe are so low that many species are unable to acquire Fe^{2+} and ligand binding has been found to serve an important role in Fe assimilation.

1.4 Cobalt in the Ocean

Cobalt (Co) is a transition metal with an atomic number of 27 and has two common oxidation states of +2 and +3, Table 1. The vertical profile of Co in the ocean is similar to Mn, exhibiting a hybrid-type profile (Knauer *et al.* 1982). The surface water has a maximum concentration of Co due to external enrichment, with low concentrations in the mixed layer during the growing season due to scavenging (Knauer *et al.* 1982). Below the euphotic zone, Co concentrations decrease with depth as its more readily scavenged rather than regenerated (Knauer *et al.* 1982). Although Mn and Co ocean profiles are similar, the concentrations of Co in the water column are much lower than that of Mn, likely due to its low abundance of 15 ppm Co in the upper continental crust (Knauer *et al.* 1982; Hu and Gao 2008). Shelf sediments represent a key source of Co to the oceans, as well as microbial co-oxidation with Mn and release of Co by Mn oxide reduction (Moffet and Ho 1996; Biller and Bruland 2013).

1.4.1 Cobalt Phytoplankton Assimilation

Co plays important roles in the growth of marine phytoplankton and bacteria, one being it acts as a metal center for carbonic anhydrase (CA). CA is predominantly a Zn containing enzyme, that is cannibalistic and can substitute both Co and Cd in the active site, to catalyze the interconversion of

bicarbonate (HCO_3^-) to carbon dioxide (CO_2) to supply the main carbon fixing enzyme with substrate (Falkowski and Raven 2007). Cyanobacteria have an absolute requirement for Co that cannot be substituted for Zn, coccolithophores have a Co requirement that can by substituted by Zn, while diatoms can co-substitute Co and Zn (Sunda and Huntsman 1995; Saito *et al.* 2002). Therefore, co-limitation by Co and Zn has been documented for some phytoplankton species (Sunda and Huntsman 1995; Saito *et al.* 2002; Boye *et al.* 2017).

Another important role of Co is metal-ligand binding to produce cobalamin (vitamin B12) (Morel *et al.* 2003). Marine cyanobacteria have an essential requirement for Co that cannot be fulfilled by other transition metals and are able to synthesize B12 while other eukaryotic phytoplankton are unable to do so (Sunda and Huntsman 1995; Saito *et al.* 2002). While the quotas for vit B12 and Co are generally low across species, there is growing evidence to suggest potential limitation of phytoplankton and bacteria production with Co limitation (Bertrand *et al*. 2013; Boye *et al.* 2017).

1.5 Cadmium in the Ocean

Cadmium (Cd) is a metal located at the end of the 4d transition series with an atomic number of 48, and only one common oxidation state of +2 (Table 1). The vertical profile of Cd in the ocean is a nutrient-type profile similar to macronutrients NO_3^- and PO_4^{3-}. Acute depletions of dCd exist in the open ocean owing to biological uptake by microbes and concentrations increase with depth as sinking organic matter is respired and breaks down with depth (Bruland 1980). Observations have shown a strong correlation between Cd and PO_4^{3-} in the global ocean, suggesting that their distributions are governed by similar processes (Boyle *et al.* 1976; Bruland *et al.* 1978; Bruland 1980; Conway and John 2015). The surface ocean is replenished with Cd via vertical mixing of deeper, more Cd-enriched water to the surface (Conway and John 2015). In coastal regions, Cd concentrations are higher due to proximal continental atmospheric, riverine, and upwelling inputs (Bruland and Franks 1983).

1.5.1 Cadmium Phytoplankton Assimilation

Like other trace metals, Cd can be beneficial to the growth of marine phytoplankton over a moderate range of bioavailability but can be toxic at higher concentrations. Similar to Co, Cd is able to substitute for Zn in CA under Zn-limiting conditions in marine surface waters (Sunda and Huntsman 1995; Lee and Morel 1995). There is also a Cd-specific form of the CA enzyme (CDCA1) that has been isolated from marine diatoms, the only known biological function for Cd in any organism (Lane and Morel 2000). However, there is a minimum Zn requirement in marine phytoplankton that cannot be substituted by another nutrient (Sunda and Huntsman 1995; Saito *et al.* 2002). During times of extreme Zn limitation, Cd uptake can become toxic to certain phytoplankton groups (Lee and Morel 1995). In the cell, Cd can compete for uptake sites with essential metals such as Mn and Fe, thereby causing deficiencies and loss of enzyme function (Lavoie *et al.* 2012). The degree of toxicity also depends on the phytoplankton species with coccolithophores and dinoflagellates being moderately sensitive, diatoms being the least sensitive and cyanobacteria the most sensitive (Brand *et al.* 1986).

1.6 Nickel in the Ocean

Nickel (Ni) is a first row transition metal with an atomic number of 28, atomic weight of 58.693 g/mol, and common oxidation state of +2 (Table 1). Vertical profiles in the ocean are nutrient-type profiles that are similar to other nutrient-like trace metals and macronutrients (Bruland 1980). Dissolved Ni is scavenged at the surface and regenerated with depth with similar rates to PO_4^{3-} down to 800m, and silicic acid (Si) in deeper waters (Bruland 1980).

1.6.1 Nickel Phytoplankton Assimilation

Nickel (Ni) plays a key role for the assimilation of nitrogen species. Urease, a Ni dependent enzyme, catalyzes the breakdown of the organic molecule urea and subsequent release of ammonia (Morel *et al.* 2003). In addition, some eukaryotic phytoplankton have adapted to replace Fe-containing SOD enzymes for those that are Ni-containing during times of Fe limitation (Cuvelier *et al*. 2010). Higher concentrations of Ni are typically found in surface waters, likely due to the inertness of Ni^{2+} and slow uptake of Ni due to lower demand by phytoplankton (Morel *et al.* 2003). Mineralized Ni is also found in the opal frustules of diatoms, resulting in up to 50% of their cellular Ni inventories (Twining *et al.* 2012).

1.7 Copper in the Ocean

Copper (Cu) is a first row transition metal with an atomic number of 29 and common oxidation states of +1 and +2 (Table 1). The vertical profile of dissolved Cu is a hybrid-type of both scavenging and regeneration (Bruland and Lohan 2014). Surface Cu is actively taken up by phytoplankton and typically recycled with depth, but can have surface maxima due to atmospheric inputs and constant concentrations in deeper waters due to a balance between regeneration by organic matter degradation and particle scavenging (Johnson *et al.* 1997;Bruland and Lohan). At mid-depths, Cu scavenging by sulfide precipitates could be possible within the suboxic region of the OMZ, as they are known to form under anoxic conditions (Janssen *et al.* 2014; Posacka *et al.* 2017). In oligotrophic waters, like the open North Pacific Ocean, sources of Cu predominantly originate from natural atmospheric inputs of dust from Central Asia, as well as anthropogenic pollutants in the aerosols that can increase Cu concentrations within the particles (Lee *et al.* 2013). In addition to atmospheric inputs, Cu can be mixed vertically to replenish surface waters with deeper, more Cu-rich water and can be enriched by continental sources through riverine and upwelling inputs (Bruland 1980).

1.7.1 Copper Phytoplankton Assimilation

Copper (Cu) is another metal nutrient that is important in the photosynthetic and electron transport chain, but can be very toxic to some phytoplankton species. In the photosynthetic process Cu acts as a metal center for proteins and enzymes such as plastocyanin, cytochrome oxidase, and SOD (Twinning and Baines 2013). The metal has a similar job during nitrogen assimilation, acting as a metal center for enzymes such as nitrate reductase to reduce NO_3^- to NH_4^+ (Harrison *et al.* 1977). However, high concentrations of Cu, or limiting amounts of other trace metals, can be toxic to marine microbes. As with Cd, the degree of sensitivity to Cu toxicity depends strongly on the phytoplankton species,

where the eukaryotic dinoflagellates and coccolithophores are moderately sensitive, prokaryotic cyanobacteria are the most sensitive, and eukaryotic diatoms are the least sensitive (Brand *et al.* 1986). Dissolved Cu can act to interfere with the uptake of other trace metals and reduce photosynthetic rates (Sunda and Huntsman 1998).

1.8 The Subarctic Northeast Pacific Ocean: Line P

1.8.1 Physical Setting

In the Gulf of Alaska (GOA), the North Pacific Current (NPC) has an eastward, surface flow that originates from the Kuroshio extension in the Central Pacific that transport waters to the northeast Pacific (Cummins and Freeland 2007). The NPC bifurcates near the west coast of North America and flows northwards as the Alaska Current (AC) and southwards as the California Current (CC) (Cummins and Freeland 2007). The AC flows to the north becoming the Alaska Coastal Current (ACC) and the Alaska Stream (AS). Located to the west of these currents is the Alaska Gyre (AG), defined by a series of connected sea surface topographic lows (Crawford et al 2007).

Line P is a transect of stations within the subarctic northeast Pacific Ocean that has been continuously sampled and monitored for nearly 70 years (Freeland 2007). The transect begins at station P1 near the southern tip of Vancouver Island, B.C. at 48.5°N, 125.5°W and travels northwest most to offshore station P26 at 50.0°N, 145.0°W, Fig. 1. The line can be split into two major regions: offshore and coastal regions. For the purposes of this study, the offshore will consist of stations P26 to P16 while the coastal will consist of P12 to P4.

1.8.2 Offshore Conditions

The offshore region of Line P is classified as a high nutrient, low chlorophyll (HNLC) environment. Due to the limited concentrations of labile and biologically available Fe, and other trace metals, phytoplankton are unable to deplete macronutrients in the surface, resulting in unused macronutrients and diminished community growth. As the open ocean is too far from the continent to be directly influenced by coastal and margin sources, the offshore region can receive micro- and macronutrients from 3 main pathways: winter mixing, atmospheric inputs, and lateral transport (Bishop and Fleisher 1987; Freeland *et al.* 1997; Crawford *et al.* 2007;). The predominant input of nutrients to the surface comes from winter mixing. During the winter months, the Aleutian Low produces storm surges that cause upwelling of deeper, more nutrient rich waters that reside below the euphotic zone (Whitney and Freeland 1999). During this time, productivity remains low until irradiance increases in the spring, resulting in increased community productivity and growth with concomitant uptake of nutrients (Whitney and Freeland 1999).

1.8.3 Coastal Conditions

The coastal region of Line P is micro- and macronutrient replete. Proximity to the continent allows for riverine nutrient transport of freshwater plumes into the ocean during the spring and summer freshets (Wong *et al.* 2002). During the growing seasons, productivity is high until NO_3 becomes depleted, resulting in NO_3 limitation. Coastal upwelling driven by local and regional wind forcing transports nutrients to the surface off the west coast of Vancouver Island (Freeland and Denman 1982). Another source of nutrients to the coastal region is the northward flow of the Vancouver Island Coastal Current (VICC). The VICC is fed by fresh Vancouver Island coastal runoff, as well as surface waters from the Juan de Fuca Strait (Ianson *et al.* 2003).

1.9 Marine Heatwaves

Marine heatwaves are extreme events where the temperatures in the surface ocean, at times extending deeper, exceed those in the 90^{th} percentile based on a 30- year average and last for more than 5 days (Hobday *et al.* 2016). They are often brought on by atmospheric anomalies resulting in changes to air-sea heat fluxes, wind forcings, and possibly large scale teleconnections (Holbrook *et al.* 2019; Oliver *et al.* 2021), and have the ability to cause drastic changes to the ecological system. The warm temperatures and lack of food sources due to decreased upwelling, and general nutrient transport to the surface, resulted in devastating effects throughout the entire marine food web. In 2015, a coastal toxic algal bloom dominated the west coast of North America, producing the neurotoxin domoic acid (DA) (Cavole *et al.* 2016). DA is bioaccumulative and can be absorbed by shellfish, fish, and marine birds resulting in death and/or disability (Cavole *et al.* 2016). Substantial population reductions in copepods, squid, crab, and some salmon species resulted in the massive die off of seabirds and sealions (Cavole *et al.* 2016). Lower in the trophic level, the marine phytoplankton community experienced a shift towards smaller, pico- to nano-phytoplankton in the northeast Pacific likely due to changes in nutrient availability (Peña *et al.* 2019).

In the subarctic northeast Pacific a multiyear marine heatwave, known colloquially as the Blob, impacted the region resulting in sea surface temperatures up to 4.5 standard deviations above normal from late 2013 to 2015 (Freeland and Ross 2019). During the winter 2013/2014, an anomalous high pressure ridge overlaid the north Pacific which blocked strong winter winds (Bond *et al.* 2015; Whitney 2015). This atmospheric change led to decreased storm mixing and mixed layer deepening, and increased surface temperatures and stratification (Bond *et al.* 2015). Whitney (2015) observed a decrease in phytoplankton biomass in the warm region, specifically the eastern North Pacific, and hypothesized it was likely due to decreased vertical transport of nutrients to the mixed layer. The marine heatwave persisted through to the following winter 2014/2015 with similarly warm sea surface temperatures and mixed layer shallowing. The multiyear persistence of the Blob was found to be due to a North Pacific Gyre Oscillation (NPGO) pattern in 2014, following a Pacific Decadal Oscillation in 2015 (Di Lorenzo and Mantua 2016). The year 2014 experienced anomalously high sea level pressure, with a high pressure lobe in the south that blocked winter winds, which was representative of a NPGO pattern. In 2015 the western Pacific sea surface temperatures cooled, while the eastern remained warm, representing a positive PDO pattern.

The subarctic northeast Pacific experienced a second marine heatwave beginning in the Fall 2018. Over the GOA during winter 2018/2019, anomalously high sea level pressure overlaid the region which was unusual due to a moderate to weak El Nino that was present concurrently (Zador *et al.* 2019). During the summer of 2019 air and sea surface temperatures rose due to diminished winds brought on

by a dipole effect of anomalously high sea level pressure in the GOA and anomalously low sea level pressure in the central North Pacific (Zador *et al.* 2019). The ecosystem responded in some positive and some negative ways. While some sea birds reproduced successfully, there were declines in early season phytoplankton biomass, zooplankton, copepods, and Pacific cod juveniles (Zador *et al.* 2019; Laurel and Rogers 2020). In addition, there were diminished humpback whale calving rates and massive grey whale mortality with 48 stranding's in Alaska alone (Zador *et al.* 2019).

As climate change continues to warm our oceans, it is imperative to have a comprehensive understanding of the effects that marine heatwaves have from the pico- scale up to the macro- scale. The possibility stands that these extreme events will become more frequent, and more adverse as time goes on. At this time there is little known about the distribution of bioavailable trace metal species during the 2014/2015 and the 2019 marine heatwaves, and how they may have affected marine phytoplankton community production and structure. These observations will provide greater insight into how marine organisms will be affected throughout the trophic level, and what outcomes we could expect for future marine heatwaves.

1.10 Thesis Focus

The aim of this thesis is to observe and understand the trace metal distributions during marine heatwave events in the subarctic northeast Pacific Ocean and their relationship to phytoplankton production and community composition. **Chapter 2** focuses on the trace metal distributions at Ocean Station PAPA (OSP) from 2012 to 2015 during the winter and summer seasons. This study was paired with hydrographic, macronutrient, and phytoplankton community composition data to determine the effects and relationships during the 2014/2015 marine heatwave, the Blob. **Chapter 3** focuses on the timeseries of trace metal distributions during winter 2012-2015 and summer 2012-2019 along the Line P transect, focusing on the major stations P26, P20, P16, P12, and P4. This study was paired with matching hydrographic and macronutrient data to observe changes during the 2014/2015 marine heatwave and the 2019 marine heatwave in the offshore and coastal regions of the subarctic northeast Pacific Ocean.

Chapter 2: Relationship between surface dissolved iron inventories and net community production during a marine heatwave at Ocean Station PAPA

2.1 Introduction

The biological carbon pump (BCP) transfers inorganic carbon from the atmosphere to the deep ocean through gravitational settling of particulate matter formed in the sunlit surface ocean by photosynthetic plankton (Falkowski and Raven 2013). Variations in the efficiency of the BCP are linked to past glacial-interglacial variations of inorganic carbon inventories in the ocean interior (Jacobel *et al.* 2017; Jacobel *et al.* 2020) and will impact the ocean's ability to absorb anthropogenic carbon dioxide (CO_2) in the future (Passow and Carison 2012). In the contemporary high nitrate-low chlorophyll (HNLC) eastern subarctic Pacific, BCP efficiency is limited by the availability of the micro-nutrient iron (Fe) (Martin and Gordon 1988; Maldonado *et al.* 1999; Boyd *et al*. 2005). Models predict that regional warming, freshening, and increased stratification due to ongoing climate change will conspire to diminish the BCP by decreasing the vertical flux of Fe and macronutrients from the pycnocline to the surface (Denman 2008). Time series observations testing this hypothesis have so far proven inconclusive, as decreasing oxygen and increasing nutrient concentrations in the pycnocline appear to offset increasing regional stratification (Whitney et al. 2013). How the biological system of the subarctic northeast Pacific ultimately responds to regional climate change remains an open question.

During the winter of 2014-15 a marine heat wave with a surface temperature anomaly greater than 4.5 standard deviations above normal (1981-2010 mean) developed in the subarctic northeast Pacific. This extreme event persisted until 2016 (Bond et al. 2015; Freeland and Ross 2019), during which time the observed temperature anomalies were linked to a persistent high pressure system that reduced ocean heat loss to the atmosphere and weakened the advection of cold water into the area. A consequence of this severe, high temperature anomaly was increased stratification of the upper ocean, affording the opportunity to investigate the resilience of the base of the marine food web and the BCP when subjected to ongoing regional warming. Remote sensing indicated that extremely low chlorophyll concentrations were present in the region of the warm temperature anomaly during the first quarter of 2014, likely related to diminished nutrient fluxes into the mixed layer (Whitney 2015). In addition, significant changes in the abundance and composition of phytoplankton were observed in the subarctic northeast Pacific as a result of the rapid warming of surface waters (Peña *et al.,* 2019). Autonomous biogeochemical (BGC) float measurements of nitrate (NO_3^-) and calculated drawdown from 2013 through 2015 allowed estimates of the temporal variability of net community production (NCP) and hence, the efficiency of the BCP (Bif et al. 2019) to be made. NCP was maintained during the first year of the warming event, but decreased significantly during spring-summer of 2015 as winter stratification persisted. Bif *et al.* (2019) suggested that NCP during the first warm year was likely sustained by Fe recycled from the previous year. In addition, a study by Hayashida *et al.* (2020) observed a relationship between marine heatwaves, nutrient-poor waters, and phytoplankton blooms. Using satellite derived chlorophyll-a and in-situ NO_3^- data the study found that phytoplankton blooms in nutrient-poor waters tended to be weak during marine heatwaves. As part of the Line P Time Series monitoring program, trace metal clean seawater samples collected at Ocean Station PAPA (OSP) (50°N, 145°W; Fig. 1) during the winter (February) and summer (August) months from 2013 to 2015 were analyzed for trace metals, including dissolved iron (dFe). This allowed us to test the hypothesis proposed by Bif *et al.* that NCP

during the first year of the marine heatwave was sustained by dFe recycling but was reduced in the second year due to (micro)macronutrient depletion and prolonged mixed layer shallowing.

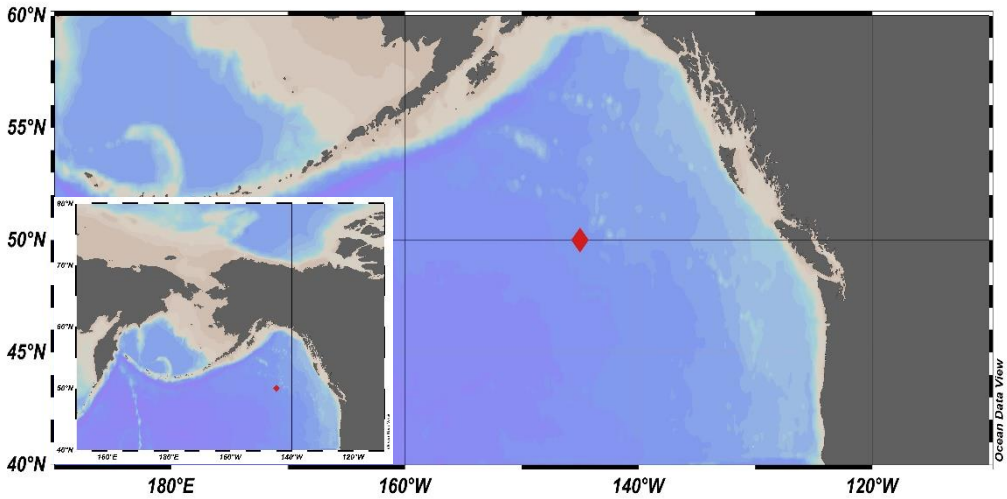

Figure 1. Map views of Ocean Station PAPA (OSP) in the subarctic northeast Pacific Ocean. Coastlines and land are denoted in grey, while bathymetry is blue. The red triangle indicates the location of OSP at 50°N, 145°W and the OSP mooring at 50.1°N, 144.9°W.

2.2 Methods

2.2.1 Sample collection

Seawater samples were collected on the *CCGS John P. Tully* at Ocean Station PAPA (OSP) (50°N, 145°W) in February and August from 2012 to 2015 (Fig. 1). Seawater was collected using either a trace metal clean, aluminum powder-coated rosette fitted with twelve 12-L GO-FLO sampling bottles (General Oceanics, FL, USA) (Measure et al. 2008) or with 10-L GO-FLO bottles deployed on a Kevlar line (Bruland *et al.* 1979). The bottles were submerged open and closed at the desired sampling depths during ascent to minimize the potential for contamination from the rosette frame and instruments. Following recovery, GO-FLO bottles were removed to a portable laboratory supplied with HEPA-filtered air or to a shared laboratory, equipped with a HEPA-filtered flow hood, where filtered (0.2-µm Acropak capsules, Pall Corporation) and unfiltered seawater was collected into 500-mL low density polyethylene (LDPE) bottles. Both filtered and unfiltered samples were acidified to pH 1.6-2.0 using ultrapure 12N HCl (SeaStar Chemicals, Sidney, BC, Canada). We followed the procedures for preparing sampling equipment and collecting samples outlined in the GEOTRACES Cookbook, version 3.0 (https://www.geotraces.org/methods-cookbook/).

2.2.2 Reagents

All reagents and standards were prepared in a Class 100 laminar flow hood located in a Class 100 clean room using ultrapure deionized water (MQ) from a Milli-Q Element system (Millipore, Darmstadt, Germany). Multi-element standards were prepared in filtered, open ocean surface seawater (subarctic northeast Pacific Ocean, Line P P26/P20) from single element standards (High-Purity Standards, SC, USA), and acidified to pH ~1.6 using ultrapure 12N HCl (SeaStar Chemicals, Sidney, BC,

Canada). Blanks (Table 1), consisting of 125 µL of 12N ultrapure HCl, and 125 µL of bulk, filtered, open ocean surface seawater in 125 mL of MQ were prepared in acid-cleaned 125mL LDPE bottles (Field *et al.* 1999).

Reagents used for sample pre-concentration (see below) included a 2N ammonia acetate buffer (pH 6.1 +/- 0.1), a 10% HNO_3 (SeaStar Chemicals, Sidney, BC, Canada) eluting solution spiked with 10 ppb rhodium (Rh) internal standard (High Purity Standards, SC, USA), and a 0.1% ultrapure HCl rinse solution. A certified reference standard (NASS-7; National Research Council. Canada) and an in-house reference material consisting of homogenized seawater from Line P in the subarctic northeast Pacific were analyzed along with each batch of seawater samples (Table 1).

Table 1. The average blanks, detection limits, and reference materials for the analysis of the winter and summer Fe and Cd profiles of 2012-2015.

	Blanks, n=10	Detection Limits, n=10	In house Reference Material, n=10	NASS-7 Measured, n=2	NASS-7 Consensus
Mn (nmol L^{-1})	0.004	0.002	0.99 ± 0.06	13.9 ± 0.7	13.6 ± 1.1
Fe (nmol L^{-1})	0.024	0.014	0.5 ± 0.1	6.3 ± 0.6	6.7 ± 0.5
Co (pmol L^{-1})	0.44	0.14	36.2 ± 1.5	255.2 ± 1.4	247.7 ± 23.8
Ni (nmol L^{-1})	0.033	0.04	5.4 ± 0.7	4.8 ± 0.7	4.2 ± 0.3
Cu (nmol L^{-1})	0.008	0.006	2.1 ± 0.1	3.21 ± 0.01	3.1 ± 0.2
Cd (nmol L^{-1})	0.0002	0.0002	0.094 ± 0.002	0.133 ± 0.002	0.14 ± 0.01

2.2.3 Extraction and Analysis

Acidified seawater samples were pre-concentrated using a seaFAST-pico SC4-DX a solid phase extraction system (Elemental Scientific, Omaha, NE, USA) fitted with a Nobias-1 column (Elemental Scientific). A concentration factor of 62.5x was achieved by loading 50 mL (5 x 10 mL aliquots) of acidified seawater and eluting with 800 uL of 10% HNO_3. Details of the extraction procedure are outlined by Jackson *et al*. (2018) while the seaFAST instrument parameters used in this study are given in Table 2.

Pre-concentrated samples were analyzed using an Agilent 8800 triple quadrupole inductively-coupled plasma tandem mass spectrometer (Agilent Technologies) as previously described (Jackson *et al.* 2018). Instrument parameters were optimized for each batch of samples to eliminate molecular and mass interferences.

Table 2. ESI seaFAST preconcentration parameters for the analyses of trace metal profiles.

seaFAST preconcentration parameters	
Parameters	
Mode of analysis	offline
Column resin	Nobias-1 EDTRiA and IDA groups
Buffer	2M ammonia acetate buffer, pH 6.1 +/ - 0.1
Eluent	10% HNO_3
Internal Standard	10 ppb Rh
Sample pH	1.6
Preconcentration factor	62.5 times
Initial volume of sample	50mL
Final elution volume	800uL

2.2.4 Mixed layer depth, estimated net community production, trace metal, and nutrient ratio average calculations

Mixed layer depth was identified as the depth at which depths did not exceed 0.02 kg/m³ from the surface density (Timmerman and Hamme 2021). Seasonally in the subarctic northeast Pacific, in the spring and summer months the mixed layer reaches a minimum depth and deepens to a maximum depth in the fall and winter months by storm surges. For the purpose of this study, mixed layer depths will be compared by the season and year, and not between two different seasons (i.e. winter 2012 mixed layer compared to winter 2014 mixed layer).

Average winter and summer NO_3^- concentrations within the mixed layer (ML) were calculated, the difference between these concentrations (ΔNO_3^-) reflecting non-integrated, seasonal estimates of net community production (NCP) solely in the mixed layer. The resulting values were converted to mol C/m³ using the Redfield Ratio, where estimated NCP = mol C/m³ = (mol ΔNO_3^-)*6.6 (Bif and Hansell 2019). Average trace metal concentrations were calculated over the same depth range, along with winter to summer dissolved iron:nitrate ($\Delta Fe:\Delta NO_3^-$), silicate:nitrate ($\Delta Si:\Delta NO_3^-$), and cadmium:phosphate ($\Delta Cd:\Delta PO_4$) ratios.

2.3 Results

2.3.1 Hydrography

Vertical profiles of sigma-t density (σ_T), temperature (T), salinity (S) and NO_3^- at OSP in winter and summer are presented in Fig.2. These allow us to compare and contrast the hydrography at OSP in 2012 and 2013 with that observed during the marine heatwave years of 2014 and 15. During the winter of 2012/13 mixed layer deepening resulted in colder, denser, more nutrient-rich water at the surface than during the following summer, when a shallower MLD was observed. During the first winter of the marine heatwave, diminished winter surface winds limited the depth of mixing. Consequently, the winter MLD in 2014 was 89 m compared with 107 m in 2012 and 116 m in 2013, whereas winter ML and surface σ_T, S, and NO_3^- were lower (25.26 kg/m³, 32.4 PSU, and 11 µmol/kg, respectively) and winterML temperature higher (8.1°C) in 2014 than in 2012 and 2013 (Fig.2). Summer 2014 ML and surface water

σ_T, T, and S values were comparable to those in 2013, while the summer ML in 2012 was denser, cooler, and more saline. However, summer 2014 ML NO_3^- concentrations (maximum NO_3^-= 5.02 µmol/kg) were lower than the previous summer (9.80 µmol/kg) , which may be due to reduced mixing at the beginning of the growing season in February 2014. The winter 2015 ML shoaled to 82 m, with lower σ_T and surface NO_3^- concentrations than in 2013 but with elevated ML T (7.5°C). Summer 2015 σ_T and T were similar to those in 2013 and 2014 while NO_3^- concentration (5.75 µmol/kg) was lower and more similar to summer 2014.

2.3.2 Vertical profiles of dissolved Fe and Cd

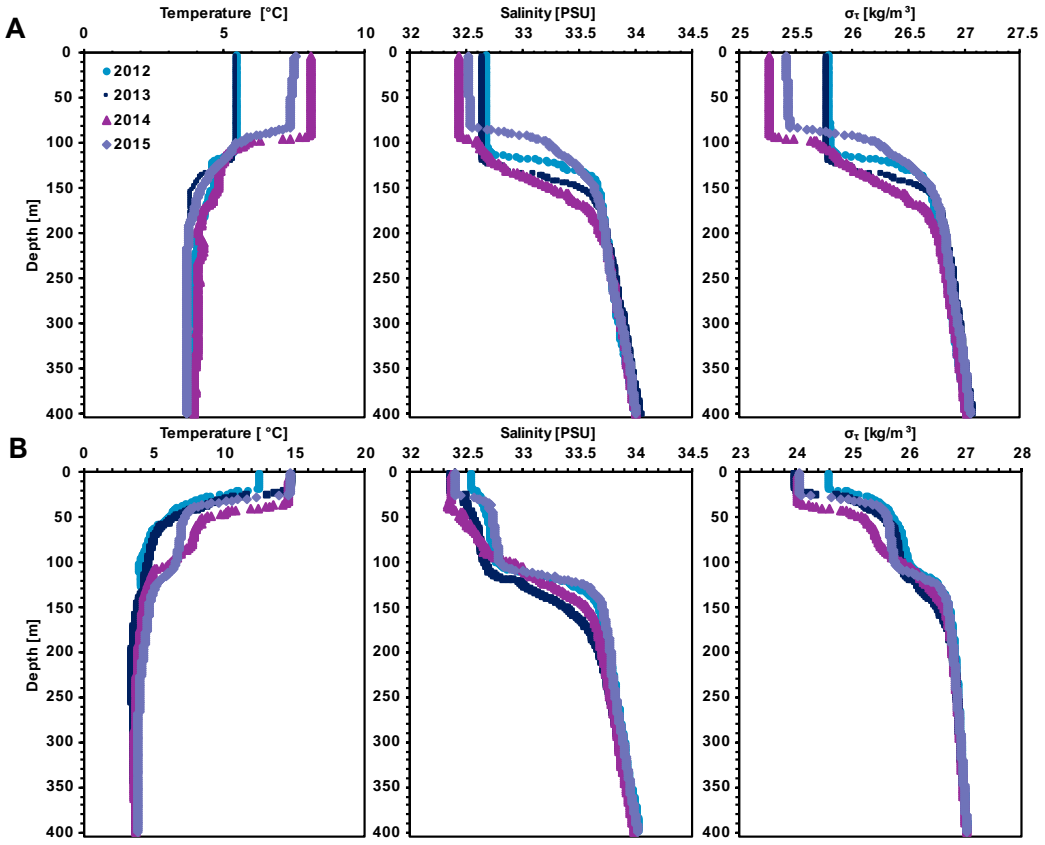

Figure 2. Hydrography of the upper 400m at OSP from 2012 to 2015. **A**: Winter (February) T, S, σ_τ profiles. **B**: Summer (August) T, S, σ_T profiles. Data collected from the Line P Program.

Vertical profiles of dissolved iron (dFe) and cadmium (dCd) concentration in February (winter) and August (summer) are shown in Fig. 3 for the upper 400 m of the water column. Subsets of these data have been used in other studies to help interpret the role of Fe and Cd in biogeochemical systems; for example, August 2012 and 2013 Fe profiles were reported by Schallenberg *et al.* (2015) and Whitby *et al.* (2020), and August 2012 and 2013 Cd profiles by Janssen *et al.* (2017). However, the analysis of multiple elements and interpretation of their distributions at OSP during the aforementioned heatwave are unique to this study.

Winter dFe concentrations were lower in 2013 than in 2012 with ML values ranging from 0.058 to 0.095 nmol dFe/kg in 2013 and from 0.131 to 0.207 nmol dFe/kg in 2012 (dFe values measured at 40, 100, and 400 m in winter 2012 were flagged and omitted due to potential sample contamination). In contrast, summer dFe values were elevated in 2013 compared to 2012. Winter dFe concentrations in

2014 were similar to those in 2012 and 2013 with values ranging from 0.123 to 0.312 nmol dFe/kg (again, values measured at 25 and 40 m in summer 2014 were flagged due to potential sample contamination). Winter dFe concentrations in 2015 were more consistent with those in 2012, ranging from 0.027 to 0.081 nmol dFe/kg in the upper 75 m. However, dFe in the summer 2015 growing season was depleted to values below the limited of detection (0.014 nmol dFe/kg) in the upper 50 m, ranging from 0.00 to0.01 nmol dFe/kg.

Winter dCd concentrations in 2012 and 2013 in the upper 75 m were similar with values ranging from 0.44 to 0.96 and 0.46 to 1.11 nmol/kg, respectively. Summer 2012 and 2013 distributions were also similar with dCd concentrations ranging from 0.44 to 0.46 and 0.456 to 0.468 nmol dCd/kg, respectively, the former being in agreement with previously published data (Janssen *et al.* 2017). The winters of 2014 and 2015 had significantly lower dCd concentrations within the upper 75m, with surface values of 0.24 and 0.253 nmol dCd/kg, respectively. These lower winter concentrations are consistent with similar drawdown of surface dCd to 0.022 and 0.04 nmol dCd/kg, respectively, during the summer growing season in 2014 and 2015.

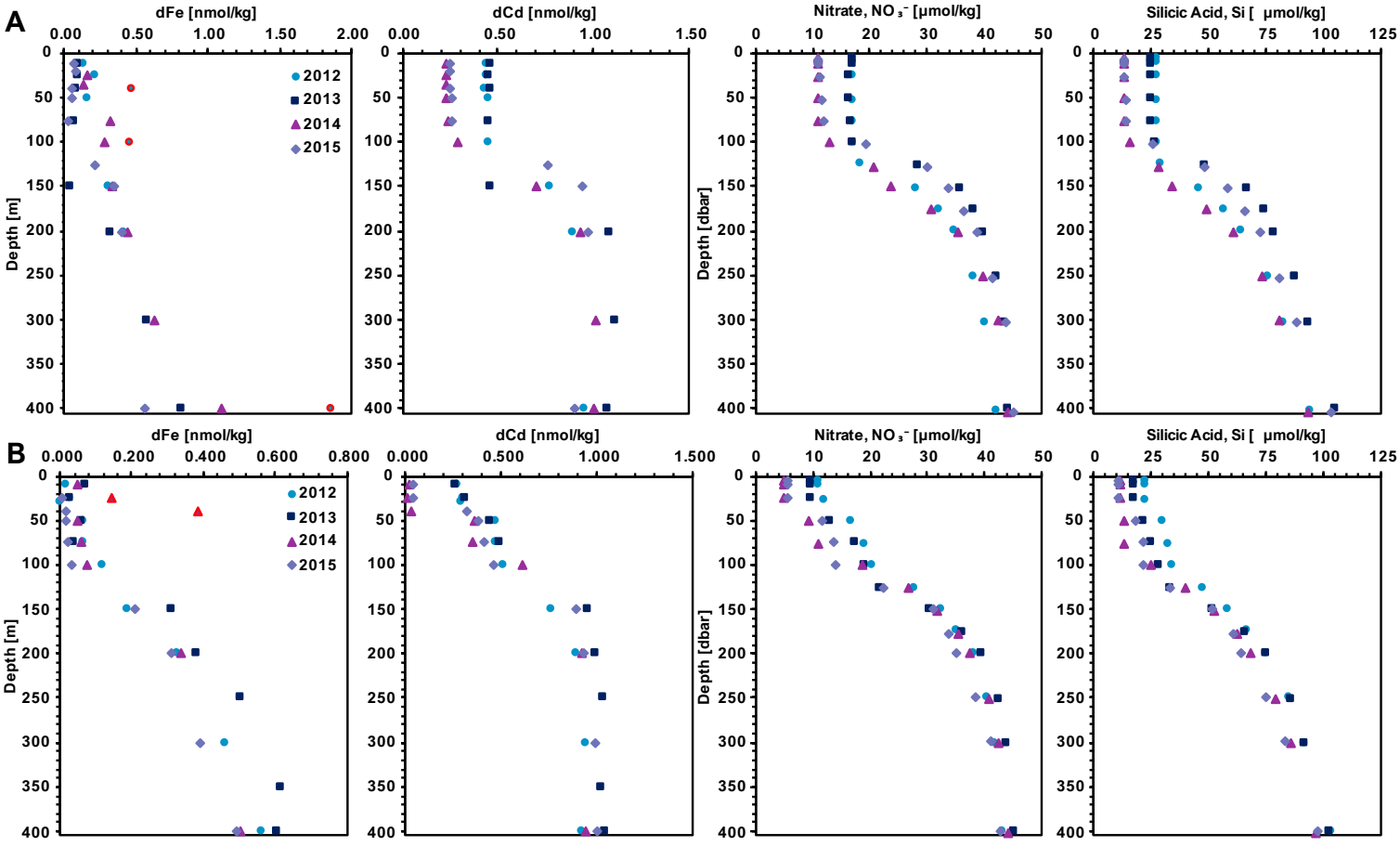

Figure 3. Micro and Macronutrient profiles in the upper 400m at OSP. Dissolved iron and cadmium are reported in nmol/kg (dFe, dCd) while nitrate and silicic acid are reported in μmol/kg in the winter(**A**) and summer (**B**).

2.3.3 Mixed layer concentrations of dissolved Fe and Cd

The mixed layer (ML) depths and ML average concentrations of dFe and dCd over the study period are presented in Fig.4. During 2014 the winter ML dFe concentration (0.20 nmol dFe/kg) was higher than in 2013 and 2015 but similar to that in 2012 (0.16 nmol dFe/kg). Less deepening of the winter ML in 2014 would be expected to limit the concentrations of micro- and macro-nutrients derived from vertical advection of deeper waters. Hence, elevated dFe in winter 2014 may be indicative of iron supply from alternate sources such as atmospheric deposition, or horizontal advection of Fe rich waters. The summer ML dFe concentration in 2014 (0.048 nmol dFe/kg) was marginally higher than in 2012 and 2013 but significantly higher than in 2015. Winter ML stratification persisted and intensified during 2015, resulting in the lowest winter ML dFe concentration (0.053 nmol/kg dFe) observed throughout the study. This led, in turn, to the unusually low summer ML dFe concentration seen in 2015, the lowest observed in this study (and below the method detection limit of 0.014 nmol dFe/kg).

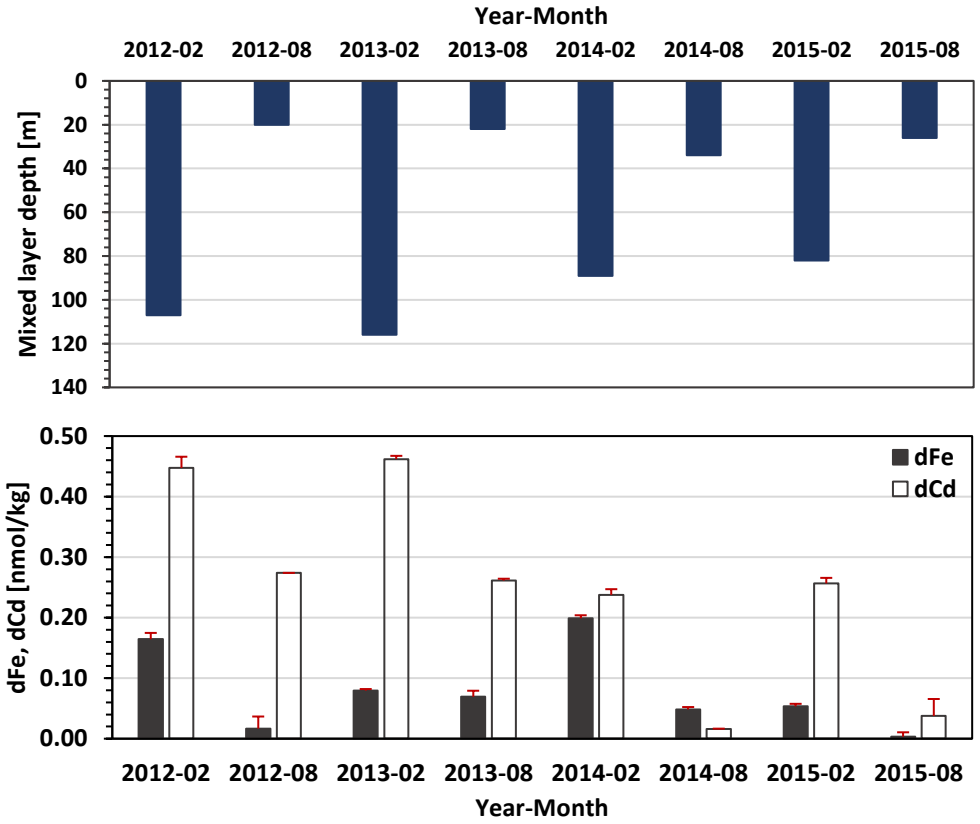

Figure 4. Top panel: the mixed layer depth (MLD) at OSP in winter (February) and summer (August) of 2012-2015. Bottom panel: the mixed layer averages of dissolved iron (dFe) and cadmium (dCd) in winter and summer 2012-2013. Red error bars indicate associated error.

Cd is less prone to abiotic scavenging and atmospheric inputs than Fe in the North Pacific (Conway & John 2015). Therefore, we decided to monitor dCd concentrations in the ML at OSP (Fig. 4) to compare the effects of the marine heatwave on these two contrasting bioactive elements. As for dFe, shallowing of the winter ML in 2014 and 2015 led to lower average surface dCd concentrations (0.24 and 0.26 nmol/kg dCd, respectively) than in 2012 and 2013 (0.45 and 0.46 nmol dCd/kg, respectively). Removal during the growing seasons in 2014 and 2015 further reduced summer dCd (to 0.02 and 0.04 nmol dCd/kg, respectively).

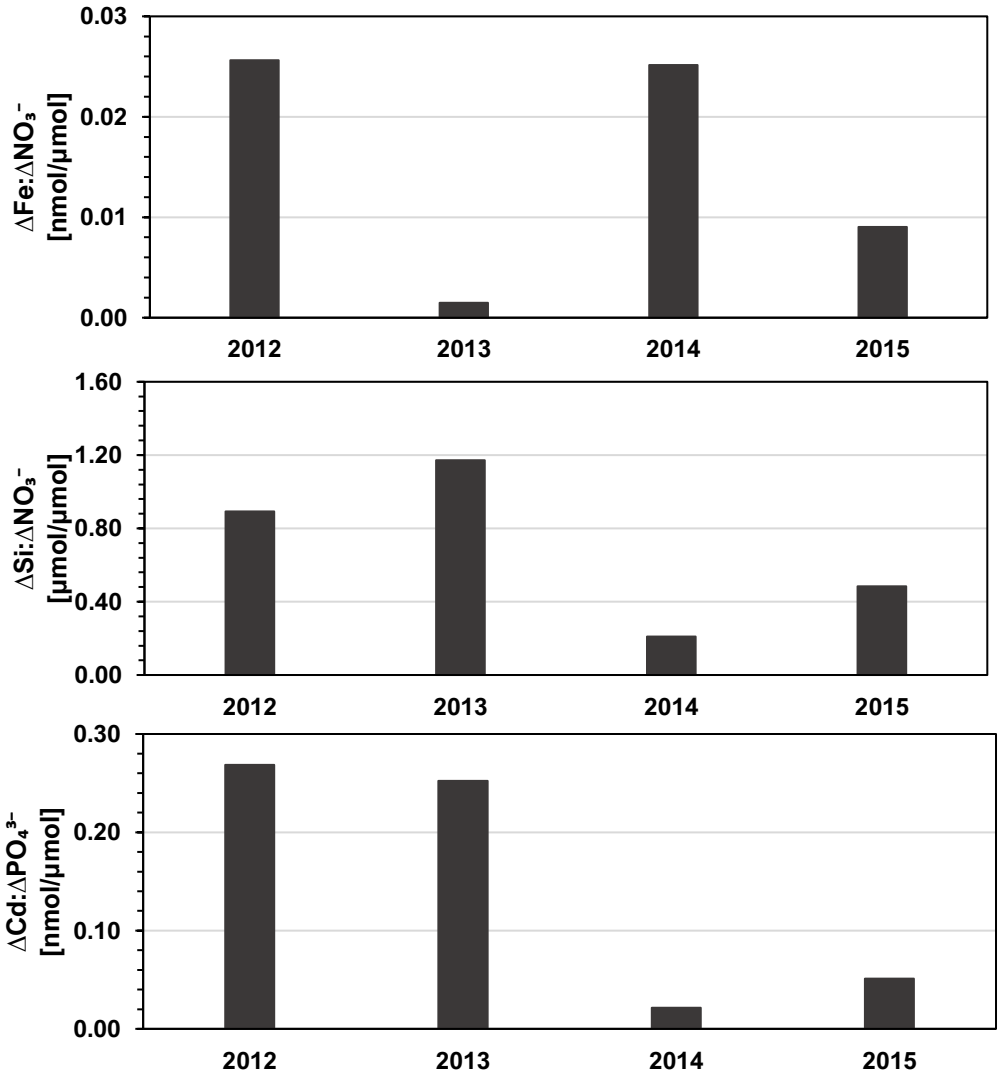

Figure 5. The winter to summer macro(micro)nutrient ratio ML averages from 2012 to 2015. From top to bottom, the ratios are presented as follows: $\Delta Fe:\Delta NO_3^-$, $\Delta Si:\Delta NO_3^-$, and $\Delta Cd:\Delta PO_4^{3-}$.

2.3.4 Nutrient ratios and net community production

The winter to summer nutrient ratios for $\Delta Fe:\Delta NO_3^-$, $\Delta Si:\Delta NO_3^-$ and $\Delta Cd:\Delta PO_4^{3-}$were calculated for the years 2012-2015 to estimate the contribution of diatom productivity to NCP over the study period, as diatoms have an absolute requirement for Si and both diatom Si and Cd quotas tend to increase under Fe-limitation (Hutchins and Bruland 1998; Brzezinski *et al.* 2005; Marchetti *et al.* 2006; Cullen *et al.* 2009). The $\Delta Fe:\Delta NO_3^-$ consumption ratio was highest in 2012 (0.026 nmol/µmol) and lowest in 2013 (0.002 nmol/µmol). In contrast, the $\Delta Si:\Delta NO_3^-$ ratio was reduced in 2012 (0.89 µmol/µmol) and elevated in 2013 (1.17 µmol/µmol) while the $\Delta Cd:\Delta PO_4^{3-}$ ratio remained unchanged (0.27 and 0.25 nmol/µmol, respectively). In 2014, the $\Delta Fe:\Delta NO_3^-$ ratio (0.025 nmol/µmol) was similarly elevated compared to 2012 while $\Delta Si:\Delta NO_3^-$ was lower (0.21 µmol/µmol) and $\Delta Cd:\Delta PO_4^{3-}$ higher (0.69 nmol/µmol) than in previous years. In 2015, the $\Delta Fe:\Delta NO_3^-$ (0.009 nmol/µmol) and $\Delta Cd:\Delta PO_4^{3-}$ (0.63 nmol/µmol) and the $\Delta Si:\Delta NO_3^-$ (0.48 µmol/µmol) increased compared to 2014.

2.3.5 Net community production in the mixed layer

Net community production was calculated for 2012 to 2015 (Fig.6) as described in section 2.2.4. In 2013, NCP was notably elevated (44.9 mol C/m³) compared to other years. Production in 2012 and 2014 was similar (38.1 and 39.5 mol C/m³, respectively) while 2015 NCP was marginally diminished (36.5 mol C/m³). Compared to NCP calculated by Bif *et al.* (2019) the values reported here trend similarly for 2012 and 2013 but dissimilar with regard to 2014 and 2015, with Bif *et al.* reporting significantly elevated and diminished NCP in 2014 (~2.7 mol C/m²) and 2015 (~1.0 mol C/m²), respectively, while this study shows more moderate changes during these periods.

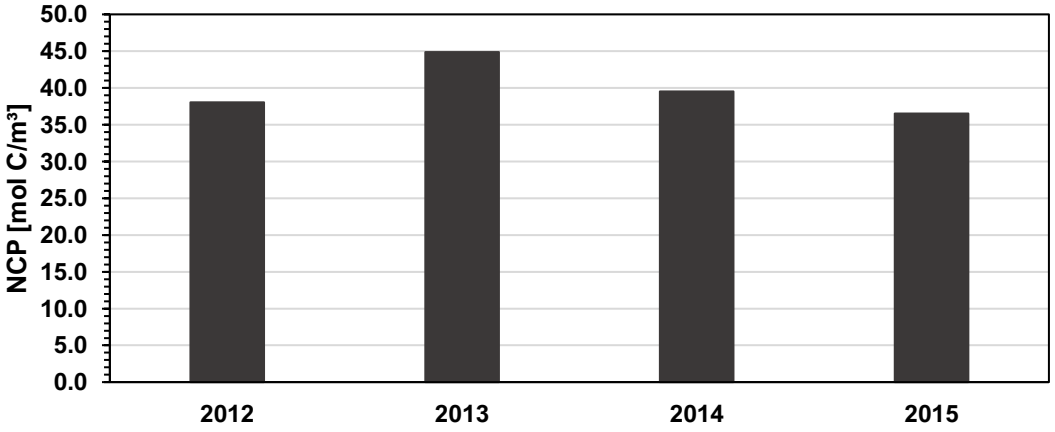

Figure 6. Net community production (NCP) in the mixed layer from the winter to summer of 2012 to 2015.

2.4 Discussion

In HNLC regions of the world ocean, NCP is governed by the resupply of bioavailable Fe and, to a lesser extent, macro- and other micronutrients to the mixed layer. This resupply can be driven via wind induced vertical mixing (Moore et al. 2013; Bif and Hansell 2019), dust deposition (Duce and Tindall 1991; Buck *et al.* 2013), and horizontal advection (Duce and Tindall 1991; Garrett and Munk 1972, 1979; Harrison et al. 1999). Here we explore how dFe may have been resupplied to the ML and whether changes in nutrient utilization, community composition, and NCP might be related to changes in dFe over the study period.

2.4.1 Micro- and macro nutrient reduction during marine heatwave

Beginning in the winter of 2013-2014 the winter mixed layer remained shallow relative to the previous year, due to diminished mixing and increased ML stratification (Bond *et al.* 2015). Similar winter conditions persisted through 2015-2016 (Freeland and Ross 2019) limiting the vertical flux of nutrients into the ML. This resulted in lower average concentrations of dFe, NO_3^-, and dCd during the winter and summer of 2014 and 2015, with the exception of dFe concentrations in 2014. The winter and summer seasons of 2013 were characterized by higher nutrient concentrations than were observed during the marine heat wave.

The 2013 winter ML depth of 114m was sufficient to reach the nutricline and to replenish surface macro- and micronutrients, resulting in average NO_3^-, dCd, and dFe concentrations of 16.5 µmol/kg, 0.462 nmol/kg, and 0.079 nmol/kg, respectively. As insolation increased and surface stratification intensified in the spring and summer, the growth of photosynthetic microbes began to consume surface nutrients. By the summer season NO_3^-, dCd, and dFe were drawn down to 9.8 µmol/kg, 0.261 nmol/kg, 0.069 nmol/kg, respectively.

The following winter, 2014, the mixed layer shoaled to 91m, which was insufficient to erode the nutricline. Re-supply of NO_3^- and dCd to the surface was thus reduced compared to 2013 with ML concentrations of 11 µmol/kg and 0.24 nmol/kg, respectively. In contrast, ML dFe increased 2-fold in winter 2014 compared to winter 2013, with an average concentration of 0.20 nmol/kg, suggesting re-supply to the system independent of vertical mixing, as further discussed below. With community growth during the summer season NO_3^-, dCd, and dFe were drawn down to 7.1 µmol/kg, 0.152 nmol/kg, and 0.053 nmol/kg, respectively.

The 2015 winter mixed layer shoaled relative to 2014, extended only 76m in depth. As in 2014, the ML did not appreciably erode the nutricline, limiting the re-supply of both macro- and micronutrients. Winter re-supply and summer drawdown of NO_3^- and dCd in 2015 were very similar to those in 2014, while dFe concentrations were reduced by August 2015. The average winter ML dFe concentration in 2015 (0.053 nmol/kg) was lower than in 2013, indicating minimal re-supply. As the 2015 growing season progressed dFe became nearly exhausted, approaching our detection limit of 0.014 nmol/kg.

2.4.2 Supply of dissolved Fe to the mixed layer

In the subarctic northeast Pacific, nutrient drawdown and subsequent NCP is correlated with bioavailable dFe (Cassar *et al.* 2011). Therefore, iron limitation will result in low nutrient drawdown and NCP, while iron replete periods will result in high drawdown and NCP. In the winter and summer of 2014, the offshore environment experienced elevated levels of dFe that resulted in NCP comparable to that observed prior to the marine heat wave, despite shallowing of the winter ML. Accordingly, we will investigate potential external sources of iron that led to elevated concentrations during the winter of 2014.

2.4.2.1 Winter dissolved Fe in 2014

While average concentrations of dFe in the winter of 2014 were elevated, they were similar to those of winter 2012, and therefore likely, an indication of natural variability or of external Fe supply at OSP. Another key point is that while dCd concentrations were diminished significantly from the first shallowing event of the marine heatwave, winter 2014, dFe remained similar to previous years. It was

not until the second shallowing event, in the winter of 2015, that average dFe diminished significantly, resulting in reduced summer NCP. Although natural variability in the marine environment, including speciation of trace metals, could have resulted in these changes, we also considered potential sources of external iron supply in order to understand what might have occurred during the first winter shallowing event.

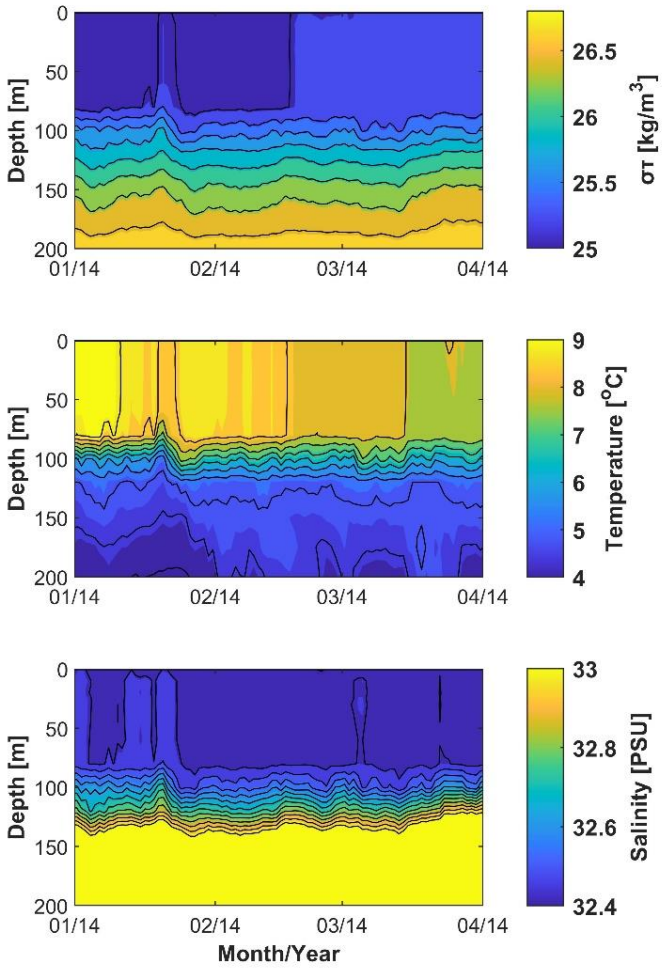

Figure 7. Density (σ_T), temperature, and salinity profiles in the upper 200m from January to March 2014, showing the anomaly that occurred in late January/early February. Data collected from the NOAA OSP mooring (https://www.pmel.noaa.gov/ocs/data/disdel/).

2.4.2.2 Subsurface features

Daily σ_T, T, and S data from the NOAA Ocean Station Papa mooring for January 1-March 31, 2014 are presented in Fig. 7. An anomaly can be observed in the σ_T, T, and S depth profiles between January 11 and 24. The peak of the anomaly represents changing conditions that led to an increase in σ_T and S, a decrease in T, and an overall heaving of the water column between the surface and a depth of 200 to 300m. At the height of this anomaly the ML σ_T, T, and S were 25.12 kg/m³, 8.38°C, and 32.46 PSU, respectively, suggesting that the encroaching water mass was denser, cooler, and more saline than the surrounding water.

In order to determine how this feature originated, sea surface height anomaly (SSHa) data was observed from December 2013 to the end of February 2014 in the subarctic northeast Pacific (Fig.8). These data were retrieved from MEaSUREs 5 day grided sea surface mean height anomalies version 1812 in the NASA Earthdata database (https://earthdata.nasa.gov/). The feature is cooler, more saline, and more dense surrounding water. Such observations are often associated with the passage of anticyclonic mesoscale eddies, which produce negative SSH anomalies. However, the data presented in

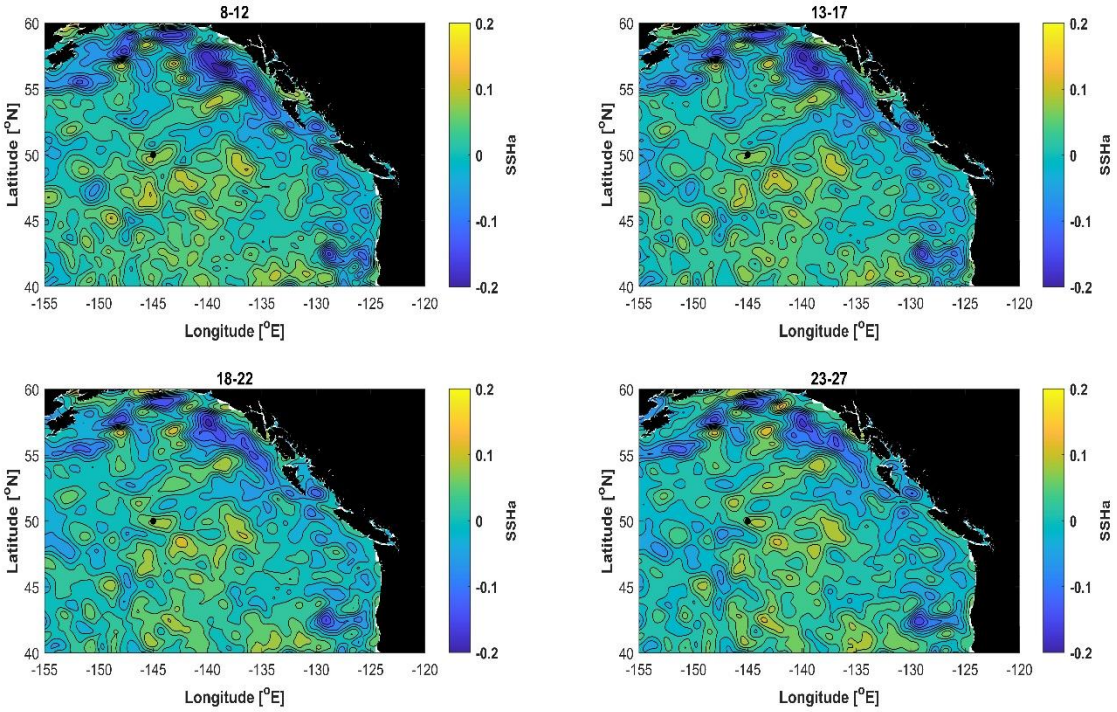

Figure 8. Sea surface height anomalies (SSHa) of the subarctic northeast Pacific Ocean in winter 2014. Panels show the 5-day gridded average of SSHa for January 8-12, 13-17, 18-22, and 23-27 2014. Black dot represents the location of OSP (50°N, -145°E). (*https://earthdata.nasa.gov/).*

Fig.8 show that, in fact, there were positive SSH anomalies during this time period. Furthermore, the subsurface did not present anticyclonic eddy features such as depressed isopycnals, or temperature and salinity contours near and below 200m (Crawford 2002; 2005). Indeed, the isolated subsurface feature and its origin remain unknown although the elevated isopycnals suggest a possible breakthrough of deeper, more nutrient rich water to the mixed layer.

2.4.2.3 Atmospheric Deposition

Dust deposition data was retrieved from NASA's Earthdata MODIS-Aqua (Fig.9). The aerosol optical depth (AOD) was averaged within an area from 45 to 60°N and 120 to 160°W, surrounding Ocean Station PAPA, from 2012 to 2015. Atmospheric transport and deposition of mineral aerosols can be a primary source of iron to open ocean environments (Duce and Tindall 1991). Deposition tends to be episodic, aerosols being delivered to the ocean surface during rain fall events, with fractional iron solubility averaging 6.4% in Pacific surface seawater (Duce and Tindall 1991;Buck et al. 2013). Relatively low dust deposition (<1.0x10^{-11} kg/m^2/s) was observed between January 28 and February 28, 2015 (Sim and Orians 2019). Hence, iron enrichment observed during the winter of 2014 was unlikely related to dust deposition.

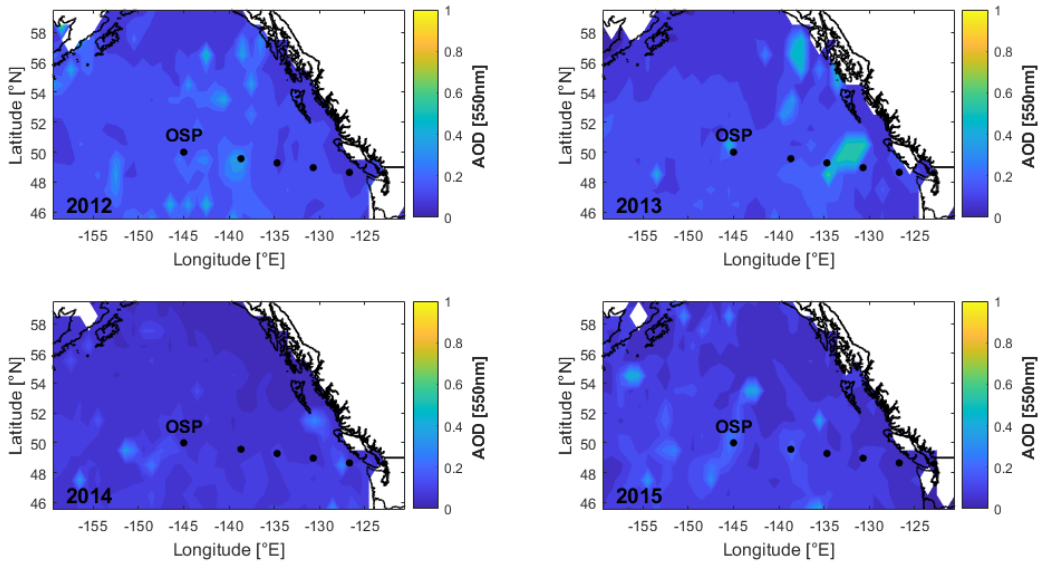

Figure 9. The February monthly mean aerosol optical depth (AOD) at 550nm in the subarctic NE Pacific from 2012 to 2015. Data collected from NASA's Earthdata MODIS-Aqua, 1° resolution. Data was gathered from NASA GIOVANNI available at https://giovanni.gsf.

2.4.2.4 Advection of iron-rich sediments from the Aleutian shelf.

Lam et al. (2006) observed Fe "hot spots" in winter 1996 in the upper 200 m at OSP, which they attribute to advection of Fe-containing sediments from the Aleutian shelf. In a simulation of ocean drift of sediments from continental shelves surrounding the Gulf of Alaska, Lam et al. showed the most likely source to be the continental shelf of the Aleutian Islands. Their simulation also showed that sediments from the southeast Alaska and northern Canada were likely sources of Fe to regions east of OSP, but not

to OSP itself. Moreover, transport from the east would most likely be via Sitka and Haida Eddies, whereas advection by ocean currents was the main conduit from the Aleutians in the west.

It is possible for this injection of iron-rich sediments from the Aleutians to exhibit interannual variability. Ueno et al. (2010) overlaid satellite-derived images of sea surface height anomaly and ocean surface chlorophyll distribution to show enhancement of chlorophyll-a concentration in anticyclonic eddies in the Alaskan Stream. They also showed that eddies are able to inject waters containing sediment far to the south where they enter the westward flowing North Pacific Current, which in turn could carry these sediments to OSP. Such episodic events might give rise to periods of enhanced Fe in the surface mixed layer of OSP in winter.

In the summer of 2013, waters within the 100m to 200m range were enriched with dFe compared to the previous winters of 2012 and 2013, and the summer of 2012 (Fig. 10). At 150m, dFe concentrations in summer 2013 are similar to that of winter 2012, and subsequently, winter 2014. In the subarctic northeast Pacific, the pycnocline typically resides near 150m, and is approximately the depth of the continental margin (Bishop *et al.* 1999; Whitney and Freeland 1999; Lam *et al.* 2006). As such, the elevated dFe observed at 150m could indeed be a product of Fe rich waters from the continental shelf. The following winter, 2014, winter storm mixing or injection by the isolated subsurface feature previously described (Section 4.2), may have resulted in the relatively high dFe observed in the winter 2014 ML.

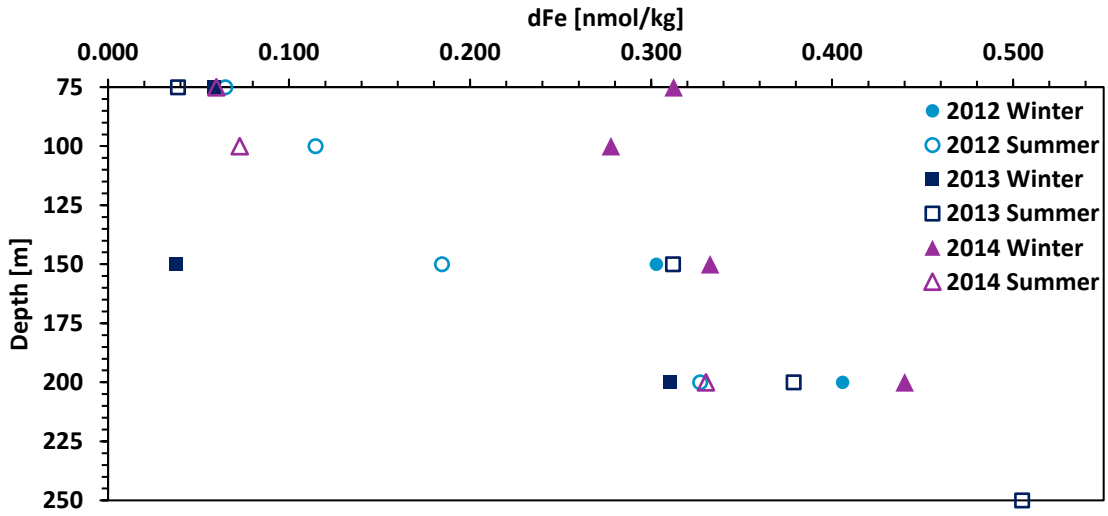

Figure 10. Depth profile of dFe at OSP in the winter and summer of 2012-2014. At 100-200m depth, summer 2013 is elevated similarly to winter 2012, potentially resulting in increased dFe in the winter 2014 ML.

2.4.3 Evidence of phytoplankton community shift from trace metal and nutrient ratios

In the offshore region of Line P macronutrients such as NO_3^- and PO_4^{3-} are typically not limiting to phytoplankton growth and, therefore, have little effect on yearly changes in NCP. Rather, it is Fe limitation in the ML during the growing season that constrains NCP (Martin *et al.* 2013). During the winter of 2013/14 atmospheric conditions resulted in sea surface heating and shallowing of the ML that affected the subarctic northeast Pacific until the end of 2015. A previous study based on autonomous

float data observed that, in the NE Pacific, NCP was sustained during 2014 but decreased significantly following a second year of shallowing, in 2015 (Bif *et al.* 2019). The authors proposed that Fe recycling preserved NCP during 2014, but that a loss of resilience in 2015 was caused by removal and export of Fe. Our macro- and micronutrient data allow us to test this hypothesis. NCP calculated from nitrate drawdown shows a stepwise trend from 2013 to 2015, wherein NCP is marginally diminished in 2014 and 2015. While our data shows lower NCP in 2015, we do not see the substantial decrease in NCP observed by Bif *et al.* 2019.

One reason for changes in NCP during the marine heatwave could be changes in Fe limitation, which can be assessed using nutrient consumption ratios $\Delta Fe:\Delta NO_3^-$, $\Delta Si:\Delta NO_3^-$, and $\Delta Cd:\Delta PO_4^{3-}$. As shallowing and stratification of the winter ML tend to reduce nutrient concentrations, average dFe values suggest that Fe re-supply to the ML in the winter of 2014 (the first year of the marine heatwave) was indeed resilient. As previously stated, this could have been due to an injection of Fe via a vertical transport event, while dCd and the macronutrients were clearly diminished compared to previous years. Mixed layer nutrient drawdown was typical for dFe, dCd, and NO_3^- during the summer of 2014, while that for Si and PO_4^{3-} were not. This suggests a shift in phytoplankton community structure, likely derived from changes in nutrient availability and/or warmer temperatures resulting in either limited growth of individual species or a selection of smaller phytoplankton.

During Fe stress, diatoms are known to alter their (micro)nutrient uptake ratios by non-selectively consuming Si relative to NO_3^- and Cd relative to PO_4^{3-}, thus impacting residual dissolved macro and micronutrient concentrations (Hutchins and Bruland 1998; Takeda 1998; Cullen *et al.* 2003; Lane *et al.* 2009). In 2014 we observed increased levels of $\Delta Cd:\Delta PO_4^{3-}$ due to low PO_4^{3-} consumption; however, we also observed decreased levels of $\Delta Si:\Delta NO_3^-$ due to low Si consumption. This, together with markedly low $\Delta Fe:\Delta NO_3^-$, suggests that our results are not fully explained by altered diatom nutrient uptake due to changes in Fe limitation, but rather by a potential transition to a community dominated by smaller phytoplankton. After a year of Fe consumption and increased shallowing of the ML, the data from winter 2015 suggest a system that is less resilient to the effects of the marine heatwave.

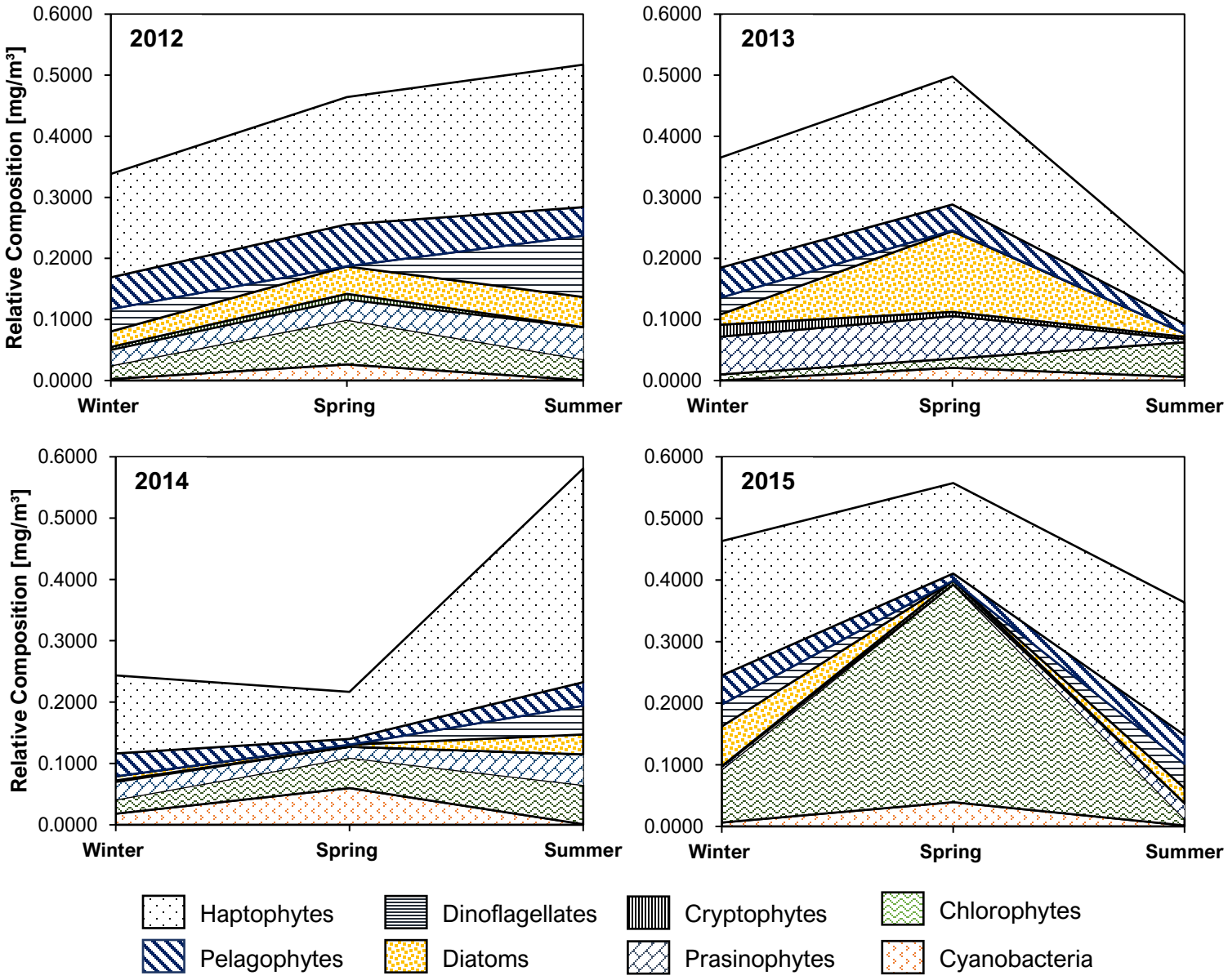

Figure 11. Composition of mixed layer phytoplankton groups (in mg total chlorophyll m^{-3}) at OSP during winter, spring, and summer from 2012 to 2015. The values were derived from CHEMTAX analysis of HPLC pigment measurements of a single depth profile within the mixed layer.

Average dFe decreased significantly resulting in reduced NCP compared to previous years. The summer 2015 experienced a substantial reduction in the $\Delta Fe:\Delta NO_3^-$ ratio due to diminished consumption of both dFe and NO_3^-. The $\Delta Si:\Delta NO_3^-$ and $\Delta Cd:\Delta PO_4^{3-}$ were also markedly lower than in 2014, and reduced consumption of both dCd and PO_4^{3-}, suggesting a shift towards smaller phytoplankton.

Indeed, throughout 2014 the community at OSP shifted towards a higher biomass of smaller phytoplankton (<5 µm) such as haptophytes, chlorophytes, and cyanobacteria, as well as a decrease in diatoms and dinoflagellates (>5 µm) (Fig. 11). During the second year of the marine heatwave, as the resilience of the system decreased, we observe a further shift towards higher biomass nano- to pico-

phytoplankton, with the winter and spring dominated primarily by chlorophytes and haptophytes, and fewer diatoms and dinoflagellates during the spring and summer. Previous studies have shown that phytoplankton at OSP is dominated by small size organisms with microplankton (> 20 µm) accounting for about 20 % of the biomass (Boyd and Harrison (1999)). The <5 µm assemblage is generally dominated by autotrophic flagellates, the 5-20 µm class is mainly composed of dinoflagellates and small pennate diatoms, while most of the cells >20 µm are both pennate and centric diatoms (Booth *et al.* (1993); Varela and Harrison (1999); Marchetti *et al*. (2006b)). Thus, although we did not measure the size of phytoplankton, the pigment data show a decrease in dinoflagellates and diatoms biomass and an increase of chlorophytes during the heatwave years indicating a shift in the phytoplankton community towards smaller size organisms.

Responses to the marine heatwave of 2014 and 2015 in the HNLC subarctic northeast Pacific include decreased vertical flux of macro- and micro-nutrients to the ML due to strong stratification and shallowing of the ML. As the resilience of the system decreased over time, the phytoplankton community shifted toward higher abundances of <5 µm phytoplankton, with limited >5 µm phytoplankton such as diatoms and dinoflagellates. As the BCP heavily relies on gravitational settling and net vertical transport of organic carbon by physical and biological processes (Siegel *et al.* 2016), a shift toward smaller phytoplankton might indicate that the conditions associated with the marine heatwave are less conducive to organic carbon export. The strong stratification and shallowing of the ML throughout the seasons decreased vertical supply of nutrients to the surface, but would also have decreased the downward transport of organic carbon out of the ML (i.e. via particle injection pumps; Boyd *et al.* 2019). Similarly, the shift in phytoplankton community toward smaller organisms could have reduced their gravitational settling efficiency and increased the remineralization of smaller cells trapped in the ML. With continued climate change, the subarctic NE Pacific could be subject to similar hydrographic and biogeochemical conditions in the future, which could have negative long-term impacts on the BCP.

Although our study did not detect a substantial decrease in NCP due to nitrate drawdown in 2015, as observed by Bif *et al.* (2019), we did see similarities between 2014 NCP and the hypothesized resilience of the system, i.e. from Fe availability during both years of the marine heatwave. As Bif *et al.* conducted their study using autonomous float data, they were able to calculate NCP at a higher resolution and over a greater area. Our study was more limited in resolution (three times per year), and geographic scale (OSP). However, this time series of micronutrient data provides insight into the mechanisms driving observed changes in biological productivity, and associated implications. We show that enhanced winter Fe availability helped to sustain elevated productivity in summer 2014. Furthermore, we document a shift in species composition during the marine heatwave, which, coupled with decreases in ML depth, may impact the efficacy of the biological carbon pump. Finally, since our data suggests that 2015 was more Fe-limited compared to previous years and dominated by smaller phytoplankton, with greater resolution we might observe noticeable differences in NCP that cannot be seen from a single station three times per year.

2.5 Conclusion

The 2014/2015 marine heatwave affected the hydrographic and biogeochemical setting at OSP. Increased sea surface temperatures resulted in increased ML stratification and shallowing during winter and summer. During 2014, the first year of the heatwave, NCP was sustained by higher average dFe in

the winter, although the consumption ratios $\Delta Si:\Delta NO_3^-$ and $\Delta Cd:\Delta PO_4^{3-}$ and phytoplankton community composition data inferred a shift towards smaller species in the phytoplankton community which remained productive, as seen from the elevated $\Delta Fe:\Delta NO_3^-$ ratio. The following winter, 2015, NCP was marginally diminished based on our observations, while Bif *et al.* (2019) reported a substantial decrease in NCP during 2015. We observed low dFe concentrations in the winter, resulting in Fe limitation during the subsequent growing season. Correspondingly low $\Delta Fe:\Delta NO_3^-$, $\Delta Si:\Delta NO_3^-$ and $\Delta Cd:\Delta PO_4$ consumption ratios, compared to 2014, suggesting a phytoplankton community more dominated by smaller species. Using community composition data we were able to confirm a shift to smaller phytoplankton species in both 2014 and 2015, and a decrease in larger phytoplankton like diatoms and dinoflagellates. As climate change progresses, the frequency of these marine heatwave events are expected to increase (Oliver *et al.* 2018), the impacts of which are not fully understood; however, if similar to the conditions presented here (2014-2015) the outcome is expected to be overall negative with regard to the biological carbon pump.

Chapter 3 : The effects of marine heatwaves on the relationship between trace metal distributions and net community production in the coastal and offshore subarctic northeast Pacific

3.1 Introduction

In the subarctic northeast Pacific, two marine heatwaves with surface temperatures greater than approximately 5 standard deviations above the mean have taken place in the last decade, Fig.12 (Freeland and Ross 2019). The first heatwave, colloquially called The Blob, began in the late winter of 2013 with surface temperature anomalies that persisted until the end of 2016 (Whitney et al. 2019). The Blob was induced by an anomalous atmospheric high-pressure system over the North Pacific. The high-pressure ridge weakened the Aleutian Low, resulting in diminished winter surface winds and diminished heat loss that led to ocean surface heating and winter mixed layer shallowing (Bond *et al.* 2015, Whitney *et al.* 2019).

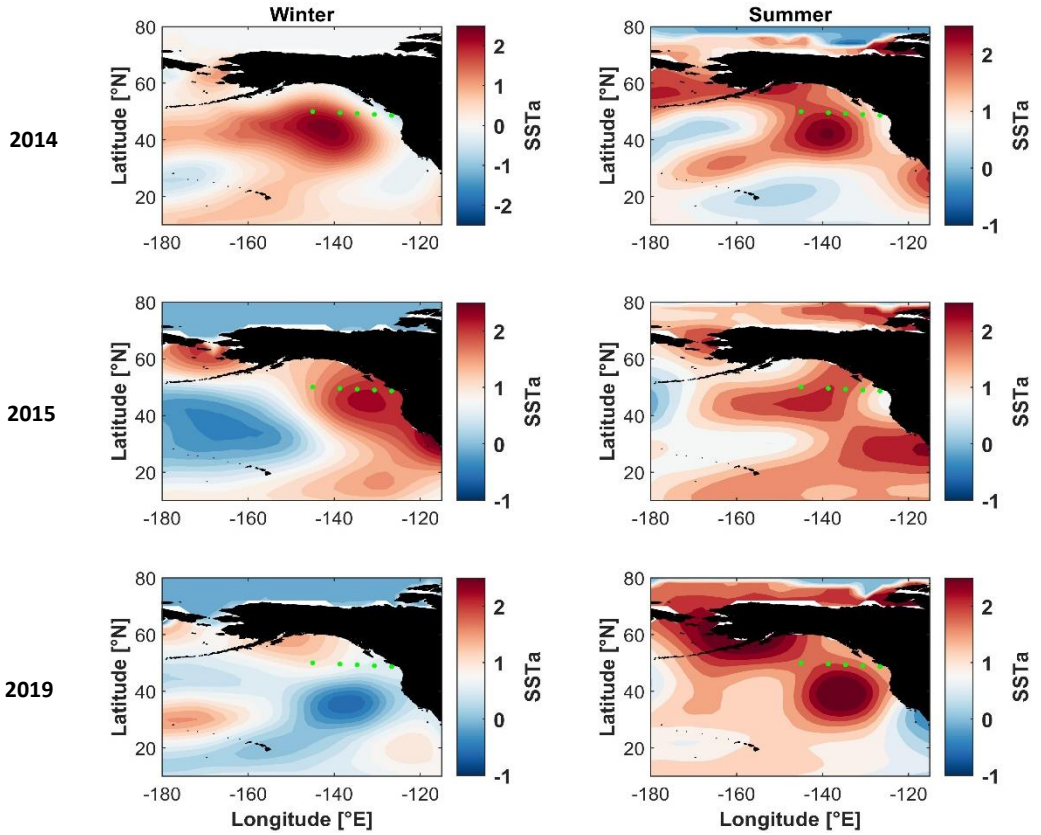

Figure 12. Monthly mean sea surface temperature anomalies (SSTa) in the subarctic northeast Pacific Ocean in winter (February) and summer (August) 2014, 2015, and 2019. Green circles represent the locations of Line P stations P26, P20, P16, P12, and P4 from offshore to coastal environments. Data collected from the NASA Earthdata Database (https://earthdata.nasa.gov/) (Huang *et al.* 2015).

Hints of the second marine heatwave began in late 2018 as observed temperatures in the Gulf of Alaska (GOA) passed above the threshold into 'heatwave' status (Zador *et al.* 2019). The winter 2018-2019 featured a weak Aleutian Low that resulted in warmer SST due to lack of winter winds- a similar physical conditions to those that initiated to The Blob (Zador *et al.* 2019). From the Bering Sea south into the GOA during the summer of 2019, high sea level pressure (SLP) was present while just south in the

Central Pacific, low SLP was dominant (Zador *et al.* 2019; Amaya *et al*. 2020). This contrast in SLP set the scene for increased sea surface temperatures in the subarctic northeast Pacific by reducing wind driven mixing and heat transport out of the surface layer (Zador *et al.* 2019). Extreme changes in the physical fields at the surface of the subarctic northeast Pacific are likely to have significant impacts on both chemical and biological fields and processes (Whitney and Freeland 1999; Freeland and Ross 2019).

In the early 1990's, an El Niño event affected the subarctic northeast Pacific (Goddard and Graham 1997). The phenomenon brought on warm sea surface temperatures, as well an increasingly buoyant mixed layer that diminished macronutrient supply to the surface (Whitney and Freeland 1999). The event was prolonged and by 1994, resulted in diminished and/or depleted concentrations of nitrate that spread from the offshore to coastal regions. In 1982 a similar El Niño event was observed that resulted in the same hydrographic and nutrient distributions (Whitney *et al.* 1998; Whitney and Freeland 1999). These events have been observed to have lasting affects on nutrient stocks that can take years to reverse (Whitney and Freeland 1999). It has been hypothesized by Whitney and Freeland 1999 that these events are leading to trends in the GOA towards warmer, less saline surface waters that are resulting in reduced nitrate and silicate concentrations. To date, observations have shown that nutrients were indeed affected comparably to these past warming events during the 2014/2015 marine heatwave event, the Blob (Peña *et al.* 2019). At this time, the most recent marine heatwave event (2019) in the subarctic northeast Pacific has not been thoroughly studied. In the offshore region, nitrate concentrations were essentially depleted, which is not typical of HNLC environments that are limited by iron rather than nitrate. As nitrate consumption is directly related to net community production, why was the region relatively productive when past events clearly show a trend in decreasing nutrient concentrations to the mixed layer and reduced phytoplankton growth?

Trace metal nutrients (eg. Mn, Fe, Co, Ni, Cu, and Cd) play key roles in regulating the growth and community composition of marine microbes (Morel *et al.* 2003). At this time, there is little known about the effects of marine heatwaves on trace metal (TM) distributions. To study this issue, trace metal clean seawater samples were collected and analyzed from 5 major stations as part of the Line P Time-Series Program in the subarctic northeast Pacific Ocean, Fig.1, P26, P20, P16, P12, and P4. Vertical profiles of dissolved manganese (dMn), cobalt (dCo), cadmium (dCd), iron (dFe), nickel (dNi), and copper (dCu) were analyzed for the winters (February) of 2012 to 2015 and the summers (August) 2012 to 2019 (excluding 2016). The hydrographic profiles and the surface mixed layer (ML) averages of macro-micronutrients were also measured to determine the effects of marine heatwaves on TM distributions and net community production (NCP) along a transect between nitrogen limited coastal waters and the Fe-limited high nutrient-low chlorophyll (HNLC) offshore waters of the subarctic northeast Pacific.

3.2 Methods

3.2.1 Sample collection

Trace metal clean seawater samples were collected in the subarctic northeast Pacific along the Line P Timeseries transect from the *CGSS John P. Tully* during the winter (February) 2012 to 2015, and the summer (August) 2012 to 2019. Samples were collected at the five major stations, Fig.12, located at P4 (48°39N, 126°40W), P12(48°58N, 130°40W), P16 (49°17N, 134°40W), P20 (49°34N, 138°40W), and P26 (50°00N, 145°00W). Trace metal clean seawater samples were collected following GEOTRACES protocols (https://www.geotraces.org/methods-cookbook/) and the methodology outlined in Chapter 2:

Relationship between surface dissolved iron inventories and net community production during a marine heatwave in the subarctic northeast Pacific.

3.2.2 Experimental

Preparation of reagents, as well as the procedure to extract and analyze trace metals from seawater samples are outlined in detail in Chapter 2: *Relationship between surface dissolved iron inventories and net community production during a marine heatwave in the subarctic northeast Pacific*. Extraction was conducted using an ESI seaFAST- pico SC4-DX, solid phase extraction system using a Nobias-1 column resin (ESI, Omaha, NE, USA). Samples were analyzed on an Agilent 8800 triple quadrupole ICP-MS/MS (Agilent Technologies) utilizing modified parameters from those outlined in Jackson *et al.* 2018. The resulting samples were run against in-house reference material and the certified references standard NASS-7 (National Research Council, Canada). Blanks, detection limits (DL), accuracy and precision of the analyses are reported in Table 4.

Table 4: The average blanks, detection limits, and consensus values for reference materials for the analysis of the winter 2012-2015 and summer 2012-2019 trace metal species profiles.

	Blanks, n=18	Detection Limits, n=18	In house Reference Material, n=18	NASS-7 Measured, n=2	NASS-7 Consensus
Mn (nmol L^{-1})	0.03	0.002	0.95 ± 0.05	13.9 ± 0.7	13.6 ± 1.1
Fe (nmol L^{-1})	0.027	0.016	0.5 ± 0.1	6.3 ± 0.6	6.7 ± 0.5
Co (pmol L^{-1})	0.41	0.14	36.5 ± 1.3	255.2 ± 1.4	247.7 ± 23.8
Ni (nmol L^{-1})	0.033	0.04	5.4 ± 0.6	4.8 ± 0.7	4.2 ± 0.3
Cu (nmol L^{-1})	0.008	0.006	2.1 ± 0.1	3.21 ± 0.01	3.1 ± 0.2
Cd (nmol L^{-1})	0.0002	0.0003	0.09 ± 0.01	0.133 ± 0.002	0.14 ± 0.01

3.2.3 Calculations

Mixed layer depth was identified as the depth at which depths did not exceed 0.02 kg/m^3 from the surface density (Timmerman and Hamme 2021). Seasonally in the subarctic northeast Pacific, in the spring and summer months the mixed layer reaches a minimum depth and deepens to a maximum depth in the fall and winter months by storm surges. For the purpose of this study, mixed layer depths will be compared by the season and year, and not between two different seasons (i.e. winter 2012 mixed layer compared to winter 2014 mixed layer).

Average winter and summer NO_3^- concentrations within the mixed layer (ML) were calculated, the difference between these concentrations (ΔNO_3^-) reflecting non-integrated, seasonal estimates of net community production (NCP) solely in the mixed layer. The resulting values were converted to mol C/m^3 using the Redfield Ratio, where estimated NCP = mol C/m^3 = (mol ΔNO_3^-)*6.6 (Bif and Hansell 2019). Average trace metal concentrations were calculated over the same depth range, along with winter to summer silicate:nitrate ($\Delta Si:\Delta NO_3^-$), and cadmium:phosphate ($\Delta Cd:\Delta PO_4$) ratios . The ML dCd and PO_4^{3-} concentrations were used to calculate seasonal (summer) averages of $Cd:PO_4^{3-}$ over the time series, instead of $\Delta Cd:\Delta PO_4^{3-}$ due to limited winter TM data.

3.3 Results

For this section, the stations P26, P20, and P16 will be grouped together as ***offshore stations***, while P12 and P4 will be grouped together as ***coastal stations***.

3.3.1 Hydrography

The density (σ_T), mixed layer depth (MLD), temperature (T), and salinity (S) of winter and summer 2012, 2014, 2015, and 2019 are shown for stations P1 to P26 along the Line P transect, Fig.13, to characterize the hydrography of 'normal' and marine heatwave conditions in the subarctic northeast Pacific. In addition, temperature- salinity (TS) plots, Fig.14, of stations P26 and P4 during the same time frame were generated to give specifics on the conditions experienced in the offshore and coastal regions.

3.3.1.1 P26 to P1 hydrography

2012 – The winter of 2012 MLD's were shallower near the continental margin and deepened moving offshore, with maximum MLD's nearing 100m in the HNLC region. The σ_T, T, and S were dense, warm, and saline near shore compared to the offshore which was less dense, cooler, and less saline ranging from approximately 23-26 kg/m^3, 8.5-5°C, and 30-32 PSU, respectively. During the summer of 2012, shallowing of the MLD was observed from near to offshore with σ_T, T, and S ranging from 23-25 kg/m^3, 11-15°C, and 30-33 PSU, respectively.

2014 – In the winter of 2014, the MLD shoaled across the offshore regions with diminished σ_T (25 kg/m^3), S (32 PSU) and elevated T (7.5-9°C). The near shore portion of the coastal region had ML S and T of 31 PSU and 6-7°C, respectively. The summer offshore MLD's experienced shallowing when compared to the summer of 2012. The offshore σ_T and S diminished while the T increased. Coastal waters had relatively unchanged MLD's with σ_T, S, and T values near 23 kg/m^3, 32 PSU, and 15-20°C, respectively.

2015 – The winter of 2015 experienced increasing ML shallowing, while some coastal, near shore stations experienced ML deepening. The σ_T varied across the line with coastal values near 24.5 kg/m^3 and offshore values near 25 kg/m^3. The offshore T (7-9°C) was similar to 2014, while coastal T increased (10-12°C). The summer of 2015 MLD's deepened compared to those of summer 2014 in the offshore and coastal regions. Across the line, the σ_T, T, and S ranged from 23-24.5 kg/m^3, 12.5-20°C, and remained near 32 PSU.

2019 – The second marine heatwave in 2019 held warmer winter temperatures similar to that of the Blob, with high T's of 9-10°C near shore and 6.5-8°C offshore. The MLD's were similarly shoaled in the offshore to 2014, with the exception of near shore where the MLD deepened. The σ_T and the S remained near 25 kg/m^3 and 32.5 PSU across the line. The following summer the MLD's appeared to be more similar to 2012, however, the hydrography followed the Blob trends. The σ_T and S values were near 23.5 kg/m^3 and 32.5 PSU, respectively, while the T was the warmest closer to the shore and ranged from 15-17°C across the line.

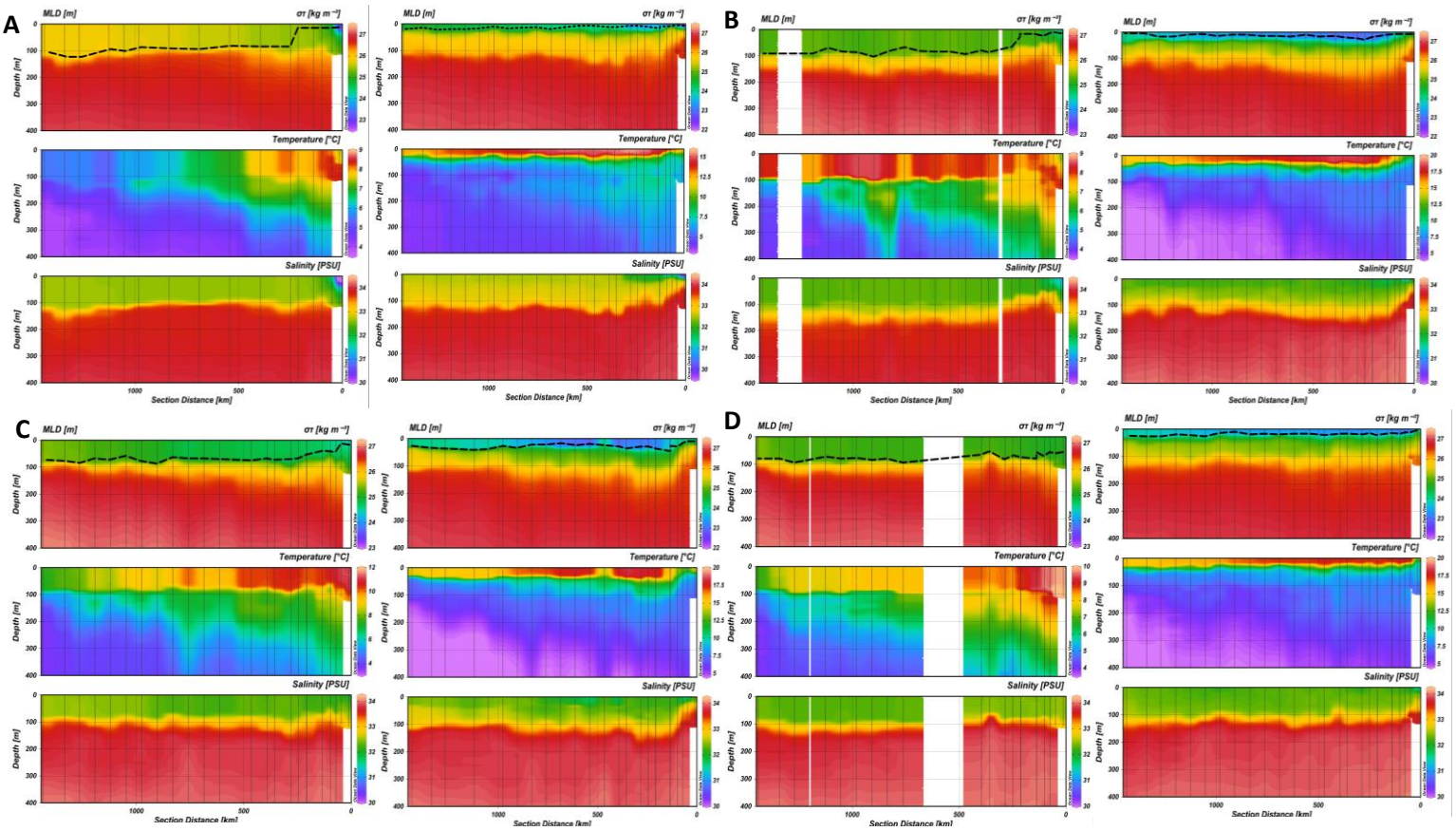

Figure 13. Hydrographic profiles of the Line P transect in the winter (left) and summer (right) of 2012 (A), 2014 (B), 2015 (C), 2019 (D). The three profiles from top to bottom are density (σ_T), temperature (T), and salinity (PSU). Density profiles have mixed layer depths as dashed black line.

3.3.1.2. P26 and P4 temperature-salinity diagrams

P26 – At station P26 (Fig.14A), the winter and summer σ_T, T, and S were noticeably affected by the marine heatwaves of 2014/2015 and 2019. During winter 2014 and 2015 at P26 the surface waters were warmer, fresher, and less dense than in the immediately preceding years. In 2019, waters were similarly fresher and less dense, but were not as warm as those in 2014 and 2015. The upper-ocean hydrography during summer seasons of the marine heatwaves were very similar. The σ_T, T, and S values for 2014, 2015, and 2019 were all near 24 kg/m³, 15°C, and 32.5 PSU, respectively.

P4 – Station P4 (Fig.14B) hydrography behaved differently under marine heatwave conditions compared to the offshore station P26. In 2014 the σ_T, T, and S were more similar to 2012 values of approximately 25 kg/m³, 8°C, and 32 PSU. The warming effects were not observed near shore until 2015, where σ_T and T at the surface changed markedly to values closer to 24.5 kg/m³ and 10.5°C. The near shore waters during the winter of 2019 were similar in σ_T and S to 2012 and 2014, but were notably warmer with T's around 8.5°C. The summer hydrography at P4 during 2014 was less dense, warmer, and less saline compared to 2012 with values near 23.75 kg/m³, 15°C, and 32 PSU. The second summer of the marine heatwave, 2015, was more dense and less warm with values near 24 kg/m³ and 13°C, respectively. The

2019 marine heatwave had a greater impact on the waters at P4 compared to the marine heatwave years 2014/2015 being less dense (σ_T = 23.16 kg/m³) and warmer (T= 18°C).

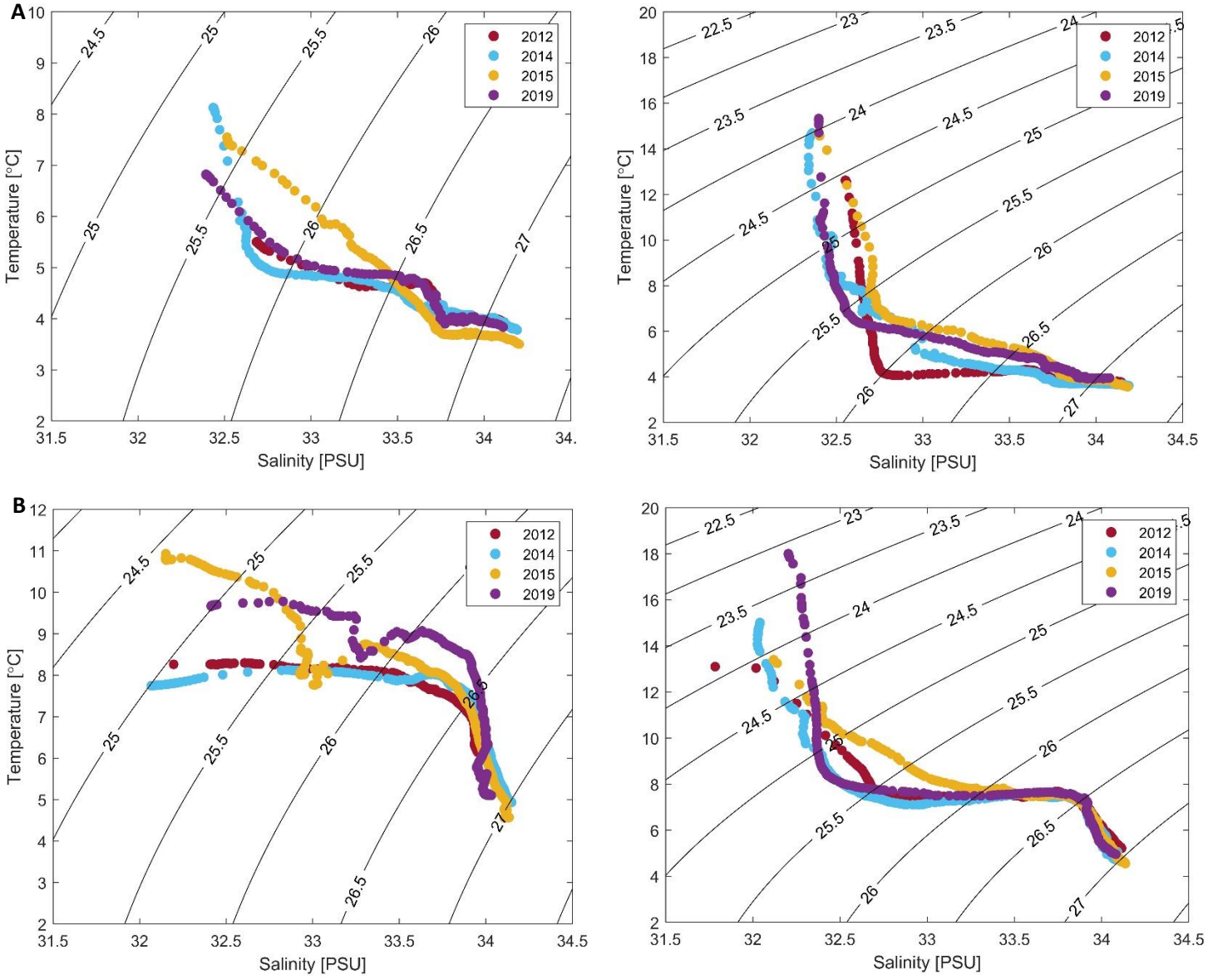

Figure 14. T/S diagrams of station winter (left) and summer (right) 2012, 2014, 2015, and 2019 at stations P26 (A) and P4 (B).

3.3.2 Trace metal and macronutrient vertical profiles

3.3.2.1 Trace metal vertical profiles

Offshore – The winter 2012 and 2013 profile ranges and trends were similar for dMn, dFe, and dCd while dCo, dNi, and dCu displayed more variation (Fig. 15,17,19). The dCo and dCu concentrations were elevated compared to 2013 with profile values being in the range of 45-60 pmol dCo/kg and 1.3-2.4 nmol dCu/kg in 2012, and 34-50 pmol dCo/kg and 0.50-2.4 nmol dCu/kg in 2013, respectively. In 2012 dNi had diminished values compared to 2013 in the range of 4.2-7.3 nmol dNi/kg and 5.5-8.5 nmol dNi/kg. During the summer of 2013, there was general elevation of TM concentrations compared to the same period in 2012. The winter 2014 and 2015 TM concentrations were much lower within the MLD's with the exception of dFe and dCu in 2014 (Fig. 15,17,19). The dFe and dCu profiles were elevated within the upper 100m in the range of 0.12 to 0.31 nmol dFe/kg and 1.23 to 2.24 nmol dCu/kg, respectively. The summer 2014 and 2015 had the lowest concentrations in our time-series, with the exception of station P16 where in 2015 some elevated concentrations of TM's were observed (Fig. 16,18,20). The most significant reductions were observed during both summers at P26 and P20 in the upper 100m were dMn, dCo, and dCd concentrations fell to 0.52-1.2 dMn/kg, 6.7-65.3 pmol dCo/kg, and 0.007-0.610 nmol dCd/kg, respectively. Station P16 in 2015 had elevated levels of dMn, dCo, dCu, and dCd at the surface of 2.72 nmol dMn/kg, 38.6 pmol dCo/kg, 2.05 nmol dCu/kg, and 0.036 nmol dCd/kg. The summers of 2017 and 2018 had TM profiles that were similar to summer 2012 and 2013 (Fig. 16,18,20). The summer of 2019 was characterized by uniformly low surface TM concentrations. The dMn, dCo, dNi, dCu, and dCd decreased to concentrations lower or similar to that of 2014 and 2015, with the exception of a higher surface dNi concentration of 2.70 nmol dNi/kg at P26.

Coastal – As coastal environments receive nutrients and trace elements from wind driven upwelling of subsurface waters, riverine discharge, atmospheric deposition, and tidal mixing (Whitney *et al.* 1998), they are known to exhibit more spatial and temporal variation in chemical distributions compared to offshore environments. In the winter of 2012, the dMn, dFe, dCo, and dCu were quite different between the P4 and P12 with higher ML concentrations of dMn, dFe, dCo at P4 and lower concentrations of dCu at P12 (no winter 2013 TM data available). The winter distributions during 2014 and 2015 varied by station, species, and year (Fig. 21,23). In 2014 at station P12, only two depths were sampled and species concentrations appear to be similar to those in 2012. In 2015 dMn and dNi were elevated while dFe, dCo, dCu, and dCd were diminished in relation to 2012 and 2014. During the winter at station P4, there was a large increase in dMn and dCo in the upper 35m. In 2015, all species were diminished compared to 2014 except for dNi which was slightly elevated (4.65-4.94 nmol dNi/kg). Similar to the winter, the two coastal stations varied in the summer months (Fig.22,24). Station P12 in 2014 profile values were similar to 2012 and 2013, while summer 2015 species distributions varied. The surface concentrations of dMn, dFe, dCo, and dCd were significantly diminished compared to the depths below. The summer of 2014 at station P4 species within the bounds of 2012 and 2013 profiles. In the summer 2015, dMn and dCo anomalously elevated, while dFe, dCd, dNi, and dCu were marginally elevated. The summer 2018 had relatively high concentrations of all species in the coastal region, especially at station P4. The summer 2019 had some of the lowest concentrations in the upper 25m for dCo, dCd, dNi, and dCu, while the remaining species and depths remained within the bounds of the timeseries (Fig.22,24).

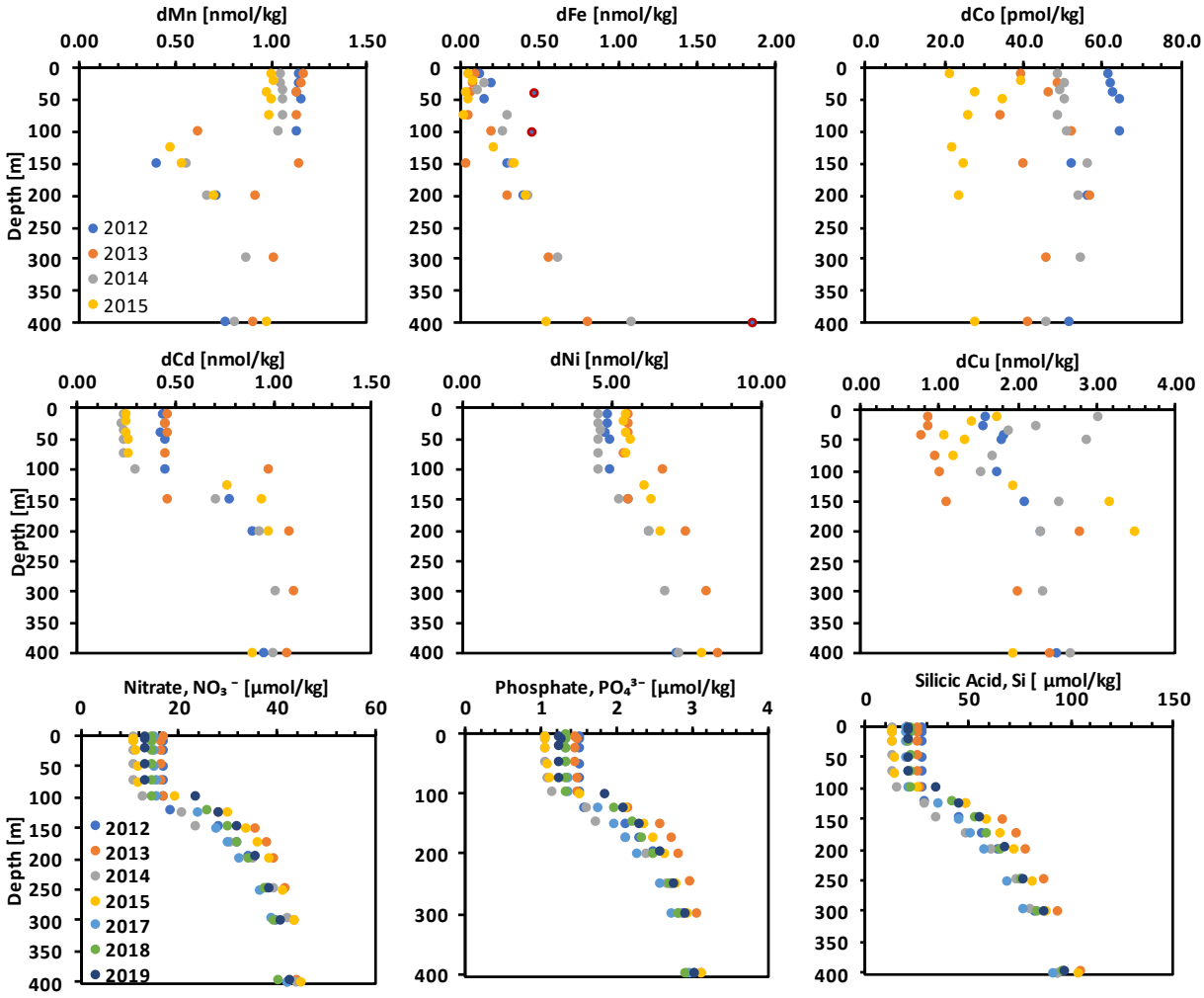

Figure 15. P26 winter trace metal and macronutrient depth profiles (0-400m) at OSP. Winter values for trace metals range from 2012-2015, while macronutrient values range 2012-2019. Data points with bordering red are flagged for contamination.

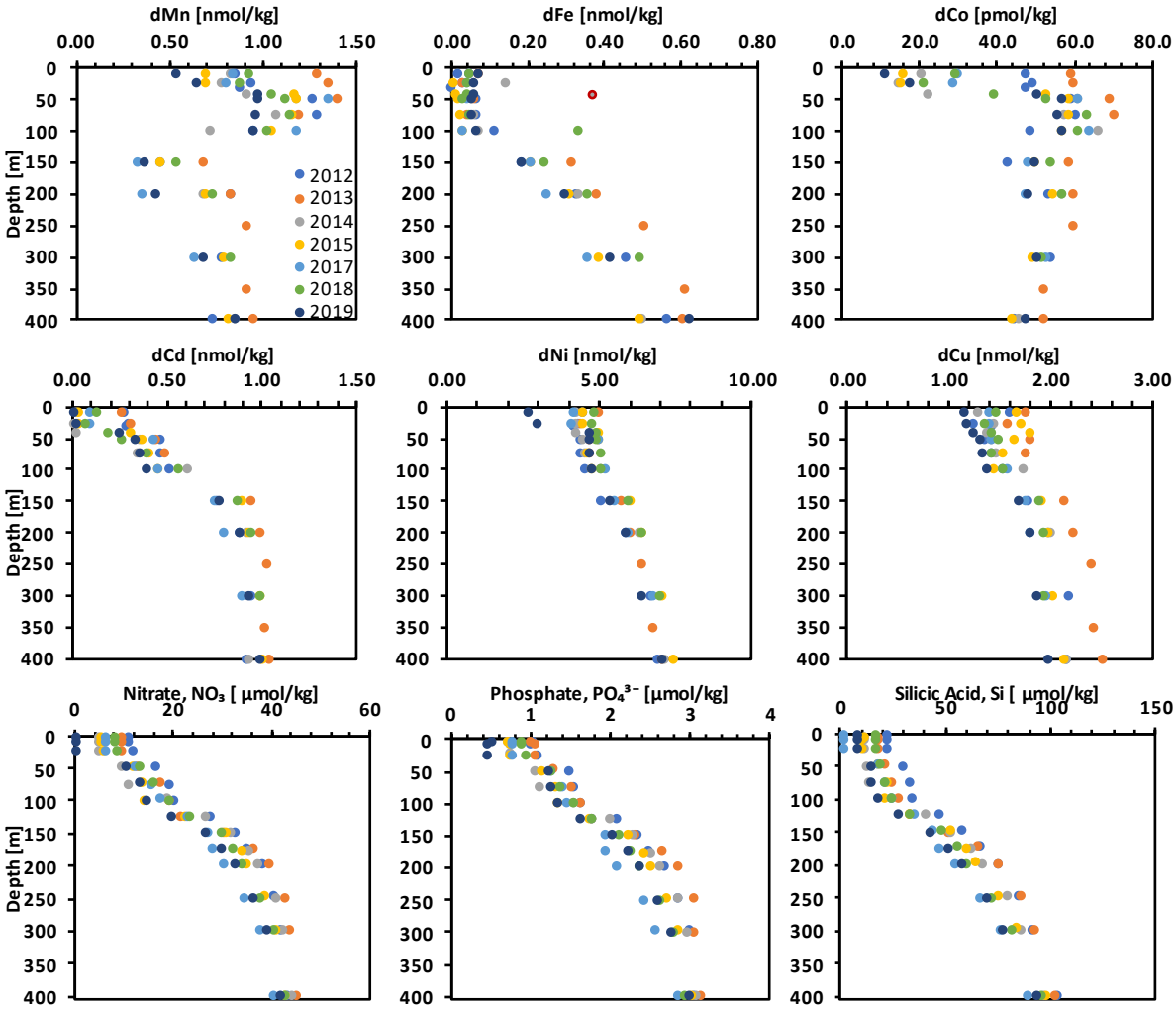

Figure 16. P26 summer trace metal and macronutrient depth profiles (0-400m) at OSP. Summer trace metal and macronutrient values range from 2012-2019. Data points with bordering red are flagged for contamination.

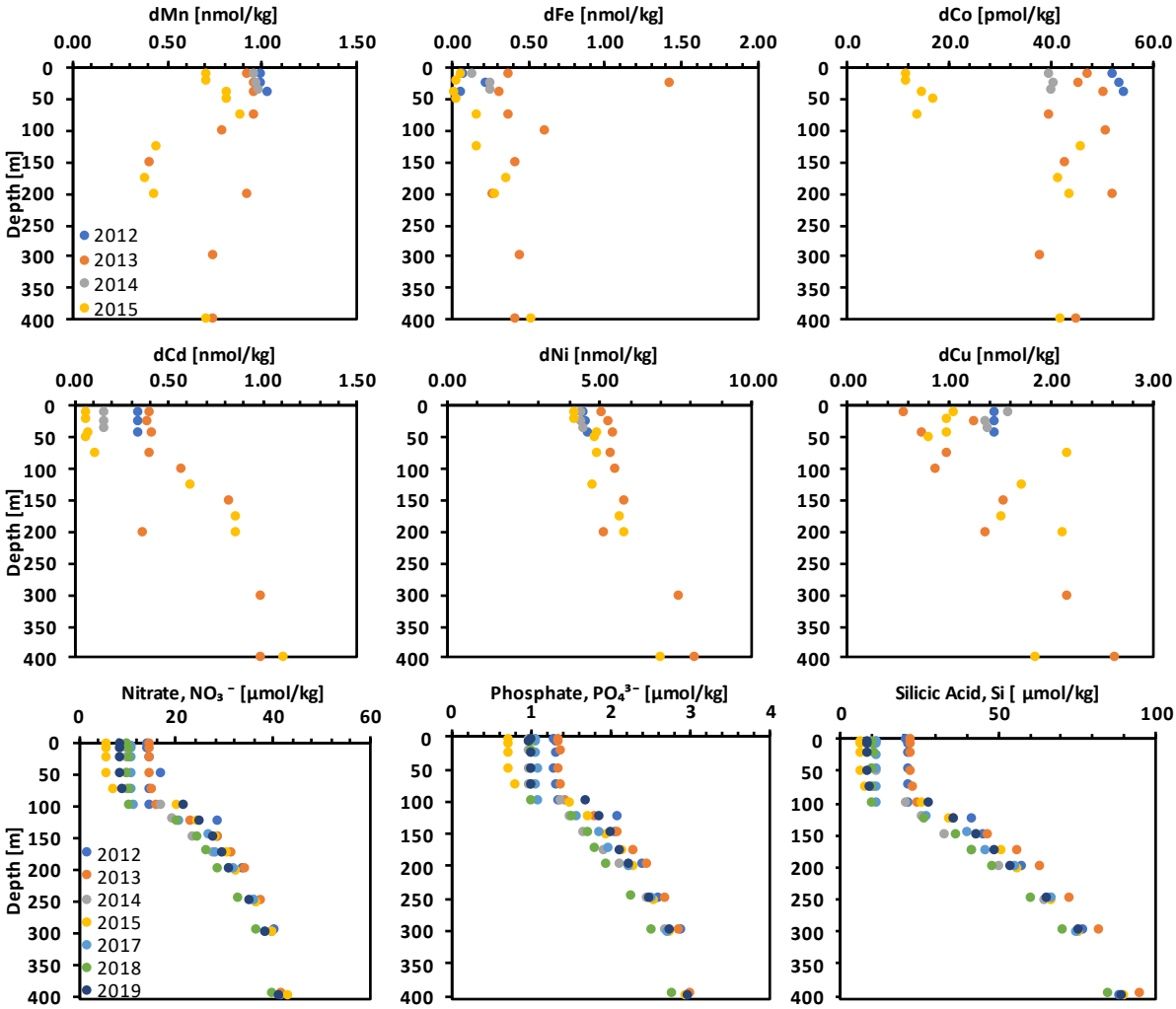

Figure 17. P20 winter trace metal and macronutrient depth profiles (0-400m) at OSP. Winter values for trace metals range from 2012-2015, while macronutrient values range 2012-2019. Data points with bordering red are flagged for contamination.

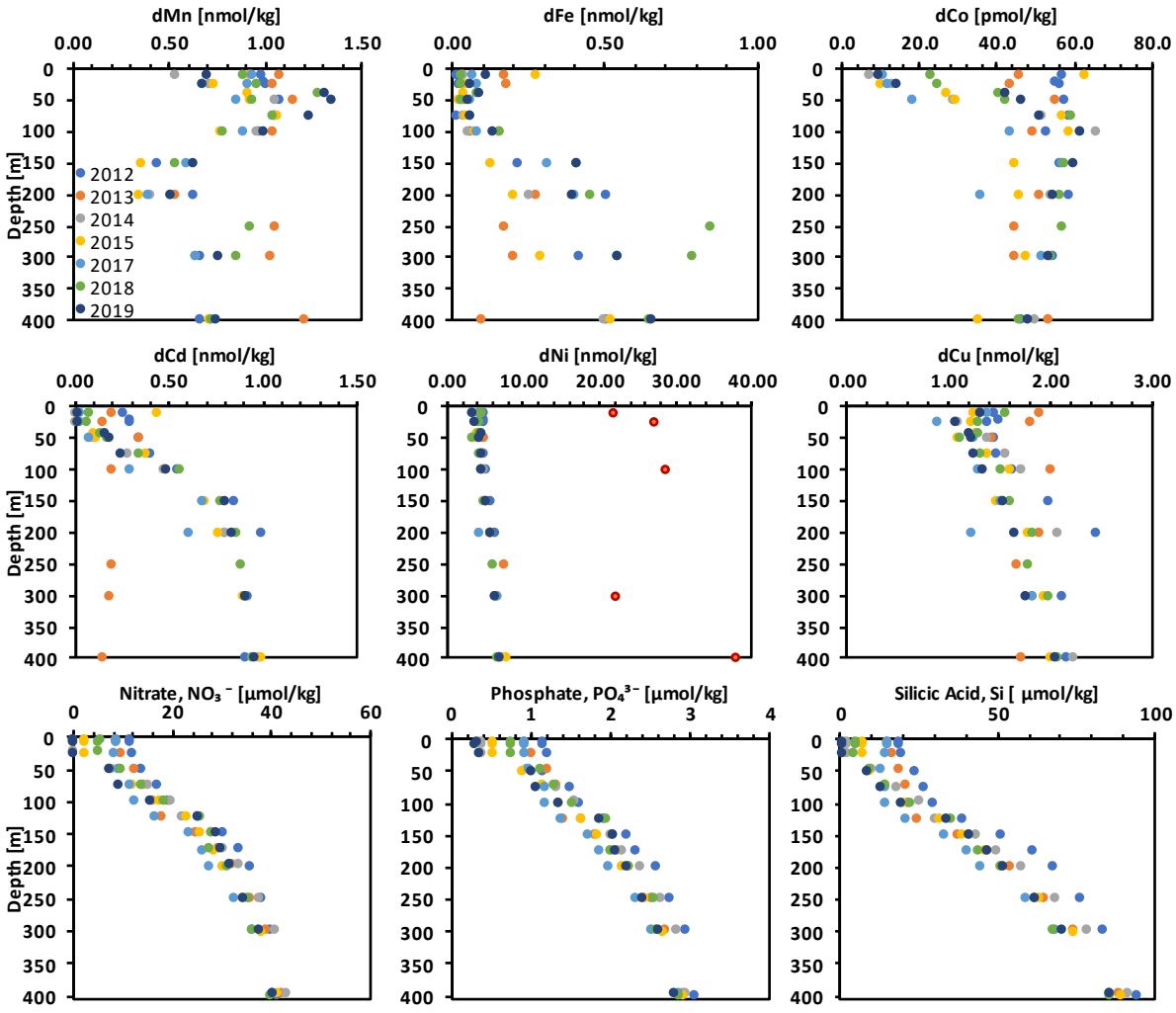

Figure 18. P20 summer trace metal and macronutrient depth profiles (0-400m) at OSP. Summer trace metal and macronutrient values range from 2012-2019. Data points with bordering red are flagged for contamination.

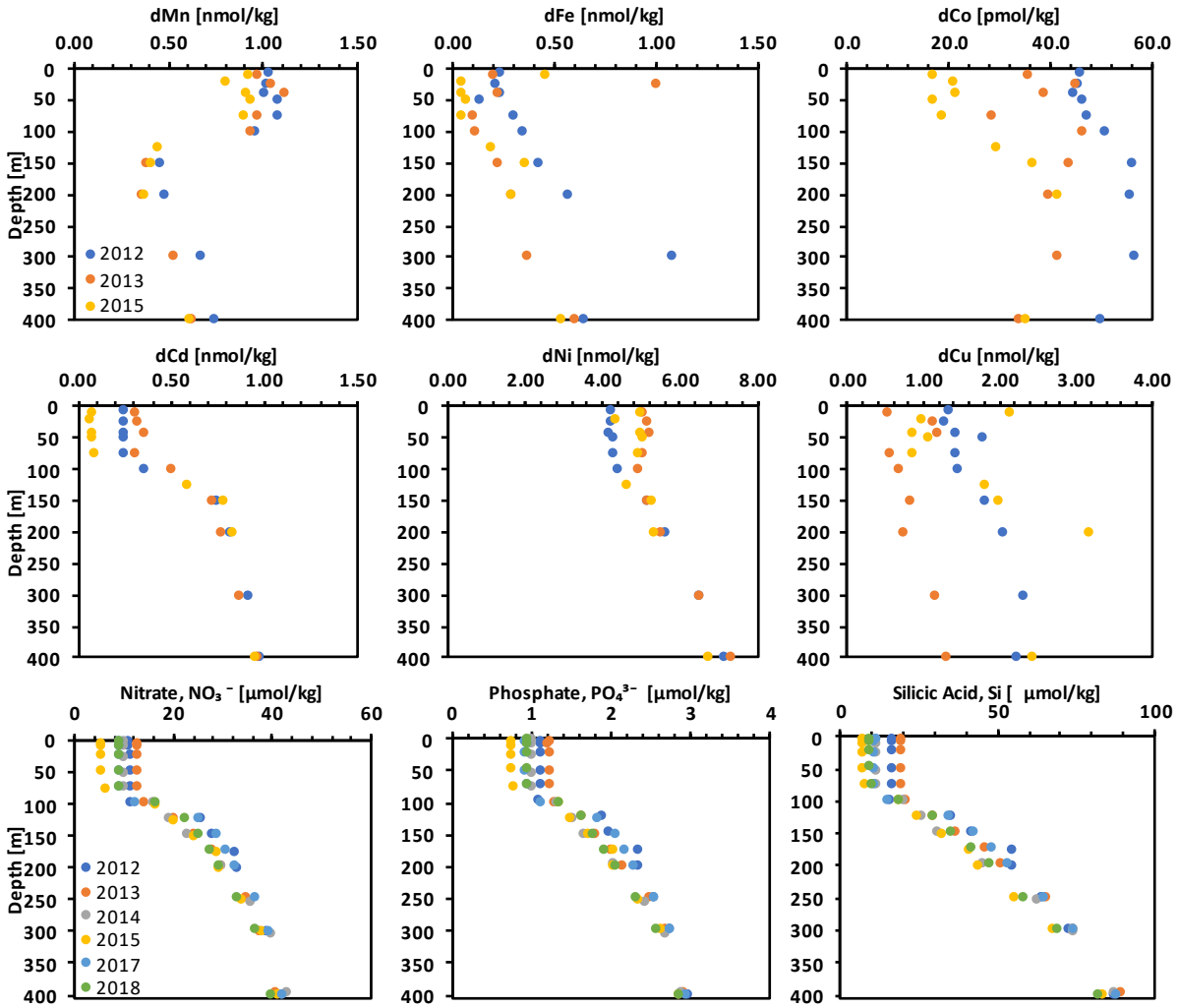

Figure 19. P16 winter trace metal and macronutrient depth profiles (0-400m) at OSP. Winter values for trace metals range from 2012-2015, while macronutrient values range 2012-2019. Data points with bordering red are flagged for contamination.

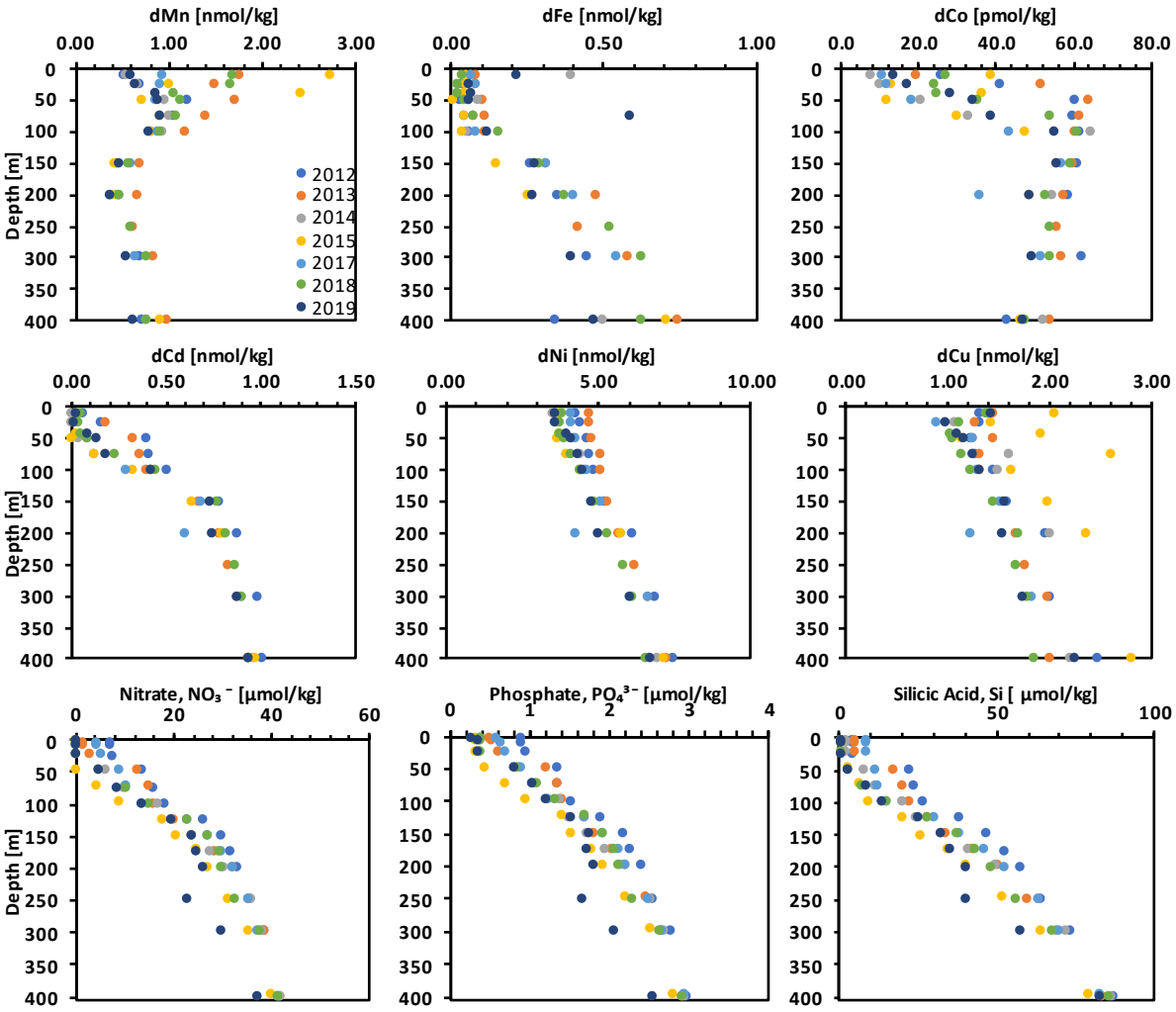

Figure 20. P16 summer trace metal and macronutrient depth profiles (0-400m) at OSP. Summer trace metal and macronutrient values range from 2012-2019. Data points with bordering red are flagged for contamination.

3.3.2.2 Macronutrient vertical profiles

Offshore – Here we focus on the upper 150m where most variation in dissolved chemical species occurred. The winter 2012 and 2013 NO_3^-concentrations were similar, with winter 2013 PO_4^{3-} and Si concentrations marginally higher in 2013 than in 2012 (Fig.15,17,19). During the 2013 summer, NO_3^-, PO_4^{3-}, and Si concentrations in the ML were diminished compared to winter values. The winters of 2014 and 2015 were characterized by ML macronutrients concentrations (11.0-23.5 µmol NO_3^-/kg; 1.05-1.75 µmol PO_4^{3-}/kg; 12.8-33.9 µmol Si/kg) that were much lower than those observed in 2012 and 2013 (10.89-33.73 µmol NO_3^-/kg; 1.06-2.36 µmol PO_4^{3-}/kg; 12.8-58.4 µmol Si/kg). At station P26 in summer 2014 and 2015, macronutrients were drawn down from winter values to similar concentrations (Fig.16,18,20). In 2015, P20 and P16 macronutrients were depleted to average surface concentrations of 5.6 µmol NO_3^-/kg, 0.73 µmol PO_4^{3-}/kg, and 6.5 µmol Si/kg. The offshore summer 2014 and 2015 drawdown resulted in low ML concentrations due to the reduced pre-growing season ML stocks. The winter macronutrient ML stocks had rebounded, but not to the extent of 2012 and 2013 values –

concentrations values were intermediate to those in 2012/13 and 2014/15. In the summer, 2018 had the most notable change with reduced ML concentrations compared to 2017, with the exception of Si, which was the lowest in the dataset in 2017 at P26. The winter 2019 macronutrients had similar concentrations to 2018 values, while NO_3^- concentrations were a bit closer to those in 2014 and 2015. The summer 2019 brought on complete depletion of NO_3^-, while PO_4^{3-} and Si were drawdown to levels close to, or below those of 2014 and 2015.

Coastal – In the winter of 2012 and 2013, macronutrient concentrations for P12 and P4 were similar to other winters in the study (Fig.21,23). In the summer, stations P12 and P4 experienced different extents of macronutrient drawdown (Fig.22,24). At P12, ML NO_3^- and PO_4^{3-} concentrations were lower in 2013 when compared to 2012, with surface values of 1.5 µmol NO_3^-/kg and 0.53 µmol PO_4^{3-}/kg, respectively. At the same time, Si concentrations remained unchanged between the two summers. At P4, NO_3^- concentrations were marginally lower, while PO_4^{3-} and Si concentrations were greater in relation to 2013 values. The winter of 2014 had relatively typical macronutrient concentrations for the coastal region, while winter 2015 macronutrients were significantly reduced to average values near 3.4 µmol NO_3^-/kg, 0.61 µmol PO_4^{3-}/kg, and 6.0 µmol Si/kg. The summer 2014 and 2015 NO_3^- was deplete with the exception of P4 2015 (1.77 µmol NO_3^-/kg). At P12, ML Si was elevated compared to other years in 2014. At station P4, Si was elevated for both 2014 and 2015 in relation to 2012 and 2013. During the winter of 2017, the coastal region macronutrient concentrations rebounded to levels close to 2012 and 2013. During the summer, typical drawdown occurred. The winter of 2018 had diminished concentrations of NO_3^- (6.83 µmol NO_3^-/kg) and Si (6.77 µmol Si/kg) at station P12, while those at P4 were the same as 2017. The summer 2018 brought on typical drawdown of macronutrients with the exception of Si at P4, which was elevated to 7.9 µmol Si/kg from the winter value of 7.74 µmol Si/kg. The winter 2019 concentrations were within the bounds of both 2015 and 2018 values for all nutrients. The summer was met with depletion of NO_3^- and low concentrations of both PO_4^{3-} and Si.

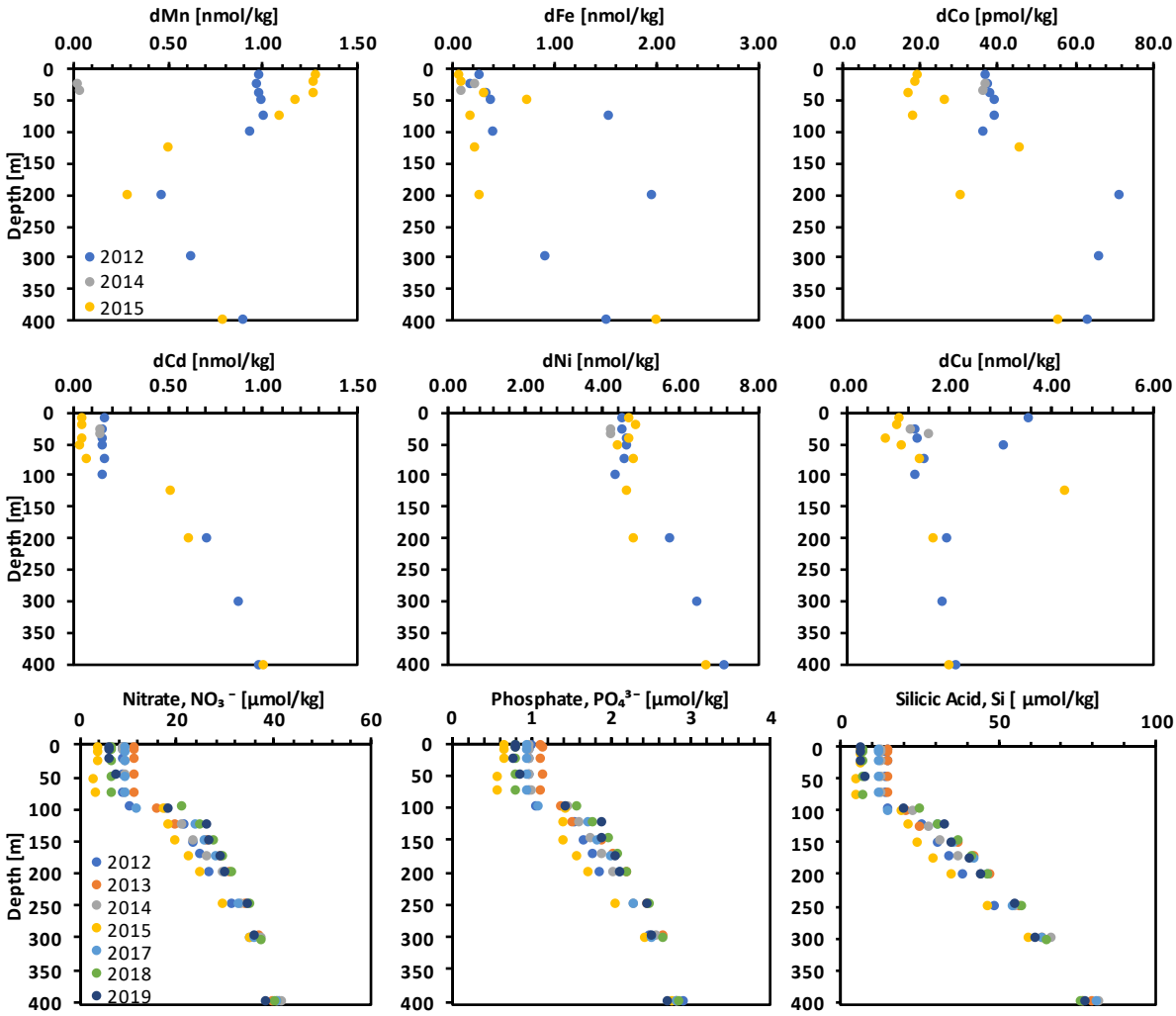

Figure 21. P12 winter trace metal and macronutrient depth profiles (0-400m) at OSP. Winter values for trace metals range from 2012-2015, while macronutrient values range 2012-2019. Data points with bordering red are flagged for contamination.

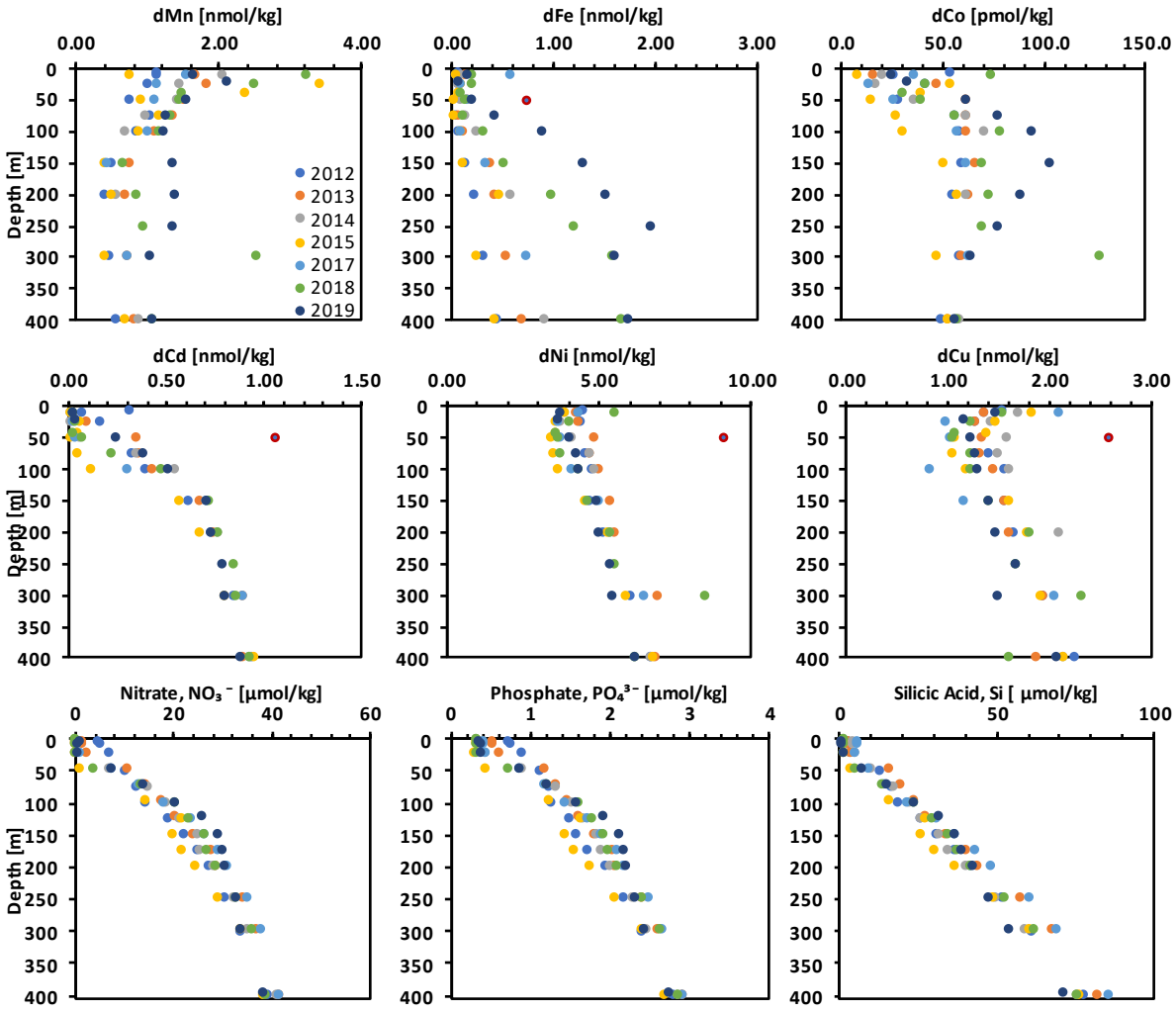

Figure 22. P12 summer trace metal and macronutrient depth profiles (0-400m) at OSP. Summer trace metal and macronutrient values range from 2012-2019. Data points with bordering red are flagged for contamination.

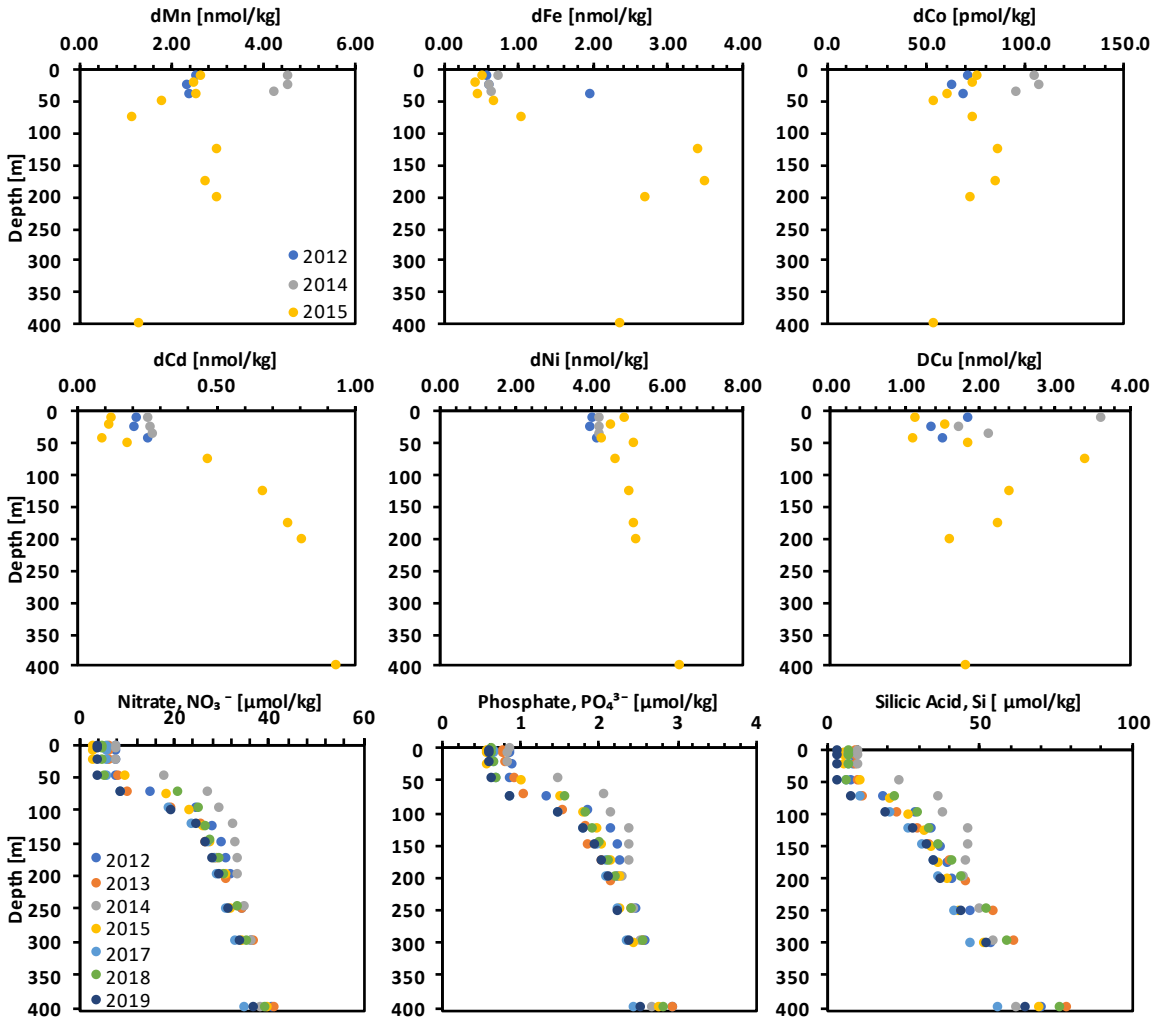

Figure 23. P4 winter trace metal and macronutrient depth profiles (0-400m) at OSP. Winter values for trace metals range from 2012-2015, while macronutrient values range 2012-2019. Data points with bordering red are flagged for contamination.

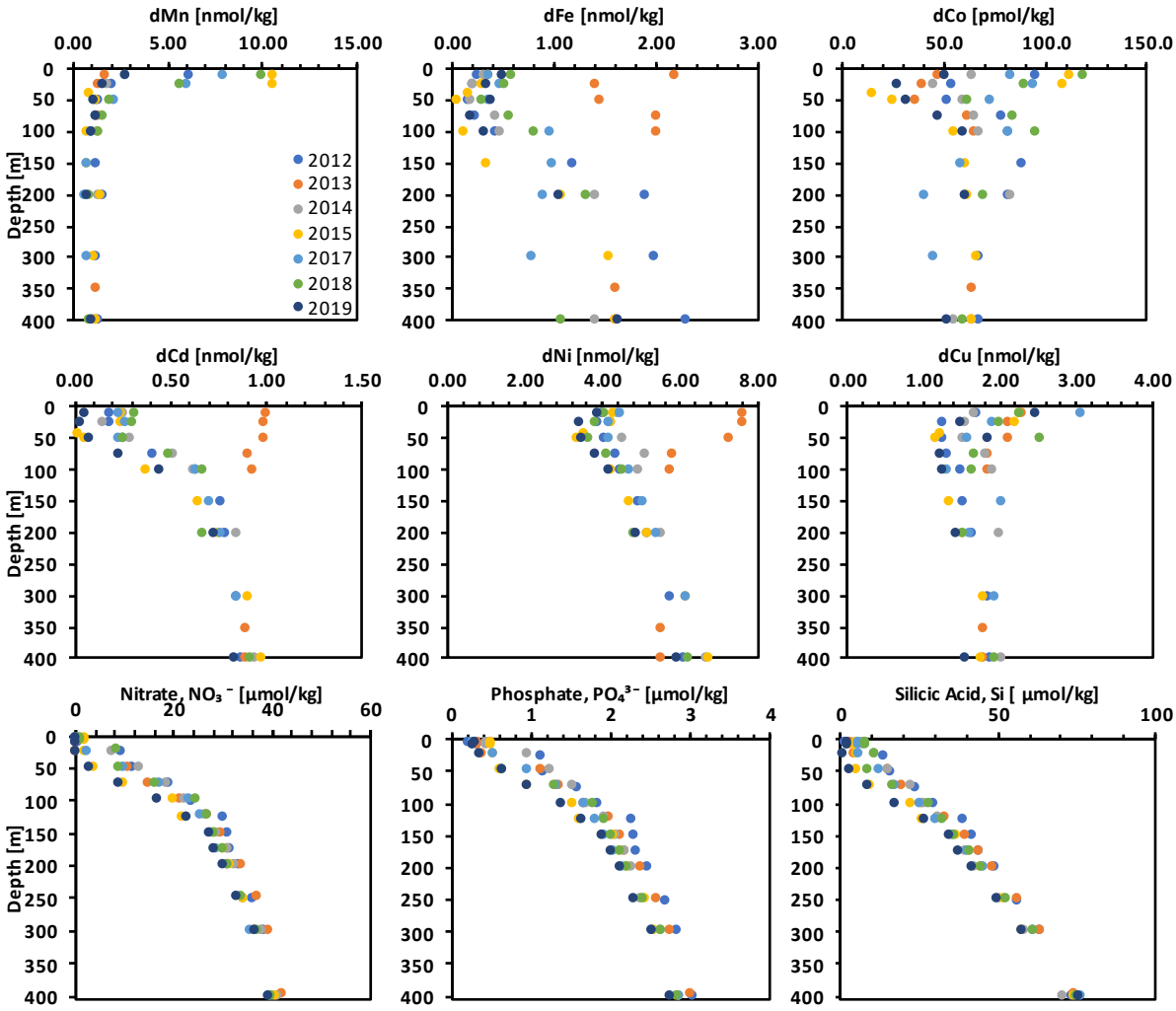

Figure 24. P4 summer trace metal and macronutrient depth profiles (0-400m) at OSP. Summer trace metal and macronutrient values range from 2012-2019. Data points with bordering red are flagged for contamination.

3.3.3 Trace metal mixed layer concentrations

Offshore – The ML trace metal concentrations observed in the winter of 2012 were similar to those in 2013 with the exception of dFe, dCo, and dCu. ML concentrations of dMn, dNi, and dCd were in the range of 0.95 to 1.15 nmol dMn/kg, 4.23 to 5.53 nmol dNi/kg, and 0.25 to 0.462 nmol dCd/kg, respectively (Fig. 25). The dFe, dCo, and dCu were distinct, with elevated concentrations of dFe at P20 in 2013 (0.34 nmol dFe/kg) and diminished concentrations of dCo and dCd in the range of 39.7 to 42.2 pmol dCo/kg and 0.75-0.94 nmol dCu/kg, respectively. The summer 2013 dMn, dFe, dNi, dCu were elevated compared to 2012 with values in the range of 1.07 to 1.76 nmol dMn/kg, 0.08 to 0.017 nmol dFe/kg, and 1.45 to1.88 nmol dCu/kg, while dCo and dCd diminished slightly at stations P20 and P16 with values 45.7 and 19.3 pmol dCo/kg, and 0.19 and 0.03 nmol dCd/kg, respectively (Fig.26). During the winter of 2014 the trace metal concentrations were within 2012 and 2013 concentrations, with the exception of dCd (0.16-0.24 nmol/kg) which was reduced by half compared to 2012 and 2013. The summer of 2014 metals were diminished to ranges 0.53-0.807 nmol dMn/kg, 6.7-17.4 pmol dCo/kg,

3.54-4.26 nmol dNi/kg, 1.32-1.40 nmol dCu/kg, and 0.003-0.016 nmol dCd/kg, while dFe varied from 0.03-0.94 nmol dFe/kg.

The second winter of the marine heatwave, 2015, the dMn, dFe, dCo, and dCd were lower than in winter 2014 and in the range of 0.76 to 1.00 nmol dMn/kg, 0.03-0.053 nmol dFe/kg, 13.6-29.7 pmol dCo/kg, and 0.07-0.257 nmol dCd/kg, respectively (Fig.25). The summer resulted in the reduction of the same trace metals at stations P26 and P20, while P16 had some elevated concentrations (Fig.26). P26 and P20 metals ranged from 0.70-0.73 nmol dMn/kg, 0.003-0.04 nmol dFe/kg, 10.0-15.4 pmol dCo/kg, and 0.01-0.04 nmol dCd/kg, and those at P16 were 2.72 nmol dMn/kg, 0.048 nmol/kg dFe, 38.6 pmol dCo/kg, and 0.036 nmol dCd/kg. The summers of 2017 and 2018 trace metals were more typical compared to non-marine heatwave years, but did not fully rebound to those concentrations. The summer 2019 offshore had another significant reduction in concentrations where values ranged 0.59-0.69 nmol dMn/kg, 0.06-0.11 nmol dFe/kg, 9.6-14.4 pmol dCo/kg, 2.8-3.42 nmol dNi/kg, 1.165-1.41 nmol dCu/kg, and 0.01-0.02 nmol dCd/kg.

Coastal – As there is no data for winter of 2013, the concentrations of 2012 will be the focus. The 2012 concentrations of dMn, dFe, dCo, dNi, dCu, and dCd ranged from 0.99-2.47 nmol dMn/kg, 0.54-0.62 nmol dFe/kg, 38.0-68.1 pmol dCo/kg, 4.04-4.57 nmol dNi/kg, 1.41-1.62 nmol dCu/kg, and 0.16-0.21 nmol dCd/kg, respectively (Fig.25). In the coastal region, there was variation between P12 and P4 in the summer of 2012 and 2013 (no data available for 2013 P4) (Fig.26). The P12 ML concentrations ranged from 1.13-6.08 nmol dMn/kg, 0.06-0.24 nmol dFe/kg, 53.9-95.0 pmol dCo/kg, 4.01-4.51 nmol dNi/kg, 1.54-1.67 nmol dCu/kg, and 0.18-0.31 nmol dCd/kg. The species dMn and dFe were elevated while dCo, dNi, dCu, and dCd were diminished compared to 2012. Coastal station P12 and P4 varied in the winter and summer of both 2014 and 2015. At P12, species values in winter 2014 were very similar for all with the exception of dFe, which dropped to 0.15 nmol dFe/kg. The summer growing season resulted in ML concentrations similar to that of 2013, with again, the exception of dFe which was lower at 0.08 nmol dFe/kg. The winter of 2015 experienced diminishing concentrations for dCo (20.3 pmol dCo/kg), dCd (0.05 nmol dCd/kg), and dCu (0.94 nmol dCu/kg) while those of dMn (1.25 nmol dMn/kg), dFe (0.30 nmol dFe/kg), and dNi (4.65 nmol dNi/kg) were marginally elevated compared to 2014 winter. The summer of 2015 had the lowest concentrations of dMn, dCo, dCd, and dFe of 0.74 nmol dMn/kg, 8.1 pmol dCo/kg, 0.006 nmol dCd/kg, and 0.049 nmol dFe/kg, respectively.

At P4, winter of 2014, species concentrations increased compared to 2012 at 4.56 nmol dMn/kg, 106.9 pmol dCo/kg, 0.26 nmol dCd/kg, 0.69 nmol dFe/kg, 4.24 nmol dNi/kg, and 2.70 nmol dCu/kg (Fig.25). The winter of 2015 had significant decrease in dMn, dCd, and dCu compared to previous with values 2.64 nmol dMn/kg, 0.12 nmol dCd/kg, and 1.15 nmol dCu/kg, respectively. The summer concentrations during 2014 and 2015 were similar ranging with the exception of dMn and dCo (Fig.26). Concentrations in 2014 and 2015 were 2.80 and 10.57 nmol dMn/kg, 63.5 and 109.8 pmol dCo/kg, 0.25 and 0.25 nmol dCd/kg, 0.32 and 0.32 nmol dFe/kg, 4.38 and 4.24 nmol dNi/kg, and 1.66 and 2.21 nmol dCu/kg, respectively. The summer of 2017 and 2018 again varied between the two stations, but there was a regional increase in ML trace metal concentrations after 2015. The summer of 2019 dMn, dFe, dCo, and dCu ranged from 1.65-2.72 nmol dMn/kg, 0.149-0.48 nmol dFe/kg, 24.2-50.5 pmol dCo/kg, 1.47-2.47 nmol dCu/kg, respectively, while dNi and dCd diminished significantly ranging 3.75-3.84 nmol dNi/kg and 0.03-0.06 nmol dCd/kg.

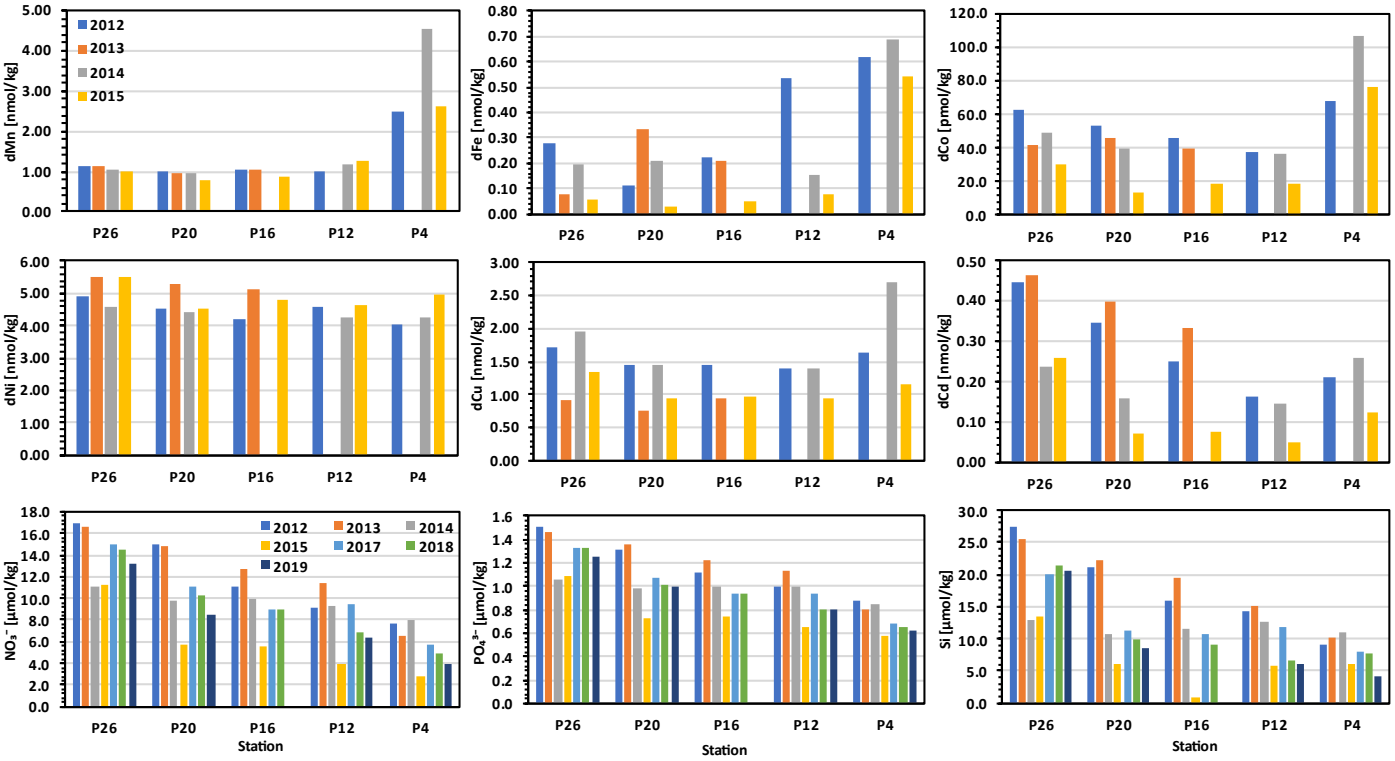

Figure 25. Winter mixed layer (ML) trace metal and macronutrient average concentrations from the offshore (stations P26, P20, P16) to the coastal (stations P12, P4) regions of the subarctic northeast Pacific Ocean. Winter trace metal values range from 2012-2014, while winter macronutrient values range from 2012-2019. No trace metal ML averages were available for P16 2014, P12 2013, and P4 2013 due to suspected sample contamination.

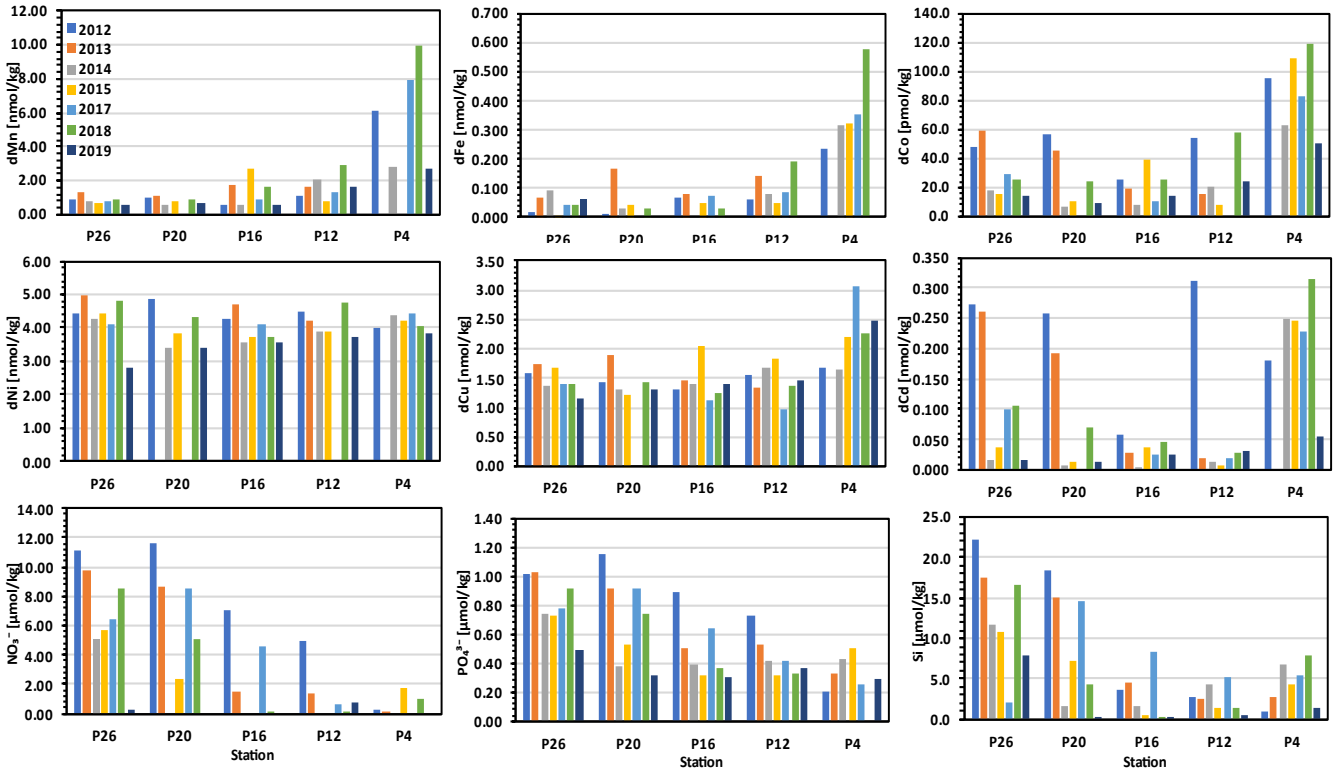

Figure 26. Summer mixed layer (ML) trace metal and macronutrient average concentrations from the offshore (stations P26, P20, P16) to the coastal (stations P12, P4) regions of the subarctic northeast Pacific Ocean. Trace metal and macronutrient values range from 2012-2019. No trace metals averages were available for P20 2017 all trace metals, P16 2014 and 2019 dFe, P12 2017 dCo, dNi, and P4 2013 all trace metals due to suspected sample contamination.

3.3.4 Macronutrient and net community production mixed layer concentration

Offshore – The winters and summers of 2012 and 2013 NO_3^-, PO_4^{3-}, and Si ML concentrations were nutrient replete. The winter and summer 2012 ML concentrations were nutrient replete (Fig.25,26). The winter and summer 2012 ML concentrations were in the range 11.2 to 16.9 µmol NO_3^-/kg, 1.1-1.5 µmol PO_4^{3-}/kg, and 15.9-27.3 µmol Si/kg, and 7.1-11.7 µmol NO_3^-/kg, 0.9-1.16 µmol PO_4^{3-}/kg, and 18.4-22.2 µmol Si/kg, respectively. The 2013 concentrations were very similar, with the exception of the summer values that diminished to 1.5-9.80 µmol NO_3^-/kg, 0.5-1.04 µmol PO_4^{3-}/kg, and 4.5-17.5 µmol Si/kg. The 2012 NCP was notably lower than 2013 with values ranging from 22.3-38.1 µmol C/m³ in 2012 and 40.1-74.3 µmol C/m³ in 2013. The winters and summers of 2014 and 2015 NO_3^-, PO_4^{3-}, and Si were much lower than values observed in 2012 or 2013. Winter 2014 and 2015 values ranged from 9.8-11.0 µmol NO_3^-/kg, 1.0-1.1 µmol PO_4^{3-}/kg, and 10.8-12.9 µmol Si/kg, and 5.6-11.3 µmol NO_3^-/kg, 0.7-1.1 µmol PO_4^{3-}/kg, and 0.7-13.5 µmol Si/kg, respectively. The summer 2014 and 2015 values ranged from 0.0-5.02 µmol NO_3^-/kg, 0.38-0.74 µmol PO_4^{3-}/kg, 1.6-11.6 µmol Si/kg, and 0.0-5.75 µmol NO_3^-/kg, 0.3-0.74 µmol PO_4^{3-}/kg, and 0.5-10.8 µmol Si/kg, respectively. The NCP in 2014 was 39.5-65.3 µmol C/m³, while NCP dropped substantially in 2015 at 21.8-36.9 µmol C/m³.

The 2017 and 2018 winter NO_3^-, PO_4^{3-}, and Si ML concentrations rebounded and had very similar values ranging from 8.5-15.0 µmol NO_3^-/kg, 0.9-1.3 µmol PO_4^{3-}/kg, and 9.0-21.4 µmol Si/kg, respectively (Fig.25,26). The summer macronutrient concentrations and NCP were quite different between years, with 2017 values 4.6-8.5 µmol NO_3^-/kg, 0.60-0.92 µmol PO_4^{3-}/kg, and 2.01-14.6 µmol Si/kg, and 16.7-56.4 µmol C/m³, respectively (Fig.27). The summer 2018 offshore had values 0.0-8.5 µmol NO_3^-/kg, 0.40-0.91 µmol PO_4^{3-}/kg, and 0.4-16.53 µmol Si/kg, and NCP values of 33.8-59.5 µmol C/m³. The winter and summer 2019 values ranged from 8.5-13.2 µmol NO_3^-/kg, 1.0-1.2 µmol PO_4^{3-}/kg, 8.4-20.45 µmol Si/kg, and 0-0.26 µmol NO_3^-/kg, 0.30-0.49 µmol PO_4^{3-}/kg, and 0.3-7.93 µmol Si/kg, respectively. The respective offshore NCP varied from 56.2-85.2 µmol C/m³.

Coastal – The coastal stations, P12 and P4, differed from one another and the results will be explained separately (Fig.25,26). Similar to P16, the winter P12 macronutrients were higher in 2013 than 2012 with NO_3^-, PO_4^{3-}, and Si values of 11.4 µmol NO_3^-/kg, 1.1 µmol PO_4^{3-}/kg, and 15.0 µmol Si/kg, respectively. The summer of 2013 observed significant drawdown of NO_3 compared to 2012, resulting in NCP of 65.8 µmol C/m³. The winter of 2014 NO_3^-, PO_4^{3-}, and Si were diminished relative to 2012/13, but NCP was sustained at 61.2 µmol C/m³. NO_3^- and PO_4^{3-} were reduced to 0 µmol NO_3^-/kg and 0.4 µmol PO_4^{3-}/kg, respectively, while Si was only drawdown to 4.3 µmol Si/kg. ML concentrations were significantly diminished during the winter of 2015. The macronutrient concentrations were reduced to 4.0 µmol NO_3^-/kg, 0.7 PO_4^{3-}µmol/kg, and 5.9 µmol Si/kg. The summer resulted in NCP dropping to 26.4 µmol C/m³, due to low winter ML NO_3^- before the growing season. While the winter of 2017 ML macronutrients were replenished, the following winters 2018 and 2019 began to diminish thereafter. Productivity during the summers followed the same trend, where NCP rebounded in 2017 (58.3 µmol C/m³) and diminished the following summers of 2018 (39.5 µmol C/m³) and 2019 (37.6 µmol C/m³).

The years 2012 and 2013 at P4 followed suit of 'normal' conditions with winter NO_3^-, PO_4^{3-}, and Si concentrations ranging from 6.5-7.6 µmol NO_3^-/kg, 0.8-0.9 µmol PO_4^{3-}/kg, and 9.1-10.2 µmol Si/kg, respectively (Fig.25). The summer months were NO_3 limited resulting in NCP levels of 48.4 µmol C/m³ in 2012 and 42.0 µmol C/m³ in 2013 (Fig.26). The winter of 2014 was met with an increase in NO_3 (8.0 µmol/kg) and Si (11.0 µmol/kg) ML concentrations, resulting in increased productivity during the summer growing season. The NCP was the highest from 2012-2019 at 52.8 µmol C/m³, with NO_3^- completely consumed. The winter of 2015 was deplete in NO_3^-, reaching only 2.8 µmol NO_3^-/kg. Typically, P4 becomes NO_3^- limited during the growing season, but in 2015 the macronutrients were

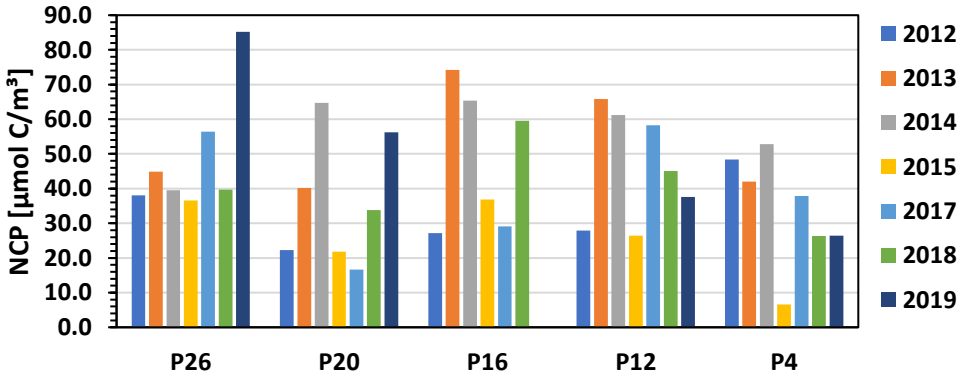

Figure 27. Net community production (NCP) within the mixed layer from the offshore (stations P26, P20, P16) to the coastal (stations P12, P4) regions of the subarctic northeast Pacific Ocean. Values range from 2012-2019. Note no data available NCP at P16 in 2019.

hardly consumed resulting in low NCP (6.6 µmol C/m³). The years 2017-2019 followed the trend at P12, with replenished macronutrient concentrations in 2017 and diminished concentrations thereafter resulting in consistently decreasing NCP.

3.4 Discussion

The subarctic NE Pacific can be divided into two main biogeochemical provinces: an offshore area where primary production is seasonally Fe-limited and more inshore waters where NO_3^- availability tends to limit phytoplankton growth (Martin and Fitzwater 1988; Whitney *et al.* 1998). For this investigation of the impacts of marine heatwaves on trace metal distributions, the stations P26, P20, and P16 are categorized as typically Fe-limited and labelled as *offshore*, while P12 and P4 are categorized as NO_3^- limited, and *coastal* (Boyd et a. 1998).

3.4.1 Marine heatwave effects during 2014

During the winter of 2014, the subarctic NE Pacific experienced anomalously high sea surface temperatures. The conditions were induced by a high-pressure ridge blocking strong, southwesterly winter winds resulting in shallowing and stratification of the ML brought on by weakened storm mixing (Bond *et al.* 2015; Whitney *et al.* 2019). The hydrography, trace metal and macronutrient distributions of 2014 are discussed to determine the effects the first year of the marine heatwave had on NCP and productivity in the offshore and coastal subarctic northeast Pacific. While these effects were observed in the offshore regions, the coastal stations were less affected by the changing conditions. In the offshore region, winter ML shallowing diminished mixing of deeper, more nutrient replete waters to the surface. This was observed clearly in the ML average concentrations of NO_3^- , PO_4^{3-}, and Si which were 1.2 to 1.5-fold lower than the winter 2012 and 2013 ML averages. Most ML trace metal concentrations were relatively unaffected, but there was a clear decrease in dCd. Without significant atmospheric or advective source terms the decrease of dCd supports the hypothesis that diminished winter mixing led to lower amounts of vertical nutrient resupply (Conway & John 2015). In the coastal region, the sea surface temperatures and ML depths were similar to previous years, as well as the macronutrient and some trace metal ML concentrations. While there was no ML trace metal data available for 2013, dMn and dCo concentrations were high at P4 in 2014 likely reflecting the importance of coastal river and continental shelf inputs.

The NCP and the nutrient ratios ($\Delta Si:\Delta NO_3^-$ and $Cd:PO_4^{3-}$) are discussed to estimate the overall community productivity and that contributed by diatoms. Diatoms have an absolute requirement for Si, and have Cd and Si cellular quotas that tend to increase under Fe-limitation (Hutchins and Bruland 1998; Brzezinski *et al.* 2005; Marchetti *et al.* 2006; Cullen *et al.* 2009). The NCP of P26 was similar to previous years, while P20 and P16 showed a substantial increase in productivity. ML NO_3^- was completely consumed (0 µmol/kg) at both stations, while trace metals dMn, dFe, dCo, and dCd were diminished. P26 had diminished concentrations of dFe, dCo and dCd, but the loss of NO_3^-, and estimated NCP, was comparable to previous years. The nutrient ratios $\Delta Si:\Delta NO_3^-$ and $Cd:PO_4^{3-}$ were both low at P26, suggesting a shift in the phytoplankton community composition towards smaller, more low nutrient adapted species that may have maintained 2014 NCP (Hutchins and Bruland 1998; Cullen *et al.* 2003). At the other two stations, P20 and P16, $\Delta Si:\Delta NO_3$ ratios were typical (approx. 1 µmol/µmol) while $Cd:PO_4^{3-}$ ratios were similarly low to P26 due to an increase in PO_4^{3-} consumption relative to DCd.

3.4.2 Marine heatwave effects during 2015

In late 2014 and early 2015, a weak El Niño sustained warm SST's, ML shallowing, and stratification continuing the marine heatwave in the study region (Di Lorenzo and Mantua 2016). The same investigation performed on the 2014 data was done for 2015 hydrography, and trace metal and macronutrient concentrations. The results are used to determine differences and similarities between the first year (2014) and the second year (2015) of the marine heatwave – did their distributions behave similarly and what impact did this have on NCP and phytoplankton community composition. For 2015, winter water properties are discussed as offshore and coastal, as previously done, and summer water properties are discussed in 3 groups: P26 and P20, P16 and P12, and P4 due to marked differences between the coastal stations.

Unlike 2014, both the offshore and coastal stations in the winter of 2015 were affected by increased winter ML warming and shallowing. The macronutrient concentrations at P26 during the winter 2015 were similar to those of 2014, while stations P20 and P16 winter NO_3^- and Si concentrations approximately 2-fold lower than 2014. The offshore TM concentrations varied between stations. Most notably, dCo, dCd, dFe, and dCu in the offshore were diminished compared to 2014, with the exception of dCd at P26, which was marginally higher than the previous winter. While dNi ML concentrations were similar to previous years, the difference between winter and summer dNi inventories suggest that Ni utilization was elevated in 2015 relative to other years (Morel *et al.* 2003; Dupont *et al.* 2010). The coastal stations macronutrients were diminished significantly compared to previous years, with the lowest ML averages in the time series. The TM concentrations inshore were similarly diminished in dCo, dCd, and dCu. The coastal dFe had more variation between stations, where P12 dFe increased and P4 dFe decreased compared to previous years.

In the summer of 2015, NCP and macronutrient concentrations at P26 and P20 varied, where P26 values were similar and those at P20 were diminished compared to 2014. P26 TM concentrations were comparable to 2014. At P20, the dCo and dCd concentrations were similar to 2012/13. Stations P16 and P12 had anomalously low S during the summer 2015, while P16 also had low σ_T, indicative of the coastal water containing eddy passing through (Whitney and Robert 2002; Crawford 2005). The NCP of both stations dropped significantly compared to the previous year with depleted NO_3^- (0 µmol/kg) and reduced Si values. At P16, summer dMn and dCo were the most elevated in relation to other years, possibly indicative of inputs from the eddy as Mn can act as a tracer for waters that have been influenced by the ocean margin and proximity to continental sources of trace elements (Landing and Bruland 1980; Bishop and Fleisher 1987; Lam *et al.* 2006). Presence of the eddy was also noted in the post cruise report from the 2015 August Line P summary, by sea surface height anomaly data (Robert 2015). On the other hand, station P12 had very low summer dMn, dCo, and dCd but similar dFe to P16. The conditions at P4 were unexpected for a marine heatwave. The summer P4 ML was the deepest (29 m), the coldest (13.4°C), and most dense (24.10 kg/m^3) in relation to 2012-2019 summer seasons. Based on TM data, the dMn and dCo were notably high indicating input from the continent (Biller and Bruland 2013). The other P4 summer TM's and macronutrients NO_3^- and PO_4^{3-} were observed to have elevated concentrations. The NCP of P4 was quite low due to higher level of summer NO_3^- with little drawdown during the growing season, as concentrations in the spring of 2015 were low. By the summer, cooler and denser waters from the continent were transported to the ML, resulting in significant injection of macronutrients and TM's.

As nutrient and metal:nutrient ratios can provide information about the presence of diatoms and Fe-limitation, the $\Delta Si:\Delta NO_3^-$ and $Cd:PO_4^{3-}$ are compared to values to 2014. At P26, the summer 2015 $Cd:PO_4^{3-}$ ratio was comparable to 2014 and the $\Delta Si:\Delta NO_3^-$ was marginally higher. Station P20 had similar summer $Cd:PO_4^{3-}$ to P26, while the $\Delta Si:\Delta NO_3^-$ was negative due to an increase in Si from winter to summer. In these offshore regions the ratios suggest that the phytoplankton community shifted towards smaller species, especially at P20 where Si remained high, suggesting that diatom growth was less prevalent. Station P16 and P12 had $\Delta Si:\Delta NO_3^-$ ratios of around 1.1 while P16 had the higher summer $Cd: PO_4^{3-}$ due to the increase in dCd at the station. The observed ratios suggest typical consumption of nutrients by a community with some larger phytoplankton species present such as diatoms. The ratios at P4 might not provide much insight to the phytoplankton community composition given the addition of nutrients from continental sources and the influence of coastal upwelling during the summer, but resulted in elevated levels of both $Cd: PO_4^{3-}$ and $\Delta Si:\Delta NO_3^-$ ratios. We cannot hypothesize the general phytoplankton community composition because of the unknown timing of nutrient input to the station's ML.

3.4.3 Marine heatwave effects during 2019

In the autumn of 2018, marine heatwave conditions prevailed in the GOA and continued through to the winter and summer of 2019 (Zador *et al.* 2019). During the winter of 2019, the Aleutian Low was weakened and resulted in reduced wind forcing and elevated sea surface temperatures that were sustained through the spring and summer seasons. The length of this time series has allowed for observation of two separate marine heatwave events. As the marine heatwave of 2019 was initiated by high sea level pressure, akin to 2014 and 2015, the results of 2019 help to identify key processes and patterns resulting from marine heatwave conditions, while simultaneously presenting contrasting effects on the system. While trace metal concentrations were not sampled for the winter 2019, hydrographic and macronutrient concentrations are used to observe similarities and differences in relation to 2014 and 2015. In the offshore subarctic northeast Pacific, the 2019 winter ML T was not as warm as T's observed in 2014 and 2015, but were evidently higher than previous, non-heatwave years. The winter NO_3^- and PO_4^{3-} ML concentrations were similarly low to those in 2014, while Si concentrations were elevated at P26 and diminished at P20. In the coastal region, station P12 had winter T, S and σ_T similar to 2014, while P4 had warmer and more saline winter waters. No trace metal data was available for the winter of 2019.

In the summer of 2019, offshore ML shallowing was combined with T's above or comparable to those of 2014 and 2015. At station P26 the NCP was the highest in the timeseries and P20 NCP was similar to 2014. The macronutrient concentrations were markedly low, causing NO_3^- to become the limiting nutrient rather than Fe. Evidence of such limitation was observed at P26, where dNi concentrations were 1.5-fold lower than previous years, suggesting that Ni may have been used in the assimilation of urea as a source of nitrogen (Morel *et al.* 2003; Dupont *et al.* 2010) indicative of regenerated rather than new production. At P26, other TM's such as dMn, dCo, and dCd were the lowest measured for the station across the time series. The TM concentrations at P20 and P16 approached, but did not diminish to values observed in 2014, with elevated dFe at P20. In the coastal region, T's at P12 were more similar to 2013/2015 while those at P4 were the highest in the time series. The NCP was relatively low for the region due to low winter NO_3^- concentrations resulting in early onset NO_3^- limitation. The TM concentrations observed at P12 appeared to be relatively consistent compared

to previous years, with natural variations. At P4, dMn, dCo, dNi, and dCd were the lowest for the station as a result of reduced winter mixing and subsequent shallowing of the winter ML.

The nutrient ratios of 2019 will be discussed to compare values to 2014 and 2015, for reasons previously stated above. In the offshore region, the summer Cd: PO_4^{3-} ratios were similarly low to 2014 and 2015 at P26 and P20 with $\Delta Si:\Delta NO_3^-$ ratios around 1. Along with the high NCP of these stations, the data suggests that the phytoplankton communities were likely dominated by larger phytoplankton such as diatoms (Hutchins and Bruland 1998). In the coastal region, P12 summer $Cd:PO_4^{3-}$ was similar to previous years with $\Delta Si:\Delta NO_3^-$ marginally lower than 1. Station P4 had the lowest summer $Cd:PO_4^{3-}$ for the station and a similar $\Delta Si:\Delta NO_3^-$ to 2014. The results suggest that the phytoplankton community at P4 was dominated by diatoms until acute NO_3^- limitation may have selected for a smaller cell-size phytoplankton community.

3.4.4 Anomalous offshore productivity of summer 2019

The offshore stations P26 and P20 experienced periods of high productivity given increased NCP and unusual drawdown of macronutrients and TM's for the region. As the winter 2019 conditions were similar to the marine heatwave of 2014 and 2015, one would assume similar effects would extend into the summer resulting in decreased NCP and reduced (but not limited) macronutrient concentrations. As discussed above, NCP increased such that NO_3^- became the limiting nutrient in the typically high nitrate low chlorophyll subarctic northeast Pacific.

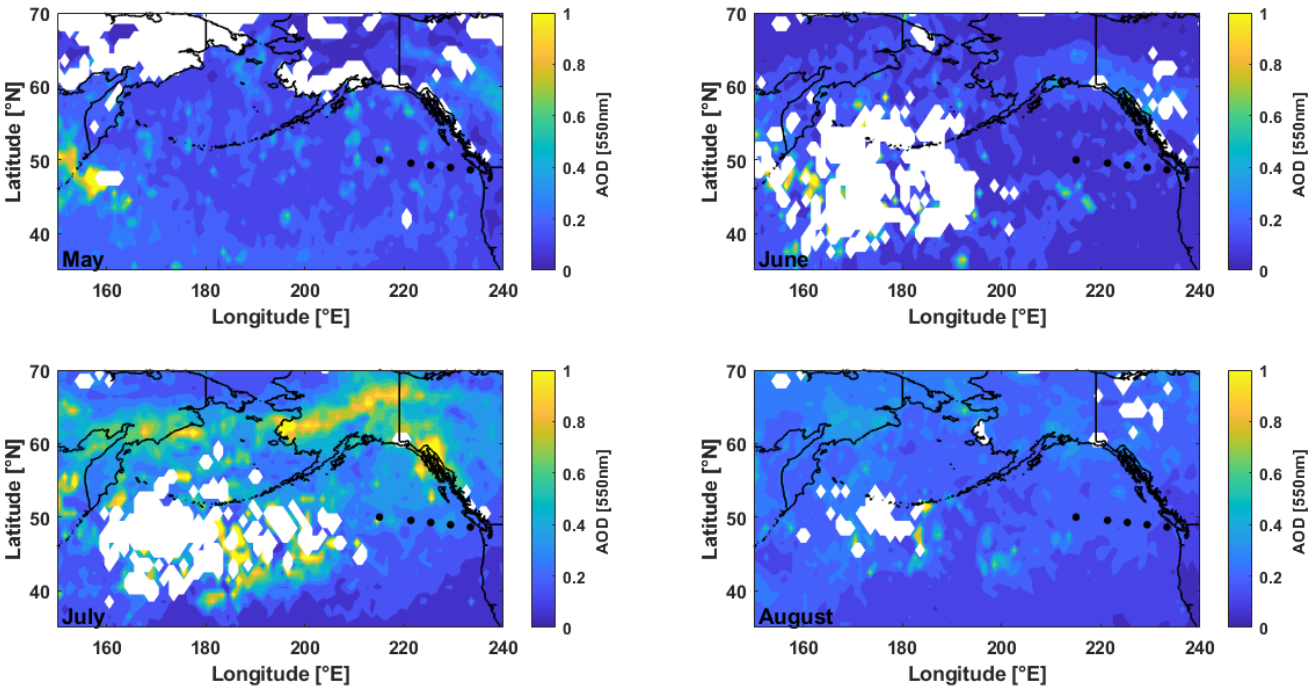

Figure 28. Monthly mean aerosol optical depth (AOD) at 550nm in the subarctic NE Pacific in May, June, July, and August 2019 (months indicated in bottom left corner of figures). Data collected from NASA's Earthdata MODIS-Aqua, 1° resolution. Data was gathered from NASA GIOVANNI available at https://giovanni.gsf.

Here, external effects on trace metal and macronutrient concentrations are explored to determine the source of the high productivity during a marine heatwave. As Fe typically limits the growth and productivity of phytoplankton in the offshore HNLC, it is probable that Fe was replenished (Martin and Gordon 1988; Maldonado *et al.* 1999; Boyd *et al*. 2005). Atmospheric inputs are recognized as an important source of Fe to the offshore (Martin 1990; Martin *et al.* 1989; Duce and Tindall 1991), and therefore, aerosolized dust concentrations were examined using aerosol optical depth (550 nm) from NASA's Giovanni MODIS in the North Pacific, Fig. 28. The subarctic North Pacific during July 2019 was clearly inundated with aerosolized dust, with continental hotspots located in Alaska, coastal Alaska/British Columbia (BC), and Asia. The point sources of these hotspots could have originated from forest fire, glacial dust, and continental dust. In Alaska, the Chalkyitsik forest fire complex began in late June and early July and burned a minimum of 203,000 hectares of forest, with local PM2.5 values typically above 350 $\mu g/m^3$ (McDonald 2019). New temperature records were set in Alaska in 2019, with lower than average 2018/2019 winter snowfall (The Alaska Climate Research Centre 2019). These events could have led to increased glacial melting and glacial dust transport off of the western coast of Alaska and northern BC, Fig. 28. Continental dust originating from Asia can be transported eastward in the spring, but the probability of summer transport diminishes due to wind direction (Duce and Tindall 1991;Boyd *et al.* 1998). Although our study cannot predict the exact aerosol source, there is without a doubt a large plume of dust in the subarctic northeast Pacific that fed the offshore stations P26 and P20. With the anomalously high-pressure system that overlaid the region, it is possible that winds were stronger in the northwesterly direction providing aerosols from North America rather than Asia.

3.4.5 Not all marine heatwaves are created equally

The subarctic northeast Pacific has experienced two marine heatwaves in recent years. The first, colloquially known as the 'Blob', warmed sea surfaces across the GOA from winter 2013/2014 into late 2016 (Bond *et al.* 2015; Whitney *et al.* 2019). A consequence of heatwave conditions is that the ML tends to shoal and stratify as density decreases at the surface (Whitney *et al.* 1998). We documented here that both macronutrient and trace metal concentrations are diminished at the beginning of the spring bloom, most likely in response to weaker upward transport of nutrient rich waters during the winter (Whitney *et al.* 1998; Whitney and Freeland 1999). Due to changes in nutrient distributions, the Blob had marked effects on the phytoplankton community composition, its productivity, and likely the function of the BCP (Denman 2008). The second marine heatwave, which began in late 2018, was similar in its effect on shallowing and stratification on the winter ML during 2019. While we did not have winter TM data to observe distributions, the winter macronutrients did diminish in the ML similarly to concentrations observed in 2014/2015. Atmospheric conditions in 2019 may have helped alleviate nutrient limitation of phytoplankton compared to the previous heatwave, as observed in Fig.28. The subarctic northeast Pacific was flooded with aerosol particles in the summer of 2019 with external sources from either fire smoke, glacial dust, or continental dust. As Fe enrichment experiments have shown that external additions of Fe can increase productivity (Martin *et al.* 1989; Boyd *et al.* 2004), natural sources of Fe from aerosols can have a similar effect. Hamme *et al.* 2010 observed increased productivity and chlorophyll a concentrations in the subarctic northeast Pacific following a volcanic eruption. Crusius *et al.* 2011 determined that glacial flour from coastal Alaskan glaciers are an important source of Fe to the GOA, providing Fe to the HNLC regions. As marine heatwaves influence the transport of nutrients to the ML internally, it is important to note that not all marine heatwaves are created equally, and external inputs can have an even greater effect on the productivity of the system.

3.5. Conclusion

The effects of marine heatwaves on TM distributions is widely unknown. Our study analyzed data collected along the Line P Timeseries to create a TM specific timeseries from 2012 to 2019 to observe any changes brought on by the 2013-2016 Blob and the 2019 North Pacific marine heatwave. The first and second year of the Blob, 2014 and 2015, were different in their own respects. During 2014 in the offshore region, ML shallowing and stratification reduced the transport of TM to the ML, resulting in low stocks for the summer growing season, a shift to smaller phytoplankton in the community, and sustained or increased NCP. The coastal region appeared to be unaffected by the first year of the marine heatwave, with nutrient concentrations and NCP similar to previous years. The second year of the marine heatwave, 2015, the offshore was characterized by a stronger reduction in TM concentrations in the ML, low NCP, and a potentially stronger shift to smaller phytoplankton. The stations closer to the coast, P16, P12, and P4 all reacted differently to the changes. An eddy passed through P16 during the summer, changing the TM and macronutrient distributions, but still resulting in low NCP compared to 2014. P12 had diminished ML nutrient concentrations in the winter that resulted in lower NCP and reduced TM concentrations. The most coastal station, P4, likely experienced transport of all nutrients to the ML with increased summer values compared to the spring, as well as a deeper, cooler ML. The 2019 marine heatwave resulted in similar reduction of nutrients to the winter ML, but the offshore stations productivity increased due to external inputs of Fe. We have observed that while marine heatwaves have similar effects on internal nutrient transport to the ML, external atmospheric inputs can have a great effect on the productivity of the system.

Chapter 4: Conclusions

Over the last 65 years, large scale increases in the heat content of the world ocean have occurred (Barnett *et al.* 2001). Changes in upper-ocean heat content is a critical variable to constrain in order to understand ongoing climate change resulting from anthropogenic CO_2 emissions (Tesdal and Abernathey 2021). The resulting variability in seasonal density stratification will likely affect the vertical flux of nutrients and essential trace elements that influence marine microbe community structure and ecosystem level productivity (Hayashida *et al.* 2020; Gao *et a.*2021; Gupta *et al.* 2020)). Ecosystem services and marine fisheries production are likely to be negatively impacted. In the subarctic northeast Pacific changes in upper-ocean heat content have been manifest as two high-temperature anomalies, or marine heatwaves, in the last decade. Here, I have presented dMn, dFe, dCo, dNi, dCu, and dCd within the subarctic northeast Pacific Ocean from 2012 to 2019 to investigate variability in essential trace metal nutrients that coincided with the 2014-2015 and 2019 marine heatwaves. Not only does this thesis provide insight into the variability of trace metal distributions, it also provides a novel time series of trace metal distributions along a transect covering productive coastal and Fe-limited high nutrient-low chlorophyll waters spanning eight years. This chapter will summarize the major findings of Chapter 2 and Chapter 3, and provide suggestions for future work.

4.1 ***Chapter 2****: Relationship between surface dissolved iron inventories and net community production during a marine heatwave in the subarctic northeast Pacific*

Chapter 2 investigated the effects of the 2014-2015 marine heatwave, colloquially referred to as the Blob, and its effects on dFe in relation to NCP and phytoplankton community structure. During the late winter of 2013 and early 2014, sea surface temperatures increased due to reduced winter winds brought on by anomalously high sea level pressure (Bond *et al.* 2015; Whitney 2015). The high sea surface temperatures persisted in the offshore region until the end of 2015, and into 2016 for the coast. Observations synthesized by Bif *et al.* 2019 determined that NCP in the offshore region of the subarctic northeast Pacific, remained unchanged in the summer of 2014 relative to 2012-2013, but was dramatically reduced in 2015. The study hypothesized the efficiency of Fe recycling and retention in the upper-ocean likely modulated NCP, where Fe was retained in 2014 relative to 2015.

With collected hydrographic (σ_T, T, S), macronutrient (NO_3^-, PO_4^{3-}, Si), and trace metal data (dFe, dCd, dCo) from Ocean Station PAPA (OSP), I was able to make key observations to test whether the Blob had affected Fe recycling and retention in the ML, how that related to local NCP, and if there were any subsequent shifts in the phytoplankton community. Calculations of the mixed layer depth (MLD) using density profiles demonstrated that shallowing of the winter mixed layer (ML) in February 2014 and 2015 was more pronounced than in years immediately preceding the Blob. Winter shallowing was limited by diminished winter storm mixing and resulting ML concentrations of NO_3^-, PO_4^{3-}, and Si were lower during both winter 2014 and 2015, but not to levels that are known to directly limit NCP. Calculated NCP at OSP, however, was maintained relative to preceding years during 2014 and decreased in 2015. These calculations differ from the dramatic drop in NCP reported by Bif *et al.* 2019. The differences between the studies are likely an artifact of resolution and depth differences, as this study utilized shipboard observations over the ML, while Bif *et al.* 2019 utilized autonomous float to depth integrate NCP over 75m. In the winter of 2014, the ML dFe was the highest compared to previous years (2012/13), while ML dFe in 2015 was much lower. There was a clear correlation between winter dFe and NCP, with sustained dFe and NCP in 2014 and diminished dFe and NCP in 2015. While the dFe

concentrations were higher in winter 2014, they were only slightly elevated compared to 2012. By comparing dFe depth profiles in the upper 400m to dCd and dCo, it was clear that while dCd was significantly lower in response to winter ML shallowing in 2014, dFe and dCo were similar to 2012-13 winters until the second winter of the marine heatwave. Clearly there are a variety and distinct set of process that control different trace metal sources and sinks in the mixed layer along Line P.

Why might dFe (and dCo) concentrations be less sensitive and more resilient to winter ML shallowing, stratification and diminished vertical fluxes up until the winter of 2015? Natural variation could have been a possibility, but as it is not easily proven, other inputs of dFe were examined. As horizontal transport of the North Pacific Current and atmospheric deposition were ruled out, an isolated feature in the pycnocline during January 2014 could have contributed to vertical transport of nutrients to the ML.

Changes in the phytoplankton community composition and structure were estimated using changes in nutrient utilization ratios and autotrophic pigment concentrations. Changes in ML $Cd:PO_4^{3-}$ and $\Delta Si:\Delta NO_3^-$ were used to determine if the importance of diatom growth diminished and a shift towards a community of smaller, pico-nano phytoplankton occurred during 2014 and 2015. Direct analysis of pigment data (CHEMTAX) to determine the proportion of phyto species further reinforced that a shift towards pico-nano phytoplankton occurred during the 2014-2015 marine heat wave.

Combined, all of these data suggest that marine heatwaves in offshore environments can contribute to decreased NCP by reductions in macronutrients and micronutrients (trace metals) by dampened vertical mixing. These changes to the physical and chemical fields appear to select for a smaller phytoplankton community, with less mineral ballast, that results in some reduction in the efficiency of the biological carbon pump (BCP).

4.2 ***Chapter 3****: The effects of marine heatwaves on the relationship between trace metal distributions and net community production in the coastal and offshore subarctic northeast Pacific*

The purpose of Chapter 3 was synthesize trace metal (dMn, dFe, dCo, dNi, dCu, dCd) observations together to discuss how marine heatwaves affect their distributions in the subarctic northeast Pacific Ocean. Similar to Chapter 2, this study used hydrographic, macronutrient, and trace metal data to observe changes upper-ocean (<400 m) metal distributions along Line P – at stations P26, P20, P16, P12, and P4 from 2012-2019. This spatial and temporal coverage allowed me to answer the question: how did the marine heatwave events of 2014/2015 and 2019 affect trace metal distributions and net community production in the offshore and coastal regions of the subarctic northeast Pacific?

The first marine heatwave studied, the 2014/2015 Blob, was a multiyear phenomenon that allowed for observation of differences in hydrographic, chemical and biological fields between the two years. In the offshore region during 2014, winter ML shallowing reduced macronutrient, and likely trace metal, transport to the surface. Interestingly, dCd was the only trace metal that was significantly diminished, whereas dMn, dFe, dCo, dNi, and dCu were relatively unchanged compared to previous years 2012 and 2013. Resulting NCP was stable in the face of upper-ocean warming although a potential shift towards a pico-nanophytoplankton dominated community was indicated by $\Delta Si:\Delta NO_3^-$ and $Cd:PO_4^{3-}$ ratios (proxies for phytoplankton community structure), during the summer growing season. The coastal region, however, appeared to be unaffected by the marine heatwave during the first year.

The winter MLD's did not experience shallowing compared to previous years, macronutrient and trace metal ML stocks remained relatively unchanged, and NCP was typical for the region.

The second year of the marine heatwave, 2015, brought on increased winter ML shallowing, diminished macronutrients and trace metal ML concentrations in the offshore and coastal regions. While most trace metal distributions and average ML concentrations were resilient in the face of upper-ocean warming during 2014, their distributions changed significantly in response to sustained temperature anomalies and diminished mixing during winter 2015, resulting in diminished ML concentrations. The summer growing season during 2015 in the offshore and coastal regions varied greatly due to events other than the marine heatwave. At offshore stations, P26 and P20, NCP dropped dramatically due to extreme iron limitation brought on by winter shallowing, and had anomalously low trace metal concentrations across the board. During sampling, offshore station P16 was in the vicinity of an eddy that resulted in higher dMn, dCo, dNi, dCu, and dCd than expected compared to the other offshore stations. While ML dFe was low, the NO_3^- concentrations were depleted and likely limited the growth of the phytoplankton community, resulting in low NCP regardless of the eddy. The coastal station, P12, appeared to have some peripheral interaction with the eddy based on low salinity of similar concentration to P16; however, the trace metal distributions were more similar to what was expected for the marine heatwave. Anomalously low dMn, dFe, dCo, and dCd were observed along with depleted NO_3^-, which attributed to low NCP. The conditions at coastal station P4 were the most unexpected for the marine heatwave. The ML depth was deep (29 m), and the ML was very cold and dense. The high concentrations of dMn and dCo were indicative of continental input, and the NO_3^- was elevated slightly. Although the NCP was the lowest within the time series due to winter shallowing, the injection of nutrient rich water likely reinvigorated the phytoplankton community and increased production that was not observed.

The marine heatwave of 2019 was notably different than that of 2014 and 2015. While trace metals were not sampled along the Line P transect in the winter of 2019, macronutrient data was available and used to determine NCP. During the summer growing season, the offshore region had some of the highest NCP in the time series – most notably at P26. In the HNLC, offshore environment, phytoplankton are typically limited by iron. In the summer of 2019, NO_3^- concentrations were depleted and became the limiting nutrient. Further evidence of this depletion was made by dNi concentrations, which were the lowest from 2012-2018, as nickel is used in the nitrogen cycle for assimilation of urea (Morel *et al.* 2003). The dMn, dFe, dCo, dCu, and dCd ML concentrations were similarly diminished in 2014 and 2015. The coastal region sustained similar NCP to the previous post Blob years of 2017 and 2018; yet from 2017-2019 there appears to be a stepwise decrease in NCP. Trace metal ML concentrations at station P12 were non-anomalous compared to previous years, while P4 had the lowest dMn, dCo, dNi, and dCd from 2012-2018.

The source of the high offshore production was determined to likely be atmospheric input by either forest fires, glacial dust, or continental dust based on aerosol optical depth data. Therefore, based on 2014-2015 data, external inputs of nutrients can overshadow marine heatwave processes which can result in diminished production. For future marine heatwaves, some processes such as winter ML shallowing and diminished vertical transport of nutrients (trace metals and macronutrients) in the subarctic northeast Pacific can be expected. Yet, other factors have the ability to change the course of productivity, as observed in 2019, and strong differences between offshore and coastal environments must be considered.

4.3 Future Work

Future studies on coastal and offshore subarctic northeast Pacific trace metal distributions could benefit from the inclusion of particulate trace metal concentrations. Due to the amount of data analyzed, time was a limitation in the ability to analyze both dissolved and particulate samples. Particulate iron data can be used as a tracer for inorganic and organic inputs of nutrients (Tagliabue *et al.* 2017). Inorganic inputs can include aerosol deposition and advection of continental waters, where the presence of inorganic sources results in greater particulate iron concentrations (Lam *et al.* 2006; Tagliabue *et al.* 2017). Organic inputs include ligand- and organically-bound iron that is produced in surface waters and either remains or sinks below the euphotic zone (Archer and Johnson 2000). By using particulate metals as tracers, the robustness of trace metal distributions during the first year of the heatwave, and the collapse during the second, could provide more direct observations for the 2014 and 2015 marine heatwave. While organic iron recycling may have played an important role in the winter of 2014, there alternatively may have been external inputs that could only be detected at the particulate level. Similarly, the 2019 marine heatwave observations could also benefit from particulate trace metal data by determining which metals were introduced by the summer growing season's atmospheric deposition. Although this trace metal time series from 2012 to 2019 will be useful for future studies, it is an incomplete record. There was no single year in which all three seasons were sampled for trace metals, resulting in only a partial story. Future trace metal monitoring would benefit immensely from consistent seasonal and yearly sampling plans where possible, providing a more detailed record.

Bibliography

Amaya, D.J., Miller, A.J., Xie, S-P., Kosaka, Y. (2020). Physical drivers of the summer 2019 North Pacific marine heatwave. *Nature Communications*. 11(1): 1903. doi: 10.1038/s41467-020-15820-w.

Barbeau, K., Rue, E. L., Trick, C. G., Bruland, K. W., Butler, A. (2003). The photochemical reactivity of siderophores produced by marine heterotrophic bacteria and cyanobacteria, based on characteristic iron(III)-binding groups. *Limnology and Oceanography*. 48(3): 1069–1078. doi: 10.4319/lo,2003.48.3.1069.

Barnett, T.P., Pierce, D.W., Schnur, R. (2001). Detection of anthropogenic climate change in the world's oceans. *Science*. 292(5515): 270-274. doi: 10.1126/science.1058304.

Bertrand, E.M., Moran, D.M., Mcllvin, M.R., Hoffman, J.M. Allen, A.E., Saito, M.A. (2013). Methionine synthase interreplacement in diatom cultures and communities: Implications for the persistence of B12 use by eukaryotic phytoplankton*. Limnology and Oceanography*. 58(4): 1431-1450. doi: 10.4319/lo.2013.58.4.1431.

Bif, M.B., Hansell, D.A. (2019). Seasonality of Dissolved Organic Carbon in the Upper Northeast Pacific Ocean. *Global Biogeochemical Cycles*. 33(5): 526-539. doi: 10.1029/2018GB006152.

Bif, M. B., Siqueira, L., Hansell, D. A. (2019). Warm events induce loss of resilience in organic carbon production in the northeast Pacific Ocean. *Global Biogeochemical Cycles*. 33(9): 1174-1186. doi: 10.1029/2019GB006327.

Biller, D.V., Bruland K.W. Sources and distribution of Mn, Fe, Co, Ni, Cu, Zn, and Cd relative to macronutrients along the central California coast during the spring and summer upwelling season. *Marine Chemistry*. 155: 50-70. doi: 10.1016/j.marchem.2013.06.003.

Bishop, J.K.B, Fleisher, M.Q. (1987). Particulate manganese dynamics in Gulf Stream warm-core rings and surrounding waters of the N.W. Atlantic. *Geochimica et Cosmochimica Acta*. 51(10): 2807-2825. doi: 10.1016/0016-7037(87)90160-8.

Bond, N.A., Cronin, M.F., Freeland, H., Mantua, N. (2015). Causes and impacts of the 2014 warm anomaly in the NE Pacific. *Geophysical Research Letters*. 42(9): 3414–3420. doi:10.1002/2015GL063306.

Booth, B.C., Lewin, J., Pastel, J.R. (1993). Microprotozooplankton distribution and their potential grazing impacts in the Antarctic circumpolar current. *Progress in Oceanography*. 32: 57-99. doi: 10.1016/S0967-0645(96)00080-X.

Boyd, P., Berges, J.A., Harrison, P.J. (1998). In vitro iron enrichment experiments at iron-rich and -poor sites in the NE subarctic Pacific. *Journal of Experimental Marine Biology and Ecology.* 227(1): 133-151. doi: 10.1016/S0022-098(97)00264-5.

Boyd, P.W., and Harrison, P.J. (1999). Colimitation of phytoplankton growth by light and Fe during winter in the NE subarctic Pacific Ocean. *Deep Sea Research II*, 46, 2405-2432. doi: 10.1016/S0967-0645(99)00072-7.

Boyd, P.W., Ellwood, M.J. (2010). The biogeochemical cycle of iron in the ocean. *Nature Geoscience*. 3(10): 675-682. doi: 10.1038/ngeo964.

Boye, M., Adjou, M.A., Dulaquais, G., Treguer, P. (2017). Trace metal limitations (Co, Zn) increase PIC/POC ratio in coccolithophore Emiliania huxleyi. *Marine Chemistry*. 192: 22-31. doi: 10.1016/j.marchem.2017.03.006.

Boyle, E.A., Sclater, F., Edmond, J.M. (1976). On the marine geochemistry of cadmium. *Nature*. 263(5572), 42-44. doi: 10.1038/263042a0.

Brand, L.E., Sunda, W.G., Guillard, R.R.L. (1986). Reduction of marine phytoplankton reproduction rates by copper and cadmium. *Journal of Experimental Marine Biology and Ecology.* 96: 225-250. doi: 10.1016/0022-0981(86)90205-4.

Bruland, K.W., Knauer, G.A., Martin, J.H. (1978). Cadmium in northeast Pacific waters 1: Cadmium in NE Pacific. *Limnology and Oceanography*. 23(4): 618-625. doi: 10.4319/lo.1978.23.4.0618.

Bruland, K.W. (1980). Oceanographic distributions of cadmium, zinc, nickel, and copper in the north Pacific. *Earth and Plan. Sci. Lett.* 47: 176-189. doi: 10.1016/0012-821X(80)90035-7.

Bruland, K.W., Middag, R., Lohan, M.C. (2014). Controls of Trace Metals in Seawater. Treatise on Geochemistry, Elsevier, 19-51. doi: 10.1016/B978-0-08-095975-7.00602-1.

Bruland K.W., Franks R.P. (1983). Mn, Ni, Cu, Zn and Cd in the Western North Atlantic. In: Wong C.S., Boyle E., Bruland K.W., Burton J.D., Goldberg E.D. (eds) Trace Metals in Sea Water. NATO Conference Series (IV Marine Sciences), vol 9. Springer, Boston, MA. doi: 10.1007/978-1-4757-6864-0_23.

Bruland, K.W., Franks, R.P., Knauer, G.A., Martin J.H. (1979). Sampling and analytical methods for the determination of copper, cadmium, zinc, and nickel at the nanogram per liter level in sea water. *Analytica Chimica Acta.* 105: 233-245. doi: 10.1016/S0003-2670(01)83754-5.

Brzezinski, M. A., Jones, J.L, Demarest, M.S. (2005). Control of silica production by iron and silicic acid during the Southern Ocean Iron Experiment (SOFeX). *Limnology and Oceanography.* 50(3): 810–824. doi:10.4319/lo.2005.50.3.0810.

Buck, C.S., Landing, W.M., Resing, J. (2013). Pacific Ocean aerosols: Deposition and solubility of iron, aluminum, and other trace elements. *Marine Chemistry*. 157: 117-130. doi: 10.1016/j.marchem.2013.09.005.

Cassar, N., DiFiore, P.J., Barnett, B.A., Bender, M.L., Bowie, A.R., Tilbrook, B., Petrou, K., Westwood, K.J., Wright, S.W., Lefevre, D. (2011). The influence of iron and light on net community production in the Subantarctic and Polar Frontal Zones. *Biogeosciences*. 8(2): 227-237. doi: 10.5194/bg-8-227-2011.

Cavole, L., Demko, A., Diner, R., Giddings, A., Koester, I., Pagniello, C.M.L.S., Paulsen, M.L., Ramirez-Valdez, A., Schwenck, S.M., Yen, N.K., Zill, M.E., Franks, P.J.S. (2016). Biological Impacts of the 2013–2015 Warm-Water Anomaly in the Northeast Pacific: Winners, Losers, and the Future. *Oceanography*. 29(2): 273-285. doi: 10.5670/oceanog.2016.32.

Conway, T.M., John, S.G. (2015). The cycling of iron, zinc and cadmium in the North East Pacific Ocean – Insights from stable isotopes. *Geochimica et Cosmochimica Acta*. 164, 262-283. doi: 10.1016/j.gca.2015.05.023

Crawford, W.R. (2002). Physical characteristics of Haida Eddies. *Journal of Oceanography.* 5: 703-713. doi: 10.1023/A:1022898424333.

Crawford, W.R. (2005). Heat and fresh water transport by eddies into the Gulf of Alaska. *Deep Sea Research Part II: Topical Studies in Oceanography.* 52(7-8): 893-908. doi: 10.1016/j.dsr2.2005.02.003.

Crawford, W.R., Brickley, P.J., Thomas, A.C. (2007). Mesoscale eddies dominate surface phytoplankton in northern Gulf of Alaska. *Progress in Oceanography*. 75(2): 287-303. doi: 10.1016/j.pocean.2007.08.017.

Croot, P.L., Streu, P., Baker, A.R. (2004). Short residence time for iron in surface seawater impacted by atmospheric dry deposition from Saharan dust events: Saharan iron in surface waters. *Geophysical Research Letters*. 31, L23S08. doi: 10.1029/2004GL020153.

Cullen, J.T., Chase, Z., Coale, K.H., Fitzwater, S.E., Sherrell, R.M. (2003). Effect of iron limitation on the cadmium to phosphorus ratio of natural phytoplankton assemblages from the Southern Ocean. *Limnology and Oceanography.* 48(3). doi: 10.4319/lo.2003.48.3.1079.

Cullen, J.T. (2006). On the nonlinear relationship between dissolved cadmium and phosphate in the modern global ocean: Could chronic iron limitation of phytoplankton growth cause the kink? *Limnology and Oceanography.* 51(3): 1369-1380. doi: 10.4319/lo.2006.51.3.1369.

Cullen, J.T., Chase, Z., Coale, K.H., Fitzwater, S.E., Sherrell, R.M. (2003). Effect of iron limitation on the cadmium to phosphorus ratio of natural phytoplankton assemblages from the Southern Ocean. *Limnology and Oceanography.* 48(3). doi: 10.4319/lo.2003.48.3.1079.

Cummins, P.F., and Freeland, H.J. (2007). Variability of the North Pacific Current and its bifurcation. *Progress in Oceanography*. 75(2), 253-265. doi: 10.1016/j.pocean.2007.08.006

Denman, K.L. (2008). Climate change, ocean processes and ocean iron fertilization. *Marine Ecology Progress Series*. 364: 219-225. doi: 10.3354/meps07542.

Di Lorenzo, E., Mantua, N. (2016). Multi-year persistence of the 2014/15 North Pacific marine heatwave. *Nature Climate Change*. 11(6): 1042-1047. doi: 10.1038/nclimate3082.

Duce, R.A., Tindale, N.W. (1991). Atmospheric transport of iron and its deposition in the ocean. *Limnology and Oceanography*. 36(8): 1507-1970. doi: 10.4319/lo.1991.36.8.1715.

Dupont, C.L., Buck, K.N., Palenik, B., Barbeau, K. (2010). Nickel utilization in phytoplankton assemblages from contrasting oceanic regimes. *Deep Sea Research Part I: Oceanographic Research Papers.* 57(4): 553-566. doi: 10.1016/j.dsr.2009.12.014.

Falkowski, P.G. and Raven, J.A. (2007). Aquatic Photosynthesis. 2nd ed. Princeton (NJ): Princeton Oxford Press. 484 p.

Field, P.M, Cullen, J.T., Sherrell, R.M. (1999). Direct determination of 10 trace metals in 50µL samples of coastal seawater using desolvating micronebulization sector field ICP-MS. *Journal of Analytical Atomic Spectrometry.* 14(9): 1425-1431. doi: 10.1039/A901693G.

Freeland, H., Denman, K. (1982). A topographically controlled upwelling center off southern Vancouver Island. *Journal of Marine Research.* 40(4): 1069-1093.

Freeland, H., Denman, K., Wong, C.S., Frank, W., Renee, J. (1997). Evidence of change in the winter mixed layer in the Northeast Pacific Ocean. *Deep Sea Research Part I: Oceanographic Research Pap*ers. 44(12): 2117-2129. doi: 10.1016/S0967-0637(97)00083-6.

Freeland, H. (2007). A short history of Ocean Station Papa and Line P. *Progress in Oceanography*. 75(2): 120-125. doi: 10.1016/j.pocean.2007.08.005

Freeland, H., Ross, T. (2019). 'The Blob' - or, how unusual were ocean temperatures in the Northeast Pacific during 2014-2018? *Deep Sea Research Part I: Oceanographic Research Papers*. 150, 103061. doi: 10.1016/j.dsr.2019.06.007.

Gao, G., Zhao, X., Jiang, M., Gao, L. (2021). Impacts of marine heatwaves on algal structure and carbon sequestration in conjunction with ocean warming and acidification. *Fontiers in Marine Science.* doi: 10.3389/fmars.2021.758651.

Garrett, C., Munk, W. (1972). Ocean mixing by breaking internal waves. *Deep-Sea Res*earch. 19(12): 823-832. doi: 10.1016/0011-7471(72)90001-0.

Garrett, C., Munk, W. (1979). Internal waves in the ocean. *Annual Review of Fluid Mechanics*. 11: 339-369. doi: 10.1146/annurev.fl.11.010179.002011.

Goddard, L., Graham, N.E. (1997). El Niño in the 1990s. *Journal of Geophysical Research: Oceans.* 102(5): 10423-10436. doi: 10.1029/97JC00463.

Gupta, A.S., Thomsen, M., Benthuysen, J.A., Hobday, A.J., Oliver, E. , Alexander, L.V., Burrows, M.T., Donat, M.G., Feng, M., Holbrook, N.J., Perkins-Kirkpatrick, S., Moore, P.J., Rodrigues, R.R., Scannell, H.A., Taschetto, A.S., Ummenhofer, C.C., Wernberg, T., Smale, D.A. (2020). Drivers and impacts of the most extreme marine heatwave events. *Scientific Reports*. 10: 19359. doi: 10.1038/s41598-020-75445-3.

Harrison, W.G., Eppley, R.W., Renger, E.H. (1977). Phytoplankton Nitrogen Metabolism, Nitrogen Budgets, and Observations on Copper Toxicity: Controlled Ecosystem Pollution Experiment. *Bulletin of Marine Science*. 27(1): 44-57.

Harrison, P.J., Boyd, P.W., Varela, D.E., Takeda, S., Shiomoto, A., Odate, T. (1999). Comparison of factors controlling phytoplankton productivity in the NE and NW subarctic Pacific gyres. *Progress in Oceanography*. 43(2-4): 205-234. doi: 10.1016/S0079-6611(99)00015-4.

Hayashida, H., Matear, R.J., Strutton, P.G. (2020). Background nutrient concentration determines phytoplankton bloom response to marine heatwaves. *Global Change Biology.* 26(9): 4800-4811. doi: 10.1111/gcb.15255.

Hobday, A.J, Alexander, L.V., Perkins, S.E., Smale, D.A., Straub, S.C., Oliver, E.C.J., Benthuysen, J.A., Burrows, M.T., Donat, M.G., Feng, M., Holbrook, N.J., Moore, P.J., Scannell, H.A., Sen Gupta, A., and Wernberg, T. (2016). A hierarchical approach to defining marine heatwaves. *Progress in Oceanography*. 141: 277-238. doi: 10.1016/j.pocean.2015.12.014.

Ho, T-Y. Quigg, A., Finkel, Z.V., Milligan, A.J., Wyman, K., Falkowski, P.G., Morel, F.M.M. (2003). The elemental composition of some marine phytoplankton. *Journal of Phycology*. 39(6): 1145-1159. doi: 10.1111/j.0022-3646.2003.03-090.x.

Holbrook, N.J., Scannell, H.A., Sen Gupta, A., Benthuysen, J.A., Ming, F., Oliver, E.C.J., Alexander, L.V., Burrows, M.T., Donat, M.G., Hobday, A.J., Moore, P.J., Perkins-Kilpatrick, S.E., Smale, D.A., Straub, S.C., Wernberg, T. (2019). A global assessment of marine heatwaves and their drivers. *Nature Communications*. 10(1): 2624. doi: 10.1038/s41467-019-10206-z.

Hu, Z., Goa, S. (2008). Upper crustal abundances of trace elements: A revision and update. *Chemical Geology*. 253 (3-4): 205-221. doi: 10.1016/j.chemgeo.2008.05.010.

Hutchins, D.A., Bruland, K.W. (1998). Iron-limited diatom growth and Si:N uptake ratios in a coastal upwelling regime. *Nature*. 393(6685): 561-564. doi: 10.1038/31203.

Ianson, D., Allen, S.E., Harris, S.L., Orians, K.J., Varela, D.E., Wong, C.S. (2003). The inorganic carbon system in the coastal upwelling region west of Vancouver Island, Canada. *Deep Sea Research I*. 50(8): 1023-1042. doi: 10.1016/S0967-0637(03)00114-6.

Jackson, S.L, Spence, J., Janssen, D.J., Ross, A.R.S., Cullen, J.T. (2018). Determination of Mn, Fe, Ni, Cu, Zn, Cd, and Pb in seawater using offline extraction and triple quadrupole ICP-MS/MS. *Journal of Analytical Atomic Spectrometry*. 33(2): 304-313.doi: 10.1039/C7A00237H.

Jacobel, A.W., McManus, J.F., Anderson, R.F., Winckler, G. (2017). Repeated storage of respired carbon in the equatorial Pacific Ocean over the last three glacial cycles. *Nature Communications.* 8(1): 1-9. doi: 10.1038/s41467-017-01938-x.

Jacobel, A.W., Anderson, R.F., Jaccard, S.L., McManus, J.F., Pavia, F.J., Winckler, G. (2020). Deep Pacific storage of respired carbon during the last ice age: Perspectives from bottom water oxygen reconstructions. *Quaternary Science Reviews*. 230. doi: 10.1016/j.quascirev.2019.106065.

Janssen, D.J., Conway, T.M., John, S.G., Christian, J.R., Kramer, D.I., Pedersen, T.F., Cullen, J.T. (2014). Undocumented water column sink for cadmium in open ocean oxygen-deficient zones. *Proceedings of the National Academy of Sciences*. 111(19): 6888-6893. doi: 10.1073/pnas.1402388111.

Johnson K. S., Gordon R. M., and Coale K. H. (1997). What controls dissolved iron concentrations in the world ocean? *Marine Chemistry*. 57(3-4): 137–161. doi: 10.1016/S0304-4203(97)00043-1.

Klinkhammer, G.P, Bender, M.L. (1980). The distribution of manganese in the Pacific Ocean. *Earth and Planetary Science Letters.* 46(3): 361-384. doi: 10.1016/0012-821X(80)90051-5.

Lam, P.J., Bishop, J.K.B., Henning, C.C., Marcus, M.A., Waychunas, G.A., Fung, I.Y. (2006). Wintertime phytoplankton bloom in the subarctic Pacific supported by continental margin iron. *Global Biogeochemical Cycles*. 20(1): GB1006. doi: 10.1029/2005GB002557.

Landing, W.M, Bruland, K.W. (1980). Manganese in the North Pacific. *Earth and Planetary Science Letters*. 49(1): 45-56. doi: 10.1016/0012-821X(80)90149-1.

Lane, E. S., D. M. Semeniuk, R. F. Strzepek, J. T. Cullen, and M. T. Maldonado. (2009). Effects of iron limitation on intracellular cadmium of cultured phytoplankton: Implications for surface dissolved cadmium to phosphate ratios. *Marine Chemistry.* 115(3): 155–162. doi: 10.1016/J.Marchem.2009.07.008.

Laurel, B.J., Rogers, L.A. (2020). Loss of spawning habitat and prerecruits of Pacific cod during a Gulf of Alaska heatwave. *Canadian Journal of Fisheries and Aquatic Sciences.* 77(4): 644-650. doi: 10.1139/cjfas-2019-0238.

Lavoie, M., Fortin, C., Campbell, P.G.C. (2012). Influence of essential elements on cadmium uptake and toxicity in a unicellular green alga: The protective effect of trace zinc and cobalt concentrations. *Environmental Toxicology and Chemistry*. 31(7): 1445-1452. doi: 10.1002/etc.1855.

Lee, J.G., Morel, F.M.M. (1995). Replacement of zinc by cadmium in marine phytoplankton. *Marine Ecology Progress Series.* 127: 305-309. doi: 10.3354/meps127305.

Lee, P.K., Youm, S.J., Ho, Y.J. (2013). Heavy metal concentrations and contamination levels from Asian dust and identification sources: A case-study. *Chemosphere*. 91(7): 1018-1025. doi: 10.1016/j.chemosphere.2013.01.074.

Maldonado, M.T., Price, N.M. (1999). Utilization of iron bound to strong organic ligands by phytoplankton communities in the subarctic Pacific Ocean. *Deep-Sea Research II*. 46(11): 2447-2473. doi: 10.1016/S0967-0645(99)00071-5.

Marchetti, A., Juneau. P., Whitney, F.A., Wong, C.S., Harrison, P.J. (2006b). Phytoplankton processes during a mesopelagic iron enrichment in the NE subarctic Pacific: Part II – Nutrient utilization. *Deep-sea Research Part II, Topical Studies in Oceanography.* 53(20): 2114-2130. doi: 10.1016/j.dsr2.2006.05.031.

Martin, J.H., Fitzwater, S.E. (1988). Iron deficiency limits phytoplankton growth in the north-east Pacific subarctic. *Nature*. 331(6154): 341-343. doi: 10.1038/331341a0.

Martin, J.H., Gordon, R.M., Fitzwater, S., Broenkow, W.W. (1989). *Deep Sea Research Part A. Oceanographic Research Papers*. 36(5): 649-680. doi: 10.1016/0198-0149(89)90144-1.

Martin, J.H. (1990). Glacial-interglacial CO_2 change: The Iron Hypothesis. *Paleoceanography*. 5(1): 1-13. doi: 10.1029/PA005i001p00001.

Martin, J.H., Coale, K.H., Johnson, K.S., Fitzwater, S.E., Gordon, R.M., et al. (1994). Testing the iron hypothesis in ecosystems of the equatorial Pacific Ocean. *Nature*. 371(6493): 123-129. doi: 10.1038/371123a0.

Martin, P., Rutgers van der Loeff, M., Cassar, N., Vandromme, P., d'Ovidio, F., Stemmann, L., Rengarajan, R., Soares, M., González, H., Ebersbach, F., Lampitt, R.S., Sanders, R., Barnett, B.A., Smetacek, V., Naqvi, S.W.A. (2013). Iron fertilization enhanced net community production but not downward particle flux during the Southern Ocean iron fertilization experiment LOHAFEX. *Global Biogeochemical Cycles*. 27(3): 871-881. doi: 10.1002/gbc.20077.

McDonald, N. (2019). Chalkyitsik Complex Incident Summary: June 17-July 3, 2019. Alaska Type 2 Green Incident Management Team, Alaska Interagency Coordination Center, Wainwright, Alaska 99703.

McGowan, J.A., Hayward, T.L. (1978). Mixing and oceanic productivity. *Deep-Sea Research*. 25(9): 771-793. doi: 10.1016/0146-6291(78)90023-1.

Measure, C.I., Landing, W.M., Brown, M.T., Buck, C.S. (2008). A commercially available rosette system for trace metal- clean sampling. *Limnology and Oceanography*. 6(9): 384-394. doi: 10.4319/lom.2008.6.384.

Moffet, J.W., Ho, J. (1996). Oxidation of cobalt and manganese in seawater via a common microbially catalyzed pathway. *Geochemica et Cosmochimica Acta*. 60(18): 3415-3424. doi: 10.1016/0016-7037(96)00176-7.

Moore, J.K, Doney, S.C., Lindsay, K. (2004). Upper ocean ecosystem dynamics and iron cycling in a global three-dimensional model. *Biogeochemical Cycles*. 18(4): GB4028. doi: 10.1029/2004GB002220.

Morel, M.M., Milligan, A.J., Saito, M.A. (2003). Marine bioinorganic chemistry: the role of trace metals in the oceanic cycles of major nutrients. *Treatise on Geochemistry.* 6: 113-143. doi: 10.1016/B0-08-043751-6/06108-9.

Neth, E.J, Flowers, P., Robinson, W.R., Theopold, K., Langley, R. (2016). Chemistry: Atoms First, OpenStax, Houston, Texas.

Oliver, E.C.J., Benthuysen, J.A., Darmaraki, S., Hobday, A.J., Holbrook, N.J., Schlegel, R.W., Sen Gupta, A. (2021). Marine Heatwaves. *Annual Review of Marine Science*. 13(1): 313-342. doi: 10.1146/annurev-marine-032720-095144.

Passow, U., Carlson, C.A. (2012). The biological pump in a high CO2 world. *Marine Ecology Progress Series.* 470: 249-271.doi: 10.3354/meps09985.

Peers, G., Price, N.M. (2004). A role for manganese in superoxide dismutases and growth of iron-deficient diatoms. *Limnology and Oceanography.* 49(5): 1774-1783. doi: 10.4319/lo.2004.49.5.1774.

Pelland, N.A., Eriksen, C.C., Cronin, M.F. (2016). Seaglider surveys at Ocean Station Papa: Circulation and water mass properties in a meander of the North Pacific Current. *Journal of Geophysical Research. Oceans*. 121(9): 6816–6846. doi:10.1002/2016JC011920.

Peña, M.A., Nemcek, N., Robert, M. (2019). Phytoplankton responses to the 2014–2016 warming anomaly in the northeast subarctic Pacific Ocean. *Limnology and Oceanography*. 64(2): 515-525. doi: 10.1002/lno.11056.

Posacka, A.M., Semeniuk, D.M., Whitby, H., van den Berg, C.M.G., Cullen, J.T., Orians, K., Maldonado, M.T. (2017). Dissolved copper (dCu) biogeochemical cycling in the subarctic Northeast Pacific and a call for improving methodologies. *Marine Chemistry*. 196: 47-61. doi: 10.1016/j.marchem.2017.05.007.

Price, N. M., Ahner, B. A., and Morel, F. M. M. (1994). The equatorial Pacific Ocean: grazer-controlled phytoplankton populations in an iron-limited system. *Limnology and Oceanogr*aphy. 39(3): 520–534. doi: 10.4319/lo.1994.39.3.0520.

Raven, J.A. (2019). Iron in diatoms. Diatoms: Fundamentals and Applications, Scrivener Publishing LLC, Beverly, MA 01915: 213-224. doi: 10.1002/9781119370741.

Robert, M. (2015). Pacific region CCG vessel post cruise report – Line P Program Fisheries and Oceans Canada, report for 2015-010. Institute of Ocean Sciences, Sidney (BC).

Rue, E.L., Bruland, K.W. (1995). Complexation of iron(II1) by natural organic ligands in the Central North Pacific as determined by a new competitive ligand equilibration/adsorptive cathodic stripping voltammetric method. *Marine Chemistry*. 50(1): 117-138. doi: 10.1016/0304-4203(95)00031-L.

Saito, M.A., Moffett, J.W., Chisholm, S.W., Waterbury, J.B. (2002). Cobalt limitation and uptake in Prochlorococcus. *Limnology and Oceanography.* 47(6): 1629-1636. doi: 10.4319/lo.2002.47.6.1629.

Sathish, K., Patil, J.S., Anil, A.C. (2020). Phytoplankton chlorophyll-breakdown pathway: implications in ecosystem assessment. *Journal of Environmental Management.* 258. doi: 10.1016/j.jenvman.2019.109989.

Schallenberg, C., Davidson, A.B., Simpson, K.G., Miller, L.A., Cullen, J.T. (2015). Iron(II) variability in the northeast subarctic Pacific Ocean. *Marine Chemistry.* 177(1): 33-44. doi: 10.1016/j.marchem.2015.04.004.

Siegel, D.A., Buesseler, K.O., Behrenfeld, M.J., Benitez-Nelson, C.R., Boss, E., Brzezinski, M.A., Burd, A., Carlson, C.A., D'Asaro, E.A., Doney, S.C., Perry, M.J., Stanley, R.H.R, Steinberg, D.K. (2016). Prediction of the export and fate of global ocean net primary production: the EXPORTS science plan. *Frontiers in Marine Science.* 3(22). doi: 10.3389/fmars.2016.00022.

Sim, N., Orians, K.J. (2019). Annual variability of dissolved manganese in Northeast Pacific along Line-P: 2010-2013. *Marine Chemistry*. 216: 103702. doi: 10.1016/j.marchem.2019.103702.

Slater, J.C. (1964). Atomic Radii in Crystals. *Journal of Chemical Physics.* 41(10): 3199. doi: 10.1063/1.1725697.

Sunda, W.G., Huntsman, S.A. (1995). Cobalt and zinc interreplacement in marine phytoplankton: Biological and geochemical implications. *Limnology and Oceanography.* 40(8): 1404-1417. doi: 10.4319/lo.1995.40.8.1404.

Sunda, W.G., Huntsman, S.A. (1998). Control of Cd Concentrations in a Coastal Diatom by Interactions among Free Ionic Cd, Zn, and Mn in Seawater. *Environmental Science and Technology*. 32(19): 2961-2968. doi: 10.1021/es980271y.

Takeda. S. (1998). Influence of iron availability on nutrient consumption ratio of diatoms in oceanic waters. *Nature*. 393(6687): 774-777. doi:10.1038/31674.

Tesdal, J-E., Abernathey, R.P. (2021). Drivers of local ocean heat content variability in ECCOv4. *Journal of Climate.* 34(8): 2941-2956. doi: 10.1175/JCLI-D-20-0058.1.

The Alaska Climate Research Center. (2019). 2019 Alaska Climate Review. American Association of State Climatologists, Fairbanks, Alaska 99775.

Timmerman, A.H.V., and Hamme, R.C. (2021). Consistent relationships among producitivty rate methods in the NE Subarctic Pacific. *Global Biogeochemical Cycles*. 35(2). e2020GB00672. doi: 10.1029/2020GB006721.

Twinning, B.S., Baines, S.B., Vogt, S., Nelson, D.M. (2012). Role of diatoms in nickel biogeochemistry in the ocean: diatoms and nickel biogeochemistry. *Global Biogeochemical Cycles.* 26(4): GB4001. doi: 10.1029/2011GB004233.

Ueno, H., Crawford, W.R., Onishi, H. (2010). Impact of Alaskan Stream eddies on chlorophyll distribution in the North Pacific. *Journal of Oceanography.* 66:319-328. doi: doi.org/10.1007/s10872-010-0028-6.

Varela, D.E., and Harrison, P.J. (1999a). Transformations of biogenic particulates from the pelagic to the deep ocean realm. *Deep Sea Research II.* 46:2405-2432. doi: 10.1016/S0967-0645(99)00083-1.

Vinyard, D.J., Ananyev, G.M., Charles Dismukes, G. (2013). Photosystem II: The Reaction Center of Oxygenic Photosynthesis. *Annual Review of Biochemistry.* 82(1): 577-606. doi: 10.1146/annurev-biochem-070511-100425.

Whitby, H., Planquette, H., Cassar, N., Bucciarelli, E., Osburn, C.L., Janssen, D.J., Cullen, J.T., Gonzalez, A.G., Volker, C., Sarthou, G. (2020). A call for refining the role of humic-like substances in the oceanic iron cycle. *Nature.* 10. doi: 10.1038/s41598-020-62266-7.

Whitney, F.A., Wong, C.S., Boyd, P.W. (1998). Interannual variability in nitrate supply to surface waters of the Northeast Pacific Ocean. *Marine Ecology. Progress Series*. 170: 15-23. doi: 10.3354/meps170015.

Whitney, F.A., Bograd, S.J., Tsuneo, O. (2013). Nutrient enrichment of the subarctic Pacific Ocean pycnocline. *Geophysical Research Letters*. 40(10): 2200-2205. doi: 10.1002/grl.50439.

Whitney, F. A. (2015). Anomalous winter winds decrease 2014 transition zone productivity in the NE Pacific. *Geophysical Research Letters*. 42(2): 428–431. doi:10.1002/ 2014GL062634.

Whitney, F.A., Freeland, H.J. (1999). Variability in upper-ocean water properties in the NE Pacific Ocean. *Deep Sea Research II*. 46(11): 2351-2370. doi: 10.1016/S0967-0645(99)00067-3.

Whitney, F.A., Robert, M. (2002). Structure of Haida Eddies and Their Transport of Nutrient from Coastal Margins into the NE Pacific Ocean. *Journal of Oceanography.* 58(5): 715-723. doi: 10.1023/A:1022850508403.

Wong, C.S., Yu, Z., Waser, N.A.D., Whitney, F.A., Johnson, W.K. (2002). Seasonal changes in the distribution of dissolved organic nitrogen in coastal and open-ocean waters in the North East Pacific: sources and sinks. *Deep-Sea Research II.* 49(24): 5759-5773. doi: 10.1016/S0967-0645(02)00213-8.

Von Damm, K.L. (1990). Seafloor hydrothermal activity: black smoker chemistry and chimneys. *Annual Review of Earth and Planetary Sciences. Sci.* 18(1): 173-204. doi: 10.1146/annurev.ea.18.050190.001133.

Yang. B., Emerson, S.R., Peña, M.A. (2018). The effect of the 2013-2016 high temperature anomaly in the subarctic Northeast Pacific (the “Blob”) on net community production. *Biogeosciences*. 15(21): 6747-6759. doi:10.5194/bg-15-6747-2018.

Zador, S., Yasumiishi, E., Whitehouse, G.A. (2019). Ecosystems Status Report 2019: Gulf of Alaska, North Pacific Fishery Management Council, 605 West 4th, Suite 306, Anchorage, Alaska 99501.

Appendix A

Data Tables of dissolved Mn, Fe, Co, Ni, Cu, and Cd at stations P26, P20, P16, P12, and P4 from 2012-2019

Table A.1 Station P26 dissolved Mn, Fe, Co, Ni, Cu, and Cd from winter 2012-2015 and summer 2012-2019. Quality flags (QF) follow the GEOTRACES Quality Flag Policy https://www.geotraces.org/geotraces-quality-flag-policy/.

Cruise	Year	Month	Latitude	Longitude	Depth	dMn	dMn Error	QF	dFe	dFe Error	QF	dCo	dCo Error	QF	dNi	dNi Error	QF	dCu	dCu Error	QF	dCd	dCd Error	QF
			°N	°E	m	nmol/kg	nmol/kg		nmol/kg	nmol/kg		pmol/kg	pmol/kg		nmol/kg	nmol/kg		nmol/kg	nmol/kg		nmol/kg	nmol/kg	
2012-01	2012	2	50.00	-145.00	10	1.14	0.01	1	0.131	0.002	1	61.4	0.5	1	4.86	0.01	1	1.59	0.01	1	0.44	0.01	1
2012-01	2012	2	50.00	-145.00	25	1.143	0.004	1	0.207	0.001	1	62.2	0.6	1	4.88	0.03	1	1.57	0.01	1	0.448	0.005	1
2012-01	2012	2	50.00	-145.00	40	1.13	0.03	1	0.47	0.01	1	62.6	1.2	1	4.81	0.10	1	1.83	0.04	1	0.44	0.02	1
2012-01	2012	2	50.00	-145.00	50	1.16	0.01	1	0.155	0.001	1	64.1	0.5	1	4.94	0.03	1	1.808	0.009	1	0.451	0.004	1
2012-01	2012	2	50.00	-145.00	100	1.132	0.007	1	0.446	0.003	1	64.4	0.8	1	4.94	0.05	1	1.74	0.01	1	0.46	0.01	1
2012-01	2012	2	50.00	-145.00	150	0.403	0.004	1	0.303	0.002	1	52.0	0.6	1	5.57	0.06	1	2.11	0.02	1	0.780	0.003	1
2012-01	2012	2	50.00	-145.00	200	0.719	0.002	1	0.406	0.004	1	56.1	0.8	1	6.29	0.06	1	2.31	0.02	1	0.900	0.005	1
2012-01	2012	2	50.00	-145.00	400	0.762	0.004	1	1.848	0.009	1	51.8	0.3	1	7.21	0.05	1	2.51	0.02	1	0.956	0.004	1
2012-13	2012	8	50.00	-144.87	10	0.851	0.000	1	0.017	0.001	1	47.58	0.06	1	4.448	0.001	1	1.590	0.001	1	0.274	0.000	1
2012-13	2012	8	50.00	-144.87	25	0.945	0.005	1	0.028	0.000	1	49.3	0.5	1	4.33	0.04	1	1.241	0.008	1	0.303	0.002	1
2012-13	2012	8	50.00	-144.87	30	0.879	0.006	1	0.000	0.001	1	47.3	0.7	1	4.21	0.02	1	1.41	0.01	1	0.291	0.002	1
2012-13	2012	8	50.00	-144.87	50	1.270	0.005	1	0.063	0.001	1	59.1	0.6	1	4.40	0.03	1	1.361	0.007	1	0.469	0.003	1
2012-13	2012	8	50.00	-144.87	75	1.297	0.009	1	0.065	0.001	1	60.3	0.5	1	4.41	0.04	1	1.43	0.01	1	0.472	0.005	1
2012-13	2012	8	50.00	-144.87	100	0.95	0.01	1	0.115	0.001	1	48.6	0.7	1	4.52	0.05	1	1.53	0.01	1	0.512	0.004	1
2012-13	2012	8	50.00	-144.87	150	0.452	0.005	1	0.184	0.004	1	42.6	0.3	1	5.10	0.02	1	1.79	0.01	1	0.765	0.005	1
2012-13	2012	8	50.00	-144.87	200	0.829	0.003	1	0.327	0.001	1	53.2	0.4	1	5.92	0.04	1	1.99	0.01	1	0.892	0.005	1
2012-13	2012	8	50.00	-144.87	300	0.779	0.003	1	0.457	0.003	1	54.0	0.8	1	6.67	0.04	1	2.19	0.01	1	0.946	0.004	1
2012-13	2012	8	50.00	-144.87	400	0.729	0.007	1	0.562	0.004	1	44.5	1.0	1	6.92	0.06	1	2.16	0.02	1	0.92	0.01	1
2013-01	2013	2	50.00	-145.99	10	1.167	0.004	1	0.095	0.001	1	39.5	0.4	1	5.60	0.05	1	0.882	0.009	1	0.465	0.004	1

Cruise	Year	Month	Latitude	Longitude	Depth	dMn	dMn Error	QF	dFe	dFe Error	QF	dCo	dCo Error	QF	dNi	dNi Error	QF	dCu	dCu Error	QF	dCd	dCd Error	QF
			°N	°E	m	nmol/kg	nmol/kg		nmol/kg	nmol/kg		pmol/kg	pmol/kg		nmol/kg	nmol/kg		nmol/kg	nmol/kg		nmol/kg	nmol/kg	
2013-01	2013	2	50.00	-145.99	25	1.15	0.01	1	0.092	0.002	1	48.7	0.8	1	5.56	0.05	1	0.88	0.01	1	0.459	0.002	1
2013-01	2013	2	50.00	-145.99	40	1.138	0.007	1	0.072	0.001	1	46.4	0.4	1	5.53	0.04	1	0.797	0.007	1	0.468	0.002	1
2013-01	2013	2	50.00	-145.99	75	1.13	0.01	1	0.058	0.001	1	34.2	0.5	1	5.42	0.04	1	0.962	0.008	1	0.456	0.003	1
2013-01	2013	2	50.00	-145.99	100	0.62	0.03	4	0.203	0.02	4	52.3	4.6	4	6.70	0.60	4	1.01	0.08	1	0.978	0.07	4
2013-01	2013	2	50.00	-145.99	150	1.14	0.01	1	0.037	0.001	1	39.7	0.5	1	5.57	0.04	1	1.10	0.02	1	0.469	0.003	1
2013-01	2013	2	50.00	-145.99	200	0.92	0.01	1	0.31	0.01	1	56.9	0.5	1	7.48	0.06	1	2.79	0.02	1	1.091	0.008	1
2013-01	2013	2	50.00	-145.99	300	1.01	0.06	1	0.57	0.04	1	45.9	3.7	1	8.2	0.7	1	2.0	0.2	1	1.11	0.05	1
2013-01	2013	2	50.00	-145.99	400	0.90	0.01	1	0.81	0.01	1	40.9	0.6	1	8.57	0.09	1	2.41	0.02	1	1.077	0.006	1
2013-18	2013	8	50.00	-145.00	10	1.29	0.01	1	0.069	0.001	1	59.3	0.9	1	4.97	0.05	1	1.749	0.007	1	0.261	0.003	1
2013-18	2013	8	50.00	-145.00	25	1.35	0.01	1	0.027	0.001	1	59.5	0.5	1	4.37	0.04	1	1.58	0.02	1	0.314	0.002	1
2013-18	2013	8	50.00	-145.00	50	1.40	0.03	1	0.058	0.002	1	68.9	1.0	1	4.66	0.09	1	1.81	0.02	1	0.441	0.004	1
2013-18	2013	8	50.00	-145.00	75	1.19	0.008	1	0.039	0.001	1	70.3	0.6	1	4.72	0.05	1	1.76	0.03	1	0.49	0.01	1
2013-18	2013	8	50.00	-145.00	150	0.68	0.01	1	0.312	0.005	1	58.2	1.0	1	5.72	0.10	1	2.14	0.03	1	0.953	0.005	1
2013-18	2013	8	50.00	-145.00	200	0.83	0.01	1	0.379	0.003	1	59.6	0.5	1	6.00	0.06	1	2.22	0.03	1	1.00	0.01	1
2013-18	2013	8	50.00	-145.00	250	0.92	0.007	1	0.50	0.01	1	59.7	0.6	1	6.43	0.06	1	2.40	0.02	1	1.031	0.009	1
2013-18	2013	8	50.00	-145.00	350	0.92	0.02	1	0.61	0.01	1	52.2	0.8	1	6.80	0.08	1	2.42	0.03	1	1.02	0.01	1
2013-18	2013	8	50.00	-145.00	400	0.95	0.02	1	0.61	0.01	1	52.2	1.1	1	7.05	0.07	1	2.52	0.03	1	1.04	0.02	1
2014-01	2014	2	50.00	-145.00	10	1.05	0.01	1	0.213	0.003	4	48.7	1.3	1	4.59	0.05	1	3.02	0.07	4	0.24	0.01	1
2014-01	2014	2	50.00	-145.00	25	1.05	0.01	1	0.161	0.001	1	50.6	1.6	1	4.57	0.08	1	2.24	0.05	1	0.233	0.004	1
2014-01	2014	2	50.00	-145.00	35	1.07	0.02	1	0.123	0.003	1	49.0	0.3	1	4.67	0.04	1	1.90	0.05	1	0.237	0.004	1
2014-01	2014	2	50.00	-145.00	50	1.07	0.01	1	1.324	0.02	4	50.7	1.5	1	4.59	0.05	1	2.89	0.7	4	0.24	0.01	1
2014-01	2014	2	50.00	-145.00	75	1.06	0.02	1	0.312	0.004	1	48.7	1.7	1	4.58	0.06	1	1.68	0.03	1	0.24	0.01	1
2014-01	2014	2	50.00	-145.00	100	1.04	0.02	1	0.278	0.003	1	50.8	1.0	1	4.61	0.07	1	1.55	0.04	1	0.30	0.01	1
2014-01	2014	2	50.00	-145.00	150	0.56	0.01	1	0.333	0.003	1	56.0	2.1	1	5.23	0.07	1	2.53	0.04	1	0.71	0.02	1
2014-01	2014	2	50.00	-145.00	200	0.66	0.01	1	0.44	0.01	1	53.7	2.4	1	6.23	0.08	1	2.29	0.04	1	0.93	0.01	1
2014-01	2014	2	50.00	-145.00	300	0.87	0.02	1	0.63	0.02	1	54.8	2.2	1	6.81	0.02	1	2.33	0.01	1	1.02	0.01	1
2014-01	2014	2	50.00	-145.00	400	0.81	0.02	1	1.09	0.03	1	45.9	1.0	1	7.28	0.10	1	2.69	0.01	1	1.008	0.005	1
2014-19	2014	8	50.00	-145.00	10	0.832	0.005	1	0.048	0.004	1	20.4	0.3	1	4.27	0.04	1	1.28	0.01	1	0.022	0.001	1
2014-19	2014	8	50.00	-145.00	25	0.781	0.006	1	0.141	0.006	1	14.4	0.2	1	4.24	0.04	1	1.44	0.01	1	0.009	0.000	1
2014-19	2014	8	50.00	-145.00	40	0.910	0.007	1	0.365	0.009	1	22.3	0.2	1	4.23	0.03	1	1.385	0.005	1	0.028	0.000	1

Cruise	Year	Month	Latitude	Longitude	Depth	dMn	dMn Error	QF	dFe	dFe Error	QF	dCo	dCo Error	QF	dNi	dNi Error	QF	dCu	dCu Error	QF	dCd	dCd Error	QF
			°N	°E	m	nmol/kg	nmol/kg		nmol/kg	nmol/kg		pmol/kg	pmol/kg		nmol/kg	nmol/kg		nmol/kg	nmol/kg		nmol/kg	nmol/kg	
2014-19	2014	8	50.00	-145.00	50	1.183	0.004	1	0.049	0.005	1	60.6	0.5	1	4.44	0.03	1	1.43	0.02	1	0.358	0.004	1
2014-19	2014	8	50.00	-145.00	75	1.08	0.01	1	0.060	0.006	1	57.2	1.0	1	4.53	0.03	1	1.461	0.008	1	0.35	0.01	1
2014-19	2014	8	50.00	-145.00	100	0.726	0.003	1	0.073	0.003	1	65.9	0.4	1	5.09	0.03	1	1.73	0.01	1	0.610	0.005	1
2014-19	2014	8	50.00	-145.00	200	0.686	0.007	1	0.33	0.01	1	56.6	0.4	1	6.36	0.06	1	2.00	0.01	1	0.920	0.005	1
2014-19	2014	8	50.00	-145.00	400	0.850	0.008	1	0.50	0.02	1	45.7	0.5	1	7.12	0.06	1	2.17	0.03	1	0.939	0.005	1
2015-01	2015	2	50.00	-145.00	10	1.00	0.02	1	0.060	0.002	1	21.1	0.5	1	5.5	0.1	1	1.74	0.02	1	0.253	0.005	1
2015-01	2015	2	50.00	-145.00	20	1.01	0.02	1	0.081	0.003	1	39.4	0.7	1	5.4	0.1	1	1.42	0.02	1	0.253	0.003	1
2015-01	2015	2	50.00	-145.00	40	0.974	0.009	1	0.048	0.001	1	27.6	0.4	1	5.47	0.05	1	1.080	0.007	1	0.251	0.004	1
2015-01	2015	2	50.00	-145.00	50	1.01	0.01	1	0.051	0.001	1	34.5	0.5	1	5.68	0.09	1	1.32	0.02	1	0.263	0.004	1
2015-01	2015	2	50.00	-145.00	75	0.99	0.02	1	0.027	0.001	1	26.1	0.7	1	5.51	0.08	1	1.20	0.02	1	0.263	0.005	1
2015-01	2015	2	50.00	-145.00	125	0.48	0.01	1	0.212	0.004	1	21.9	0.3	1	6.1	0.1	1	1.96	0.04	1	0.77	0.02	1
2015-01	2015	2	50.00	-145.00	150	0.54	0.01	1	0.345	0.004	1	24.9	0.6	1	6.37	0.08	1	3.16	0.04	1	0.95	0.01	1
2015-01	2015	2	50.00	-145.00	200	0.70	0.01	1	0.42	0.01	1	23.4	0.4	1	6.6	0.1	1	3.49	0.04	1	0.98	0.02	1
2015-01	2015	2	50.00	-145.00	400	0.98	0.02	1	0.56	0.01	1	27.5	0.8	1	8.1	0.1	1	1.95	0.04	1	0.90	0.02	1
2015-01	2015	2	50.00	-145.00	600	0.68	0.01	1	0.56	0.01	1	18.8	0.5	1	8.5	0.2	1	2.02	0.06	1	0.87	0.01	1
2015-10	2015	8	50.00	-145.00	10	0.696	0.003	1	0.000	0.005	6	15.80	0.02	1	4.47	0.01	1	1.68	0.01	1	0.04	0.02	1
2015-10	2015	8	50.00	-145.00	25	0.69	0.01	1	0.01	0.00	6	15.03	0.01	1	4.44	0.01	1	1.70	0.02	1	0.04	0.02	1
2015-10	2015	8	50.00	-145.00	40	1.17	0.01	1	0.01	0.00	6	52.48	0.01	1	5.03	0.01	1	1.81	0.01	1	0.315	0.008	1
2015-10	2015	8	50.00	-145.00	50	1.19	0.01	1	0.01	0.00	6	58.56	0.01	1	5.03	0.01	1	1.64	0.01	1	0.376	0.005	1
2015-10	2015	8	50.00	-145.00	75	1.15	0.02	1	0.020	0.000	1	58.3	0.8	1	4.63	0.09	1	1.53	0.03	1	0.407	0.005	1
2015-10	2015	8	50.00	-145.00	100	1.05	0.01	1	0.029	0.000	1	56.9	1.4	1	4.74	0.06	1	1.44	0.02	1	0.459	0.005	1
2015-10	2015	8	50.00	-145.00	150	0.45	0.01	1	0.206	0.007	1	49.9	2.2	1	6.04	0.10	1	1.92	0.00	1	0.895	0.004	1
2015-10	2015	8	50.00	-145.00	200	0.70	0.01	1	0.307	0.007	1	54.2	2.3	1	6.40	0.05	1	1.97	0.01	1	0.934	0.006	1
2015-10	2015	8	50.00	-145.00	300	0.79	0.02	1	0.388	0.007	1	49.2	2.4	1	7.08	0.03	1	2.03	0.02	1	0.994	0.005	1
2015-10	2015	8	50.00	-145.00	400	0.81	0.02	1	0.491	0.023	1	43.7	1.7	1	7.47	0.24	1	2.14	0.01	1	1.005	0.008	1
2017-08	2017	8	50.00	-145.00	10	0.836	0.008	1	0.044	0.001	1	29.8	0.3	1	4.14	0.06	1	1.40	0.02	1	0.099	0.001	1
2017-08	2017	8	50.00	-145.00	25	0.810	0.008	1	0.043	0.001	1	28.9	0.2	1	4.13	0.05	1	1.41	0.01	1	0.100	0.001	1
2017-08	2017	8	50.00	-145.00	50	1.35	0.01	1	0.043	0.000	1	60.7	0.7	1	5.02	0.04	1	1.43	0.02	1	0.43	0.01	1
2017-08	2017	8	50.00	-145.00	100	1.18	0.01	1	0.027	0.001	1	64.0	0.7	1	5.23	0.05	1	1.57	0.02	1	0.462	0.003	1
2017-08	2017	8	50.00	-145.00	150	0.329	0.002	1	0.205	0.002	1	48.1	0.6	1	5.53	0.02	1	1.76	0.01	1	0.760	0.007	1

Cruise	Year	Month	Latitude	Longitude	Depth	dMn	dMn Error	QF	dFe	dFe Error	QF	dCo	dCo Error	QF	dNi	dNi Error	QF	dCu	dCu Error	QF	dCd	dCd Error	QF
			°N	°E	m	nmol/kg	nmol/kg		nmol/kg	nmol/kg		pmol/kg	pmol/kg		nmol/kg	nmol/kg		nmol/kg	nmol/kg		nmol/kg	nmol/kg	
2017-08	2017	8	50.00	-145.00	200	0.352	0.003	1	0.249	0.002	1	47.1	0.5	1	5.95	0.04	1	1.80	0.02	1	0.800	0.007	1
2017-08	2017	8	50.00	-145.00	300	0.63	0.01	1	0.356	0.004	1	52.8	0.9	1	6.79	0.09	1	1.96	0.02	1	0.895	0.006	1
2017-08	2017	8	50.00	-145.00	500	0.70	0.01	1	0.593	0.005	1	44.9	0.5	1	7.93	0.09	1	2.27	0.03	1	0.968	0.009	1
2018-040	2018	8	50.00	-145.00	10	0.93	0.01	1	0.046	0.002	1	29.5	0.3	1	4.84	0.07	1	1.46	0.02	1	0.137	0.001	1
2018-040	2018	8	50.00	-145.00	25	0.88	0.01	1	0.042	0.001	1	21.3	0.5	1	4.77	0.03	1	1.36	0.01	1	0.072	0.001	1
2018-040	2018	8	50.00	-145.00	40	1.04	0.02	1	0.041	0.001	1	39.0	0.5	1	4.95	0.06	1	1.43	0.02	1	0.191	0.003	1
2018-040	2018	8	50.00	-145.00	50	1.13	0.01	1	0.031	0.001	1	52.9	0.9	1	4.95	0.06	1	1.489	0.008	1	0.265	0.003	1
2018-040	2018	8	50.00	-145.00	75	1.14	0.02	1	0.048	0.001	1	63.0	0.4	1	5.09	0.06	1	1.42	0.03	1	0.393	0.004	1
2018-040	2018	8	50.00	-145.00	100	1.03	0.01	1	0.33	0.01	1	60.8	0.5	1	5.03	0.06	1	1.54	0.02	1	0.57	0.01	1
2018-040	2018	8	50.00	-145.00	150	0.534	0.005	1	0.245	0.004	1	53.6	0.5	1	5.93	0.07	1	1.89	0.02	1	0.877	0.007	1
2018-040	2018	8	50.00	-145.00	200	0.73	0.01	1	0.358	0.005	1	57.0	1.0	1	6.38	0.06	1	1.93	0.02	1	0.950	0.007	1
2018-040	2018	8	50.00	-145.00	300	0.84	0.01	1	0.49	0.01	1	51.2	0.5	1	7.02	0.05	1	1.938	0.017	1	0.992	0.007	1
2019-008	2019	8	50.00	-145.00	10	0.542	0.004	1	0.069	0.001	1	11.2	0.3	1	2.70	0.02	1	1.16	0.01	1	0.012	0.000	1
2019-008	2019	8	50.00	-145.00	25	0.64	0.01	1	0.056	0.001	1	17.7	0.5	1	2.96	0.04	1	1.17	0.01	1	0.021	0.000	1
2019-008	2019	8	50.00	-145.00	40	0.98	0.01	1	0.060	0.001	1	50.0	0.5	1	4.73	0.02	1	1.234	0.006	1	0.256	0.001	1
2019-008	2019	8	50.00	-145.00	50	0.979	0.006	1	0.054	0.001	1	57.0	0.5	1	4.71	0.03	1	1.315	0.008	1	0.337	0.003	1
2019-008	2019	8	50.00	-145.00	75	0.966	0.009	1	0.050	0.002	1	55.7	0.9	1	4.67	0.04	1	1.33	0.01	1	0.361	0.002	1
2019-008	2019	8	50.00	-145.00	100	0.95	0.01	1	0.064	0.002	1	56.9	0.9	1	4.75	0.06	1	1.38	0.01	1	0.397	0.005	1
2019-008	2019	8	50.00	-145.00	150	0.367	0.002	1	0.181	0.002	1	49.6	0.5	1	5.34	0.02	1	1.70	0.01	1	0.781	0.004	1
2019-008	2019	8	50.00	-145.00	200	0.431	0.005	1	0.297	0.001	1	47.8	0.6	1	5.91	0.06	1	1.80	0.02	1	0.893	0.002	1
2019-008	2019	8	50.00	-145.00	300	0.68	0.01	1	0.416	0.003	1	50.3	0.8	1	6.40	0.07	1	1.87	0.02	1	0.94	0.01	1
2019-008	2019	8	50.00	-145.00	400	0.852	0.003	1	0.62	0.01	1	47.6	0.7	1	7.11	0.08	1	1.97	0.02	1	0.997	0.008	1

Table A.2 Station P20 dissolved Mn, Fe, Co, Ni, Cu, and Cd from winter 2012-2015 and summer 2012-2019. Quality flags (QF) follow the GEOTRACES Quality Flag Policy https://www.geotraces.org/geotraces-quality-flag-policy/.

Cruise	Year	Month	Latitude	Longitude	Depth	dMn	dMn Error	QF	dFe	dFe Error	QF	dCo	dCo Error	QF	dNi	dNi Error	QF	dCu	dCu Error	QF	dCd	dCd Error	QF
			°N	°E	m	nmol/kg	nmol/kg		nmol/kg	nmol/kg		pmol/kg	pmol/kg		nmol/kg	nmol/kg		nmol/kg	nmol/kg		nmol/kg	nmol/kg	
2012-01	2012	2	49.57	-138.67	10	0.998	0.006	1	0.065	0.001	1	52.1	0.7	1	4.51	0.03	1	1.44	0.01	1	0.342	0.002	1
2012-01	2012	2	49.57	-138.67	25	0.998	0.007	1	0.215	0.002	1	53.3	0.4	1	4.57	0.05	1	1.45	0.02	1	0.344	0.003	1
2012-01	2012	2	49.57	-138.67	40	1.030	0.005	1	0.057	0.001	1	54.1	0.2	1	4.59	0.03	1	1.435	0.009	1	0.347	0.003	1
2012-13	2012	8	49.57	-138.66	10	0.980	0.000	1	0.0143	0.0003	1	56.45	0.05	1	4.884	0.001	1	1.445	0.000	1	0.257	0.000	1
2012-13	2012	8	49.57	-138.66	20	0.987	0.009	1	0.0308	0.0005	4	54.9	0.9	1	4.67	0.06	1	1.49	0.02	1	0.288	0.003	1
2012-13	2012	8	49.57	-138.66	25	0.997	0.007	1	0.02	0.01	1	56.2	0.5	1	4.68	0.05	1	1.38	0.02	1	0.287	0.003	1
2012-13	2012	8	49.57	-138.66	50	1.075	0.009	1	0.032	0.001	1	57.1	0.7	1	4.72	0.03	1	1.44	0.01	1	0.341	0.003	1
2012-13	2012	8	49.57	-138.66	75	1.05	0.01	1	0.016	0.001	1	58.6	0.5	1	4.70	0.05	1	1.47	0.01	1	0.405	0.003	1
2012-13	2012	8	49.57	-138.66	100	0.97	0.01	1	0.0582	0.0002	1	52.9	0.5	1	5.20	0.03	1	1.63	0.01	1	0.550	0.003	1
2012-13	2012	8	49.57	-138.66	150	0.431	0.005	1	0.217	0.001	1	56.0	0.8	1	5.75	0.03	1	1.98	0.01	1	0.846	0.003	1
2012-13	2012	8	49.57	-138.66	200	0.627	0.004	1	0.501	0.002	1	58.4	0.3	1	6.34	0.07	1	2.44	0.02	1	0.99	0.01	1
2012-13	2012	8	49.57	-138.66	300	0.654	0.005	1	0.417	0.006	1	54.2	0.9	1	6.57	0.07	1	2.11	0.03	1	0.91	0.01	1
2012-13	2012	8	49.57	-138.66	400	0.661	0.005	1	0.503	0.003	1	46.5	0.5	1	6.75	0.07	1	2.17	0.01	1	0.90	0.01	1
2013-01	2013	2	49.57	-138.67	10	0.929	0.007	1	0.367	0.004	1	47.0	0.3	1	5.10	0.04	1	0.55	0.01	1	0.400	0.003	1
2013-01	2013	2	49.57	-138.67	25	0.96	0.01	1	1.429	0.02	4	45.5	0.3	1	5.28	0.06	1	1.23	0.02	4	0.385	0.004	1
2013-01	2013	2	49.57	-138.67	40	0.955	0.006	1	0.307	0.001	1	50.5	1.0	1	5.41	0.04	1	0.722	0.006	1	0.414	0.004	1
2013-01	2013	2	49.57	-138.67	75	0.959	0.005	1	0.37	0.01	1	39.4	0.4	1	5.34	0.04	1	0.973	0.008	1	0.401	0.003	1
2013-01	2013	2	49.57	-138.67	100	0.80	0.01	1	0.61	0.01	1	51.0	0.9	1	5.51	0.05	1	0.852	0.007	1	0.57	0.01	1
2013-01	2013	2	49.57	-138.67	150	0.409	0.003	1	0.419	0.004	1	42.6	0.7	1	5.78	0.05	1	1.53	0.02	1	0.83	0.01	1
2013-01	2013	2	49.57	-138.67	200	0.918	0.007	1	0.267	0.003	1	52.2	0.6	1	5.16	0.04	1	1.35	0.02	1	0.359	0.003	1

Cruise	Year	Month	Latitude	Longitude	Depth	dMn	dMn Error	QF	dFe	dFe Error	QF	dCo	dCo Error	QF	dNi	dNi Error	QF	dCu	dCu Error	QF	dCd	dCd Error	QF
			°N	°E	m	nmol/kg	nmol/kg		nmol/kg	nmol/kg		pmol/kg	pmol/kg		nmol/kg	nmol/kg		nmol/kg	nmol/kg		nmol/kg	nmol/kg	
2013-01	2013	2	49.57	-138.67	300	0.742	0.006	1	0.446	0.004	1	37.7	0.6	1	7.63	0.08	1	2.15	0.02	1	1.00	0.01	1
2013-01	2013	2	49.57	-138.67	400	0.75	0.01	1	0.411	0.004	1	44.7	0.6	1	8.1	0.1	1	2.62	0.04	1	1.00	0.01	1
2013-18	2013	8	49.57	-138.67	10	1.07	0.02	1	0.171	0.003	1	45.7	1.5	1	21.8	0.6	4	1.88	0.04	1	0.193	0.002	1
2013-18	2013	8	49.57	-138.67	25	1.03	0.02	1	0.177	0.004	1	43.3	0.9	1	27.1	0.2	4	1.79	0.02	1	0.149	0.003	1
2013-18	2013	8	49.57	-138.67	50	1.138	0.004	1	0.045	0.001	1	55.2	0.4	1	4.75	0.05	1	1.41	0.02	1	0.337	0.005	1
2013-18	2013	8	49.57	-138.67	100	1.04	0.01	1	0.152	0.003	1	49.1	1.2	1	28.7	0.9	4	1.99	0.04	1	0.201	0.003	1
2013-18	2013	8	49.57	-138.67	200	0.530	0.004	1	0.273	0.003	1	51.1	0.5	1	5.73	0.06	1	1.88	0.02	1	0.802	0.006	1
2013-18	2013	8	49.57	-138.67	250	1.051	0.006	1	0.170	0.001	1	44.5	0.5	1	7.54	0.06	1	1.67	0.02	1	0.199	0.002	1
2013-18	2013	8	49.57	-138.67	300	1.02	0.02	1	0.203	0.004	1	44.3	0.9	1	22.0	0.8	4	1.82	0.02	1	0.187	0.003	1
2013-18	2013	8	49.57	-138.67	400	1.19	0.01	1	0.097	0.002	1	53.5	0.8	1	37.9	0.8	4	1.72	0.04	1	0.153	0.003	1
2014-01	2014	2	49.57	-138.67	10	0.96	0.01	1	0.126	0.003	1	39.6	2.3	1	4.38	0.07	1	1.58	0.07	1	0.16	0.01	1
2014-01	2014	2	49.57	-138.67	25	0.975	0.005	1	0.253	0.004	1	40.5	0.8	1	4.42	0.04	1	1.4	0.1	1	0.16	0.01	1
2014-01	2014	2	49.57	-138.67	35	0.99	0.01	1	0.257	0.002	1	39.8	1.3	1	4.50	0.09	1	1.37	0.03	1	0.162	0.003	1
2014-19	2014	8	49.57	-138.67	10	0.527	0.005	1	0.032	0.001	2	6.7	0.3	1	3.41	0.04	1	1.32	0.01	1	0.007	0.000	1
2014-19	2014	8	49.57	-138.67	25	0.703	0.006	1	0.0539	0.0005	1	12.7	0.2	1	3.78	0.03	1	1.09	0.01	1	0.007	0.000	1
2014-19	2014	8	49.57	-138.67	50	1.05	0.06	1	0.029	0.003	2	28.6	1.6	1	4.31	0.23	1	1.37	0.07	1	0.11	0.01	1
2014-19	2014	8	49.57	-138.67	75	1.05	0.04	1	0.037	0.002	1	51.4	2.5	1	4.58	0.18	1	1.56	0.05	1	0.28	0.01	1
2014-19	2014	8	49.57	-138.67	100	0.948	0.009	1	0.048	0.001	1	65.3	0.8	1	4.74	0.04	1	1.71	0.01	1	0.468	0.003	1
2014-19	2014	8	49.57	-138.67	200	0.406	0.004	1	0.250	0.001	1	53.7	0.4	1	5.73	0.03	1	2.08	0.02	1	0.802	0.004	1
2014-19	2014	8	49.57	-138.67	400	0.72	0.01	1	0.501	0.006	1	50.0	0.6	1	7.10	0.09	1	2.23	0.03	1	0.975	0.009	1
2015-01	2015	2	49.57	-138.67	10	0.71	0.01	5	0.052	0.002	5	11.5	0.2	5	4.18	0.05	5	1.04	0.02	5	0.066	0.001	5
2015-01	2015	2	49.57	-138.67	20	0.70	0.02	5	0.024	0.002	5	11.5	0.3	5	4.19	0.09	5	0.98	0.02	5	0.064	0.001	5
2015-01	2015	2	49.57	-138.67	40	0.82	0.01	1	0.014	0.001	6	14.6	0.4	1	4.90	0.05	1	0.97	0.01	1	0.073	0.001	1
2015-01	2015	2	49.57	-138.67	50	0.82	0.01	1	0.029	0.001	1	17.0	0.3	1	4.86	0.05	1	0.80	0.01	1	0.069	0.001	1
2015-01	2015	2	49.57	-138.67	75	0.89	0.02	1	0.163	0.004	1	13.6	0.3	1	4.89	0.08	1	2.16	0.04	1	0.11	0.00	1
2015-01	2015	2	49.57	-138.67	125	0.44	0.01	1	0.165	0.002	1	46.0	0.5	1	4.74	0.06	1	1.71	0.02	1	0.617	0.006	1
2015-01	2015	2	49.57	-138.67	175	0.384	0.002	5	0.35	0.01	5	41.3	0.7	5	5.7	0.1	5	1.51	0.02	5	0.86	0.01	5
2015-01	2015	2	49.57	-138.67	200	0.43	0.01	1	0.284	0.005	1	43.4	0.4	1	5.79	0.05	1	2.12	0.02	1	0.86	0.01	1
2015-01	2015	2	49.57	-138.67	400	0.714	0.007	1	0.512	0.003	1	41.8	0.3	1	7.04	0.05	1	1.837	0.009	1	1.113	0.006	1
2015-10	2015	8	49.57	-138.67	10	0.92	0.01	4	0.28	0.01	4	62.8	2.1	4	4.50	0.05	4	1.25	0.01	4	0.442	0.008	4

Cruise	Year	Month	Latitude	Longitude	Depth	dMn	dMn Error	QF	dFe	dFe Error	QF	dCo	dCo Error	QF	dNi	dNi Error	QF	dCu	dCu Error	QF	dCd	dCd Error	QF
			°N	°E	m	nmol/kg	nmol/kg		nmol/kg	nmol/kg		pmol/kg	pmol/kg		nmol/kg	nmol/kg		nmol/kg	nmol/kg		nmol/kg	nmol/kg	
2015-10	2015	8	49.57	-138.67	15	0.73	0.02	1	0.044	0.001	1	10.0	0.3	1	3.85	0.05	1	1.22	0.06	1	0.013	0.001	1
2015-10	2015	8	49.57	-138.67	40	0.90	0.02	1	0.034	0.000	1	27.0	0.6	1	4.00	0.05	1	1.26	0.04	1	0.095	0.004	1
2015-10	2015	8	49.57	-138.67	50	0.92	0.02	1	0.019	0.000	1	29.5	1.4	1	3.98	0.04	1	1.10	0.05	1	0.108	0.004	1
2015-10	2015	8	49.57	-138.67	75	1.06	0.01	1	0.040	0.001	1	56.8	2.3	1	4.41	0.03	1	1.38	0.07	1	0.372	0.006	1
2015-10	2015	8	49.57	-138.67	100	0.76	0.01	1	0.075	0.001	1	58.6	2.2	1	4.41	0.05	1	1.59	0.04	1	0.484	0.008	1
2015-10	2015	8	49.57	-138.67	150	0.36	0.01	1	0.123	0.009	1	44.7	2.8	1	5.00	0.03	1	1.47	0.00	1	0.687	0.009	1
2015-10	2015	8	49.57	-138.67	200	0.35	0.01	1	0.197	0.007	1	45.7	2.9	1	5.57	0.10	1	1.79	0.01	1	0.757	0.008	1
2015-10	2015	8	49.57	-138.67	300	0.63	0.01	1	0.289	0.011	1	47.2	1.5	1	6.47	0.04	1	1.94	0.03	1	0.892	0.004	1
2015-10	2015	8	49.57	-138.67	400	0.71	0.01	1	0.519	0.009	1	35.1	2.2	1	7.76	0.10	1	2.01	0.01	1	0.987	0.008	1
2017-08	2017	8	49.57	-138.67	ND	ND	ND	ND	ND	ND	ND	ND	ND	ND	ND	ND	ND	ND	ND	ND	ND	ND	ND
2018-040	2018	8	49.57	-138.67	10	0.88	0.01	1	0.030	0.001	1	23.0	0.6	1	4.41	0.08	1	1.55	0.03	1	0.073	0.001	1
2018-040	2018	8	49.57	-138.67	25	0.949	0.009	1	0.031	0.000	1	24.6	0.3	1	4.22	0.04	1	1.29	0.02	1	0.068	0.001	1
2018-040	2018	8	49.57	-138.67	40	1.27	0.01	2	0.081	0.002	2	40.2	0.4	1	4.34	0.08	1	1.30	0.02	1	0.133	0.002	1
2018-040	2018	8	49.57	-138.67	50	0.93	0.01	1	0.025	0.001	1	42.1	0.3	1	3.29	0.02	2	1.10	0.01	1	0.176	0.001	1
2018-040	2018	8	49.57	-138.67	75	1.03	0.01	1	0.059	0.001	1	58.9	0.7	1	4.10	0.03	1	1.30	0.02	1	0.34	0.01	1
2018-040	2018	8	49.57	-138.67	100	0.77	0.01	1	0.157	0.004	1	61.5	1.0	1	4.53	0.06	1	1.51	0.02	1	0.562	0.005	1
2018-040	2018	8	49.57	-138.67	150	0.535	0.004	1	0.410	0.002	1	57.2	0.9	1	4.85	0.03	1	1.61	0.01	1	0.775	0.003	1
2018-040	2018	8	49.57	-138.67	200	0.51	0.03	1	0.45	0.03	1	55.9	3.7	1	5.6	0.3	1	1.8	0.1	1	0.86	0.04	1
2018-040	2018	8	49.57	-138.67	250	0.92	0.01	1	0.846	0.006	1	57.0	0.5	1	5.90	0.08	1	1.78	0.01	1	0.88	0.01	1
2018-040	2018	8	49.57	-138.67	300	0.848	0.008	1	0.79	0.01	1	54.1	0.6	1	6.17	0.08	1	1.97	0.02	1	0.91	0.01	1
2018-040	2018	8	49.57	-138.67	400	0.72	0.01	1	0.65	0.01	1	45.6	0.7	1	6.65	0.07	1	2.06	0.02	1	0.940	0.009	1
2019-008	2019	8	49.57	-138.67	10	0.69	0.01	1	0.111	0.002	1	9.6	0.2	1	3.42	0.02	1	1.320	0.008	1	0.012	0.001	1
2019-008	2019	8	49.57	-138.67	25	0.68	0.01	1	0.055	0.001	1	14.3	0.3	1	3.55	0.03	1	1.07	0.01	1	0.017	0.000	1
2019-008	2019	8	49.57	-138.67	40	1.311	0.008	1	0.091	0.001	1	42.4	0.5	1	4.36	0.03	1	1.191	0.009	1	0.158	0.002	1
2019-008	2019	8	49.57	-138.67	50	1.34	0.02	1	0.054	0.001	1	46.1	0.2	1	4.31	0.03	1	1.22	0.01	1	0.186	0.002	1
2019-008	2019	8	49.57	-138.67	75	1.221	0.009	1	0.061	0.001	1	50.9	0.9	1	4.35	0.03	1	1.242	0.009	1	0.248	0.003	1
2019-008	2019	8	49.57	-138.67	100	0.99	0.01	1	0.129	0.001	1	61.4	0.6	1	4.56	0.03	1	1.322	0.006	1	0.485	0.004	1
2019-008	2019	8	49.57	-138.67	150	0.627	0.005	1	0.410	0.005	1	59.8	0.2	1	5.16	0.05	1	1.54	0.02	1	0.803	0.007	1
2019-008	2019	8	49.57	-138.67	200	0.510	0.005	1	0.395	0.003	1	54.4	0.9	1	5.57	0.05	1	1.65	0.01	1	0.832	0.006	1
2019-008	2019	8	49.57	-138.67	300	0.752	0.007	1	0.541	0.002	1	53.2	0.6	1	6.36	0.05	1	1.76	0.01	1	0.912	0.007	1
2019-008	2019	8	49.57	-138.67	400	0.738	0.004	1	0.657	0.005	1	48.1	0.2	1	6.94	0.03	1	2.05	0.02	1	0.959	0.004	1

Table A.3 Station P16 dissolved Mn, Fe, Co, Ni, Cu, and Cd from winter 2012-2015 and summer 2012-2019. Quality flags (QF) follow the GEOTRACES Quality Flag Policy https://www.geotraces.org/geotraces-quality-flag-policy/.

Cruise	Year	Month	Latitude	Longitude	Depth	dMn	dMn Error	QF	dFe	dFe Error	QF	dCo	dCo Error	QF	dNi	dNi Error	QF	dCu	dCu Error	QF	dCd	dCd Error	QF
			°N	°E	m	nmol/kg	nmol/kg		nmol/kg	nmol/kg		pmol/kg	pmol/kg		nmol/kg	nmol/kg		nmol/kg	nmol/kg		nmol/kg	nmol/kg	
2012-01	2012	2	49.28	-134.67	5	1.029	0.006	1	0.232	0.002	1	46.0	0.5	1	4.22	0.05	1	1.318	0.006	1	0.246	0.002	1
2012-01	2012	2	49.28	-134.67	25	1.024	0.007	1	0.211	0.001	1	45.2	0.5	1	4.20	0.04	1	1.28	0.01	1	0.247	0.002	1
2012-01	2012	2	49.28	-134.67	40	1.01	0.01	1	0.234	0.002	1	44.6	0.7	1	4.17	0.03	1	1.43	0.01	1	0.242	0.001	1
2012-01	2012	2	49.28	-134.67	50	1.083	0.007	1	0.132	0.002	1	46.3	0.4	1	4.29	0.03	1	1.79	0.00	1	0.250	0.002	1
2012-01	2012	2	49.28	-134.67	75	1.085	0.004	1	0.294	0.002	1	47.2	0.2	1	4.25	0.02	1	1.43	0.01	1	0.252	0.003	1
2012-01	2012	2	49.28	-134.67	100	0.96	0.01	1	0.342	0.004	1	50.7	0.7	1	4.39	0.04	1	1.43	0.02	1	0.354	0.002	1
2012-01	2012	2	49.28	-134.67	150	0.455	0.004	1	0.420	0.003	1	56.2	0.4	1	5.18	0.06	1	1.81	0.02	1	0.747	0.006	1
2012-01	2012	2	49.28	-134.67	200	0.485	0.002	1	0.56	0.01	1	55.6	0.9	1	5.63	0.07	1	2.05	0.02	1	0.818	0.005	1
2012-01	2012	2	49.28	-134.67	300	0.67	0.01	1	1.084	0.008	1	56.6	0.7	1	6.51	0.04	1	2.31	0.01	1	0.913	0.004	1
2012-01	2012	2	49.28	-134.67	400	0.739	0.006	1	0.645	0.005	1	49.9	0.4	1	7.15	0.06	1	2.21	0.02	1	0.975	0.004	1
2012-13	2012	8	49.28	-134.66	10	0.524	0.004	1	0.066	0.001	1	25.9	0.2	1	4.26	0.03	1	1.30	0.01	1	0.059	0.000	1
2012-13	2012	8	49.28	-134.66	25	0.679	0.005	1	0.036	0.001	1	41.2	0.5	1	4.39	0.06	1	1.30	0.02	1	0.152	0.002	1
2012-13	2012	8	49.28	-134.66	50	1.21	0.01	1	0.031	0.001	1	60.2	0.5	1	4.61	0.03	1	1.22	0.01	1	0.392	0.003	1
2012-13	2012	8	49.28	-134.66	75	1.062	0.008	1	0.0401	0.0002	1	59.4	0.4	1	4.70	0.04	1	1.259	0.009	1	0.410	0.005	1
2012-13	2012	8	49.28	-134.66	100	0.815	0.005	1	0.056	0.001	1	61.5	0.6	1	4.82	0.03	1	1.45	0.01	1	0.50	0.01	1
2012-13	2012	8	49.28	-134.66	150	0.456	0.004	1	0.256	0.002	1	60.8	0.3	1	5.24	0.05	1	1.58	0.01	1	0.78	0.01	1
2012-13	2012	8	49.28	-134.66	200	0.475	0.003	1	0.350	0.002	1	58.7	0.4	1	6.10	0.02	1	1.96	0.02	1	0.875	0.003	1
2012-13	2012	8	49.28	-134.66	300	0.694	0.006	1	0.442	0.005	1	61.8	0.8	1	6.88	0.07	1	1.99	0.02	1	0.982	0.007	1
2012-13	2012	8	49.28	-134.66	400	0.720	0.006	1	0.344	0.002	1	43.0	0.5	1	7.42	0.07	1	2.47	0.02	1	1.009	0.008	1
2013-01	2013	2	49.28	-134.67	10	0.97	0.03	1	0.20	0.01	1	35.5	1.1	1	5.1	0.1	1	0.52	0.01	1	0.31	0.01	1

Cruise	Year	Month	Latitude	Longitude	Depth	dMn	dMn Error	QF	dFe	dFe Error	QF	dCo	dCo Error	QF	dNi	dNi Error	QF	dCu	dCu Error	QF	dCd	dCd Error	QF
			°N	°E	m	nmol/kg	nmol/kg		nmol/kg	nmol/kg		pmol/kg	pmol/kg		nmol/kg	nmol/kg		nmol/kg	nmol/kg		nmol/kg	nmol/kg	
2013-01	2013	2	49.28	-134.67	25	1.044	0.006	1	1.00	0.01	4	44.9	0.9	1	5.14	0.01	1	1.135	0.007	1	0.316	0.002	1
2013-01	2013	2	49.28	-134.67	40	1.116	0.008	1	0.222	0.002	1	38.8	0.7	1	5.22	0.05	1	1.181	0.007	1	0.363	0.003	1
2013-01	2013	2	49.28	-134.67	75	0.97	0.01	1	0.098	0.002	1	28.2	0.5	1	5.0	0.1	1	0.54	0.01	1	0.31	0.01	1
2013-01	2013	2	49.28	-134.67	100	0.93	0.01	1	0.110	0.000	1	46.3	0.8	1	4.94	0.05	1	0.69	0.01	1	0.50	0.01	1
2013-01	2013	2	49.28	-134.67	150	0.384	0.005	1	0.224	0.002	1	43.4	0.4	1	5.13	0.07	1	0.82	0.01	1	0.72	0.01	1
2013-01	2013	2	49.28	-134.67	200	0.364	0.003	1	0.286	0.004	1	39.6	0.6	1	5.51	0.07	1	0.729	0.006	1	0.77	0.01	1
2013-01	2013	2	49.28	-134.67	300	0.53	0.01	1	0.36	0.01	1	41.4	0.6	1	6.52	0.06	1	1.16	0.01	1	0.87	0.01	1
2013-01	2013	2	49.28	-134.67	400	0.627	0.005	1	0.604	0.004	1	33.6	0.7	1	7.30	0.02	1	1.314	0.007	1	0.967	0.007	1
2013-18	2013	8	49.28	-134.67	10	1.76	0.03	1	0.078	0.002	1	19.3	0.4	1	4.68	0.08	1	1.45	0.02	1	0.027	0.001	1
2013-18	2013	8	49.28	-134.67	25	1.50	0.02	1	0.082	0.002	1	51.7	1.0	1	4.67	0.08	1	1.26	0.02	1	0.187	0.003	1
2013-18	2013	8	49.28	-134.67	50	1.72	0.02	1	0.105	0.002	1	63.6	1.3	1	4.75	0.07	1	1.44	0.02	1	0.328	0.004	1
2013-18	2013	8	49.28	-134.67	75	1.40	0.02	1	0.110	0.002	1	61.3	1.0	1	5.06	0.08	1	1.31	0.02	1	0.362	0.004	1
2013-18	2013	8	49.28	-134.67	100	1.19	0.02	1	0.112	0.004	1	60.1	1.0	1	5.1	0.1	1	1.30	0.03	1	0.40	0.01	1
2013-18	2013	8	49.28	-134.67	150	0.693	0.006	1	0.314	0.005	1	60.0	0.9	1	5.3	0.1	1	1.54	0.03	1	0.672	0.001	1
2013-18	2013	8	49.28	-134.67	200	0.656	0.005	1	0.47	0.01	1	57.1	0.9	1	5.67	0.09	1	1.67	0.04	1	0.776	0.007	1
2013-18	2013	8	49.28	-134.67	250	0.61	0.01	1	0.416	0.005	1	55.4	0.6	1	6.20	0.09	1	1.76	0.03	1	0.834	0.008	1
2013-18	2013	8	49.28	-134.67	300	0.840	0.005	1	0.581	0.005	1	56.5	0.8	1	6.65	0.09	1	1.98	0.03	1	0.881	0.008	1
2013-18	2013	8	49.28	-134.67	400	0.972	0.009	1	0.74	0.01	1	54.0	0.8	1	7.2	0.1	1	1.99	0.04	1	0.938	0.008	1
2014-01	2014	2	49.28	-134.66	ND	ND	ND	ND	ND	ND	ND	ND	ND	ND	ND	ND	ND	ND	ND	ND	ND	ND	ND
2014-19	2014	8	49.28	-134.67	10	0.539	0.001	1	0.395	0.002	4	7.5	0.2	1	3.54	0.01	1	1.40	0.01	1	0.003	0.058	2
2014-19	2014	8	49.28	-134.67	25	0.656	0.004	1	0.0449	0.0005	1	10.1	0.1	1	3.74	0.02	1	1.07	0.01	1	0.005	0.037	2
2014-19	2014	8	49.28	-134.67	50	0.96	0.02	1	0.089	0.002	1	20.5	0.4	1	4.18	0.07	1	1.24	0.01	1	0.035	0.000	1
2014-19	2014	8	49.28	-134.67	75	1.01	0.01	1	0.074	0.001	1	32.7	0.6	1	4.43	0.04	1	1.61	0.02	1	0.126	0.002	1
2014-19	2014	8	49.28	-134.67	100	0.927	0.005	1	0.054	0.001	1	64.5	0.5	1	4.55	0.03	1	1.49	0.01	1	0.415	0.004	1
2014-19	2014	8	49.28	-134.67	200	0.46	0.01	1	0.269	0.003	1	54.5	0.5	1	5.74	0.06	1	2.00	0.02	1	0.800	0.006	1
2014-19	2014	8	49.28	-134.67	400	0.76	0.04	1	0.50	0.03	1	52.2	2.6	1	6.9	0.3	1	2.21	0.09	1	0.96	0.04	1
2015-01	2015	2	49.28	-134.67	10	0.92	0.02	1	0.451	0.01	4	17.0	0.5	1	4.98	0.07	1	2.13	0.03	4	0.078	0.001	1
2015-01	2015	2	49.28	-134.67	20	0.80	0.01	5	0.042	0.001	5	20.9	0.2	5	4.31	0.04	5	0.98	0.02	5	0.068	0.001	5
2015-01	2015	2	49.28	-134.67	40	0.91	0.01	1	0.044	0.001	1	21.1	0.2	1	4.96	0.08	1	0.85	0.02	1	0.076	0.001	1
2015-01	2015	2	49.28	-134.67	50	0.94	0.02	1	0.060	0.002	1	16.9	0.3	1	5.0	0.1	1	1.07	0.02	1	0.078	0.002	1

Cruise	Year	Month	Latitude	Longitude	Depth	dMn	dMn Error	QF	dFe	dFe Error	QF	dCo	dCo Error	QF	dNi	dNi Error	QF	dCu	dCu Error	QF	dCd	dCd Error	QF
			°N	°E	m	nmol/kg	nmol/kg		nmol/kg	nmol/kg		pmol/kg	pmol/kg		nmol/kg	nmol/kg		nmol/kg	nmol/kg		nmol/kg	nmol/kg	
2015-01	2015	2	49.28	-134.67	75	0.89	0.02	1	0.042	0.002	1	18.7	0.4	1	4.9	0.1	1	0.85	0.02	1	0.095	0.001	1
2015-01	2015	2	49.28	-134.67	125	0.44	0.01	1	0.186	0.002	1	29.4	0.4	1	4.64	0.04	1	1.81	0.01	1	0.59	0.01	1
2015-01	2015	2	49.28	-134.67	150	0.403	0.002	1	0.350	0.003	1	36.6	0.2	1	5.29	0.04	1	1.971	0.008	1	0.787	0.005	1
2015-01	2015	2	49.28	-134.67	200	0.371	0.004	1	0.285	0.003	1	41.4	0.6	1	5.34	0.06	1	3.18	0.03	1	0.830	0.007	1
2015-01	2015	2	49.28	-134.67	400	0.61	0.01	1	0.532	0.002	1	35.3	0.3	1	6.75	0.09	1	2.42	0.02	1	0.956	0.006	1
2015-10	2015	8	49.28	-134.67	10	2.72	0.03	1	0.048	0.007	1	38.57	0.99	1	3.73	0.04	1	2.05	0.04	1	0.036	0.003	1
2015-10	2015	8	49.28	-134.67	25	1.01	0.02	1	0.049	0.006	1	12.76	0.86	1	3.68	0.04	1	1.429	0.010	1	0.015	0.002	1
2015-10	2015	8	49.28	-134.67	40	2.42	0.01	1	0.041	0.008	1	35.98	1.59	1	3.74	0.03	1	1.91	0.03	1	0.031	0.002	1
2015-10	2015	8	49.28	-134.67	50	0.72	0.01	1	0.004	0.007	1	11.63	0.87	1	3.65	0.03	1	1.13	0.02	1	0.003	0.000	1
2015-10	2015	8	49.28	-134.67	75	0.91	0.01	1	0.043	0.007	1	29.9	1.6	1	3.97	0.03	1	2.60	0.03	4	0.115	0.005	1
2015-10	2015	8	49.28	-134.67	100	0.82	0.01	1	0.037	0.007	1	47.4	1.1	1	4.40	0.06	1	1.63	0.02	1	0.320	0.007	1
2015-10	2015	8	49.28	-134.67	150	0.43	0.01	1	0.148	0.009	1	55.8	1.7	1	4.84	0.05	1	1.99	0.02	1	0.631	0.016	1
2015-10	2015	8	49.28	-134.67	200	0.40	0.01	1	0.254	0.010	1	48.7	2.0	1	5.73	0.07	1	2.37	0.00	1	0.792	0.014	1
2015-10	2015	8	49.28	-134.67	400	0.92	0.01	1	0.707	0.016	4	46.3	3.2	1	7.16	0.08	1	2.80	0.03	1	0.977	0.000	1
2017-008	2017	8	49.28	-134.67	10	0.936	0.008	1	0.069	0.001	1	10.4	0.2	1	4.10	0.03	1	1.38	0.01	1	0.023	0.001	1
2017-008	2017	8	49.28	-134.67	25	0.91	0.01	1	0.078	0.001	1	11.4	0.2	1	4.11	0.04	1	0.882	0.006	1	0.027	0.001	1
2017-008	2017	8	49.28	-134.67	50	0.848	0.007	1	0.059	0.001	1	18.1	0.4	1	4.23	0.05	1	1.24	0.02	1	0.082	0.002	1
2017-008	2017	8	49.28	-134.67	100	0.886	0.008	1	0.078	0.002	1	43.2	0.4	1	4.59	0.03	1	1.29	0.01	1	0.293	0.003	1
2017-008	2017	8	49.28	-134.67	150	0.590	0.004	1	0.312	0.001	1	56.5	0.7	1	5.09	0.03	1	1.51	0.02	1	0.681	0.005	1
2017-008	2017	8	49.28	-134.67	200	0.384	0.004	1	0.399	0.004	1	35.5	0.4	1	4.23	0.06	1	1.23	0.02	1	0.605	0.005	1
2017-008	2017	8	49.28	-134.67	300	0.632	0.004	1	0.543	0.005	1	51.3	0.6	1	6.60	0.06	1	1.83	0.02	1	0.90	0.01	1
2017-008	2017	8	49.28	-134.67	500	0.88	0.01	1	0.77	0.01	1	41.5	0.8	1	7.8	0.1	1	2.16	0.04	1	0.988	0.008	1
2018-040	2018	8	49.28	-134.67	10	1.69	0.02	1	0.038	0.001	1	27.0	0.7	1	3.77	0.04	1	1.374	0.006	1	0.051	0.001	1
2018-040	2018	8	49.28	-134.67	25	1.66	0.02	1	0.018	0.001	1	24.3	0.7	1	3.72	0.05	1	1.12	0.01	1	0.040	0.001	1
2018-040	2018	8	49.28	-134.67	40	1.05	0.01	1	0.022	0.000	1	24.5	0.3	1	3.73	0.06	1	1.02	0.01	1	0.048	0.001	1
2018-040	2018	8	49.28	-134.67	50	1.12	0.01	1	0.041	0.001	1	35.0	0.4	1	3.85	0.05	1	1.03	0.01	1	0.086	0.002	1
2018-040	2018	8	49.28	-134.67	75	1.09	0.02	1	0.070	0.001	1	53.9	0.8	1	4.10	0.05	1	1.14	0.01	1	0.231	0.004	1
2018-040	2018	8	49.28	-134.67	100	0.90	0.01	1	0.154	0.003	1	60.8	0.9	1	4.38	0.04	1	1.23	0.01	1	0.446	0.004	1
2018-040	2018	8	49.28	-134.67	150	0.57	0.01	1	0.292	0.004	1	59.1	0.8	1	4.85	0.03	1	1.436	0.008	1	0.764	0.006	1
2018-040	2018	8	49.28	-134.67	200	0.46	0.01	1	0.37	0.01	1	52.6	0.7	1	5.30	0.08	1	1.68	0.03	1	0.814	0.006	1

Cruise	Year	Month	Latitude °N	Longitude °E	Depth m	dMn nmol/kg	dMn Error nmol/kg	QF	dFe nmol/kg	dFe Error nmol/kg	QF	dCo pmol/kg	dCo Error pmol/kg	QF	dNi nmol/kg	dNi Error nmol/kg	QF	dCu nmol/kg	dCu Error nmol/kg	QF	dCd nmol/kg	dCd Error nmol/kg	QF
2018-040	2018	8	49.28	-134.67	250	0.60	0.01	1	0.52	0.01	1	53.5	0.5	1	5.82	0.05	1	1.66	0.02	1	0.869	0.004	1
2018-040	2018	8	49.28	-134.67	300	0.769	0.005	1	0.625	0.005	1	53.7	0.6	1	6.14	0.07	1	1.79	0.02	1	0.903	0.004	1
2018-040	2018	8	49.28	-134.67	400	0.75	0.01	1	0.62	0.01	1	47.6	0.6	1	6.59	0.05	1	1.86	0.02	1	0.935	0.006	1
2019-008	2019	8	49.28	-134.67	10	0.60	0.01	1	0.218	0.004	1	13.5	0.2	1	3.59	0.04	1	1.41	0.01	1	0.025	0.001	1
2019-008	2019	8	49.28	-134.67	25	0.636	0.004	1	0.054	0.000	1	16.9	0.4	1	3.61	0.03	1	0.973	0.008	1	0.014	0.000	1
2019-008	2019	8	49.28	-134.67	40	0.870	0.008	1	0.066	0.001	1	27.9	0.4	1	3.99	0.05	1	1.09	0.01	1	0.086	0.001	1
2019-008	2019	8	49.28	-134.67	50	0.874	0.003	1	0.059	0.001	1	33.9	0.4	1	4.10	0.02	1	1.148	0.009	1	0.136	0.002	1
2019-008	2019	8	49.28	-134.67	75	0.898	0.008	1	0.588	0.005	4	38.7	0.7	1	4.32	0.05	1	1.23	0.01	1	0.183	0.003	1
2019-008	2019	8	49.28	-134.67	100	0.798	0.006	1	0.117	0.002	1	54.8	0.2	1	4.45	0.06	1	1.32	0.01	1	0.426	0.003	1
2019-008	2019	8	49.28	-134.67	150	0.464	0.003	1	0.271	0.002	1	55.6	0.6	1	4.79	0.04	1	1.54	0.02	1	0.736	0.006	1
2019-008	2019	8	49.28	-134.67	200	0.367	0.002	1	0.265	0.002	1	48.3	0.7	1	4.99	0.05	1	1.53	0.01	1	0.739	0.006	1
2019-008	2019	8	49.28	-134.67	300	0.546	0.003	1	0.391	0.002	1	49.2	0.7	1	6.05	0.03	1	1.725	0.009	1	0.871	0.006	1
2019-008	2019	8	49.28	-134.67	400	0.609	0.003	1	0.464	0.004	1	46.8	0.5	1	6.67	0.06	1	2.24	0.02	1	0.933	0.005	1

Table A.4 Station P12 dissolved Mn, Fe, Co, Ni, Cu, and Cd from winter 2012-2015 and summer 2012-2019. Quality flags (QF) follow the GEOTRACES Quality Flag Policy https://www.geotraces.org/geotraces-quality-flag-policy/.

Cruise	Year	Month	Latitude	Longitude	Depth	dMn	dMn Error	QF	dFe	dFe Error	QF	dCo	dCo Error	QF	dNi	dNi Error	QF	dCu	dCu Error	QF	dCd	dCd Error	QF
			°N	°E	m	nmol/kg	nmol/kg		nmol/kg	nmol/kg		pmol/kg	pmol/kg		nmol/kg	nmol/kg		nmol/kg	nmol/kg		nmol/kg	nmol/kg	
2012-01	2012	2	48.97	-130.67	10	0.982	0.009	1	0.269	0.001	1	36.6	0.4	1	4.51	0.04	1	3.57	0.02	4	0.167	0.002	1
2012-01	2012	2	48.97	-130.67	25	0.97	0.04	1	0.16	0.01	1	37.1	1.6	1	4.5	0.2	1	1.33	0.06	1	0.160	0.002	1
2012-01	2012	2	48.97	-130.67	40	0.98	0.02	1	0.34	0.01	1	38.0	0.8	1	4.6	0.1	1	1.36	0.03	1	0.157	0.001	1
2012-01	2012	2	48.97	-130.67	50	1.00	0.05	1	0.37	0.02	1	39.0	2.3	1	4.6	0.2	1	3.1	0.1	4	0.157	0.004	1
2012-01	2012	2	48.97	-130.67	75	1.01	0.02	1	1.53	0.03	4	39.4	0.9	1	4.57	0.07	1	1.52	0.02	1	0.163	0.001	1
2012-01	2012	2	48.97	-130.67	100	0.93	0.01	1	0.400	0.003	1	36.1	0.6	1	4.33	0.07	1	1.30	0.02	1	0.155	0.003	1
2012-01	2012	2	48.97	-130.67	200	0.47	0.01	1	1.95	0.05	4	71.5	1.7	1	5.74	0.09	1	1.95	0.03	1	0.71	0.01	1
2012-01	2012	2	48.97	-130.67	300	0.621	0.005	1	0.902	0.006	1	66.1	0.9	1	6.45	0.06	1	1.85	0.03	1	0.87	0.01	1
2012-01	2012	2	48.97	-130.67	400	0.904	0.008	1	1.52	0.01	1	63.2	0.5	1	7.16	0.05	1	2.11	0.02	1	0.980	0.008	1
2012-13	2012	8	48.97	-130.67	5	1.13	0.01	1	0.063	0.001	1	53.9	0.5	1	4.51	0.06	1	1.54	0.01	1	0.310	0.004	1
2012-13	2012	8	48.97	-130.67	10	1.12	0.01	1	0.045	0.001	1	25.3	0.4	1	4.32	0.07	1	1.34	0.02	1	0.072	0.001	1
2012-13	2012	8	48.97	-130.67	25	1.00	0.01	1	0.064	0.001	1	41.1	0.6	1	4.42	0.05	1	1.26	0.01	1	0.16	0.00	1
2012-13	2012	8	48.97	-130.67	50	0.74	0.01	1	0.73	0.01	4	28.3	0.3	1	9.1	0.1	4	2.58	0.03	4	1.06	0.01	4
2012-13	2012	8	48.97	-130.67	75	1.039	0.008	1	0.046	0.001	1	55.3	0.3	1	4.56	0.06	1	1.40	0.01	1	0.326	0.002	1
2012-13	2012	8	48.97	-130.67	100	0.845	0.007	1	0.056	0.001	1	58.3	1.1	1	4.74	0.05	1	1.55	0.01	1	0.399	0.001	1
2012-13	2012	8	48.97	-130.67	150	0.50	0.01	1	0.131	0.002	1	58.6	0.9	1	4.70	0.06	1	1.55	0.02	1	0.619	0.006	1
2012-13	2012	8	48.97	-130.67	200	0.395	0.003	1	0.208	0.001	1	55.0	0.5	1	5.17	0.07	1	1.65	0.01	1	0.73	0.01	1
2012-13	2012	8	48.97	-130.67	300	0.452	0.005	1	0.317	0.005	1	57.9	0.6	1	6.07	0.02	1	1.94	0.02	1	0.841	0.004	1
2012-13	2012	8	48.97	-130.67	400	0.557	0.005	1	0.449	0.003	1	48.5	0.5	1	6.74	0.05	1	2.24	0.02	1	0.942	0.008	1
2013-01	2013	2	48.97	-130.67	ND	ND	ND	ND	ND	ND	ND	ND	ND	ND	ND	ND	ND	ND	ND	ND	ND	ND	ND

Cruise	Year	Month	Latitude	Longitude	Depth	dMn	dMn Error	QF	dFe	dFe Error	QF	dCo	dCo Error	QF	dNi	dNi Error	QF	dCu	dCu Error	QF	dCd	dCd Error	QF
			°N	°E	m	nmol/kg	nmol/kg		nmol/kg	nmol/kg		pmol/kg	pmol/kg		nmol/kg	nmol/kg		nmol/kg	nmol/kg		nmol/kg	nmol/kg	
2013-18	2013	8	48.97	-130.67	10	1.68	0.04	1	0.136	0.003	1	15.6	0.2	1	4.23	0.07	1	1.35	0.01	1	0.020	0.001	1
2013-18	2013	8	48.97	-130.67	25	1.84	0.02	1	0.076	0.001	1	46.9	0.7	1	4.35	0.03	1	1.26	0.01	1	0.095	0.002	1
2013-18	2013	8	48.97	-130.67	50	1.51	0.02	1	0.158	0.002	1	61.5	0.5	1	4.81	0.06	1	1.32	0.02	1	0.35	0.01	1
2013-18	2013	8	48.97	-130.67	75	1.36	0.01	1	0.070	0.001	1	61.1	0.8	1	4.73	0.06	1	1.32	0.01	1	0.363	0.002	1
2013-18	2013	8	48.97	-130.67	100	1.09	0.02	1	0.114	0.002	1	61.3	0.4	1	4.96	0.06	1	1.43	0.02	1	0.43	0.01	1
2013-18	2013	8	48.97	-130.67	150	0.74	0.01	1	0.365	0.005	1	65.9	1.3	1	5.4	0.1	1	1.56	0.03	1	0.674	0.006	1
2013-18	2013	8	48.97	-130.67	200	0.684	0.005	1	0.423	0.005	1	62.7	1.3	1	5.52	0.07	1	1.60	0.02	1	0.74	0.01	1
2013-18	2013	8	48.97	-130.67	300	0.71	0.01	1	0.53	0.01	1	58.7	0.8	1	6.9	0.1	1	1.94	0.02	1	0.89	0.01	1
2013-18	2013	8	48.97	-130.67	400	0.821	0.007	1	0.69	0.01	1	52.9	0.7	1	6.9	0.1	1	1.87	0.03	1	0.891	0.007	1
2014-01	2014	2	48.97	-130.67	25	1.18	0.02	1	0.213	0.004	1	36.9	1.6	1	4.23	0.09	1	1.23	0.06	1	0.145	0.004	1
2014-01	2014	2	48.97	-130.67	35	1.17	0.04	1	0.095	0.001	1	36.5	1.8	1	4.2	0.1	1	1.57	0.06	1	0.144	0.003	1
2014-19	2014	8	48.97	-130.67	10	2.061	0.019	1	0.080	0.001	1	20.3	0.4	1	3.91	0.03	1	1.686	0.008	1	0.013	0.000	1
2014-19	2014	8	48.97	-130.67	25	1.43	0.02	1	0.071	0.002	1	16.2	0.4	1	3.71	0.05	1	1.42	0.02	1	0.014	0.000	1
2014-19	2014	8	48.97	-130.67	50	1.41	0.02	1	0.082	0.001	1	35.2	0.6	1	4.07	0.05	1	1.57	0.02	1	0.056	0.001	1
2014-19	2014	8	48.97	-130.67	75	0.978	0.004	1	0.133	0.001	1	61.8	0.9	1	4.70	0.03	1	1.50	0.01	1	0.349	0.003	1
2014-19	2014	8	48.97	-130.67	100	0.700	0.002	1	0.235	0.001	1	69.8	0.6	1	4.85	0.04	1	1.59	0.02	1	0.542	0.002	1
2014-19	2014	8	48.97	-130.67	200	0.569	0.005	1	0.584	0.002	1	61.5	0.3	1	5.337	0.007	1	2.08	0.02	1	0.762	0.007	1
2014-19	2014	8	48.97	-130.67	400	0.869	0.018	1	0.90	0.02	1	58.4	0.7	1	6.7	0.1	1	2.15	0.05	1	0.93	0.02	1
2015-01	2015	2	48.97	-130.66	10	1.29	0.02	1	0.057	0.001	1	19.1	0.4	1	4.71	0.08	1	1.01	0.02	1	0.052	0.001	1
2015-01	2015	2	48.97	-130.66	20	1.27	0.02	1	0.093	0.001	1	18.8	0.2	1	4.84	0.05	1	0.95	0.01	1	0.051	0.001	1
2015-01	2015	2	48.97	-130.66	40	1.27	0.05	1	0.30	0.01	1	17.1	0.8	1	4.7	0.2	1	0.76	0.03	1	0.049	0.001	1
2015-01	2015	2	48.97	-130.66	50	1.17	0.02	5	0.73	0.01	5	26.0	0.3	5	4.40	0.06	5	1.05	0.02	5	0.043	0.001	5
2015-01	2015	2	48.97	-130.66	75	1.09	0.02	1	0.181	0.002	1	18.3	0.1	1	4.83	0.05	1	1.43	0.03	1	0.073	0.002	1
2015-01	2015	2	48.97	-130.66	125	0.51	0.01	1	0.226	0.002	1	45.4	0.5	1	4.65	0.05	1	4.26	0.03	4	0.52	0.01	1
2015-01	2015	2	48.97	-130.66	200	0.288	0.001	1	0.255	0.002	1	30.2	0.5	1	4.81	0.05	1	1.66	0.01	1	0.61	0.01	1
2015-01	2015	2	48.97	-130.66	400	0.80	0.01	1	2.00	0.02	1	55.8	0.6	1	6.65	0.07	1	2.01	0.01	1	1.007	0.009	1
2015-10	2015	8	48.97	-130.67	10	0.74	0.01	1	0.049	0.002	1	8.1	0.8	1	3.90	0.02	1	1.82	0.02	1	0.006	0.000	1
2015-10	2015	8	48.97	-130.67	25	3.41	0.01	1	0.074	0.005	1	53.9	2.7	1	3.61	0.01	1	1.46	0.03	1	0.063	0.006	1
2015-10	2015	8	48.97	-130.67	40	2.38	0.01	1	0.056	0.004	1	38.5	0.7	1	3.60	0.03	1	1.38	0.02	1	0.051	0.004	1
2015-10	2015	8	48.97	-130.67	50	0.89	0.01	1	0.020	0.005	6	14.5	0.4	1	3.43	0.04	1	1.05	0.01	1	0.013	0.002	1

Cruise	Year	Month	Latitude	Longitude	Depth	dMn	dMn Error	QF	dFe	dFe Error	QF	dCo	dCo Error	QF	dNi	dNi Error	QF	dCu	dCu Error	QF	dCd	dCd Error	QF
			°N	°E	m	nmol/kg	nmol/kg		nmol/kg	nmol/kg		pmol/kg	pmol/kg		nmol/kg	nmol/kg		nmol/kg	nmol/kg		nmol/kg	nmol/kg	
2015-10	2015	8	48.97	-130.67	75	1.16	0.02	1	0.026	0.004	1	26.4	1.2	1	3.52	0.05	1	1.05	0.02	1	0.049	0.002	1
2015-10	2015	8	48.97	-130.67	100	0.89	0.01	1	0.085	0.006	1	29.7	1.8	1	3.64	0.03	1	1.18	0.01	1	0.113	0.002	1
2015-10	2015	8	48.97	-130.67	150	0.40	0.01	1	0.117	0.008	1	49.8	1.4	1	4.58	0.06	1	1.60	0.02	1	0.572	0.004	1
2015-10	2015	8	48.97	-130.67	200	0.51	0.01	1	0.47	0.01	4	57.3	2.5	1	5.26	0.02	1	1.78	0.02	1	0.675	0.000	1
2015-10	2015	8	48.97	-130.67	300	0.39	0.01	1	0.248	0.008	1	46.3	1.4	1	5.86	0.05	1	1.91	0.03	1	0.800	0.001	1
2015-10	2015	8	48.97	-130.67	400	0.68	0.01	1	0.420	0.009	1	51.9	3.1	1	6.78	0.06	1	2.14	0.03	1	0.953	0.005	1
2017-08	2017	8	48.97	-130.67	10	1.54	0.01	1	0.584	0.003	4	35.7	0.3	4	4.29	0.04	4	2.09	0.02	4	0.024	0.001	1
2017-08	2017	8	48.97	-130.67	25	1.14	0.01	1	0.087	0.001	1	13.9	0.2	1	3.66	0.03	1	0.98	0.01	1	0.018	0.001	1
2017-08	2017	8	48.97	-130.67	50	1.09	0.01	1	0.149	0.002	4	25.4	0.4	1	3.76	0.06	1	1.02	0.01	4	0.035	0.000	1
2017-08	2017	8	48.97	-130.67	100	0.996	0.007	1	0.076	0.001	1	57.3	0.9	1	4.14	0.04	1	0.82	0.01	1	0.302	0.004	1
2017-08	2017	8	48.97	-130.67	150	0.437	0.004	1	0.324	0.004	1	61.2	1.2	1	4.96	0.04	1	1.15	0.01	1	0.70	0.01	1
2017-08	2017	8	48.97	-130.67	300	0.720	0.007	1	0.732	0.005	1	62.1	1.0	1	6.45	0.06	1	2.04	0.02	1	0.895	0.005	1
2017-08	2017	8	48.97	-130.67	500	0.986	0.007	1	1.253	0.008	1	48.3	0.6	1	7.39	0.08	1	2.12	0.02	1	0.944	0.004	1
2018-040	2018	8	48.97	-130.67	10	3.24	0.04	1	0.192	0.003	1	73.1	0.6	1	5.49	0.05	1	1.53	0.01	1	0.028	0.001	1
2018-040	2018	8	48.97	-130.67	25	2.51	0.07	1	0.20	0.01	1	41.6	1.1	1	4.04	0.09	1	1.22	0.02	1	0.029	0.001	1
2018-040	2018	8	48.97	-130.67	40	1.48	0.02	1	0.083	0.001	1	30.4	0.3	1	3.58	0.03	1	1.069	0.008	1	0.028	0.000	1
2018-040	2018	8	48.97	-130.67	50	1.457	0.008	1	0.121	0.002	1	38.9	0.5	1	3.65	0.02	1	1.039	0.007	1	0.073	0.000	1
2018-040	2018	8	48.97	-130.67	75	1.33	0.02	1	0.102	0.002	1	56.2	1.0	1	3.75	0.04	1	1.217	0.009	1	0.217	0.003	1
2018-040	2018	8	48.97	-130.67	100	1.17	0.05	1	0.31	0.01	1	77.7	3.2	1	4.3	0.1	1	1.23	0.03	1	0.47	0.02	1
2018-040	2018	8	48.97	-130.67	150	0.659	0.003	1	0.52	0.01	1	68.7	0.3	1	4.63	0.04	1	1.39	0.02	1	0.721	0.004	1
2018-040	2018	8	48.97	-130.67	200	0.85	0.01	1	0.99	0.01	1	72.0	1.4	1	5.34	0.06	1	1.79	0.02	1	0.76	0.01	1
2018-040	2018	8	48.97	-130.67	250	0.93	0.06	1	1.20	0.09	1	69.1	4.9	1	5.5	0.4	1	1.7	0.1	1	0.84	0.04	1
2018-040	2018	8	48.97	-130.67	300	2.53	0.03	4	1.58	0.02	2	127.3	1.1	4	8.5	0.079	4	2.3	0.01	4	0.85	0.01	1
2018-040	2018	8	48.97	-130.67	400	1.07	0.02	1	1.66	0.03	1	57.1	0.9	1	6.2	0.1	1	1.59	0.02	1	0.926	0.006	1
2019-008	2019	8	48.97	-130.67	10	1.65	0.02	1	0.149	0.001	1	24.2	0.5	1	3.75	0.05	1	1.47	0.02	1	0.026	0.001	1
2019-008	2019	8	48.97	-130.67	20	2.12	0.01	1	0.064	0.001	1	32.2	0.3	1	3.65	0.04	1	1.16	0.01	1	0.035	0.001	1
2019-008	2019	8	48.97	-130.67	50	1.55	0.01	1	0.198	0.001	1	61.8	0.6	1	4.00	0.03	1	1.22	0.01	1	0.238	0.003	1
2019-008	2019	8	48.97	-130.67	75	1.26	0.02	1	0.430	0.005	1	77.3	0.9	1	4.22	0.05	1	1.27	0.02	1	0.378	0.001	1
2019-008	2019	8	48.97	-130.67	100	1.22	0.01	1	0.885	0.005	1	93.7	0.7	1	4.33	0.04	1	1.292	0.007	1	0.51	0.01	1
2019-008	2019	8	48.97	-130.67	150	1.357	0.009	1	1.282	0.007	1	102.3	0.9	1	4.88	0.05	1	1.39	0.01	1	0.703	0.005	1
2019-008	2019	8	48.97	-130.67	200	1.388	0.008	1	1.522	0.006	1	87.7	0.8	1	4.98	0.03	1	1.47	0.01	1	0.735	0.005	1
2019-008	2019	8	48.97	-130.67	250	1.36	0.02	1	1.95	0.02	4	76.7	1.2	1	5.34	0.07	1	1.67	0.02	1	0.79	0.01	1
2019-008	2019	8	48.97	-130.67	300	1.042	0.009	1	1.61	0.01	1	63.4	0.5	1	5.45	0.03	1	1.495	0.007	1	0.795	0.005	1
2019-008	2019	8	48.97	-130.67	400	1.06	0.01	1	1.74	0.02	1	55.8	0.7	1	6.18	0.06	1	2.06	0.02	1	0.879	0.007	1

Table A.5 Station P4 dissolved Mn, Fe, Co, Ni, Cu, and Cd from winter 2012-2015 and summer 2012-2019. Quality flags (QF) follow the GEOTRACES Quality Flag Policy https://www.geotraces.org/geotraces-quality-flag-policy/.

Cruise	Year	Month	Latitude	Longitude	Depth	dMn	dMn Error	QF	dFe	dFe Error	QF	dCo	dCo Error	QF	dNi	dNi Error	QF	dCu	dCu Error	QF	dCd	dCd Error	QF
			°N	°E	m	nmol/kg	nmol/kg		nmol/kg	nmol/kg		pmol/kg	pmol/kg		nmol/kg	nmol/kg		nmol/kg	nmol/kg		nmol/kg	nmol/kg	
2012-01	2012	2	48.65	-126.67	10	2.57	0.03	1	0.611	0.004	1	71.7	0.7	1	4.09	0.03	1	1.87	0.02	1	0.212	0.002	1
2012-01	2012	2	48.65	-126.67	25	2.37	0.02	1	0.630	0.003	1	64.5	0.6	1	3.99	0.02	1	1.384	0.009	1	0.204	0.003	1
2012-01	2012	2	48.65	-126.67	40	2.406	0.003	1	1.97	0.02	1	69.7	0.7	1	4.21	0.03	1	1.53	0.02	1	0.256	0.001	1
2012-13	2012	8	48.65	-126.67	10	6.08	0.00	1	0.24	0.00	1	94.99	0.02	1	4.011	0.000	1	1.675	0.001	1	0.182	0.000	1
2012-13	2012	8	48.65	-126.67	25	2.1	0.2	1	0.203	0.003	1	53.9	1.2	1	3.88	0.07	1	1.23	0.02	1	0.187	0.003	1
2012-13	2012	8	48.65	-126.67	50	1.35	0.01	1	0.15	0.00	1	51.1	0.8	1	4.06	0.04	1	1.23	0.02	1	0.259	0.001	1
2012-13	2012	8	48.65	-126.67	75	1.23	0.01	1	0.23	0.00	1	77.8	0.5	1	4.31	0.03	1	1.30	0.01	1	0.410	0.006	1
2012-13	2012	8	48.65	-126.67	100	1.02	0.02	1	0.424	0.003	1	81.3	0.6	1	4.43	0.05	1	1.47	0.01	1	0.629	0.004	1
2012-13	2012	8	48.65	-126.67	150	1.22	0.01	1	1.185	0.003	1	88.7	1.1	1	4.93	0.06	1	1.51	0.01	1	0.76	0.01	1
2012-13	2012	8	48.65	-126.67	200	1.52	0.01	1	1.900	0.009	1	81.9	0.9	1	5.17	0.04	1	1.64	0.01	1	0.79	0.01	1
2012-13	2012	8	48.65	-126.67	300	1.19	0.02	1	1.993	0.015	1	66.7	0.9	1	5.72	0.06	1	1.85	0.02	1	0.85	0.01	1
2012-13	2012	8	48.65	-126.67	400	1.29	0.01	1	2.304	0.011	1	66.6	0.6	1	6.10	0.05	1	1.87	0.02	1	0.87	0.01	1
2013-01	2013	2	48.65	-126.67	ND	ND	ND	ND	ND	ND	ND	ND	ND	ND	ND	ND	ND	ND	ND	ND	ND	ND	ND
2013-18	2013	8	48.65	-126.67	10	1.67	0.02	1	2.19	0.03	1	47.4	0.6	1	7.61	0.07	1	2.29	0.03	1	0.99	0.01	1
2013-18	2013	8	48.65	-126.67	25	1.29	0.02	1	1.40	0.01	1	39.2	0.5	1	7.61	0.07	1	2.11	0.02	1	0.99	0.01	1
2013-18	2013	8	48.65	-126.67	50	1.20	0.02	1	1.451	0.013	1	35.2	0.2	1	7.24	0.06	1	2.11	0.04	1	0.98	0.01	1
2013-18	2013	8	48.65	-126.67	75	1.33	0.02	1	1.997	0.020	1	61.3	1.2	1	5.81	0.06	1	1.82	0.02	1	0.91	0.01	1
2013-18	2013	8	48.65	-126.67	100	1.33	0.02	1	2.02	0.02	1	64.3	0.9	1	5.77	0.06	1	1.82	0.01	1	0.93	0.01	1
2013-18	2013	8	48.65	-126.67	350	1.20	0.02	1	1.60	0.03	1	63.7	1.7	1	5.5	0.1	1	1.77	0.03	1	0.89	0.01	1
2013-18	2013	8	48.65	-126.67	400	1.20	0.02	1	1.60	0.03	1	63.6	1.7	1	5.5	0.1	1	1.77	0.03	1	0.89	0.01	1

Cruise	Year	Month	Latitude	Longitude	Depth	dMn	dMn Error	QF	dFe	dFe Error	QF	dCo	dCo Error	QF	dNi	dNi Error	QF	dCu	dCu Error	QF	dCd	dCd Error	QF
			°N	°E	m	nmol/kg	nmol/kg		nmol/kg	nmol/kg		pmol/kg	pmol/kg		nmol/kg	nmol/kg		nmol/kg	nmol/kg		nmol/kg	nmol/kg	
2014-01	2014	2	48.65	-126.67	10	4.57	0.04	1	0.742	0.006	1	105.8	4.1	1	4.24	0.01	1	3.65	0.08	1	0.26	0.01	1
2014-01	2014	2	48.65	-126.67	25	4.55	0.04	1	0.640	0.005	1	108.1	2.0	1	4.25	0.03	1	1.75	0.03	1	0.26	0.01	1
2014-01	2014	2	48.65	-126.67	35	4.27	0.05	1	0.652	0.004	1	96.2	2.2	1	4.25	0.03	1	2.13	0.04	1	0.28	0.01	1
2014-19	2014	8	48.65	-126.67	10	2.80	0.03	1	0.319	0.005	1	63.5	0.9	1	4.38	0.03	1	1.66	0.01	1	0.248	0.002	1
2014-19	2014	8	48.65	-126.67	25	1.80	0.01	1	0.188	0.003	1	44.2	0.5	1	4.21	0.03	1	1.54	0.01	1	0.152	0.001	1
2014-19	2014	8	48.65	-126.67	50	1.20	0.02	1	0.163	0.003	1	59.0	1.2	1	4.52	0.07	1	1.51	0.02	1	0.29	0.01	1
2014-19	2014	8	48.65	-126.67	75	1.22	0.02	1	0.419	0.006	1	64.4	1.5	1	5.11	0.06	1	1.79	0.03	1	0.52	0.01	1
2014-19	2014	8	48.65	-126.67	100	1.01	0.01	1	0.460	0.007	1	67.3	0.8	1	4.91	0.05	1	1.90	0.02	1	0.62	0.01	1
2014-19	2014	8	48.65	-126.67	200	1.34	0.01	1	1.40	0.02	1	83.0	1.4	1	5.49	0.08	1	1.99	0.02	1	0.84	0.01	1
2014-19	2014	8	48.65	-126.67	400	1.13	0.02	1	1.41	0.03	1	54.5	1.0	1	6.7	0.1	1	2.02	0.03	1	0.940	0.009	1
2015-01	2015	2	48.65	-126.67	10	2.64	0.07	1	0.54	0.01	1	76.3	1.5	1	4.94	0.07	1	1.15	0.02	1	0.122	0.004	1
2015-01	2015	2	48.65	-126.67	20	2.50	0.07	5	0.44	0.01	5	74.3	1.6	5	4.56	0.07	5	1.55	0.03	5	0.113	0.001	5
2015-01	2015	2	48.65	-126.67	40	2.6	0.1	5	0.48	0.01	5	62.0	1.5	5	4.31	0.09	5	1.14	0.01	5	0.092	0.001	5
2015-01	2015	2	48.65	-126.67	50	1.79	0.05	1	0.70	0.01	1	54.9	1.2	1	5.13	0.08	1	1.88	0.03	1	0.182	0.003	1
2015-01	2015	2	48.65	-126.67	75	1.17	0.02	1	1.06	0.01	1	74.3	1.3	1	4.70	0.05	1	3.43	0.03	1	0.470	0.005	1
2015-01	2015	2	48.65	-126.67	125	3.02	0.07	1	3.43	0.08	1	87.1	0.4	1	5.03	0.04	1	2.42	0.01	1	0.668	0.005	1
2015-01	2015	2	48.65	-126.67	175	2.74	0.06	1	3.51	0.04	1	85.7	1.0	1	5.14	0.03	1	2.27	0.02	1	0.76	0.01	1
2015-01	2015	2	48.65	-126.67	200	2.99	0.05	1	2.713	0.025	1	73.0	1.0	1	5.20	0.05	1	1.62	0.02	1	0.81	0.01	1
2015-01	2015	2	48.65	-126.67	400	1.326	0.006	1	2.366	0.021	1	54.3	0.6	1	6.37	0.07	1	1.83	0.02	1	0.93	0.01	1
2015-10	2015	8	48.65	-126.67	10	10.6	0.1	1	0.356	0.006	1	111.2	0.8	1	4.26	0.04	1	2.24	0.03	1	0.247	0.005	1
2015-10	2015	8	48.65	-126.67	25	10.6	0.1	1	0.285	0.005	1	108.3	2.7	1	4.21	0.08	1	2.18	0.07	1	0.245	0.005	1
2015-10	2015	8	48.65	-126.67	40	0.86	0.01	1	0.159	0.002	1	14.0	1.3	1	3.49	0.06	1	1.21	0.03	1	0.016	0.003	1
2015-10	2015	8	48.65	-126.67	50	1.18	0.02	1	0.048	0.001	1	24.9	0.7	1	3.36	0.06	1	1.14	0.02	1	0.050	0.002	1
2015-10	2015	8	48.65	-126.67	100	0.77	0.01	1	0.100	0.001	1	54.9	1.3	1	4.19	0.06	1	1.26	0.02	1	0.369	0.012	1
2015-10	2015	8	48.65	-126.67	150	0.69	0.01	1	0.324	0.006	1	59.9	2.1	1	4.71	0.05	1	1.33	0.01	1	0.638	0.008	1
2015-10	2015	8	48.65	-126.67	200	1.42	0.02	1	1.059	0.020	1	60.8	3.3	1	5.15	0.06	1	1.50	0.02	1	0.749	0.001	1
2015-10	2015	8	48.65	-126.67	300	1.11	0.02	1	1.535	0.021	1	66.0	2.1	1	6.13	0.08	1	1.79	0.00	1	0.905	0.006	1
2015-10	2015	8	48.65	-126.67	400	1.24	0.01	1	1.603	0.020	1	63.6	1.6	1	6.76	0.09	1	1.75	0.00	1	0.976	0.006	1
2017-08	2017	8	48.65	-126.67	10	8.0	0.1	1	0.354	0.004	1	83.0	1.3	1	4.45	0.06	1	3.06	0.02	1	0.228	0.003	1
2017-08	2017	8	48.65	-126.67	25	6.0	0.1	1	0.469	0.004	1	94.2	1.3	1	4.18	0.04	1	1.89	0.02	1	0.261	0.003	1

Cruise	Year	Month	Latitude	Longitude	Depth	dMn	dMn Error	QF	dFe	dFe Error	QF	dCo	dCo Error	QF	dNi	dNi Error	QF	dCu	dCu Error	QF	dCd	dCd Error	QF
			°N	°E	m	nmol/kg	nmol/kg		nmol/kg	nmol/kg		pmol/kg	pmol/kg		nmol/kg	nmol/kg		nmol/kg	nmol/kg		nmol/kg	nmol/kg	
2017-08	2017	8	48.65	-126.67	50	2.115	0.015	1	0.361	0.002	1	72.0	0.7	1	4.18	0.05	1	1.56	0.02	1	0.234	0.002	1
2017-08	2017	8	48.65	-126.67	100	1.006	0.009	1	0.949	0.008	1	81.2	0.7	1	4.70	0.05	1	1.30	0.02	1	0.637	0.004	1
2017-08	2017	8	48.65	-126.67	150	0.695	0.004	1	0.976	0.008	1	57.7	0.7	1	5.01	0.05	1	2.02	0.02	1	0.700	0.002	1
2017-08	2017	8	48.65	-126.67	200	0.64	0.01	1	0.89	0.01	1	40.3	0.5	1	5.39	0.08	1	1.59	0.02	1	0.76	0.01	1
2017-08	2017	8	48.65	-126.67	300	0.683	0.006	1	0.787	0.007	1	44.6	0.5	1	6.13	0.05	1	1.93	0.02	1	0.85	0.01	1
2017-08	2017	8	48.65	-126.67	500	1.28	0.01	1	2.41	0.02	1	48.3	0.4	1	7.34	0.07	1	1.86	0.02	1	0.961	0.006	1
2018-040	2018	8	48.65	-126.67	10	9.9	0.1	1	0.58	0.01	1	118.8	1.6	1	4.04	0.05	1	2.26	0.02	1	0.31	0.01	1
2018-040	2018	8	48.65	-126.67	25	5.60	0.07	1	0.508	0.005	1	89.5	0.4	1	3.83	0.01	1	1.99	0.02	1	0.300	0.002	1
2018-040	2018	8	48.65	-126.67	50	1.96	0.03	1	0.28	0.00	1	61.6	1.2	1	3.63	0.05	1	2.53	0.04	4	0.25	0.00	1
2018-040	2018	8	48.65	-126.67	75	1.63	0.02	1	0.543	0.005	1	84.0	0.9	1	4.08	0.07	1	1.66	0.02	1	0.49	0.01	1
2018-040	2018	8	48.65	-126.67	100	1.32	0.07	1	0.81	0.04	1	95.0	5.3	1	4.5	0.2	1	1.64	0.08	1	0.67	0.03	1
2018-040	2018	8	48.65	-126.67	200	0.89	0.01	1	1.31	0.02	1	69.0	1.5	1	4.79	0.04	1	1.51	0.02	1	0.67	0.01	1
2018-040	2018	8	48.65	-126.67	400	0.86	0.01	1	1.08	0.01	1	59.2	0.5	1	6.19	0.05	1	1.94	0.02	1	0.915	0.005	1
2019-008	2019	8	48.65	-126.67	10	2.72	0.03	1	0.48	0.01	1	50.5	0.7	1	3.84	0.06	1	2.47	0.02	1	0.056	0.001	1
2019-008	2019	8	48.65	-126.67	25	1.58	0.01	1	0.341	0.004	1	26.3	0.6	1	3.39	0.04	1	1.47	0.02	1	0.026	0.001	1
2019-008	2019	8	48.65	-126.67	50	1.13	0.01	1	0.366	0.004	1	30.9	0.4	1	3.45	0.03	1	1.85	0.02	1	0.075	0.001	1
2019-008	2019	8	48.65	-126.67	75	1.24	0.01	1	0.167	0.001	1	47.1	0.3	1	3.83	0.04	1	1.20	0.01	1	0.235	0.003	1
2019-008	2019	8	48.65	-126.67	100	0.927	0.005	1	0.303	0.002	1	58.7	0.9	1	4.13	0.03	1	1.235	0.009	1	0.439	0.005	1
2019-008	2019	8	48.65	-126.67	200	0.70	0.01	1	1.04	0.01	1	59.9	1.1	1	4.88	0.05	1	1.42	0.02	1	0.724	0.007	1
2019-008	2019	8	48.65	-126.67	400	0.99	0.02	1	1.62	0.05	1	51.5	1.5	1	5.9	0.2	1	1.55	0.03	1	0.838	0.007	1

Appendix B

Data Tables of NO_3^-, PO_4^{3-}, and Si at stations P26, P20, P16, P12, and P4 from 2012-2019

Table B.1 Stations P26, P20, P16, P12, and P4 macronutrient concentrations of NO_3^-, PO_4^{3-}, and Si from 2012 to 2019. Data was retrieved from the Water Properties Line P Program https://www.waterproperties.ca/linep/.

			P26				P20				P16				P12				P4			
Cruise	Year	Month	Depth	NO_3^-	PO_4^{3-}	Si	Depth	NO_3^-	PO_4^{3-}	Si	Depth	NO_3^-	PO_4^{3-}	Si	Depth	NO_3^-	PO_4^{3-}	Si	Depth	NO_3^-	PO_4^{3-}	Si
			dbar	µmol kg^{-1}	µmol kg^{-1}	µmol kg^{-1}	dbar	µmol kg^{-1}	µmol kg^{-1}	µmol kg^{-1}	dbar	µmol kg^{-1}	µmol kg^{-1}	µmol kg^{-1}	dbar	µmol kg^{-1}	µmol kg^{-1}	µmol kg^{-1}	dbar	µmol kg^{-1}	µmol kg^{-1}	µmol kg^{-1}
2012-01	2012	2	5.2	16.8	1.5	27.3	4.6	14.3	1.29	20.9	4.7	11.1	1.12	16	4.9	9.1	1.01	14.5	5.5	7.6	0.86	9.2
2012-01	2012	2	9.9	16.9	1.51	27.3	10.9	14.4	1.33	21.1	10.2	11.1	1.13	15.9	10.6	9.1	0.97	14.4	10.6	7.6	0.88	9.1
2012-01	2012	2	24.8	16.9	1.51	27.3	25.4	14.6	1.31	21.1	24.6	11.2	1.12	15.9	25.1	9.2	0.99	14.5	26.1	7.7	0.89	9.1
2012-01	2012	2	51.6	17	1.5	27.3	50.2	17.1	1.29	21.3	50.6	11.2	1.12	15.9	49.6	9.1	0.99	14.2	49.6	7.7	0.88	8.8
2012-01	2012	2	75.1	17	1.52	27.3	75.2	14.5	1.31	21	75.2	11.2	1.12	16	75.5	9.1	0.99	14.3	76.1	15.3	1.34	18.9
2012-01	2012	2	100.1	16.9	1.51	27.3	100.6	14.8	1.34	21.5	99.3	11.3	1.1	15.8	98.9	10.6	1.06	15	99.6	24.7	1.88	29.3
2012-01	2012	2	124	18.3	1.58	28.8	126.6	28.8	2.08	41.7	124.3	25.8	1.89	35.2	124.6	21.7	1.55	26	125.6	28.2	2.16	35.1
2012-01	2012	2	150.9	28	2.12	45.8	151.1	28.5	2.06	44.9	148.8	28	1.98	41.6	153.2	23.7	1.65	30.6	151.2	30.1	2.24	37.8
2012-01	2012	2	174.4	31.9	2.31	56.6	1749	31.5	2.27	52.3	176.2	32.6	2.35	54.5	173.3	25.1	1.76	34.2	176.3	31.3	2.28	40
2012-01	2012	2	199.7	34.5	2.5	64.3	199.9	33.6	2.41	57.5	201.5	32.8	2.34	54.6	200.6	26.7	1.86	38.7	201.5	32	2.26	41.5
2012-01	2012	2	250.5	38	2.74	76.1	251.6	36	2.6	66.6	251.3	ND	2.55	63.8	250.4	31.5	ND	48.9	251	34.5	2.48	47.8
2012-01	2012	2	301.9	39.9	2.87	82.9	299.2	40.3	2.87	76.6	300.5	38.8	2.74	72.4	300.4	35.4	2.48	ND	301	36.2	2.6	54.1
2012-01	2012	2	401.6	42.1	3.04	94.3	402	41.8	2.96	88.2	400.2	42	2.97	86.8	400.9	41.5	2.91	76.8	400.6	40.8	2.94	70.9
2012-13	2012	8	4.9	11.1	1.03	22.1	5.4	11.6	1.15	18.4	5.9	7	0.89	3.7	5.6	4.8	0.72	2.6	5.4	0.3	0.2	0.9
2012-13	2012	8	10.6	11.2	1.01	22.2	10.3	11.6	1.16	18.4	10.8	7.1	0.89	3.7	10	5	0.74	2.7	11.1	0.5	0.32	1.6
2012-13	2012	8	25.9	12.2	1.1	22	25.5	11.8	1.19	19	25.8	7.5	0.95	4.2	25.4	7.1	0.89	3	26.2	9.2	1.13	13.4
2012-13	2012	8	50.9	16.8	1.5	30.1	50.9	13.6	1.15	23.3	50.5	13.4	1.34	21.9	50.6	10.1	1.13	12.6	50.8	11.5	1.16	15.4
2012-13	2012	8	76.3	19.3	1.54	32.7	75.6	16.8	1.49	26.7	76	15.9	1.34	23.3	75.9	12.5	1.22	16.3	75.9	18.7	1.57	23.2
2012-13	2012	8	100.8	20.4	1.62	34	101.7	19	1.61	29.5	101.1	18.3	1.52	26.1	100.7	14.2	1.27	18.3	101	23.7	1.82	29.5
2012-13	2012	8	125.1	27.7	2.07	47.2	124.9	25	1.91	38.9	125.7	25.9	1.89	38	125.9	19.1	1.49	25.3	126.1	29.9	2.25	38.9

			P26				P20				P16				P12				P4			
Cruise	Year	Month	Depth	NO_3^-	PO_4^{3-}	Si	Depth	NO_3^-	PO_4^{3-}	Si	Depth	NO_3^-	PO_4^{3-}	Si	Depth	NO_3^-	PO_4^{3-}	Si	Depth	NO_3^-	PO_4^{3-}	Si
			dbar	µmol kg^{-1}	µmol kg^{-1}	µmol kg^{-1}	dbar	µmol kg^{-1}	µmol kg^{-1}	µmol kg^{-1}	dbar	µmol kg^{-1}	µmol kg^{-1}	µmol kg^{-1}	dbar	µmol kg^{-1}	µmol kg^{-1}	µmol kg^{-1}	dbar	µmol kg^{-1}	µmol kg^{-1}	µmol kg^{-1}
2012-13	2012	8	148.9	32.6	2.33	58.3	150.8	30.2	2.21	51	150.4	30	2.16	46.8	150.4	22.3	1.57	30.5	151.1	30.8	2.28	41.5
2012-13	2012	8	174.2	35.2	2.49	66.6	175.4	33.6	2.3	61.1	176	31.8	2.26	52.3	175.4	25.1	1.71	36.7	175.6	31.3	2.31	43.4
2012-13	2012	8	199.9	38.2	2.68	75.4	200.3	35.7	2.57	67.5	200.6	33.2	2.39	57.1	200.4	27	1.93	41.5	200.8	33.3	2.46	48.4
2012-13	2012	8	249.5	40.7	2.84	84.8	250.5	38.2	2.75	76.1	250.9	35.8	2.55	64.2	250.9	30.6	2.17	52	251.8	36	2.67	56.3
2012-13	2012	8	300	41.8	2.99	91.7	299.5	39.9	2.94	83.2	300.5	38.7	2.77	73.4	301.1	33.7	2.39	60.7	300.7	38.1	2.82	63.5
2012-13	2012	8	400.1	43.2	3.05	103.4	400.5	41.3	3.05	94.2	400.9	41.6	2.96	86.8	400.5	39.2	2.79	77.7	400.4	40.3	3.01	73.3
2013-01	2013	2	5.2	16.8	1.46	25.3	4.3	14.6	1.35	22.3	6.1	12.7	1.23	19.3	4.7	11.3	1.13	15	5.1	6.4	0.8	10.2
2013-01	2013	2	10.7	16.7	1.47	25.2	9.9	14.8	1.35	22.3	10.5	12.6	1.2	19.4	9.8	11.3	1.14	15	10.4	6.5	0.8	10.2
2013-01	2013	2	24.5	16.3	1.44	25.2	24.7	14.8	1.36	22.3	25	12.7	1.22	19.4	24.7	11.4	1.12	15	25.3	6.5	0.81	10.2
2013-01	2013	2	49.7	16.3	1.44	25.3	50.7	14.8	1.35	22.3	50.9	12.8	1.22	19.4	49.8	11.5	1.14	14.9	49.7	8.3	0.92	10.8
2013-01	2013	2	75.1	16.5	1.49	25.3	75.6	14.9	1.36	22.4	75.1	12.7	1.23	19.3	75	11.5	1.13	14.9	74.8	10.1	1.04	12.2
2013-01	2013	2	99.7	17	1.48	26.5	101	16.2	1.44	24.5	101.2	14.2	1.3	20.7	100.7	15.9	1.38	20.9	99.8	19.3	1.56	23.3
2013-01	2013	2	125.4	28.3	2.15	48.6	125.8	23.1	1.81	35.9	124.6	20.2	1.63	29.5	125.7	19.6	1.53	25.2	124.4	25.6	1.85	30.6
2013-01	2013	2	151.2	35.6	2.59	66.4	149.6	28.5	2.09	46.9	149.9	24.4	1.81	36.7	150.9	26.5	1.89	36.9	149.7	26.7	1.88	34.3
2013-01	2013	2	174.5	38	2.74	73.9	176	31.7	2.29	55.7	175.6	27.8	2	45.6	173.8	29.1	2.04	42.6	175	29.3	2.04	40.5
2013-01	2013	2	200.4	39.5	2.81	78.1	199.5	34.1	2.45	62.9	199.5	29.8	2.15	50.9	200.8	30.9	2.19	47.3	206.3	31	2.16	46
2013-01	2013	2	249.6	41.9	2.97	87.3	251.1	37.5	2.68	72.8	250	34.8	2.49	65.7	250	34.5	2.45	56.8	250.9	34.7	2.42	55.4
2013-01	2013	2	301.2	43.4	3.06	93.8	300.5	40	2.84	81.9	300.7	37.5	2.67	73.9	300.1	37.2	2.65	63.6	300	36.8	2.57	61.5
2013-01	2013	2	400.2	44.1	3.12	105.5	399.6	41.8	2.99	95	399	40.6	2.9	89.5	399.7	40	2.81	79.9	400.3	41.5	2.94	78.9
2013-18	2013	8	5.6	9.8	1	17.5	5.4	8.7	0.91	15.1	4.9	1.4	0.49	4.5	5	1.5	0.53	2.6	4.8	0.1	0.33	2.7
2013-18	2013	8	10.1	9.8	1.07	17.5	10	8.7	0.92	15	10	1.5	0.51	4.4	9.8	1.3	0.53	2.5	10.4	0	0.32	2.7
2013-18	2013	8	25.3	9.8	1.05	17.5	25.2	9.4	1	16.4	25	3	0.61	4.7	24.7	2.5	0.62	3.1	24.8	0.2	0.39	3.8
2013-18	2013	8	49.6	13.1	1.29	21.2	50	12.2	1.19	18.5	50	12.5	1.21	16.9	49.9	10.8	1.17	15.8	49.7	10.7	1.13	15
2013-18	2013	8	75.2	17.5	1.51	24.7	74.9	14.2	1.31	20.7	74.9	14.8	1.34	20.1	74.9	14.3	1.31	19.5	75.2	14.8	1.35	19.3
2013-18	2013	8	100.2	19.3	1.62	28	100.5	16	1.35	21.3	100.2	15.9	1.4	22.1	99.6	17.3	1.47	23.2	100.1	21.1	1.65	25.7
2013-18	2013	8	125	21.9	1.76	33.4	125	17.8	1.41	24.2	125.2	19.9	1.7	27.6	124.1	20.2	1.6	27.4	124.6	26.6	1.96	32.9
2013-18	2013	8	150.6	30.5	2.32	51.8	150.4	24.8	1.8	37.1	150	23.8	1.79	33.7	149.7	23.9	1.81	33.4	150.4	29.4	2.11	39.4
2013-18	2013	8	174.6	36.3	2.66	65.9	174.6	29.2	2.08	46.7	175.1	28.5	2.02	42.2	175.5	27.8	2.02	40.4	174.9	31.1	2.18	43.9
2013-18	2013	8	199.5	39.6	2.86	75.5	200	32	2.23	53.6	200.2	32.1	2.21	50.3	200.2	28.8	2.06	43.9	200.1	33.5	2.37	48.2
2013-18	2013	8	250.1	42.7	3.04	85.6	249.6	35.8	2.5	64.6	249.8	35.2	2.44	59.9	249.6	34	2.39	57.5	249.4	36.7	2.58	56.3

			P26				P20				P16				P12				P4			
Cruise	Year	Month	Depth	NO_3^-	PO_4^{3-}	Si	Depth	NO_3^-	PO_4^{3-}	Si	Depth	NO_3^-	PO_4^{3-}	Si	Depth	NO_3^-	PO_4^{3-}	Si	Depth	NO_3^-	PO_4^{3-}	Si
			dbar	µmol kg^{-1}	µmol kg^{-1}	µmol kg^{-1}	dbar	µmol kg^{-1}	µmol kg^{-1}	µmol kg^{-1}	dbar	µmol kg^{-1}	µmol kg^{-1}	µmol kg^{-1}	dbar	µmol kg^{-1}	µmol kg^{-1}	µmol kg^{-1}	dbar	µmol kg^{-1}	µmol kg^{-1}	µmol kg^{-1}
2013-18	2013	8	300.5	43.9	3.06	92.1	300.3	38.8	2.69	74.3	299.8	38.4	2.64	68.8	299.9	36.9	2.59	67.3	300	39	2.75	62.9
2013-18	2013	8	400.6	45.4	3.13	102.6	399.6	42.1	2.91	88.8	400.4	42.1	2.9	83.7	401.1	41.4	2.9	82.2	399.6	41.9	2.98	74.3
2014-01	2014	2	4.8	11	1.05	12.9	5.2	9.8	0.98	10.9	4.4	9.9	1	11.5	5.4	9.2	0.99	12.6	4.4	8	0.86	11
2014-01	2014	2	10.1	11	1.06	12.9	10	9.8	0.98	10.8	11.3	9.9	1	11.5	10.4	9.2	0.99	12.6	10.3	8	0.85	11
2014-01	2014	2	26	11	1.05	12.9	25	9.8	0.99	10.8	27	9.9	1.01	11.5	25.4	9.3	0.99	12.6	24.8	8	0.85	11
2014-01	2014	2	49.7	11	1.06	12.8	50.6	9.8	0.99	10.9	54.1	9.9	1	11.4	49.7	9.3	0.99	12.7	50	17.8	1.48	23.9
2014-01	2014	2	74.8	11	1.08	12.9	76.2	9.8	0.99	10.8	75.8	9.9	1	11.5	75.3	9.4	1	12.8	74.1	27.3	2.08	37.3
2014-01	2014	2	100.4	12.7	1.14	15.4	100.8	16.9	1.36	20.6	100.4	16	1.33	19.6	101.3	17.7	1.45	22.5	100.1	29.7	2.17	38.4
2014-01	2014	2	126.5	20.5	1.59	28.2	123.8	19.2	1.5	25.5	125.2	19.4	1.52	25.4	125.5	21	1.61	27.6	125	32.6	2.4	47
2014-01	2014	2	149.2	23.5	1.74	33.9	149.9	23.4	1.67	32.9	150.2	22.7	1.66	30.4	149.9	23.3	1.73	31.6	150.9	33.2	2.41	47.1
2014-01	2014	2	175.4	30.6	2.13	48.8	175.8	27.8	1.91	41.6	166	ND	ND	ND	174.9	26.5	1.88	37.4	174.6	33.6	2.39	46.1
2014-01	2014	2	201	35.2	2.41	60.9	199.8	31	2.12	50	198.7	29.6	2.03	45.3	200.1	29.6	2.04	44.2	200.6	33.4	2.32	45.2
2014-01	2014	2	250	39.5	2.66	73.3	252.1	36	2.45	64.3	255.6	35.6	2.43	62.3	250.5	33.4	2.28	55.2	250.3	35.1	2.47	50.4
2014-01	2014	2	300	42.2	2.81	80.7	301.8	39.9	2.68	75.7	305	39.6	2.68	73.9	300.4	37.5	2.56	67.1	300	36.3	2.54	54.7
2014-01	2014	2	402.7	44.1	2.95	93.9	399.9	ND	ND	90.5	397.6	42.8	2.88	87	400.4	41.6	2.83	82.2	401.6	38.3	2.69	62.8
2014-19	2014	8	5.6	5	0.735	11.65	5.5	0	0.375	1.7	5.1	0	0.386	1.64	4.9	0	0.404	4.05	5.4	0	0.424	6.9
2014-19	2014	8	10	5.03	0.739	11.59	10	0	0.379	1.71	10.2	0	0.389	1.63	10.3	0	0.407	4.04	10.7	0	0.431	6.83
2014-19	2014	8	25	5.02	0.738	11.56	25	0	0.387	1.54	24.8	0	0.386	1.61	24.4	0	0.443	4.95	24.9	7.15	0.934	10.59
2014-19	2014	8	50.5	9.56	1.048	12.92	50	7.74	0.946	9.85	50.5	6.12	0.85	7.29	49.7	6.74	0.878	9.61	49.2	12.81	1.221	14.65
2014-19	2014	8	76.1	11.09	1.128	13.54	75.5	15.23	1.321	17.77	75.6	10	1.037	11.09	75.6	14.81	1.309	17.08	75.2	18.46	1.522	22.14
2014-19	2014	8	99.5	18.83	1.539	24.58	99.8	19.67	1.537	25.08	100.4	16.79	1.383	19.51	100.1	18.47	1.51	22.02	100.2	21.96	1.696	26.42
2014-19	2014	8	125.3	26.74	1.996	40.27	125.9	22.13	1.616	30.1	125.2	19.38	1.491	24.24	125.1	21.27	1.652	25.8	124.5	26.31	1.91	31.04
2014-19	2014	8	151.8	31.82	2.293	52.57	150.4	27.98	1.988	42.99	150.7	23.61	1.711	32.37	150.7	25.04	1.834	31.72	150.5	28.83	2.05	35.12
2014-19	2014	8	177.7	35.46	2.512	62.74	175.1	30.31	2.14	49.67	175.3	27.49	1.941	41.1	175.5	25.54	1.875	34.58	174.7	31.04	2.177	39.26
2014-19	2014	8	200	37.53	2.637	68.18	199.9	33.33	2.358	57.72	199.7	30.2	2.15	49.17	200.8	28.29	2.005	39.84	200.5	32.29	2.252	42.33
2014-19	2014	8	250.4	41.03	2.854	79.35	250.7	37.47	2.634	68.55	250.8	35.61	2.504	63.49	249.8	32.37	2.283	49.6	250.4	34.25	2.38	50.33
2014-19	2014	8	300.7	42.66	2.972	86.3	300.6	40.77	2.833	78.51	300.8	38.08	2.68	72.01	300.6	35.03	2.452	58.91	300.5	37.78	2.622	57.96
2014-19	2014	8	401.2	44.28	3.065	97.06	399.6	42.84	2.944	91.24	400.5	42.05	2.938	86.16	401.1	40.9	2.86	75.75	400.3	41.15	2.857	70.47
2015-01	2015	2	5.8	10.89	1.056	12.8	5.6	5.65	0.725	6.05	5.3	5.58	0.736	6.92	5.7	4.02	0.653	5.95	5.7	2.77	0.57	6.06
2015-01	2015	2	11.8	10.96	1.068	13.02	11.1	5.65	0.727	6.05	11.8	5.56	0.741	6.88	11.7	3.97	0.65	5.84	11.1	2.78	0.568	6.04

			P26				P20				P16				P12				P4			
Cruise	Year	Month	Depth	NO_3^-	PO_4^{3-}	Si	Depth	NO_3^-	PO_4^{3-}	Si	Depth	NO_3^-	PO_4^{3-}	Si	Depth	NO_3^-	PO_4^{3-}	Si	Depth	NO_3^-	PO_4^{3-}	Si
			dbar	µmol kg^{-1}	µmol kg^{-1}	µmol kg^{-1}	dbar	µmol kg^{-1}	µmol kg^{-1}	µmol kg^{-1}	dbar	µmol kg^{-1}	µmol kg^{-1}	µmol kg^{-1}	dbar	µmol kg^{-1}	µmol kg^{-1}	µmol kg^{-1}	dbar	µmol kg^{-1}	µmol kg^{-1}	µmol kg^{-1}
2015-01	2015	2	26.6	11.19	1.068	13.26	25.4	5.64	0.721	6.05	25.8	5.59	0.741	6.88	26.4	4	0.651	5.83	25.8	2.79	0.58	6.01
2015-01	2015	2	52.4	11.66	1.1	14.18	51.8	5.78	0.735	6.15	50.4	5.62	0.741	6.9	53.4	3.09	0.568	4.62	50.8	9.92	1.011	11.31
2015-01	2015	2	76.8	11.73	1.115	14.32	75.8	7.2	0.817	7.57	76.8	6.31	0.782	7.49	76.5	3.4	0.584	4.74	76.5	18.62	1.527	20.93
2015-01	2015	2	101.2	19.28	1.519	25.38	102.2	20.21	1.488	25.34	102.1	16.36	1.343	18.16	102.5	17.22	1.419	18.94	101.9	23.16	1.817	27.5
2015-01	2015	2	126.9	29.92	2.135	48.43	126	24.4	1.714	34.41	126.6	20.01	1.484	24.06	125.1	18.52	1.396	21.06	127.4	26.06	1.984	32.24
2015-01	2015	2	151.3	33.73	2.355	58.39	152	28.01	1.954	43.33	152.1	24.38	1.721	32.16	151.4	19.85	1.414	24	151.4	27.47	2.045	34.51
2015-01	2015	2	176	36.3	2.5	66.1	175.7	30.61	2.145	50.6	175.9	29	2.026	41.06	176.4	22.5	1.566	29.45	176.5	28.87	2.158	36.67
2015-01	2015	2	200.7	38.48	2.627	72.43	202.9	32.62	2.287	56.23	202.1	29.2	2.023	43.54	201.1	24.9	1.729	35.29	200.9	31.01	2.267	40.15
2015-01	2015	2	252	41.41	2.804	81.05	254.5	36.42	2.54	66.58	251.8	33.98	2.353	55.53	250.7	29.57	2.048	46.75	250.9	31.85	2.269	43.64
2015-01	2015	2	302.1	43.48	2.957	88.48	302.1	39.74	2.739	75.37	300.7	38.19	2.627	67.43	302.5	35.31	2.424	59.3	301.5	34.6	2.451	52.3
2015-01	2015	2	402.8	45.13	3.121	103.72	401.6	43.01	2.945	89.73	401.1	41.28	2.845	83.48	400.7	40.86	2.774	77.24	401.4	39.84	2.783	69.8
2015-10	2015	8	5.8	5.75	0.731	10.86	5.1	2.38	0.527	7.13	4.5	0	0.315	0.54	4.7	0	0.315	1.39	5.4	1.77	0.494	4.36
2015-10	2015	8	9.9	5.75	0.741	10.81	11	2.37	0.528	7.12	9.9	0	0.311	0.52	10.5	0	0.31	1.37	9.5	1.73	0.507	4.32
2015-10	2015	8	25.5	5.76	0.744	10.79	25.6	2.38	0.528	7.11	24.9	0	0.327	0.15	24.7	0	0.297	0.96	25.1	1.84	0.515	4.41
2015-10	2015	8	50	11.86	1.147	18.01	51.4	7.05	0.884	8.96	48.7	0.08	0.425	2.2	50	0.78	0.448	3.42	50.3	3.58	0.614	4.68
2015-10	2015	8	74.9	13.94	1.323	21.69	75.2	12.06	1.136	13.83	73.8	4.32	0.703	6.01	99.7	14.39	1.239	15.77	75	9.8	0.962	9.29
2015-10	2015	8	100.4	14.26	1.353	21.15	101.3	17.24	1.34	19.9	99	8.92	0.934	9.06	125.4	21.59	1.625	27.35	100.1	19.73	1.518	21.73
2015-10	2015	8	125.9	22.53	1.734	33.1	126.1	22.72	1.631	31.53	124.9	17.75	1.404	20.08	152.5	20.03	1.438	25.67	125.3	21.89	1.613	25.93
2015-10	2015	8	150.2	31.14	2.24	52.08	150.4	25.61	1.817	38.58	151.4	20.51	1.524	25.29	175.8	21.7	1.534	29.92	150.3	28.34	2.024	36.45
2015-10	2015	8	177.1	34.02	2.42	60.5	176.4	28.34	2.011	45.73	173.9	24.75	1.772	34.14	200.4	24.48	1.734	36.83	175.2	29.95	2.114	40.72
2015-10	2015	8	198.9	35.29	2.499	64.37	201.6	30.08	2.133	50.58	200	26.85	1.911	39.96	250.4	28.86	2.047	48.47	200.7	31.31	2.211	44.24
2015-10	2015	8	249.3	38.72	2.718	74.8	251	34.31	2.434	63.23	249	30.98	2.196	51.61	299.8	33.72	2.388	60.25	250.6	34.25	2.411	51.95
2015-10	2015	8	299	41.22	2.85	83.76	302.5	37.8	2.662	73.79	298.8	35.59	2.517	63.67	400.5	38.43	2.693	76.15	301	36.31	2.548	57.18
2015-10	2015	8	400.3	43.01	3.012	97.86	399.9	41.38	2.895	89	399.8	39.93	2.802	79.04					400.6	40.5	2.852	73.8
2017-01	2017	2	4.8	14.9	1.314	19.85	6.1	11.01	1.056	11.18	5.2	9.03	0.932	10.85	5.1	9.43	0.939	11.85	5.7	5.75	0.677	7.98
2017-01	2017	2	9.8	14.86	1.317	19.83	10.8	11.02	1.068	11.15	10.6	8.93	0.937	10.82	11	9.41	0.941	11.84	10.6	5.73	0.677	7.99
2017-01	2017	2	26	14.92	1.32	19.83	26.5	11.02	1.069	11.14	25.6	8.97	0.918	10.82	25.6	9.47	0.946	11.84	24.9	5.72	0.682	7.93
2017-01	2017	2	50.6	15.07	1.33	20.07	50.2	11.01	1.076	11.13	51.3	9.08	0.927	10.81	50.3	9.4	0.942	11.8	49.8	5.74	0.693	7.35
2017-01	2017	2	74.7	15.41	1.353	20.75	75.4	11.02	1.067	11.15	75	9.13	0.941	10.84	74.9	9.43	0.938	11.74	75.3	8.75	0.879	11.56
2017-01	2017	2	100.2	15.55	1.36	20.91	101	11.3	1.077	11.53	100.2	12.44	1.125	14.94	100.6	11.86	1.077	14.5	100.1	18.74	1.501	21.5

			P26				P20				P16				P12				P4			
Cruise	Year	Month	Depth	NO_3^-	PO_4^{3-}	Si	Depth	NO_3^-	PO_4^{3-}	Si	Depth	NO_3^-	PO_4^{3-}	Si	Depth	NO_3^-	PO_4^{3-}	Si	Depth	NO_3^-	PO_4^{3-}	Si
			dbar	µmol kg^{-1}	µmol kg^{-1}	µmol kg^{-1}	dbar	µmol kg^{-1}	µmol kg^{-1}	µmol kg^{-1}	dbar	µmol kg^{-1}	µmol kg^{-1}	µmol kg^{-1}	dbar	µmol kg^{-1}	µmol kg^{-1}	µmol kg^{-1}	dbar	µmol kg^{-1}	µmol kg^{-1}	µmol kg^{-1}
2017-01	2017	2	126.6	24.12	1.764	34.93	124.2	20.94	1.564	27.33	125.1	25.31	1.828	34.51	124.2	23.81	1.708	30.81	125.1	23.91	1.818	27.41
2017-01	2017	2	152.3	27.92	1.971	45.27	148.8	26.61	1.867	39.83	149.8	28.92	2.068	42.41	150.6	26.05	1.834	36.07	149.8	26.99	1.989	31.58
2017-01	2017	2	174.7	29.84	2.115	51.06	174.7	28.35	1.976	45.87	175.5	30.75	2.158	47.81	176.2	28.42	1.988	42.06	175	28.55	2.101	35.56
2017-01	2017	2	202.2	32.23	2.286	57.82	201.5	31.94	2.239	55.44	199.8	32.62	2.274	53.18	200.6	30.17	2.106	46.93	200.7	29.2	2.109	37.08
2017-01	2017	2	252	36.5	2.571	69.23	251.3	35.95	2.517	66.71	250.1	36.44	2.55	64.31	250.6	32.87	2.296	54.26	250.7	31.06	2.238	42.34
2017-01	2017	2	300.2	38.78	2.721	77.36	301.9	38.54	2.697	74.91	300.8	39.3	2.742	74.1	301.7	36.36	2.516	64.27	300.4	32.89	2.361	47.54
2017-01	2017	2	401.6	42.32	2.971	91.9	400.7	ND	ND	ND	400.7	42.21	2.937	87.58	400.9	40.67	2.827	80.96	400.7	34.91	2.452	56.35
2017-08	2017	8	5.2	6.52	0.782	2.07	5.2	8.63	0.923	14.65	5	4.29	0.576	8.09	5.4	0.6	0.412	5.26	5.1	0	0.259	5.47
2017-08	2017	8	10.2	6.45	0.775	1.94	10.2	8.45	0.913	14.54	10.4	4.38	0.649	8.02	10.3	0.49	0.404	5.2	9.8	0	0.272	5.52
2017-08	2017	8	25.1	6.39	0.783	2	25.2	8.29	0.911	14.3	24.7	5.19	0.706	8.64	25.4	0.71	0.424	4.86	25.7	2.37	0.51	5.4
2017-08	2017	8	50.2	12.64	1.253	18.25	50	9.02	0.983	12.7	49.9	8.8	0.898	11.28	50.1	7.34	0.857	9.24	49.9	9.82	0.942	11.59
2017-08	2017	8	75.7	15.58	1.398	20.65	75.9	11.56	1.172	13.99	75	10.41	1.049	11.71	75.2	13.06	1.163	14.33	75	16.94	1.319	16.63
2017-08	2017	8	99.8	17.42	1.467	24.48	100.7	12.31	1.188	14	100.6	13.51	1.221	15.03	100.2	17.77	1.424	21.32	100.3	22.97	1.667	24.65
2017-08	2017	8	124.9	22.87	1.758	35.01	125.3	16.65	1.382	20.49	125.2	22.91	1.694	30.28	125	23.53	1.714	30.51	124.9	25.47	1.806	29.63
2017-08	2017	8	150.1	27.39	1.928	43.68	150.1	23.34	1.71	33.01	149.9	26.98	1.913	38.13	150	26.15	1.874	36.44	150.9	27.51	1.904	35.45
2017-08	2017	8	175.8	28.01	1.938	47.51	176.1	25.86	1.869	40.31	175	29.58	2.115	46.05	175.1	29.23	2.082	42.7	175.6	28.72	2.026	40
2017-08	2017	8	200.4	30.57	2.097	54.96	200.3	27.6	1.973	44.5	201.2	31.93	2.189	52.41	200	30.97	2.176	47.7	200.4	30.75	2.144	44.81
2017-08	2017	8	251.1	34.7	2.425	67.07	250.6	32.26	2.314	58.67	251.6	35.2	2.493	63.26	250	35.17	2.473	60.03	250.2	ND	ND	ND
2017-08	2017	8	300	37.84	2.573	75.98	300.2	35.95	2.523	68.28	300.4	37.46	2.647	69.54	300.6	38.04	2.663	68.82	299.7	35.61	2.511	60.72
2017-08	2017	8	400.8	40.58	2.851	89.91	399.7	40.33	2.854	85.77	399.9	41.36	2.933	82.66	400.3	41.54	2.91	85.55	400.2	39.79	2.857	76.55
2018-001	2018	2	4.7	14.46	1.321	21.34	4.8	10.17	1.015	9.96	4.3	8.97	0.937	8.88	4.7	6.83	0.809	6.77	4	4.98	0.647	7.74
2018-001	2018	2	9.8	14.51	1.322	21.38	10.1	10.23	1.003	9.93	9.2	9.12	0.934	8.98	8.8	6.87	0.804	6.63	9.9	4.91	0.645	7.66
2018-001	2018	2	24.6	14.58	1.32	21.32	24.5	10.28	1.006	10.2	24.3	9.05	0.94	8.83	25.5	6.84	0.808	6.65	24.9	5.08	0.654	7.52
2018-001	2018	2	50	14.63	1.327	21.46	50.1	10.16	1.009	10.07	49.5	9.03	0.942	8.82	49.9	6.86	0.802	6.63	49.6	5.18	0.69	7.15
2018-001	2018	2	74.2	14.51	1.327	21.35	75.3	10.29	1.008	10	75.1	9.08	0.944	9.57	75.8	6.92	0.812	6.82	75.4	20.73	1.589	22.44
2018-001	2018	2	100.2	14.6	1.324	21.49	100.5	10.21	1.011	9.95	100	16.34	1.339	18.63	99	21.37	1.587	24.68	100.3	25.37	1.845	30.08
2018-001	2018	2	124.1	26.06	1.977	42.37	126	20.06	1.505	26.35	124.1	22.29	1.639	28.95	125.4	24.93	1.785	30.9	125.8	26.69	1.938	33.87
2018-001	2018	2	149.4	30.24	2.221	53.57	149.5	24.62	1.713	36.45	149.8	24.98	1.782	35.14	150	27.81	1.957	36.88	149.1	27.88	2.028	36.92
2018-001	2018	2	174.4	32.13	2.349	59.14	174.1	26.14	1.787	41.27	174.1	27.25	1.924	41.36	174.6	29.77	2.078	41.67	175	29.51	2.125	41.21
2018-001	2018	2	200.3	34.24	2.481	65.58	199.4	28.51	1.955	48.03	199.5	29.36	2.044	47.28	200.5	31.48	2.205	46.76	200.1	30.6	2.207	44.68

			P26				P20				P16				P12				P4			
Cruise	Year	Month	Depth	NO_3^-	PO_4^{3-}	Si	Depth	NO_3^-	PO_4^{3-}	Si	Depth	NO_3^-	PO_4^{3-}	Si	Depth	NO_3^-	PO_4^{3-}	Si	Depth	NO_3^-	PO_4^{3-}	Si
			dbar	µmol kg^{-1}	µmol kg^{-1}	µmol kg^{-1}	dbar	µmol kg^{-1}	µmol kg^{-1}	µmol kg^{-1}	dbar	µmol kg^{-1}	µmol kg^{-1}	µmol kg^{-1}	dbar	µmol kg^{-1}	µmol kg^{-1}	µmol kg^{-1}	dbar	µmol kg^{-1}	µmol kg^{-1}	µmol kg^{-1}
2018-001	2018	2	250	37.37	2.693	75.78	249.1	32.81	2.263	60.52	249.4	32.9	2.316	57.87	250.3	35.1	2.468	57.5	250.2	33.75	2.429	52.91
2018-001	2018	2	300.7	39.37	2.822	83.45	298.9	36.49	2.523	70.67	299.2	36.39	2.568	68.64	304.4	37.5	2.65	65.37	299.1	35.27	2.563	59.73
2018-001	2018	2	400.1	40.38	2.926	95.71	399.4	40	2.772	85.19	400	40.04	2.839	81.9	399.8	40.13	2.859	76.08	400.6	39.23	2.845	76.58
2018-040	2018	8	4.3	8.4	0.9	16.5	4.9	5.2	0.75	4.6	5.7	0	0.37	0.4	2.8	0	0.33	1.4	5.3	0.9	ND	7.9
2018-040	2018	8	10.6	8.4	0.9	16.5	10.4	5.1	0.74	4.5	10.1	0	0.37	0.4	4.6	0	0.33	1.4	9.8	1	ND	7.8
2018-040	2018	8	25.1	8.8	0.94	16.6	25	5	0.75	4.1	25	0.1	0.37	0.4	10.3	0	0.33	1.3	23.8	8.2	ND	10.6
2018-040	2018	8	50.2	13.6	1.25	18.9	50.1	9.4	1.11	9.3	50.4	4.9	0.84	2.5	25.4	0.1	0.33	1.4	50.2	8.6	0.64	8.6
2018-040	2018	8	74.9	16.3	1.38	21	75.1	13.5	1.28	13.8	75.4	10.2	1.08	7.2	50.4	3.5	0.73	4.4	74.6	16.1	1.3	16.2
2018-040	2018	8	100.2	19.3	1.54	24.9	100.4	18.1	1.53	21.8	100.3	14.9	1.31	14.7	74.9	13.3	1.21	13.6	100.4	24.5	1.78	27.7
2018-040	2018	8	124.7	23.7	1.77	33	125	25.8	1.93	35.1	124.9	22.6	1.69	28	100.1	20.4	1.6	23.5	125	26.9	1.91	31.9
2018-040	2018	8	150.3	29.8	2.11	47.9	150.2	27.9	2.04	40.9	150.3	26.9	1.92	37.3	125.2	23.3	1.76	28.9	149.9	28.2	1.99	36.1
2018-040	2018	8	174.4	32.3	2.26	55.3	175.2	27.5	1.99	43.4	175	29.2	2.05	43.3	150.9	26.3	1.92	34.2	175.1	29.8	2.11	40.5
2018-040	2018	8	199.3	34.3	2.38	60.5	200.7	30.9	2.22	50.9	200.4	30	2.1	47.7	175.1	26.9	1.96	37	200.3	31.1	2.2	44.3
2018-040	2018	8	251.1	37.9	2.61	71.7	249.9	35.1	2.53	61.7	250.4	32.6	2.29	56	200.1	28.6	2.08	41.8	250.1	33.8	2.41	52.3
2018-040	2018	8	301.3	40.4	2.78	81.3	299.9	36.3	2.58	67.5	300.8	37.7	2.63	67.8	250.2	32.6	2.4	52.7	300.1	36.7	2.61	61
2018-040	2018	8	399.6	42.9	2.94	95.9	403	40	2.85	85.5	400.3	41.3	2.91	85.3	300.7	35.8	2.63	61.6	400.8	39.7	2.82	75.1
2018-040	2018	8													400.9	38.8	2.85	75.3				
2019-001	2019	2	5.1	13.1	1.25	20.55	5.2	8.45	1	8.33	ND	ND	ND	ND	4.3	6.41	0.813	6.08	5	3.99	0.612	4.16
2019-001	2019	2	9.2	13.17	1.256	20.5	10.2	8.42	0.985	8.32	ND	ND	ND	ND	10.2	6.43	0.796	6.11	9.9	3.96	0.623	4.17
2019-001	2019	2	23.7	13.25	1.238	20.5	25.2	8.42	0.992	8.33	ND	ND	ND	ND	24.5	6.33	0.789	5.99	25.4	3.99	0.623	4.18
2019-001	2019	2	50.4	13.11	1.245	20.5	50.9	8.4	0.994	8.29	ND	ND	ND	ND	49.8	7.47	0.869	7.24	49.9	4.1	0.63	4.25
2019-001	2019	2	75.1	13.17	1.247	20.46	76.6	8.88	1.018	8.92	ND	ND	ND	ND	99.6	18.15	1.428	19.91	75.9	8.64	0.887	8.36
2019-001	2019	2	101	23.48	1.844	34.77	100.5	21.58	1.688	28.04	ND	ND	ND	ND	124.4	26.4	1.898	32.69	101	19.26	1.492	19.79
2019-001	2019	2	125.9	28.02	2.084	44.94	125.4	25.15	1.863	36.09	ND	ND	ND	ND	150.4	26.99	1.899	35.25	124.7	24.56	1.808	29.09
2019-001	2019	2	150.5	31.71	2.303	55.22	150.8	27.96	2.003	43.31	ND	ND	ND	ND	175.2	29.25	2.045	40.81	150.6	26.95	1.969	33.42
2019-001	2019	2	199.5	35.85	2.592	68.45	176.1	29.6	2.114	48.84	ND	ND	ND	ND	200.7	30.26	2.125	44.27	174.5	28.37	2.058	35.67
2019-001	2019	2	250.2	38.34	2.762	76.7	200	31.12	2.223	53.67	ND	ND	ND	ND	249.3	34.78	2.457	55.15	201.2	29.55	2.133	38.16
2019-001	2019	2	301.1	40.85	2.918	86.5	250.8	35.05	2.49	65.3	ND	ND	ND	ND	300.3	35.95	2.506	61.94	251.8	31.37	2.264	44.59
2019-001	2019	2	399.9	42.62	3.022	96.88	300.9	38.39	2.737	75.53	ND	ND	ND	ND	399.3	38.49	2.698	77.6	300.9	33.82	2.41	52.66
2019-001	2019	2					401.7	41.41	2.959	89.28									401	37.04	2.553	65.84

			P26				P20				P16				P12				P4			
Cruise	Year	Month	Depth	NO_3^-	PO_4^{3-}	Si	Depth	NO_3^-	PO_4^{3-}	Si	Depth	NO_3^-	PO_4^{3-}	Si	Depth	NO_3^-	PO_4^{3-}	Si	Depth	NO_3^-	PO_4^{3-}	Si
			dbar	µmol kg^{-1}	µmol kg^{-1}	µmol kg^{-1}	dbar	µmol kg^{-1}	µmol kg^{-1}	µmol kg^{-1}	dbar	µmol kg^{-1}	µmol kg^{-1}	µmol kg^{-1}	dbar	µmol kg^{-1}	µmol kg^{-1}	µmol kg^{-1}	dbar	µmol kg^{-1}	µmol kg^{-1}	µmol kg^{-1}
2019-008	2019	8	4.7	0.24	0.513	7.94	5.4	0	0.318	0.3	4.6	0	0.258	0.24	4.9	0.8	0.362	0.53	5.1	0	0.293	1.5
2019-008	2019	8	10.4	0.27	0.469	7.92	10.6	0	0.309	0.25	9.8	0	0.34	0.27	10.3	0.6	0.371	0.48	10.4	0	0.28	1.52
2019-008	2019	8	25.6	0.45	0.467	8.02	25.2	0	0.343	0.22	25.4	0	0.34	0.28	25	0.59	0.386	0.8	25.1	0	0.348	0.04
2019-008	2019	8	50.8	10.57	1.24	14.96	50.6	7.22	1.012	7.97	50.2	4.82	0.801	2.53	49.7	7.28	0.849	7.23	50	2.72	0.632	2.66
2019-008	2019	8	74.6	13.28	1.259	15.08	75.3	9.12	1.062	12.43	75.6	8.57	1.03	8.53	74.7	13.97	1.205	14.94	75	8.98	0.96	8.05
2019-008	2019	8	100.5	14.97	1.348	17.86	100.6	15.59	1.339	18.88	100.2	13.36	1.209	13.69	100.5	20.22	1.585	23.17	100.4	16.69	1.37	17.24
2019-008	2019	8	125.1	19.89	1.627	27.32	125.5	25.25	1.862	33.88	125.4	19.57	1.52	24.59	124.6	25.69	1.919	31.11	125.3	22.73	1.621	26.64
2019-008	2019	8	150.7	26.98	2.015	43.32	150.3	28.62	2.028	40.47	150.1	23.99	1.744	32.39	150.6	28.92	2.105	36.46	149.9	27.01	1.886	34.26
2019-008	2019	8	175.4	30	2.223	51.62	175.4	29.94	2.067	46.31	175.4	24.83	1.714	35.2	174.4	30	2.157	38.98	175	28.28	1.99	37.42
2019-008	2019	8	200.5	32.91	2.365	58.41	200	31.54	2.21	51.88	200.4	26.12	1.809	40.32	200.4	30.64	2.211	42.37	200	29.9	2.101	41.82
2019-008	2019	8	250.9	36.36	2.589	69.74	250	34.25	2.4	61.39	250.9	23.04	1.668	40.28	250.3	32.54	2.304	47.41	250.3	32.58	2.272	49.38
2019-008	2019	8	300.3	39.19	2.763	77.73	300.6	37.44	2.584	70.61	300.4	29.94	2.052	57.3	300.3	33.88	2.424	53.82	300.4	36.24	2.499	57.16
2019-008	2019	8	399.3	42.07	2.993	93.52	399.6	40.46	2.8	85.91	400.3	37.04	2.544	82.62	399.4	38.44	2.744	71.07	400.1	39.11	2.746	75.19

Appendix C

Data Tables of hydrography at stations P26, P20, P16, P12, and P4 from 2012-2019

Table C.1 Stations P26, P20, P16, P12, and P4 temperature (T), salinity (S), and density (στ) from 2012 to 2019. Data was retrieved from the Water Properties Line P Program https://www.waterproperties.ca/linep/.

				P26			P20			P16			P12			P4		
Cruise	Year	Month	Depth	T	S	στ	T	S	στ	T	S	στ	T	S	στ	T	S	στ
			m	°C	PSU	10^3-kgm^{-3}	°C	PSU	10^3-kgm^{-3}	°C	PSU	10^3-kgm^{-3}	°C	PSU	10^3-kgm^{-3}	°C	PSU	10^3-kgm^{-3}
2012-01	2012	2	5	5.5044	32.6846	25.8084	5.9017	32.6387	25.7249	6.7642	32.6351	25.6133	7.8076	32.646	25.4791	8.2639	32.412	25.2293
2012-01	2012	2	10	5.5041	32.6844	25.8082	5.9012	32.6388	25.725	6.7644	32.635	25.6132	7.8076	32.6461	25.4791	8.2652	32.4207	25.2359
2012-01	2012	2	20	5.4999	32.6846	25.8089	5.902	32.6389	25.725	6.7609	32.6349	25.6136	7.8129	32.6471	25.4792	8.2654	32.4251	25.2394
2012-01	2012	2	30	5.501	32.6847	25.8088	5.9009	32.6387	25.7249	6.7393	32.6336	25.6154	7.8121	32.6471	25.4793	8.2661	32.4238	25.2382
2012-01	2012	2	40	5.5016	32.6854	25.8093	5.9014	32.6389	25.725	6.7326	32.6335	25.6162	7.8108	32.6466	25.4791	8.2572	32.4468	25.2576
2012-01	2012	2	50	5.5039	32.6873	25.8106	5.8949	32.642	25.7283	6.7311	32.6334	25.6163	7.8127	32.6468	25.479	8.2812	32.4781	25.2786
2012-01	2012	2	60	5.5043	32.6882	25.8112	5.8942	32.6427	25.7289	6.7307	32.6339	25.6167	7.8134	32.647	25.479	8.2813	32.5297	25.319
2012-01	2012	2	70	5.5048	32.6884	25.8113	5.8944	32.6431	25.7292	6.7314	32.634	25.6167	7.8134	32.6471	25.4791	8.2817	32.6546	25.4169
2012-01	2012	2	80	5.5059	32.6884	25.8112	5.8848	32.6446	25.7316	6.732	32.6345	25.617	7.8065	32.6469	25.4799	8.1894	32.8568	25.5892
2012-01	2012	2	90	5.5058	32.6886	25.8114	5.888	32.6493	25.7349	6.734	32.6382	25.6197	7.7421	32.8848	25.676	8.1735	33.1709	25.8379
2012-01	2012	2	100	5.5051	32.689	25.8118	5.9319	32.7052	25.7737	6.7354	32.8273	25.7685	7.5	33.2022	25.9597	8.1218	33.34	25.9783
2012-01	2012	2	125	4.6399	33.3566	26.438	6.588	33.7526	26.5173	6.6187	33.8156	26.5629	7.38	33.6629	26.3389	7.8359	33.6095	26.2318
2012-01	2012	2	150	4.6784	33.6675	26.6805	6.2743	33.8293	26.6186	6.2326	33.8427	26.6345	7.3701	33.7622	26.4184	7.568	33.7498	26.3806
2012-01	2012	2	175	4.3852	33.7225	26.7557	5.8204	33.8351	26.6803	5.7799	33.8352	26.6854	7.1415	33.8622	26.5289	7.4052	33.8238	26.4619
2012-01	2012	2	200	4.165	33.744	26.7959	5.4026	33.8385	26.7335	5.393	33.837	26.7334	6.734	33.8717	26.5918	7.2199	33.8714	26.5253
2012-01	2012	2	250	3.9875	33.8007	26.8592	4.8772	33.858	26.8096	4.9043	33.8534	26.8029	6.1373	33.8808	26.6768	6.8212	33.9313	26.6271
2012-01	2012	2	300	4.0048	33.8662	26.9095	4.6654	33.9188	26.8813	4.5891	33.8913	26.8678	5.8219	33.8916	26.7248	6.2569	33.9414	26.7094
2012-01	2012	2	400	3.9526	34.0022	27.023	4.2581	33.9886	26.9806	4.2902	33.9888	26.9774	5.0616	34.0073	26.907	5.6937	34.0374	26.8558
2012-13	2012	8	5	12.6199	32.5516	24.5968	13.813	32.515	24.332	14.82	32.517	24.1233	15.3652	32.5082	23.9988	14.1618	31.1473	23.205
2012-13	2012	8	10	12.6191	32.5523	24.5975	13.7958	32.5143	24.3349	14.8075	32.5171	24.1261	15.1309	32.5148	24.0548	13.6227	31.214	23.3655

				P26			P20			P16			P12			P4		
Cruise	Year	Month	Depth	T	S	στ	T	S	στ	T	S	στ	T	S	στ	T	S	στ
			m	°C	PSU	10^3-kgm^{-3}	°C	PSU	10^3-kgm^{-3}	°C	PSU	10^3-kgm^{-3}	°C	PSU	10^3-kgm^{-3}	°C	PSU	10^3-kgm^{-3}
2012-13	2012	8	20	12.5836	32.5561	24.6073	11.3553	32.552	24.8326	14.6297	32.5161	24.1631	13.5445	32.5777	24.4349	9.4652	32.5115	25.1225
2012-13	2012	8	30	8.8423	32.633	25.3154	8.7374	32.6197	25.3211	11.4262	32.5483	24.8169	11.7481	32.6096	24.8059	8.4182	32.6437	25.3881
2012-13	2012	8	40	7.1504	32.6669	25.5869	7.8024	32.6444	25.4785	8.2581	32.629	25.4003	10.4595	32.6306	25.0508	7.968	32.6769	25.4803
2012-13	2012	8	50	6.4307	32.6854	25.696	6.5689	32.6745	25.6697	7.1264	32.6692	25.5919	8.6112	32.6466	25.3613	7.65	32.7104	25.552
2012-13	2012	8	60	5.5283	32.71	25.8257	5.9798	32.6955	25.7602	6.611	32.6892	25.6759	7.6357	32.6767	25.5275	7.5612	32.783	25.6216
2012-13	2012	8	70	4.9433	32.7199	25.8999	5.6038	32.7113	25.8178	6.3523	32.6972	25.7153	7.2655	32.687	25.587	7.4104	32.9567	25.7792
2012-13	2012	8	80	4.7177	32.7284	25.9312	5.2375	32.7299	25.8749	6.1101	32.7058	25.7523	7.1435	32.7354	25.6417	7.4633	33.2288	25.9857
2012-13	2012	8	90	4.4728	32.7438	25.9694	5.0031	32.7647	25.9288	5.7367	32.7427	25.8269	7.0145	32.7803	25.6945	7.5204	33.4411	26.1446
2012-13	2012	8	100	4.1956	32.7648	26.0145	4.6435	32.7709	25.9728	5.651	32.7748	25.8625	6.9687	32.8105	25.7244	7.4518	33.5621	26.2495
2012-13	2012	8	125	4.2217	33.4154	26.5289	5.1576	33.3925	26.4088	6.0625	33.4482	26.3445	6.8139	33.3161	26.1433	7.5737	33.7859	26.4082
2012-13	2012	8	150	4.1602	33.6778	26.7438	5.1064	33.7276	26.6802	6.2349	33.7856	26.5892	7.1501	33.7421	26.4332	7.3617	33.854	26.4918
2012-13	2012	8	175	4.0009	33.7316	26.8029	4.7058	33.7645	26.7544	5.915	33.8488	26.6794	7.1189	33.8742	26.5415	7.0905	33.8963	26.5628
2012-13	2012	8	200	3.8822	33.7672	26.8431	4.5892	33.8048	26.7992	5.7004	33.8536	26.7097	6.7102	33.8904	26.6097	6.7817	33.9399	26.6392
2012-13	2012	8	250	3.813	33.8387	26.907	4.3803	33.8556	26.862	5.1141	33.8684	26.7909	5.9547	33.8763	26.6962	6.3769	33.9753	26.7206
2012-13	2012	8	300	3.8478	33.907	26.9578	4.2825	33.9099	26.9155	4.6689	33.9	26.866	5.3422	33.877	26.7711	6.0596	34.0094	26.7882
2012-13	2012	8	400	3.791	34.0392	27.0687	4.2197	34.0211	27.0105	4.2393	34.0058	26.9962	4.6252	33.9399	26.9025	5.6091	34.0671	26.8896
2013-01	2013	2	5	5.4152	32.6312	25.7765	6.1836	32.569	25.6352	7.0872	32.5686	25.518	7.5442	32.529	25.4243	8.3419	32.1062	24.9781
2013-01	2013	2	10	5.4146	32.6313	25.7766	6.1824	32.5691	25.6355	7.0823	32.5688	25.5189	7.5442	32.5286	25.424	8.3381	32.1059	24.9784
2013-01	2013	2	20	5.4138	32.6313	25.7767	6.1887	32.5691	25.6347	7.0803	32.5685	25.5189	7.5478	32.5294	25.4241	8.3435	32.107	24.9785
2013-01	2013	2	30	5.4106	32.6314	25.7772	6.1892	32.5691	25.6346	7.0784	32.5688	25.5194	7.561	32.5383	25.4293	8.3476	32.1109	24.9809
2013-01	2013	2	40	5.4115	32.6314	25.7771	6.1805	32.5697	25.6362	7.0787	32.5689	25.5194	7.5662	32.553	25.4401	8.1545	32.3242	25.1765
2013-01	2013	2	50	5.4127	32.6315	25.777	6.1803	32.5698	25.6363	7.0787	32.5691	25.5196	7.5658	32.5538	25.4408	7.9466	32.4112	25.2748
2013-01	2013	2	60	5.4143	32.6313	25.7766	6.179	32.5707	25.6372	7.0792	32.5691	25.5195	7.5643	32.5556	25.4424	7.7871	32.4619	25.3374
2013-01	2013	2	70	5.4137	32.6315	25.7769	6.1756	32.5762	25.6419	7.079	32.569	25.5195	7.3982	32.6099	25.5082	7.706	32.4689	25.3544
2013-01	2013	2	80	5.4135	32.6315	25.7769	6.1788	32.5777	25.6427	7.0745	32.5701	25.5209	7.0549	32.694	25.6211	7.97	32.6599	25.4667
2013-01	2013	2	90	5.4146	32.6315	25.7768	6.1661	32.5828	25.6483	6.7564	32.6365	25.6154	6.6046	32.8448	25.7993	7.4659	32.9876	25.7957
2013-01	2013	2	100	5.4149	32.6317	25.7769	5.7523	32.6474	25.7497	6.1802	32.7476	25.7766	6.5923	32.9358	25.8727	7.4851	33.1249	25.901
2013-01	2013	2	125	4.828	32.8182	25.9905	4.9781	33.1599	26.2448	5.6913	33.2417	26.2268	6.8677	33.3462	26.1598	7.6739	33.572	26.2257
2013-01	2013	2	150	3.9346	33.5183	26.6399	5.2753	33.7016	26.64	6.0118	33.7025	26.5518	7.1309	33.6628	26.3734	7.4064	33.7887	26.4341
2013-01	2013	2	175	3.8234	33.7018	26.797	5.1504	33.7767	26.714	5.8667	33.8173	26.6605	7.0916	33.8503	26.5264	7.0293	33.8743	26.5539

				P26			P20			P16			P12			P4		
Cruise	Year	Month	Depth	T	S	στ	T	S	στ	T	S	στ	T	S	στ	T	S	στ
			m	°C	PSU	10^3-kgm^{-3}	°C	PSU	10^3-kgm^{-3}	°C	PSU	10^3-kgm^{-3}	°C	PSU	10^3-kgm^{-3}	°C	PSU	10^3-kgm^{-3}
2013-01	2013	2	200	3.7672	33.7519	26.8424	4.8156	33.7894	26.762	5.5581	33.8353	26.7124	6.7738	33.8892	26.6003	6.7205	33.8881	26.6066
2013-01	2013	2	250	3.7267	33.8298	26.9084	4.3653	33.8305	26.8436	4.9459	33.8579	26.8017	5.8777	33.8954	26.7209	6.0563	33.9189	26.7171
2013-01	2013	2	300	3.7537	33.907	26.9672	4.2286	33.8936	26.9082	4.6737	33.9052	26.8696	5.4025	33.908	26.7885	5.6524	33.9344	26.7794
2013-01	2013	2	400	3.7659	34.0491	27.0791	4.1104	34.0089	27.0122	4.3441	33.9992	26.9799	4.6233	33.9891	26.9417	5.199	34.0294	26.9086
2013-18	2013	8	5	14.9142	32.3667	23.9874	15.7985	32.3971	23.8178	16.0389	32.3092	23.6965	16.8829	32.2287	23.4421	17.435	32.013	23.1475
2013-18	2013	8	10	14.8871	32.3664	23.9929	15.7951	32.3971	23.8185	16.0164	32.3098	23.702	16.8855	32.2286	23.4415	16.9681	32.0117	23.256
2013-18	2013	8	20	14.7718	32.3619	24.0141	13.9671	32.4405	24.2429	16.004	32.312	23.7065	16.6398	32.2339	23.5022	14.9226	32.0308	23.7268
2013-18	2013	8	30	10.6827	32.4929	24.9052	11.0123	32.5023	24.855	9.6051	32.4267	25.0338	11.0386	32.3754	24.7516	11.9776	32.1791	24.4293
2013-18	2013	8	40	8.6571	32.5179	25.2536	10.012	32.5346	25.0514	7.84	32.484	25.3472	9.1465	32.4205	25.1019	9.6088	32.2971	24.932
2013-18	2013	8	50	6.9199	32.5532	25.5283	8.0283	32.57	25.3877	7.0673	32.5384	25.4969	8.3488	32.4875	25.276	8.0331	32.4294	25.2766
2013-18	2013	8	60	5.6617	32.5925	25.7171	6.776	32.594	25.5794	6.6833	32.5716	25.5738	7.6386	32.5231	25.4065	7.5629	32.5545	25.4417
2013-18	2013	8	70	5.2855	32.6153	25.7787	6.4524	32.6105	25.6342	6.4606	32.5877	25.6151	7.2726	32.5636	25.489	7.298	32.6113	25.523
2013-18	2013	8	80	5.0206	32.6263	25.8172	6.2139	32.6071	25.6615	6.2845	32.598	25.6455	7.0698	32.5728	25.5237	7.1781	32.7428	25.6428
2013-18	2013	8	90	4.8513	32.641	25.8474	6.1829	32.6251	25.6796	6.3389	32.6397	25.6716	6.8883	32.5827	25.5557	7.1421	32.9506	25.8113
2013-18	2013	8	100	4.7201	32.6605	25.8771	6.1259	32.6386	25.6973	6.2	32.6821	25.7225	6.8022	32.6166	25.5937	7.2548	33.2032	25.9946
2013-18	2013	8	125	4.488	32.9925	26.1652	5.6681	32.7374	25.8309	6.2904	33.0276	25.9838	6.5113	32.7665	25.7497	7.4199	33.562	26.2539
2013-18	2013	8	150	3.9474	33.3476	26.5028	5.2538	33.1426	26.1999	6.3369	33.5324	26.3762	6.45	33.1606	26.0683	7.3332	33.7785	26.4364
2013-18	2013	8	175	3.6781	33.5916	26.7235	5.2391	33.5508	26.5248	6.2812	33.7591	26.5623	6.6981	33.6782	26.4441	7.0719	33.8826	26.5546
2013-18	2013	8	200	3.5773	33.682	26.8052	5.1546	33.7357	26.681	6.1128	33.8439	26.6507	6.4948	33.7792	26.5505	6.9278	33.9163	26.6008
2013-18	2013	8	250	3.5757	33.7836	26.8863	4.6971	33.8079	26.7898	5.5093	33.8671	26.7434	5.7349	33.8539	26.7057	6.4911	33.9529	26.688
2013-18	2013	8	300	3.6536	33.8564	26.9368	4.4015	33.8699	26.8711	5.0091	33.8951	26.824	5.104	33.8892	26.8085	6.0389	33.9833	26.7702
2013-18	2013	8	400	3.7353	34.0133	27.0537	4.1169	33.9799	26.9884	4.5823	34.0021	26.9566	4.6309	33.9842	26.937	5.5629	34.0537	26.8846
2014-01	2014	2	5	8.1222	32.4348	25.2679	8.5342	32.4528	25.2211	8.1704	32.4651	25.2847	8.142	32.4227	25.2556	7.747	32.0678	25.0336
2014-01	2014	2	10	8.1215	32.4349	25.2681	8.534	32.4526	25.221	8.1711	32.4657	25.285	8.1521	32.423	25.2543	7.7493	32.0673	25.0329
2014-01	2014	2	20	8.1234	32.4349	25.2678	8.5476	32.453	25.2193	8.1714	32.4652	25.2846	8.1297	32.4222	25.257	7.7514	32.0696	25.0344
2014-01	2014	2	30	8.1277	32.4346	25.267	8.5438	32.4529	25.2198	8.1727	32.465	25.2843	8.1357	32.4228	25.2566	7.7695	32.1263	25.0763
2014-01	2014	2	40	8.1263	32.4353	25.2677	8.5429	32.453	25.22	8.1741	32.4649	25.284	8.1209	32.4211	25.2574	7.832	32.2352	25.153
2014-01	2014	2	50	8.1269	32.4354	25.2677	8.5431	32.4533	25.2202	8.1722	32.4662	25.2853	8.1206	32.4212	25.2575	8.1257	32.8668	25.6064
2014-01	2014	2	60	8.1269	32.4359	25.2681	8.5393	32.4543	25.2215	8.1667	32.4679	25.2874	8.1149	32.4207	25.2579	8.0754	33.1665	25.8489
2014-01	2014	2	70	8.1284	32.4357	25.2677	8.5412	32.454	25.221	8.1717	32.4678	25.2866	8.106	32.42	25.2587	7.9964	33.3203	25.9812

				P26			P20			P16			P12			P4		
Cruise	Year	Month	Depth	T	S	στ	T	S	στ	T	S	στ	T	S	στ	T	S	στ
			m	°C	PSU	10^3-kgm^{-3}	°C	PSU	10^3-kgm^{-3}	°C	PSU	10^3-kgm^{-3}	°C	PSU	10^3-kgm^{-3}	°C	PSU	10^3-kgm^{-3}
2014-01	2014	2	80	8.1259	32.4367	25.2689	8.5336	32.4541	25.2222	8.1614	32.4691	25.2891	8.1038	32.4198	25.2588	7.874	33.4843	26.1279
2014-01	2014	2	90	8.0713	32.443	25.2818	8.3023	32.4968	25.2901	7.5347	32.5563	25.4471	7.7995	32.481	25.3506	7.884	33.5661	26.1907
2014-01	2014	2	100	5.9184	32.5891	25.6836	6.5662	32.6959	25.6869	6.5024	32.6626	25.6689	6.6133	32.6474	25.6426	8.0225	33.668	26.2504
2014-01	2014	2	125	4.9014	32.8026	25.9701	5.5447	32.739	25.8467	5.5837	32.8436	25.9248	6.213	32.8674	25.8671	7.7208	33.8234	26.4165
2014-01	2014	2	150	4.7747	33.2593	26.3461	5.5409	33.1155	26.145	5.9547	33.3376	26.2705	6.1934	33.2122	26.1417	7.656	33.8656	26.459
2014-01	2014	2	175	4.2461	33.6087	26.6799	5.4784	33.4981	26.4551	5.9434	33.6087	26.4862	6.3381	33.5969	26.427	7.4941	33.9154	26.5213
2014-01	2014	2	200	4.1081	33.6931	26.7613	5.4633	33.7173	26.6304	5.7479	33.7859	26.6503	6.1763	33.769	26.5835	7.2476	33.9367	26.5728
2014-01	2014	2	250	4.1143	33.8034	26.8484	4.8724	33.7778	26.7465	4.9615	33.7946	26.7498	5.595	33.8668	26.7329	6.9418	33.9756	26.6456
2014-01	2014	2	300	4.0809	33.869	26.904	4.2972	33.8312	26.8514	4.4517	33.8469	26.8475	5.0245	33.8937	26.8212	6.63	33.9907	26.6995
2014-01	2014	2	400	3.9926	34.0099	27.0251	4.0259	33.9362	26.963	4.1649	33.9633	26.9702	4.6191	33.9658	26.9237	6.1724	34.0206	26.7827
2014-19	2014	8	5	14.6978	32.3604	24.0286	16.8051	32.233	23.4635	17.5668	32.2994	23.3355	18.6514	32.2152	23.0077	14.9662	32.0402	23.7248
2014-19	2014	8	10	14.6836	32.3592	24.0307	16.8084	32.2355	23.4646	17.5527	32.2991	23.3387	18.6474	32.2152	23.0086	14.6021	32.0305	23.7946
2014-19	2014	8	20	14.6776	32.3589	24.0318	16.7074	32.2345	23.4872	16.5358	32.2961	23.5738	18.6312	32.2155	23.0129	13.2315	32.0765	24.1098
2014-19	2014	8	30	14.6652	32.3577	24.0335	15.0197	32.2724	23.8921	12.9283	32.3576	24.3868	17.6064	32.2159	23.2622	11.2381	32.2378	24.6093
2014-19	2014	8	40	13.0504	32.3393	24.3487	9.8352	32.369	24.9513	10.6423	32.4376	24.8691	14.7422	32.2374	23.9244	9.5803	32.3491	24.9772
2014-19	2014	8	50	9.1697	32.4391	25.1128	9.0337	32.419	25.1183	9.8487	32.4823	25.0375	11.3346	32.2681	24.6156	8.7001	32.4221	25.172
2014-19	2014	8	60	8.0586	32.5069	25.3338	8.8015	32.4556	25.1828	9.3207	32.4824	25.1228	9.1373	32.383	25.074	7.9544	32.5265	25.3642
2014-19	2014	8	70	7.9368	32.5921	25.4182	8.3427	32.4733	25.2657	9.1348	32.4876	25.1562	8.5413	32.4497	25.2176	7.6243	32.61	25.4767
2014-19	2014	8	80	7.7557	32.6504	25.4899	7.5098	32.5859	25.4738	8.6447	32.5006	25.2419	8.0469	32.5256	25.3501	7.4377	32.6883	25.5643
2014-19	2014	8	90	6.8494	32.6487	25.6128	6.7104	32.7175	25.6852	8.2069	32.5877	25.3755	7.4434	32.664	25.5444	7.1948	32.8072	25.6912
2014-19	2014	8	100	6.3833	32.8899	25.8633	6.1519	32.8471	25.8587	7.3066	32.8126	25.6802	7.189	32.7618	25.6563	7.1243	32.9721	25.8306
2014-19	2014	8	125	4.661	33.1814	26.2967	5.8486	33.1617	26.1446	6.8148	33.1929	26.0461	6.9257	32.985	25.8675	7.419	33.3579	26.0935
2014-19	2014	8	150	4.2809	33.5618	26.639	5.8153	33.5838	26.4823	6.5789	33.6141	26.4093	6.9562	33.3111	26.1203	7.4799	33.6319	26.3004
2014-19	2014	8	175	4.111	33.6674	26.7406	5.4694	33.7366	26.6449	6.0603	33.7664	26.5961	6.9815	33.6984	26.4219	7.4142	33.8148	26.4535
2014-19	2014	8	200	3.914	33.7013	26.7875	5.0203	33.759	26.7149	5.4607	33.779	26.6795	6.7752	33.8297	26.5532	7.2647	33.882	26.5274
2014-19	2014	8	250	3.7403	33.7794	26.8669	4.3991	33.7849	26.8038	4.8146	33.8022	26.7723	6.1954	33.9028	26.6868	6.5933	33.9193	26.6481
2014-19	2014	8	300	3.7065	33.8537	26.9294	4.1196	33.8422	26.8787	4.4444	33.8407	26.8433	5.5993	33.9141	26.7698	6.2147	33.9782	26.7438
2014-19	2014	8	400	3.7195	33.9943	27.0401	4.014	33.9584	26.9819	4.1973	33.9553	26.9605	5.0583	34.0062	26.9065	5.5945	34.028	26.8605
2015-01	2015	2	5	7.5412	32.5145	25.4133	9.2486	32.4409	25.1018	9.4389	32.2396	24.9143	10.2846	32.2626	24.7937	10.9287	32.1512	24.5965
2015-01	2015	2	10	7.5226	32.5153	25.4165	9.2458	32.4406	25.102	9.4386	32.2399	24.9146	10.2703	32.2631	24.7965	10.8269	32.1499	24.6132

				P26			P20			P16			P12			P4		
Cruise	Year	Month	Depth	T	S	στ	T	S	στ	T	S	στ	T	S	στ	T	S	στ
			m	°C	PSU	10^3-kgm^{-3}	°C	PSU	10^3-kgm^{-3}	°C	PSU	10^3-kgm^{-3}	°C	PSU	10^3-kgm^{-3}	°C	PSU	10^3-kgm^{-3}
2015-01	2015	2	20	7.4977	32.5183	25.4224	9.2454	32.4408	25.1022	9.4387	32.2403	24.9149	10.2562	32.263	24.7988	10.7834	32.1522	24.6225
2015-01	2015	2	30	7.4764	32.5198	25.4265	9.2461	32.4408	25.1021	9.4365	32.2407	24.9155	10.2482	32.2634	24.8004	10.779	32.1541	24.6247
2015-01	2015	2	40	7.4713	32.5204	25.4277	9.2465	32.4409	25.1021	9.4227	32.2412	24.9181	10.2415	32.2735	24.8094	10.766	32.3092	24.7477
2015-01	2015	2	50	7.4126	32.5248	25.4393	9.2435	32.4409	25.1026	9.4206	32.2411	24.9184	10.2364	32.281	24.8161	10.4163	32.5171	24.9698
2015-01	2015	2	60	7.4129	32.5262	25.4403	9.2202	32.442	25.1071	9.4175	32.2411	24.9189	10.2278	32.2859	24.8214	9.845	32.8009	25.2868
2015-01	2015	2	70	7.4083	32.5277	25.4421	9.1776	32.4478	25.1184	9.4044	32.2422	24.9218	10.0584	32.3427	24.894	8.5857	32.9298	25.5871
2015-01	2015	2	80	7.4007	32.5331	25.4474	9.0315	32.4767	25.1638	8.5014	32.5289	25.2857	8.6326	32.6212	25.3382	8.0351	32.9258	25.6659
2015-01	2015	2	90	6.3252	32.9692	25.9333	7.552	32.911	25.7234	7.7906	32.7868	25.5921	7.9785	32.7469	25.5337	7.7658	33.0126	25.773
2015-01	2015	2	100	5.4562	33.2304	26.2458	7.2292	33.1816	25.9811	7.1588	33.1042	25.9299	7.6485	32.8507	25.6625	8.7249	33.3236	25.8744
2015-01	2015	2	125	4.7682	33.4773	26.5197	6.8194	33.5865	26.3556	7.0679	33.4893	26.2454	7.4229	33.2129	25.9789	8.4078	33.5416	26.0937
2015-01	2015	2	150	4.2041	33.6324	26.7031	6.4724	33.7747	26.5499	7.1033	33.6734	26.3855	7.8593	33.6891	26.2909	8.1762	33.6345	26.2013
2015-01	2015	2	175	3.9452	33.7032	26.7859	5.8908	33.7864	26.6331	6.6832	33.7852	26.5304	7.7123	33.8222	26.4168	8.0698	33.7113	26.2774
2015-01	2015	2	200	3.77	33.739	26.8319	5.3798	33.7897	26.6975	6.4065	33.8142	26.5896	7.2546	33.857	26.5091	7.7977	33.8115	26.396
2015-01	2015	2	250	3.6923	33.7896	26.8798	4.58	33.7754	26.7768	5.7153	33.8429	26.6994	6.4635	33.8534	26.6131	7.3268	33.8875	26.523
2015-01	2015	2	300	3.7144	33.8752	26.9458	4.196	33.8182	26.8517	5.1682	33.8909	26.8024	5.415	33.8404	26.7335	6.6323	33.9489	26.6662
2015-01	2015	2	400	3.6721	34.0055	27.0537	4.0719	33.9628	26.9795	4.5402	33.9579	26.926	4.7859	33.939	26.884	5.7345	34.0223	26.8389
2015-10	2015	8	5	14.7052	32.3938	24.0528	15.8147	32.4219	23.8332	17.6145	32.0132	23.1051	17.8683	31.8103	22.8891	13.4033	32.1193	24.1088
2015-10	2015	8	10	14.7062	32.3939	24.0527	15.8164	32.4221	23.833	17.6154	32.0142	23.1056	17.7046	31.8186	22.9346	13.3986	32.1197	24.11
2015-10	2015	8	20	14.7055	32.3941	24.053	15.8156	32.4223	23.8333	17.666	32.1846	23.224	17.6667	31.8829	22.9929	13.3937	32.12	24.1112
2015-10	2015	8	30	12.4136	32.5604	24.6431	12.6845	32.5638	24.5938	17.6137	32.2443	23.2822	17.2763	32.0579	23.2193	13.3809	32.1214	24.1149
2015-10	2015	8	40	7.9832	32.7009	25.4969	10.2108	32.5867	25.0588	12.6591	32.2814	24.3799	13.1875	32.413	24.3788	11.0618	32.3931	24.7613
2015-10	2015	8	50	7.3133	32.7295	25.6139	9.2562	32.6263	25.2456	10.7434	32.3203	24.7603	10.8104	32.3142	24.7439	10.5854	32.4462	24.8856
2015-10	2015	8	60	7.0116	32.7422	25.6648	8.3796	32.6651	25.4106	10.039	32.3383	24.8937	10.5247	32.4619	24.9082	10.0214	32.5791	25.0845
2015-10	2015	8	70	6.9568	32.7517	25.6797	7.8607	32.6929	25.5083	9.8128	32.3805	24.9639	10.1784	32.5927	25.0689	9.602	32.7227	25.2655
2015-10	2015	8	80	6.8879	32.7695	25.7028	7.6077	32.7955	25.6248	9.5374	32.4276	25.0454	9.5951	32.6478	25.2081	8.6825	32.9071	25.5546
2015-10	2015	8	90	6.787	32.78	25.7244	7.5559	32.9829	25.7794	9.4517	32.5155	25.1278	8.9613	32.7794	25.4116	8.2301	33.0181	25.7097
2015-10	2015	8	100	6.6501	32.7961	25.755	7.42	33.3413	26.0803	9.0854	32.6062	25.2567	8.4304	32.9497	25.6262	7.9565	33.1567	25.8586
2015-10	2015	8	125	5.2635	33.5235	26.5004	6.9435	33.6712	26.4056	7.6216	33.2824	26.0055	7.8114	33.5532	26.1911	7.6034	33.5012	26.1801
2015-10	2015	8	150	4.7436	33.7045	26.7027	6.6467	33.7922	26.5408	7.3007	33.6285	26.3229	7.5667	33.7928	26.4146	7.5501	33.7281	26.3661
2015-10	2015	8	175	4.5555	33.7465	26.7565	6.376	33.8334	26.6087	6.9625	33.7595	26.4726	7.2619	33.8509	26.5033	7.2919	33.8559	26.5031

				P26			P20			P16			P12			P4		
Cruise	Year	Month	Depth	T	S	στ	T	S	στ	T	S	στ	T	S	στ	T	S	στ
			m	°C	PSU	10^3-kgm^{-3}	°C	PSU	10^3-kgm^{-3}	°C	PSU	10^3-kgm^{-3}	°C	PSU	10^3-kgm^{-3}	°C	PSU	10^3-kgm^{-3}
2015-10	2015	8	200	4.3503	33.7776	26.8032	6.0084	33.8323	26.6547	6.4412	33.8181	26.5882	6.7858	33.8574	26.5736	7.0753	33.8985	26.5666
2015-10	2015	8	250	4.0643	33.8263	26.8717	5.1624	33.8298	26.7547	5.6811	33.8318	26.6948	5.9244	33.8381	26.6698	6.6305	33.9485	26.6662
2015-10	2015	8	300	3.9531	33.8948	26.9375	4.6702	33.8424	26.8202	5.0671	33.8582	26.7882	5.2609	33.8337	26.7463	6.1461	33.9599	26.7381
2015-10	2015	8	400	3.8638	34.0242	27.0495	4.1055	33.9308	26.9506	4.5603	33.9604	26.9258	4.4585	33.8913	26.882	5.5253	34.0264	26.8676
2017-001	2017	2	5	5.9071	32.721	25.7892	6.6168	32.7851	25.7507	7.2732	32.5226	25.4567	7.4251	32.559	25.4644	9.0304	32.352	25.0664
2017-001	2017	2	10	5.9095	32.7212	25.7891	6.6184	32.7854	25.7507	7.2442	32.5234	25.4612	7.4271	32.5591	25.4642	9.0279	32.3511	25.0661
2017-001	2017	2	20	5.9057	32.7214	25.7897	6.6243	32.7866	25.7509	7.243	32.5257	25.4632	7.4242	32.5587	25.4643	9.0481	32.3572	25.0677
2017-001	2017	2	30	5.9045	32.7213	25.7898	6.6261	32.7872	25.7512	7.2427	32.5274	25.4646	7.4172	32.5582	25.4649	9.2374	32.4277	25.0933
2017-001	2017	2	40	5.8986	32.7214	25.7906	6.6238	32.7868	25.7511	7.2386	32.5327	25.4693	7.4164	32.5582	25.465	9.2747	32.4508	25.1054
2017-001	2017	2	50	5.883	32.722	25.7929	6.6231	32.7863	25.7508	7.2311	32.535	25.4721	7.4157	32.5584	25.4652	9.3119	32.4682	25.1131
2017-001	2017	2	60	5.8194	32.7232	25.8016	6.6257	32.787	25.751	7.2289	32.536	25.4732	7.4165	32.5598	25.4662	9.3257	32.4943	25.1314
2017-001	2017	2	70	5.8141	32.7235	25.8024	6.6298	32.7878	25.7511	7.228	32.5364	25.4737	7.4163	32.5628	25.4686	9.4171	32.7855	25.3444
2017-001	2017	2	80	5.8127	32.7237	25.8028	6.6306	32.7884	25.7515	7.2284	32.5378	25.4747	7.4171	32.5722	25.4759	9.4096	32.9325	25.4605
2017-001	2017	2	90	5.8079	32.7245	25.804	6.6326	32.7886	25.7514	7.229	32.5399	25.4763	7.4174	32.5806	25.4825	9.5253	33.1239	25.5914
2017-001	2017	2	100	5.8037	32.7263	25.8059	6.6318	32.7906	25.7531	7.2357	32.5514	25.4844	7.4582	32.6533	25.534	9.5199	33.2289	25.6744
2017-001	2017	2	125	5.9191	33.7344	26.5885	6.8369	33.1565	26.0145	7.3925	33.3242	26.0707	7.4703	33.5883	26.2675	9.053	33.5921	26.0333
2017-001	2017	2	150	5.6025	33.7954	26.6755	6.4315	33.7854	26.5637	6.8588	33.6937	26.4348	7.1944	33.7923	26.4666	8.6176	33.7618	26.2343
2017-001	2017	2	175	5.3046	33.8073	26.7203	5.941	33.8238	26.6564	6.4564	33.7827	26.5583	6.8305	33.8512	26.5627	8.2603	33.8406	26.3504
2017-001	2017	2	200	5.1077	33.8297	26.7609	5.6286	33.8377	26.7058	5.9682	33.8287	26.6569	6.54	33.8737	26.6191	7.6983	33.8489	26.4398
2017-001	2017	2	250	4.7818	33.8703	26.83	5.0249	33.8547	26.7902	5.4421	33.8526	26.74	5.7723	33.8827	26.7239	7.4955	33.9294	26.5322
2017-001	2017	2	300	4.5591	33.9103	26.8862	4.5427	33.8868	26.8693	4.7614	33.9041	26.8591	5.1407	33.9007	26.8134	7.0186	33.9609	26.6236
2017-001	2017	2	400	4.1534	33.9848	26.9885	4.2537	33.994	26.9853	4.383	33.9992	26.9758	4.6551	33.9888	26.938	6.1109	33.9349	26.7229
2017-008	2017	8	5	13.2069	32.3588	24.333	14.2336	32.4321	24.1814	15.2119	32.551	24.0651	16.3246	32.4485	23.739	15.1396	32.0062	23.6613
2017-008	2017	8	10	13.2105	32.3586	24.3321	14.2116	32.4332	24.1868	15.2119	32.5511	24.0652	16.3252	32.4484	23.7388	14.5656	32.0219	23.7956
2017-008	2017	8	20	13.1808	32.3587	24.3381	14.1658	32.4393	24.201	15.2107	32.5515	24.0657	16.2676	32.4462	23.7502	12.6549	32.104	24.2433
2017-008	2017	8	30	12.7033	32.3732	24.4425	14.0722	32.4433	24.2234	14.4225	32.5703	24.2486	14.2152	32.4317	24.1849	11.5118	32.2913	24.6017
2017-008	2017	8	40	7.8919	32.4478	25.3114	9.4746	32.6283	25.2123	9.1805	32.6605	25.2843	10.6336	32.5004	24.9195	9.9781	32.4193	24.967
2017-008	2017	8	50	5.9032	32.5089	25.6221	7.5848	32.6904	25.5455	8.129	32.7184	25.4894	8.8658	32.5509	25.2475	9.2064	32.5694	25.2089
2017-008	2017	8	60	5.4658	32.5448	25.7023	7.0535	32.7279	25.648	7.5018	32.7569	25.6093	8.1845	32.5946	25.3842	8.5853	32.6792	25.3908
2017-008	2017	8	70	5.171	32.5685	25.7546	6.8425	32.7419	25.6871	7.2386	32.7736	25.6588	7.6774	32.6444	25.4963	8.8523	32.9548	25.5658

				P26			P20			P16			P12			P4		
Cruise	Year	Month	Depth	T	S	στ	T	S	στ	T	S	στ	T	S	στ	T	S	στ
			m	°C	PSU	10^3-kgm^{-3}	°C	PSU	10^3-kgm^{-3}	°C	PSU	10^3-kgm^{-3}	°C	PSU	10^3-kgm^{-3}	°C	PSU	10^3-kgm^{-3}
2017-008	2017	8	80	4.999	32.5816	25.7842	6.641	32.7534	25.7226	6.9018	32.7934	25.7198	7.375	32.7278	25.6041	8.8452	33.2964	25.8344
2017-008	2017	8	90	4.8082	32.5957	25.8162	6.4982	32.7656	25.7506	6.6799	32.8158	25.7667	7.2963	32.872	25.7283	8.8445	33.4425	25.9489
2017-008	2017	8	100	4.5978	32.6331	25.8684	6.3212	32.8009	25.801	6.4273	32.8581	25.8327	7.2512	32.9849	25.8233	8.761	33.5896	26.0771
2017-008	2017	8	125	5.132	33.3876	26.4079	6.6864	33.4706	26.282	6.9667	33.3854	26.1774	7.3107	33.3359	26.0913	8.2082	33.7689	26.302
2017-008	2017	8	150	5.6836	33.7704	26.6459	6.6285	33.8347	26.5767	7.0286	33.6521	26.379	7.1677	33.6626	26.3682	7.8197	33.8641	26.4341
2017-008	2017	8	175	5.4645	33.8107	26.7041	6.2955	33.8412	26.6253	6.6212	33.8129	26.5605	7.004	33.828	26.5209	7.4756	33.904	26.515
2017-008	2017	8	200	5.2538	33.8356	26.7487	5.9413	33.8513	26.6781	6.2823	33.8402	26.6262	6.5277	33.8646	26.6136	7.1361	33.9263	26.5801
2017-008	2017	8	250	4.7605	33.8422	26.81	5.2674	33.8511	26.7594	5.4353	33.8659	26.7513	5.6755	33.9073	26.7552	6.6068	33.9437	26.6655
2017-008	2017	8	300	4.5216	33.8937	26.8771	4.8121	33.8811	26.8352	4.9167	33.8871	26.8282	5.0844	33.9224	26.8371	5.945	33.9436	26.7506
2017-008	2017	8	400	4.2461	33.9995	26.9905	4.2632	33.963	26.9597	4.4484	33.9643	26.941	4.5416	33.9795	26.943	5.2874	34.0204	26.8911
2018-001	2018	2	5	5.8892	32.4995	25.6164	6.7468	32.4391	25.4611	7.0726	32.478	25.4487	7.9755	32.507	25.3458	8.6766	32.2074	25.0074
2018-001	2018	2	10	5.8782	32.5008	25.6187	6.7548	32.4393	25.4602	7.0818	32.479	25.4482	7.9766	32.5076	25.3462	8.6833	32.2079	25.0068
2018-001	2018	2	20	5.8786	32.5012	25.619	6.7588	32.4394	25.4598	7.0819	32.4784	25.4478	7.9757	32.5075	25.3462	8.6893	32.2098	25.0074
2018-001	2018	2	30	5.8787	32.5015	25.6192	6.7594	32.4396	25.4599	7.0892	32.4788	25.4471	7.9683	32.5112	25.3502	8.6656	32.2739	25.0612
2018-001	2018	2	40	5.8795	32.5017	25.6193	6.7607	32.4398	25.4599	7.0897	32.4788	25.447	7.9796	32.5154	25.3519	8.5409	32.2989	25.0995
2018-001	2018	2	50	5.8796	32.5017	25.6193	6.7608	32.4393	25.4595	7.0885	32.4783	25.4468	8.0114	32.5239	25.3539	8.4194	32.3404	25.1502
2018-001	2018	2	60	5.8802	32.5018	25.6193	6.7625	32.4396	25.4595	7.089	32.4782	25.4466	8.0935	32.5531	25.3649	8.5278	33.1195	25.7446
2018-001	2018	2	70	5.8803	32.502	25.6194	6.763	32.4402	25.4599	7.0904	32.4787	25.4469	7.9428	33.062	25.7863	8.4881	33.3074	25.8979
2018-001	2018	2	80	5.8804	32.5021	25.6195	6.7643	32.441	25.4604	7.0888	32.4786	25.447	7.7874	33.2833	25.9825	8.4765	33.5028	26.0528
2018-001	2018	2	90	5.8817	32.502	25.6193	6.7651	32.4411	25.4603	7.1131	32.8213	25.7134	7.7978	33.4908	26.144	8.4022	33.6419	26.1732
2018-001	2018	2	100	5.8763	32.5038	25.6213	6.4217	32.6539	25.6723	6.9879	33.0918	25.9433	7.7991	33.6081	26.236	8.2809	33.7497	26.276
2018-001	2018	2	125	4.61	33.359	26.4431	6.6911	33.617	26.3967	7.0598	33.3454	26.1332	7.711	33.8203	26.4155	8.0641	33.8482	26.3857
2018-001	2018	2	150	4.3452	33.6022	26.6644	6.5618	33.8469	26.5951	7.0501	33.6663	26.3872	7.4225	33.8786	26.5025	7.7713	33.8852	26.4578
2018-001	2018	2	175	4.1943	33.6824	26.7439	6.2839	33.8567	26.639	6.7773	33.7995	26.5291	7.0782	33.9069	26.5729	7.4157	33.9163	26.5332
2018-001	2018	2	200	4.116	33.7194	26.7814	5.9047	33.8623	26.6914	6.3296	33.8512	26.6288	6.7456	33.9294	26.6358	7.0858	33.9335	26.5928
2018-001	2018	2	250	4.1114	33.8046	26.8496	5.4393	33.8743	26.7575	5.7141	33.8671	26.7187	6.1255	33.9515	26.7341	6.5658	33.9734	26.6944
2018-001	2018	2	300	3.9876	33.8496	26.8981	4.9454	33.8897	26.827	5.1761	33.8836	26.7957	5.7607	33.9749	26.7982	6.0704	33.9958	26.7761
2018-001	2018	2	400	4.0611	34.0021	27.0118	4.2789	33.9664	26.9608	4.4944	33.9583	26.9313	5.2387	34.0249	26.9004	5.3088	34.0538	26.915
2018-040	2018	8	5	14.1328	32.2687	24.0762	15.1595	32.3465	23.919	15.8903	32.305	23.7265	16.5717	32.3135	23.579	15.4676	32.1922	23.7332
2018-040	2018	8	10	14.1355	32.269	24.0758	15.163	32.3461	23.918	15.815	32.3044	23.7428	16.5707	32.3143	23.5798	15.066	32.1849	23.8148

				P26			P20			P16			P12			P4		
Cruise	Year	Month	Depth	T	S	στ	T	S	στ	T	S	στ	T	S	στ	T	S	στ
			m	°C	PSU	10^3-kgm^{-3}	°C	PSU	10^3-kgm^{-3}	°C	PSU	10^3-kgm^{-3}	°C	PSU	10^3-kgm^{-3}	°C	PSU	10^3-kgm^{-3}
2018-040	2018	8	20	14.1361	32.2693	24.0759	15.1629	32.3462	23.9181	15.7461	32.3049	23.7585	16.5685	32.3175	23.5828	12.9549	32.2898	24.3291
2018-040	2018	8	30	14.136	32.2702	24.0767	12.402	32.3433	24.477	15.7311	32.3058	23.7625	16.551	32.3178	23.587	10.8477	32.4222	24.8215
2018-040	2018	8	40	9.8287	32.4047	24.9802	9.059	32.4129	25.1096	12.8522	32.3692	24.4106	14.2037	32.3553	24.1283	9.5452	32.5206	25.1168
2018-040	2018	8	50	7.8183	32.4862	25.352	8.1725	32.4352	25.2609	9.9249	32.4064	24.9657	10.1424	32.4253	24.9444	8.9374	32.5825	25.2612
2018-040	2018	8	60	6.8672	32.5211	25.5099	6.9501	32.4653	25.455	8.5017	32.4392	25.2153	9.0037	32.4979	25.1847	8.6715	32.7263	25.4146
2018-040	2018	8	70	6.3928	32.5474	25.592	6.7161	32.4834	25.5	7.6811	32.4615	25.3521	8.583	32.5763	25.3105	8.542	33.0861	25.7162
2018-040	2018	8	80	6.166	32.5633	25.6329	6.3945	32.5252	25.5742	7.2797	32.4729	25.4167	8.3013	32.6247	25.3906	8.4154	33.2697	25.8793
2018-040	2018	8	90	5.82	32.6369	25.7333	6.3573	32.6857	25.7056	6.9868	32.4871	25.4673	8.0278	32.7818	25.554	8.336	33.4143	26.0046
2018-040	2018	8	100	5.5473	32.8255	25.9148	6.5276	32.9908	25.9244	6.9553	32.6997	25.6389	7.9261	33.0564	25.7843	8.3062	33.5695	26.1309
2018-040	2018	8	125	4.9539	33.3066	26.3638	6.8765	33.5491	26.3185	6.8891	33.5264	26.2989	7.7669	33.4562	26.1213	8.1724	33.7705	26.3086
2018-040	2018	8	150	4.7874	33.5751	26.5952	6.7886	33.7589	26.4956	6.7348	33.7716	26.5128	7.8215	33.8088	26.3904	7.8877	33.8615	26.4222
2018-040	2018	8	175	4.5506	33.6704	26.6967	6.5004	33.8371	26.5954	6.5289	33.8299	26.586	7.4284	33.8919	26.5122	7.6066	33.8999	26.4931
2018-040	2018	8	200	4.2458	33.6947	26.7483	6.1622	33.8547	26.653	6.3291	33.8575	26.6338	6.9687	33.9128	26.5925	7.3882	33.9163	26.5371
2018-040	2018	8	250	4.0198	33.7542	26.8189	5.6591	33.8864	26.7406	5.7056	33.864	26.7172	6.5196	33.9376	26.6722	6.7739	33.9501	26.6483
2018-040	2018	8	300	4.0088	33.8377	26.8864	5.0767	33.9139	26.8312	5.2693	33.8966	26.7952	6.0795	33.972	26.7561	6.298	33.9732	26.7292
2018-040	2018	8	400	3.9815	33.9853	27.0066	4.6246	33.9862	26.9393	4.5207	33.9609	26.9305	5.4363	34.0229	26.8755	5.1935	33.97	26.8622
2019-001	2019	2	5	6.8121	32.3929	25.4162	8.0292	32.3103	25.1837	ND	ND	ND	8.6979	32.4072	25.1607	9.6695	32.414	25.0134
2019-001	2019	2	10	6.8156	32.3931	25.4159	8.0301	32.3103	25.1836	ND	ND	ND	8.697	32.4074	25.161	9.6767	32.4143	25.0125
2019-001	2019	2	20	6.8169	32.3933	25.4159	8.0301	32.3103	25.1836	ND	ND	ND	8.7012	32.4078	25.1606	9.6819	32.4146	25.0119
2019-001	2019	2	30	6.8184	32.3932	25.4156	8.0314	32.3103	25.1834	ND	ND	ND	8.7081	32.4144	25.1648	9.6815	32.4169	25.0138
2019-001	2019	2	40	6.8191	32.3932	25.4155	8.0327	32.3102	25.1831	ND	ND	ND	8.7063	32.4262	25.1743	9.6838	32.4175	25.0139
2019-001	2019	2	50	6.8199	32.3932	25.4154	8.0281	32.311	25.1844	ND	ND	ND	8.6059	32.4546	25.2117	9.6895	32.4191	25.0142
2019-001	2019	2	60	6.8237	32.3929	25.4147	8.0218	32.3115	25.1857	ND	ND	ND	8.5642	32.4686	25.229	9.6967	32.4234	25.0164
2019-001	2019	2	70	6.8225	32.3945	25.4161	8.02	32.312	25.1864	ND	ND	ND	8.5204	32.482	25.2461	9.7423	32.5967	25.1443
2019-001	2019	2	80	6.7443	32.4185	25.4452	8.0011	32.3151	25.1916	ND	ND	ND	8.5086	32.4918	25.2555	9.5432	33.0199	25.5073
2019-001	2019	2	90	5.4933	32.7612	25.8703	6.6525	32.5541	25.564	ND	ND	ND	8.0552	32.9516	25.6832	9.3541	33.2517	25.719
2019-001	2019	2	100	5.0547	32.9783	26.0923	6.1249	32.7723	25.803	ND	ND	ND	7.3796	33.1616	25.9446	8.4465	33.277	25.8803
2019-001	2019	2	125	4.8354	33.5127	26.5404	6.1118	33.2743	26.201	ND	ND	ND	8.021	33.7428	26.3093	8.9626	33.6934	26.1269
2019-001	2019	2	150	4.5976	33.66	26.6833	6.0296	33.6538	26.511	ND	ND	ND	7.8502	33.8243	26.3984	8.6431	33.8174	26.2739
2019-001	2019	2	175	4.3061	33.7114	26.7553	6.1441	33.8176	26.626	ND	ND	ND	7.5474	33.8796	26.4856	8.4437	33.9012	26.3702

				P26			P20			P16			P12			P4		
Cruise	Year	Month	Depth	T	S	στ	T	S	στ	T	S	στ	T	S	στ	T	S	στ
			m	°C	PSU	10^3-kgm^{-3}	°C	PSU	10^3-kgm^{-3}	°C	PSU	10^3-kgm^{-3}	°C	PSU	10^3-kgm^{-3}	°C	PSU	10^3-kgm^{-3}
2019-001	2019	2	200	4.1145	33.7439	26.801	5.8076	33.8408	26.6864	ND	ND	ND	7.1679	33.914	26.5661	8.175	33.9177	26.4238
2019-001	2019	2	250	3.9718	33.798	26.8586	5.2104	33.8646	26.7767	ND	ND	ND	6.6414	33.9445	26.6616	7.5034	33.9681	26.5615
2019-001	2019	2	300	3.9438	33.872	26.9203	4.8188	33.8981	26.8479	ND	ND	ND	6.1114	33.9641	26.7459	6.8921	33.9937	26.6667
2019-001	2019	2	400	3.9589	34.0046	27.0243	4.3926	33.9934	26.9701	ND	ND	ND	5.2314	34.0049	26.8854	5.6806	33.9575	26.7942
2019-008	2019	8	5	15.3296	32.3978	23.9216	16.1644	32.1477	23.5442	17.2561	32.2934	23.4045	17.3556	32.3054	23.3902	17.9979	32.2039	23.159
2019-008	2019	8	10	15.3296	32.3979	23.9216	16.1645	32.1475	23.5441	17.2568	32.2935	23.4044	17.356	32.3057	23.3904	18.0039	32.2039	23.1575
2019-008	2019	8	20	15.3235	32.3978	23.9229	14.6071	32.3219	24.0181	15.2747	32.2851	23.8468	16.0897	32.301	23.6788	16.9616	32.2764	23.4604
2019-008	2019	8	30	14.7094	32.3984	24.0555	11.5627	32.3057	24.6037	10.6101	32.2874	24.7577	12.9837	32.3055	24.3356	13.7029	32.3168	24.2012
2019-008	2019	8	40	10.5377	32.4194	24.8729	9.0322	32.3195	25.0407	9.3058	32.2996	24.9823	10.2158	32.3531	24.8758	11.6607	32.3547	24.6239
2019-008	2019	8	50	8.524	32.4833	25.2465	8.2385	32.3452	25.1807	8.7308	32.3078	25.0778	9.2384	32.4048	25.0752	10.3423	32.3676	24.8658
2019-008	2019	8	60	7.9245	32.4963	25.3448	7.9025	32.3778	25.2549	8.4476	32.3083	25.1208	8.6954	32.4988	25.2328	9.2175	32.3787	25.0581
2019-008	2019	8	70	7.5287	32.527	25.4249	7.7316	32.3894	25.2883	8.3045	32.3104	25.1437	8.297	32.6236	25.3904	8.6222	32.406	25.1712
2019-008	2019	8	80	7.2544	32.5461	25.4777	7.4883	32.4013	25.3317	8.0951	32.3352	25.1937	8.2883	32.8424	25.5632	8.243	32.4576	25.2681
2019-008	2019	8	90	6.8673	32.5583	25.5392	7.038	32.7048	25.6319	7.8618	32.401	25.2789	8.2421	33.0053	25.6979	7.8668	32.6045	25.438
2019-008	2019	8	100	6.5715	32.5941	25.606	6.877	33.0248	25.9054	7.1406	32.6623	25.5846	8.3196	33.1999	25.8389	7.6752	32.8566	25.6633
2019-008	2019	8	125	5.8896	32.9571	25.9779	6.8648	33.5867	26.3497	6.4881	33.3805	26.2369	8.3841	33.5043	26.068	7.528	33.3912	26.1043
2019-008	2019	8	150	5.0761	33.4308	26.4484	6.6341	33.7871	26.5384	6.5751	33.6593	26.4454	8.1847	33.7167	26.2646	7.6494	33.6862	26.3189
2019-008	2019	8	175	4.8154	33.6091	26.619	6.1077	33.8321	26.6421	6.4425	33.8007	26.5743	7.9095	33.8383	26.4007	7.4373	33.8598	26.4857
2019-008	2019	8	200	4.6385	33.6931	26.7051	5.7159	33.826	26.6859	5.9855	33.8255	26.6522	7.6602	33.8818	26.4711	7.2362	33.9168	26.5588
2019-008	2019	8	250	4.3797	33.7735	26.7968	5.2553	33.8604	26.7682	5.6245	33.8571	26.7216	7.0822	33.9229	26.5849	6.567	33.9289	26.6591
2019-008	2019	8	300	4.2708	33.8353	26.8574	4.8714	33.907	26.8491	5.2117	33.8822	26.7905	6.4209	33.9373	26.6849	6.0912	33.96	26.7452
2019-008	2019	8	400	3.965	33.939	26.9715	4.4492	33.9771	26.9511	4.5233	33.9542	26.9249	5.4192	33.9766	26.8408	5.3282	34.0113	26.8791